Hierarchical Control and Optimization Strategies Applied to Solar Membrane Distillation Facilities

Ph.D. in Computer Science

UNIVERSITY OF ALMERÍA

Author:

Juan Diego Gil Vergel

Supervisors:
Prof. Manuel Berenguel Soria
Dr. Lidia Roca Sobrino

Almería, June 2020

Ph.D. Thesis

Hierarchical Control and Optimization Strategies Applied to Solar Membrane Distillation Facilities

Estrategias de Control Jerárquico y Optimización Aplicadas a Plantas de Destilación por Membranas Alimentadas con Energía Solar

University of Almería

Department of Informatics

Ph.D. in Computer Science (RD99/11)

Author:
Juan Diego Gil Vergel

Supervisors:
Prof. Manuel Berenguel Soria
Dr. Lidia Roca Sobrino

Almería, June 2020

A mi familia,
Ainoa
y
amigos.

———-

To my family,
Ainoa
and
friends.

Why does this magnificent applied science which saves work and makes life easier bring us so little happiness? The simple answer runs: because we have not yet learned to make sensible use of it. [...] It is not enough that you should understand about applied science in order that your work may increase man's blessings. Concern for the man himself and his fate must always form the chief interest of all technical endeavors; [...] concern for the great unsolved problems of the organization of labor and the distribution of goods in order that the creations of our mind shall be a blessing and not a curse to mankind. Never forget this in the midst of your diagrams and equations.

Albert Einstein

Agradecimientos

Me gustaría utilizar estas primeras páginas para expresar mi más sincero agradecimiento a todas las personas que me han apoyado y animado a lo largo del desarrollo de esta tesis.

Voy a comenzar con mis directores, Manuel Berenguel y Lidia Roca. Manuel Berenguel fue mi profesor en el Grado de Ingeniería Electrónica Industrial, todavía recuerdo el primer correo que intercambié con él y la primera vez que fui a su despacho, todo esto terminó conmigo rumbo a Brescia (Italia) durante seis meses (donde viví una experiencia muy gratificante por cierto, gracias Antonio por tu acogida, hospitalidad y ayuda). Desde aquel momento en adelante, has sabido como transmitirme la curiosidad y el entusiasmo por la investigación en general, y la pasión por el control automático en particular, animándome a adentrarme en un mundo que yo nunca había imaginado. Lidia, también recuerdo la primera vez que me encontré contigo en la Plataforma Solar de Almería cuando inicié mi trabajo fin de grado. Desde un principio, y mucho antes de comenzar la tesis, has tenido un papel fundamental en mi progreso. No sabría como expresar con palabras todo el apoyo que me has dado, gracias por escuchar siempre mis ideas y por estar dispuesta a ayudarme en todo lo que he necesitado. Manolo y Lidia, muchas gracias por vuestra paciencia, por comprenderme y confiar en mí, y por todo el conocimiento y experiencias que me habéis transmitido; todo esto junto me ha ayudado a crecer tanto académicamente como personalmente. Ambos tenéis mi admiración, aprecio y respeto.

Me gustaría agradecer también a mis compañeros de la Plataforma Solar de Almería por su profesionalidad, dedicación y buena recepción. Guillermo, muchas gracias por introducirme en el mundo de la destilación por membranas y por todo el conocimiento que me has transmitido, tu contribución ha sido esencial para el exitoso desarrollo de esta tesis. Alba, muchas gracias por enseñarme a operar la planta y por estar siempre dispuesta a resolver mis dudas, especialmente al principio, que quizás es la etapa más difícil de cualquier tesis. Rafa y Agustín, gracias también por toda la ayuda que me habéis dado en aspectos técnicos y, en gran medida, por hacer el trabajo de campo más fácil. Por último, me gustaría expresar mi gratitud a todos los miembros de la Unidad de Desalación Solar de la Plataforma Solar de Almería por su hospitalidad y compañerismo.

También quiero agradecer a todos mis compañeros del grupo de Automática, Robótica y Mecatrónica por hacer estos años en la Universidad de Almería inolvidables. Trabajar y compartir el día a día con ellos es, sin lugar a dudas, un privilegio. Quiero hacer una mención especial a Francisco Rodríguez y José Luis Guzmán, ambos siempre habéis estado dispuestos a ayudarme y habéis participado activamente en mi formación académica, mis sinceros agradecimientos a los dos. Gracias también, José Luis, por todos los buenos momentos vividos fuera del ambiente universitario. De la misma manera, me gustaría agradecer a José Carlos, Manuel Pérez, Domingo, Jorge, María del Mar y Andrzej que, de alguna manera y por diferentes motivos, habéis contribuido a mi progreso. También, tengo que hacer una mención especial al grupo de "Los compadres", muchas gracias por las risas y todos los momentos divertidos vividos durante estos años. Y por supuesto, tengo que agradecer a Jero, mi conpañero más cercano en esta experiencia. Nunca olvidaré todas las aventuras superadas juntos: el viaje al primer congreso, los nervios por la primera presentación, la estancia en Brasil y muchos más. Lo creas o no, he aprendido muchas cosas de tu personalidad y has influido de una forma muy positiva en mí. Muchas gracias, amigo.

Me gustaría expresar mi gratitud también hacia los miembros del Departamento de Sistemas y Automática de la Universidad Federal de Santa Catarina (Brasil) por recibirme durante tres meses. Al profesor Julio Normey-Rico quiero agradecer su amable acogida en Florianópolis, su hospitalidad y su notable contribución a esta tesis. Al profesor Eduardo Camponogara me gustaría darle las gracias por todos los conocimientos que me ha transmitido sobre optimización no lineal, ha sido un placer colaborar con usted. Por supuesto, a Paulo y Gustavo les tengo que agradecer toda la ayuda que nos prestaron tanto en aspectos académicos como en las experiencias fuera del ámbito universitario. Especialmente Paulo, gracias amigo, por intentar mostrarnos toda la cultura de Brasil y todos los rincones de la isla y, por supuesto, por todos los buenos momentos vividos en la Lagoa da Conceição.

También me gustaría agradecer a los miembros del Departamento de Informática y al personal del servicio de investigación de la Universidad de Almería, por todo el apoyo institucional y por ayudarme con todos los procedimientos administrativos respectivamente.

Debo dar las gracias también a mis amigos que, aunque no he estado mucho tiempo con ellos durante esta etapa, siempre me han ayudado a desconectar cuando lo he necesitado.

Naturalmente, quiero resaltar el apoyo incondicional de mis padres, Juan y Maribel. Tengo que agredecer, no solo el apoyo durante esta etapa, sino el que he recibido a lo largo de mi vida. Me habéis dado la libertad para elegir mi camino y hacer lo que me guste, pero siempre guiándome y aconsejándome desde la barrera. Llegar hasta aquí no habría sido posible sin vosotros. Me gustaría extender este agradecimiento a mi familia en general y, especialmente, a mi hermana María Isabel. Muchas gracias por todo vuestro apoyo y ayuda.

Finalmente y sobre todo, me gustaría agredecer a Ainoa por su constante apoyo, compresión y paciencia, por estar conmigo en los malos momentos, y por ser protagonista de la mayoría de los buenos. No podría haber finalizado la tesis sin ti.

Muchas gracias a todos,
Juan Diego

Acknowledgements

I would like to use these first pages to express my sincere gratitude to all the people who have supported and encouraged me throughout the development of the thesis.

I am going to start by thanking my supervisors Manuel Berenguel and Lidia Roca for their guidance and support. Manuel Berenguel was my professor in the Bachelor's Degree in Industrial Electronics Engineering. I still remember the first email I exchanged with him and the first time I went to his office, all this ended with me heading to Brescia (Italy) for six months (where I lived a rewarding experience indeed, Antonio thank you for your welcome, hospitality and help). From that first moment on, you have known how to transmit to me the curiosity and enthusiasm for research in general, and the passion for automatic control in particular, encouraging me to get involved in a new world that I had never imagined. Lidia, I also remember the first time I met you at the Plataforma Solar de Almería when I started my final degree work. From the beginning, and long before starting the Ph.D. thesis, you have played a fundamental role in my progress. I would not know how to express in words all the support you have given me, thanks for always listening to my ideas and for being willing to help me in everything I have needed. Manolo and Lidia, thank you very much for your patience, for understanding and trusting me, and for all the knowledge and experiences that you have transmitted to me; everything together has helped me grow both academically and personally. Both of you have my admiration, appreciation and respect.

I would like to thank my colleagues at Plataforma Solar de Almería for their professionalism, dedication and good reception. Guillermo, thank you very much for introducing me to the world of membrane distillation and for all the knowledge you have transmitted to me, your contribution has been essential for the successful development of this Ph.D. thesis. Alba, thank you for teaching me how to operate the plant and for being willing to always answer my questions, especially at the beginning, which is perhaps the most difficult stage of any thesis. Rafa and Agustín, thanks also to you for all the help in the technical aspects and, largely, for making fieldwork easier. Finally, I would like to express my gratitude to all the members of the Solar Desalination Unit at Plataforma Solar de Almería for their hospitality and fellowship.

Resumen

El crecimiento de la población junto con el de las actividades industriales y agrícolas está provocando que las reservas de agua dulce se encuentren bajo una situación de pronunciado estrés. Así mismo, los efectos del cambio climático están alterando el ciclo natural del agua a través de fenómenos meteorológicos extremos como sequías e inundaciones, agravando aún más la situación y causando que acuíferos de todo mundo se agoten o contaminen. Ante este panorama, la humanidad se enfrenta a uno de los mayores retos de su historia, el cual se debe abordar urgentemente mediante una modificación del modelo actual de uso y abastecimiento del agua.

Pese a que muchos países de todo el mundo están desarrollando políticas dirigidas a la realización de un uso racional de este recurso, en la mayoría de los casos estas no son suficientes y se necesitan nuevas fuentes de agua dulce para satisfacer las demandas. En consecuencia, la desalación ha emergido como una de las soluciones más prometedoras para extender los recursos hídricos naturales, provocando que muchos países apuesten por su uso. Sin embargo, las tecnologías de desalación convencionales presentan dos problemas principales. Por un lado, aunque los procesos de desalación han sufrido un gran desarrollo en las últimas décadas, estos siguen siendo energéticamente ineficientes por lo que su uso, junto con fuentes de energía convencionales, puede hacer que el problema del agua derive en un problema energético. Por otro lado, estos procesos no pueden ser reducidos fácilmente a plantas de medio o pequeño tamaño y, además, requieren el uso de infraestructuras específicas y la conexión a la red eléctrica para evitar operaciones discontinuas. Este hecho impide su implementación en zonas rurales o aisladas, como islas con bajo consumo per-cápita, lugares donde se concentra una gran parte de la población que sufre escasez de agua actualmente.

La destilación por membranas es un proceso de desalación alternativo impulsado térmicamente a media-baja temperatura (generalmente inferior a 85 ºC). Esta característica le permite ser fácilmente alimentada mediante energía solar o fuentes térmicas de baja entalpía, como calor residual, reduciendo así la huella de carbón de los procesos convencionales. Además, esta tecnología permite su uso descentralizado a pequeña escala y la realización de operaciones intermitentes, lo que la convierte en una solución adecuada para ser implantada en lugares remotos

con buenas condiciones de irradiancia solar. De este modo, la destilación por membranas se erige como una de las tecnologías más convenientes, eficientes y sostenibles para expandir la gama de posibilidades de los procesos de desalación convencionales. Sin embargo, esta tecnología no se encuentra todavía implementada industrialmente y, en la actualidad, está en una etapa pre-comercial, siendo su gran consumo energético por unidad de destilado producida uno de los mayores impedimentos para su completa comercialización.

Hasta la fecha, la mayoría de trabajos de investigación en el campo de la tecnología de destilación por membranas se han centrado en la mejora del diseño interno del módulo y en la prueba de diferentes membranas, con el objetivo de minimizar el consumo térmico y aumentar la producción de destilado. Estos trabajos han provocado un gran avance en términos de consumo térmico, desencadenando que la tecnología entre en una fase de madurez avanzada, lo que se ha confirmado con la aparición de los primeros módulos a escala comercial y la instalación de las primeras plantas a escala piloto. Por lo tanto, la tecnología de destilación por membranas ha entrado en una nueva fase de investigación, en la cual, los trabajos deben estar dirigidos al desarrollo de estrategias de operación que optimicen el funcionamiento de los módulos en tiempo real, especialmente cuando estos se alimentan mediante una fuente de energía con una naturaleza tan intermitente e impredecible como es el caso de la energía solar.

Esta tesis tiene como objetivo el desarrollo de estrategias de operación, mediante el uso de técnicas de modelado, control y optimización, para plantas de destilación por membranas. Los métodos de operación propuestos están centrados principalmente en la reducción del consumo térmico de los módulos y la maximización de su producción de destilado, dos de los puntos débiles de la tecnología, así como la minimización de los costes operativos tratando de reducir el precio del agua desalada. El desarrollo de la tesis se ha dividido en cuatro fases, siguiendo las etapas clásicas de un proyecto de ingeniería de control. En primer lugar, se realizó una etapa de modelado y diseño de controladores de bajo nivel para plantas de destilación por membranas alimentadas con energía solar. Para ello, se utilizaron modelos dinámicos basados en primeros principios ya propuestos en la literatura para el circuito de generación de energía térmica, y se desarrolló un modelo basado en datos experimentales de un módulo de destilación por membranas a escala comercial. Estos modelos sirvieron de base para el desarrollo de una arquitectura de control completa de bajo nivel, formada por cuatro bucles de control gobernados mediante un generador de referencias, la cual permite mantener una temperatura estable a la entrada del módulo de destilación por membranas a pesar de perturbaciones en la radiación solar. Además, esta estrategia fue probada experimentalmente en una planta piloto localizada en la Plataforma Solar de Almería validando los resultados obtenidos en simulación y evidenciando cómo, el tiempo para establecer una temperatura adecuada de operación a la entrada del módulo, se puede reducir entorno al 50 % en comparación con operaciones manuales llevadas a cabo por operadores cualificados.

La segunda fase de desarrollo de la tesis se centró en el diseño de estrategias de control jerárquicas. Estos controladores tienen objetivos de alto nivel como la maximización de la eficiencia térmica, la producción de destilado, o la reducción de los costes operativos, los cuales se consiguen actuando sobre las referencias de los bucles de control de bajo nivel desarrollados en la etapa anterior. En particular, se desarrollaron dos arquitecturas de control, una para la fase de operación, la cual trata de optimizar en tiempo real los objetivos mencionado anteriormente, y otra para el procedimiento de arranque de la planta, que trata de reducir el tiempo empleado en dicho procedimiento. Como en la etapa anterior, ambos controladores fueron probados experi-

mentalmente demostrando, por ejemplo, cómo la producción de destilado se puede aumentar en torno a un 5-7 %, los costes operativos se pueden reducir en un 9-10 %, y el tiempo empleado en la fase de arranque se puede reducir también en un 11 % respecto a operaciones manuales.

La tercera fase de desarrollo se focalizó en el diseño de estrategias de control para plantas de destilación por membranas a escala industrial, donde el paradigma de control difiere de los enfoques anteriores debido a la presencia de múltiples módulos de destilación por membranas y a un agente consumidor de agua. Las estrategias de control propuestas tienen como objetivo reducir el consumo térmico de la unidad de desalación al mismo tiempo que aseguran la demanda de agua variable del agente consumidor, objetivos que requieren condiciones de operación contrarias en el caudal de alimentación de los módulos. El principal reto desde el punto de vista de control en este tipo de aplicaciones radica en el tiempo empleado para calcular las acciones de control óptimas, el cual crece exponencialmente a medida que crece el número de módulos en la unidad de desalación. Así, la primera arquitectura de control propuesta se basó en un controlador predictivo basado en modelo distribuido. En este caso, el controlador se encarga de gestionar el caudal de alimentación de los diferentes módulos para conseguir cumplir los objetivos previamente mencionados. Las pruebas realizadas demostraron cómo el consumo térmico específico de la unidad de desalación se reduce en un 5 % de media respecto a operaciones manuales, mientras que el tiempo de resolución del problema de optimización se redujo notablemente respecto a controladores centralizados. Del mismo modo, se propuso un algoritmo para gestionar no solo el caudal de alimentación, sino también el número de módulos encendidos en cada instante en base a la demanda de agua del agente consumidor, convirtiendo el problema de control en un problema de enteros mixtos no lineal. El algoritmo propuesto para su resolución se basó en la técnica de descomposición de Benders generalizada. Las pruebas mostraron cómo el tiempo de resolución se puede reducir considerablemente. Por ejemplo, para un caso con 64 módulos, el tiempo de un resolvedor de enteros mixtos no lineal es de entorno a 1600 s, mientras que el del algoritmo propuesto es de entorno a 5 s sin que se vea afectada significativamente la solución. Por otra parte, la cantidad de energía térmica consumida por la unidad de desalación también se reduce significativamente, ahorrando hasta un 65 % de la energía requerida en una operación manual en dias soleados.

La última fase de desarrollo de la tesis consistió en la elaboración de un tutorial de técnicas de modelado y control aplicadas en la tecnología de destilación por membranas. En este tutorial se resumen todas las técnicas aplicadas durante el desarrollo de la tesis así como otras propuestas en la literatura, describiendo el desarrollo tecnológico que se consigue con su aplicación.

Para concluir, este resumen termina describiendo la estructura del presente documento, el cual se ha dividido en cuatro partes de acuerdo a las descritas en la normativa de la Universidad de Almería para tesis presentadas en la modalidad por compendio:

- En el capítulo 1 se describe la unidad temática de la tesis y se introducen las principales metodologías empleadas. Además, se indica la estructura de desarrollo de la tesis y las publicaciones que tratan cada uno de los temas abordados.
- En el capítulo 2 se presentan las publicaciones científicas que avalan el trabajo realizado.
- En el capítulo 3 se recogen las conclusiones que se derivan de las diferentes publicaciones así como las recomendaciones para trabajos futuros.
- Por último, el capítulo 4 contiene un listado con otras aportaciones científicas que se derivan de la tesis doctoral.

Abstract

Population growth coupled with industrial and agricultural activities is placing freshwater reserves under severe stress. Also, the effects of climate change are altering the natural water cycle through extreme meteorological phenomena such as droughts and floods, further aggravating the situation and causing aquifers worldwide to become depleted or polluted. Considering this panorama, humanity faces one of the greatest challenges in its history, which must be addressed urgently by modifying the current model of water use and supply.

Even though many countries around the world are developing policies aimed at achieving rational use of this resource, in most cases these are not enough and new sources of freshwater are needed to meet demands. In consequence, desalination has emerged as one of the most promising solutions for extending natural water resources, promoting many countries opt for its use. However, conventional desalination technologies present two main problems. On the one hand, although desalination processes have undergone major development in the last decades, these are still energy inefficient, so if they are powered with conventional energy sources, the water problem can turn into an energy problem. On the other hand, these processes cannot easily be reduced to a medium or small scale. In addition, they require the use of specific infrastructures and on-grid power connections to avoid discontinued operations. This fact prevents its implementation in rural or isolated areas, such as islands with low per capita consumption, where a large part of the population currently suffering from water shortages is concentrated.

Membrane distillation is an alternative thermally-driven desalination process powered at medium-low temperature (generally below 85 °C). This feature allows this technique to be easily powered by solar energy or low enthalpy heat sources such as waste heat, thus reducing the carbon footprint of conventional processes. Besides, this technology allows its decentralized use on a small scale and the intermittent operation, which makes it a suitable solution to be implanted in remote places with good conditions of solar irradiance. In this way, membrane distillation stands out as one of the most convenient, efficient and sustainable technologies to expand the range possibilities of conventional desalination processes. However, this technology is not yet industrially implemented and it is currently in a pre-commercial stage, being its high

energy consumption per unit of distillate produced one of the major impediments to its complete commercialization.

So far the majority of research works in the field of membrane distillation technology have focused on improving the internal design of the module and on testing different membranes, intending to minimize thermal consumption and increase distillate production. These works have caused a great advance in terms of thermal consumption, allowing the technology to enter in an advanced stage of maturity, which was confirmed with the appearance of the first modules on a commercial scale and the installation of the first plants at pilot scale. Therefore, membrane distillation technology has entered in a new research phase, in which the efforts must be devoted to the development of operating strategies that optimize the operation of the modules in real-time, especially when these are powered by an energy source with such as intermittent and unpredictable nature as solar energy.

This thesis aims to develop operating strategies, through the use of modelling, control and optimization techniques for membrane distillation plants. The proposed operating methods are mainly focused on reducing the thermal consumption of the modules and on maximizing their distillate production, two of the main weak points of the technology, as well as minimizing operating costs trying to reduce the price of desalinated water. The development of the thesis has been divided into four phases, following the classic steps of a control engineering project. First, a stage of modelling and design of low-level controllers for membrane distillation plants powered by solar energy was performed. For this, dynamic models based on first principles already proposed in the literature were used to characterize the heat generation circuit, and a model based on experimental data for a commercial-scale membrane distillation module was developed. These models served as the basis for the design of a complete low-level control architecture consisting of four loops governed by a reference generator, which allows a stable temperature to be maintained at the inlet of the membrane distillation module despite disturbances in solar irradiance. This strategy was experimentally tested in a pilot plant located at the Plataforma Solar of Almería validating the results obtained in simulation and evidencing how, the time for establishing an adequate operating temperature at the module inlet, can be reduced by 50 % compared to manual operations performed by qualify operators.

The second phase of the development of the thesis focused on the design of hierarchical control strategies. These controllers were tasked with high-level control objectives such as maximizing the thermal efficiency, distillate production, or reducing operating costs, which are achieved by acting on the references of the low-level control loops developed in the previous stage. In particular, two control architectures were developed, one for the phase of operation, which tries to optimize in real-time the objectives mentioned above, and another for the plant start-up procedure, which tries to reduce the time spent on said procedure. As in the previous stage, both controllers were experimentally tested, demonstrating, for example, how distillate production can be increased by around 5-7 %, operating costs can be reduced by 9-10 %, and the time spent in the start-up phase can be reduced by 11 % compared to manual operations.

The third development phase focused on the design of control strategies for membranes distillation plants at the industrial scale, where the control paradigm differs from previous approaches due to the presence of multiple membrane distillation modules and a water-consuming agent. The proposed control strategies aim to reduce the thermal consumption of the desalination unit while ensuring the variable water demand of the consuming agent, objectives that require contrary

operating conditions in the fluid flow rate of the modules. The main challenge from a control point of view in these types of applications lies in the time spent to calculate optimal control actions, which grows exponentially as the number of distillation modules in the desalination unit increases. Thus, the first control architecture proposed was based on a distributed model predictive control technique. In this case, the controller was responsible for managing the feed flow rate of the different modules to achieve the abovementioned goals. The tests carried out showed how the specific thermal consumption of the desalination unit can be reduced by 5 % on average compared to manual operations, while the computing time was significantly reduced compared to centralized controllers. Additionally, a control algorithm was also proposed to manage, apart from the feed flow rate, the number of modules turned on at each sampling time according to the water demand of the consuming agent, turning the control problem into a nonlinear mixed integer problem. The proposed algorithm for its resolution was based on the generalized Benders decomposition. The tests showed how the computing time can be considerably reduced, for example, for a case with 64 modules, the time spent by a solver for the nonlinear mixed integer problem was around 1600 s, while that of the proposed algorithm was 5 s without significantly affecting the solution. Besides, the amount of thermal energy consumed by the desalination unit was also significantly reduced, saving up to 65 % of the energy required by manual operation on a sunny day.

The last development phase of the thesis consisted in the elaboration of a tutorial of modelling and control techniques applied to the membrane distillation technology. In this tutorial, all the techniques applied during the development of the thesis as well as other proposals in the literature are summarized, describing the technological development that can be achieved with its application.

To conclude, this summary ends by depicting the structure of this document, which has been divided into four parts according to those described in the University of Almería regulation for Ph.D. theses presented in the compendium modality:

- Chapter 1 describes the framework of the thesis and introduces the main methodologies used. In addition, this chapter describes the development structure of the thesis and indicates the publications dealing with each of the topics covered.
- Chapter 2 presents the scientific publications that support the work done.
- Chapter 3 summarizes the conclusions derived from the different publications as well as the recommendations for future work.
- Finally, Chapter 4 contains a list of other scientific contributions that are directly derived from the Ph.D. thesis.

Contents

List of Figures

List of Acronyms

Please note that each of the articles included in Chapter 2 has its
specific list of acronyms which is independent of the one below

AGMD	Air-Gap Membrane Distillation
ANN	Artificial Neural Networks
CIEMAT	Centro de Investigaciones Energéticas, Medioambientales y Tecnológicas
DCMD	Direct Contact Membrane Distillation
DMPC	Distributed Model Predictive Control
DOI	Digital Object Identifier
ERDF	European Regional Development Fund
FEDER	Fondo Europeo de Desarrollo Regional
GA	Genetic Algorithms
GBD	Generalized Benders Decomposition
IF	Impact Factor
IFAC	International Federation of Automatic Control
JCR	Journal Citation Report
LGMD	Liquid-Gap Membrane Distillation
LP	Linear Programming
MD	Membrane Distillation
MINLP	Mixed-Integer NonLinear Programming
MIP	Mixed Integer Programming
MLP	Multi-Layer feedforward Perceptron
MPC	Model Predictive Control
MSF	Multi-Stage Flash Distillation
NLP	NonLinear Programming

PGMD	Permeate-Gap Membrane Distillation
PID	Proportional, Integral and Derivative
PSA	Plataforma Solar de Almería
QP	Quadratic Programming
RO	Reverse Osmosis
RSM	Response Surface Methodology
SGMD	Sweeping Gas Membrane Distillation
SMD	Solar Membrane Distillation
UAL	Universidad de Almería
UN	United Nations
VMD	Vacuum Membrane Distillation
WHO	World Health Organization

List of Symbols

Please note that each of the articles included in Chapter 2 has its specific list of symbols which is independent of the one below

a	Argument of the summing junction in a neural network
b	Bias vector
c	Vector used to define the objective function in QP problems
$e, e(t)$	Control error, and control error at time t
$f(\cdot)$	Function of its arguments
$g(\cdot)$	Inequality constraint function
H	Symmetric matrix used to define the objective function in QP problems
$h(\cdot)$	Equality constraint function
$J(\cdot)$	Objective function
J^*	Optimal objective function value
K	PID proportional gain
$L(\cdot)$	Lagrange function related to the optimallity cut in the GBD method
$\bar{L}(\cdot)$	Lagrange function related to the feasibility cut in the GBD method
L^1, L^2	Last iteration counters at which the optimallity and feasibility cuts, respectively, are updated in the GBD method
LB	Lower bound used in the GBD method
l	Iteration counter used in the GBD method
m	Number of inputs variables in the model
N	Prediction horizon
N_u	Control horizon
q	Output variable of the model
$\Re$	Set of all real number

$\Re^n$	Real vector space
$\Re^{n_x}$	Real vector space delimiting x-domain
R^2	Coefficient of determination
T_d	PID derivative time
T_i	PID integral time
t	Time
t_s	Sampling time
UB	Upper bound used in the GBD method
$u, u(t), u(t+j\|t)$	Control variable, control variable at time t, and value of the control variable at time $t+j$ calculated with the information available at time t
u_{max}, u_{min}	Maximum and minimum values of the control signal
w	Weighting coefficient
w_0	Offset coefficient
X	Feasible or search space of continuous variables
x	Vector of continuous decision variables
x^*	Optimal solution of the optimization problem concerning continuous variables
$y, y(t), \hat{y}(t+j\|t)$	Process variable, process variable at time t, and expected value of $y(t+j)$ with available information at instant t
$y_{sp}, y_{sp}(t+j\|t)$	Setpoint of the process variable, and value of the setpoint at time $t+j$
y_{max}, y_{min}	Maximum and minimum values of the process variable
z	Input variable of the model
α	Weighting factor to penalize tracking errors in MPC control
γ	Weighting factor to penalize control efforts in MPC control
Δ	Increment
ε	Tolerance factor
λ	Lagrange multiplier related to equality constraints in the feasible *primal* problem of the GBD method
$\bar{\lambda}$	Lagrange multiplier related to equality constraints in the infeasible *primal* problem of the GBD method
μ	Lagrange multiplier related to inequality constraints in the feasible *primal* problem of the GBD method
$\bar{\mu}$	Lagrange multiplier related to inequality constraints in the infeasible *primal* problem of the GBD method
μ_0	Auxiliary continuous variable used to define the *master* problem in the GBD method
υ	Auxiliary continuous variable used to define the infeasible *primal* problem in the GBD method
Φ^{n_y}	Vector space delimiting ϕ-domain
ϕ	Vector of binary decision variables
$(\cdot)^T$	Traspose of $(\cdot)$
$\hat{\cdot}$	Expected value

1. Introduction

This chapter is aimed at providing the reader with a general overview of the research work carried out. Firstly, Section 1.1 describes the frame of reference and the main interest of the Ph.D. thesis project, standing out the problem of water shortage and the use of desalination processes as a solution. In addition, Section 1.2 presents a brief description of the Membrane Distillation (MD) technology in which the work, in essence, is focused. Secondly, as the research lines of the Ph.D. thesis project cover the application of modelling, control and optimization strategies to MD based facilities, Sections 1.3, 1.4 and 1.5 briefly depict each, introducing the main techniques and methodologies used. Finally, Section 1.6 is devoted to explaining the research work done, including background and main contributions of each task performed.

1.1 Context and motivation

Water is a fundamental resource of our society and the maintenance of its supply both in quantity and sufficient quality for human consumption is a matter of the survival of humanity. The water scarcity is increasing steadily so that the planning and the proper management of water resources, as well as the search for alternative sustainable water sources, are forefront topics in recent decades [10, 11].

1.1.1 Water: a great problem in our time

The growth of world population, industrial and agricultural activities together with the reduction of water reserves, due to climate change and contamination, are compounding the problem of water shortage worldwide. These facts have caused the use of water to increase around 1 % per year since the 1980s. Agriculture is the leading water consumer, accounting for 69 % of annual global water consumption while industry and domestic use account for 19 % and 12 % respectively [1]. The water demand is expected to continue increasing according to the socio-economic development of the aforementioned activities so that, some studies report that around 5.7 billions people (around 60 % of world population) can suffer water scarcity in 2050 [12]. These figures highlight that conventional water sources are not enough to meet human necessities

in water-scarce areas, conflicting with goal 6 of the sustainable development goals established by the United Nations (UN) in 2015, which deals with ensuring access to water and sanitation for all [13].

Water is not only limited in terms of quantity but also the sufficient quality for human consumption [14]. One of the main consequences of climate change is the degradation of water resources since extreme precipitation phenomena transport pathogens and other pollutants to waterways through runoff and flooding. Thus, the quality of the water resources is another issue to take into account in this water-scarce panorama [15]. Besides, it must be added other consequences of climate change such as drought and desertification, which are increasing significantly in diverse areas of the planet. This fact is especially relevant in Mediterranean countries, as can be seen in Fig. 1.1, where the water resources are almost exhausted [16]. Nevertheless, Fig. 1.1 only shows the physical water stress which is the ratio between the freshwater withdrawn and freshwater resources. But at the same time, there are communities where the water is not physically limited but the limitation appears as a result of a lack of infrastructures. This phenomenon is known as economic water scarcity and it arises in many regions of Australia, South America and Sub-Saharan Africa [1].
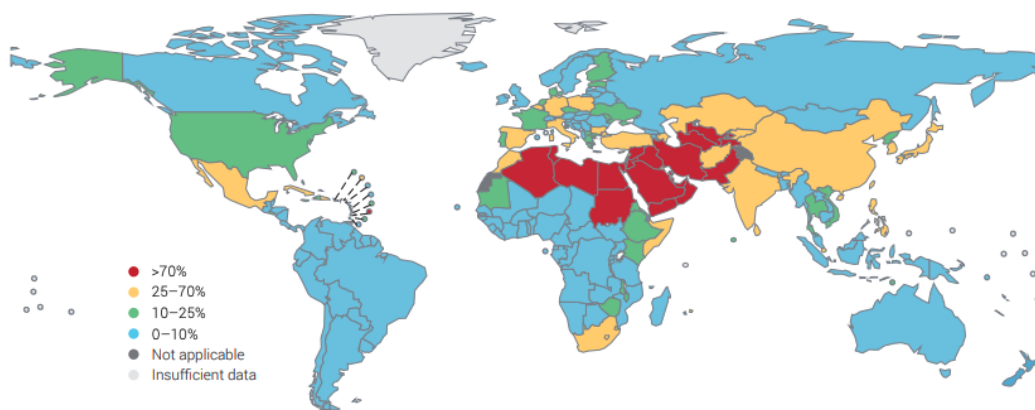
Figure 1.1: Level of physical water stress, obtained from [1].

Considering the above issues, water-scarce countries need an extreme re-think of water resources management and planning to avoid irreversible environmental and social problems very shortly. These efforts should be aimed at performing conscious exploitation of conventional resources leading to sustainable development in terms of water use [11]. However, even though some arid regions are already putting into practice actions in this line, in most cases they are not enough to overcome the problem, and the use of new water sources to close the supply-demand gap is required [17].

1.1.2 Importance of desalination

The problem associated with the lack of freshwater is paradoxical if one takes into account that two-thirds of the planet's surface is covered with water. However, about 99 % of the total is too salty (brackish or seawater) or inaccessible (ice sheets and aquifers) [18]. Thus, pure water in a liquid state can hardly be found in nature, and what is called freshwater is a solution of various salts in water. According to World Health Organization (WHO), water is drinkable if it has a salinity of less than 500 ppm [19], in this context is where desalination, which is defined as the

process of removing salts and dissolved minerals from saline water to produce freshwater, can be a very attractive alternative to alleviate the water deficit.

Desalination of brackish or sea water is getting more and more attention as a way to enhance water supply options in places where the conventional sources are highly limited. This technology is increasingly seen as a viable alternative source, as it can extend the freshwater sources beyond what is available naturally, independently of the weather conditions and providing a steady supply of high-quality product [20]. These favourable features have made desalination an essential agent in the freshwater model of regions like the Middle East or some island communities. Indeed, in countries like Qatar and Kuwait desalination is not a marginal or complementary resource but these countries totally depend on desalinated water to meet domestic and industrial water needs [21]. But desalination is not only implemented in these regions in fact, there are around 15,900 desalination facilities in operation which are placed in 177 different countries spread all over the world, with a total capacity of more than 95 million of m^3 per day. However, it should be remarked that around 45 % of this capacity is installed in regions of the Middle East and North Africa [10].

1.1.3 Water-energy nexus in desalination

Although desalination is one of the most promising solutions to mitigate the water shortage, intensive and irresponsible use of this technology can cause serious environmental problems; mainly related to the high energy consumption of current desalination technologies [22]. By and large, desalination processes can be divided in two main techniques: i) thermal-powered processes which are based on an evaporation process, and ii) membrane processes which function similar to a mechanical filter. In thermal powered desalination techniques, large amounts of thermal energy are needed to reach the latent heat required for evaporation while, in membrane techniques, electrical energy is used as power source for the filtration process. It should be noted that both techniques are considered energy-intensive processes. From 1950 to 2000, thermal-powered processes predominated the desalination panorama whereas, in the last two decades, membrane desalination techniques have reversed the situation with around 60 % of the total capacity due to their low energy requirements compared to thermal powered techniques [23]. For example, one of the most implemented thermal powered desalination processes in the Middle East, the Multi-stage Flash Distillation (MSF), has a specific thermal energy consumption of 7.5-12 kWh/m^3 and an electrical energy consumption of around 2.5-4 kWh/m^3. In contrast, Reverse Osmosis (RO), which is a membrane technique principally installed in Europe, Australia, and the USA, requires only electric power with a consumption of about 2-4 kWh/m^3 [21].

The freshwater problem can derived in a serious energy problem if one observes that most of the aforementioned energy requirements come from on-grid power obtained by conventional sources like fossil fuel. So, current desalination facilities lead to relevant emissions of greenhouse gasses. For example, if the Sydney RO plant, which has a total capacity of 250,000 m^3 per day, operates at a specific energy consumption of 3.6 kWh/m^3, it will emit 950 tons of CO_2 per m^3 of freshwater produced [22]. What is more, the world desalination industry has an estimated emission of 120,000,000 tons of CO_2 per year [24]. This is partly caused since only about 1 % of total desalination facilities are powered with renewable energy [22].

Therefore, to reduce the problem of the water-energy nexus and, in order to develop a viable and environmental-friendly desalination industry, regulatory policies, support schemes, as well

as a deeper knowledge in alternative and sustainable energy sources are required to be scattered worldwide [25].

1.1.4 Desalination technologies powered with renewable energy

The problem reported in the previous section makes the case for combining desalination plants with renewable energy sources. These kinds of systems offer a beneficial and greener solution to meet the growing desalinated water demand. Accordingly, they are attracting more and more interest as the price of renewable energy decreases [26]. Nevertheless, desalination plants powered with renewable energy are not economically competitive yet compared to those plants powered with conventional energy sources [27, 28].

The coupling between desalination facilities and renewable energy presents a main challenge that appears as a result of the intermittent nature of renewable energy sources. This circumstance makes the production of the desalination plant to fluctuate, and consequently, the efficiency of the system to decrease. In this way, most of these plants are small-medium size facilities and they are connected to the on-grid power to assure a steady freshwater supply [29].
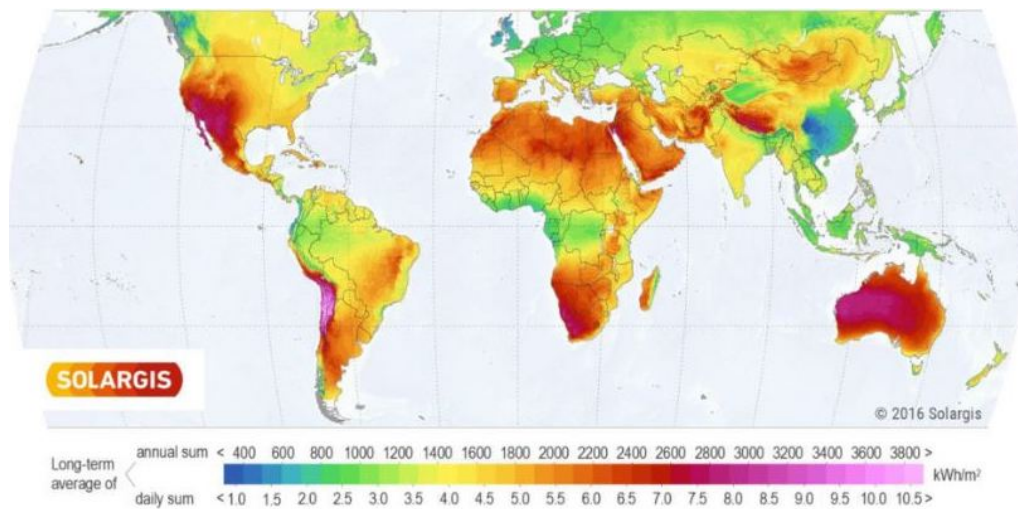
Figure 1.2: World map of direct normal irradiance, obtained from [2].

Solar energy, wind, geothermal, and wave energy are the main renewable energy sources, in addition to hydroelectric power and biomass. However, these two last are not suitable for combining with desalination processes as they require water resources that cannot be available in places with water deficit. Wave and wind energy are the most suitable for coastal areas. These sources are mainly combined with membrane processes as they are suitable to generate the electrical power required by these processes. Geothermal energy is adequate to be combined with thermal desalination processes as this source takes advantage of the heat of subsoil to produce vapor or thermal energy. The main advantage of this combination is that geothermal energy can produce energy throughout a 24 h daily cycle, thus avoiding the use of thermal storage to perform night operation. However, this source can be only used in determined locations due to the nature of the soil of the place at hand [30]. Finally, solar energy is the renewable energy source most widely used to power desalination processes. This source can be employed to produce both electrical and thermal energy so that it can be combined with membrane and thermal processes [22]. One of its main advantages is that solar energy is more abundant and

predictable than the rest of renewable sources. However, what makes it especially appropriate to power desalination facilities is the usual geographical coincidence between water stress (see Fig. 1.1) and high solar irradiance (see Fig. 1.2) [2].

Therefore, the combination of desalination plants with renewable energy is a solid technique to meet small-medium freshwater requirements. Nevertheless, it is required to improve the performance of these systems to implement large-scale plants. It is also necessary to modify conventional desalination processes to make them more suitable to be integrated with renewable energies, as well as to explore non-conventional desalination techniques that have more appropriate characteristics to be powered by these sources [22, 28].

1.2 An overview of membrane distillation

In the line of the search for alternative desalination processes that face the drawbacks mentioned in the previous section, one of the main techniques that is gaining interest in recent decades is the MD technology. This technique stands out for its low operating temperature which enables the use of low-grade thermal solar energy, waste heat, or any type of low-grade renewable thermal energy source for providing the necessary heat [31, 32], thus forming greener and sustainable plants that reduce the carbon footprint of conventional desalination processes [3]. This section aims to provide the reader with a general idea of this technology in which this thesis project focuses. Thus, a brief description of the MD technique is presented. In addition, a revision of its state of art and development and a description of the plant used as reference are provided.

1.2.1 Membrane distillation: Concept, characteristics and potential applications

Concept

MD technology is a thermally-driven separation process, not yet fully commercialized, based on the transport of vapor through a hydrophobic and microporous membrane. This vapor is then condensed somehow with a cooling current on the other side of the membrane [33]. The surface tension of the membrane prevents liquid compounds of the feed solution from passing through its pores, while the volatile compounds pass through them thanks to the partial pressure gradient originated across the membrane; which is established by a temperature difference. Despite this principle being the basis of the operation of MD modules, they can be classified in several configurations depending on how the driving force, i.e., the partial pressure gradient, is maintained in the permeate side of the membrane (see Fig. 1.3):

- **Direct contact membrane distillation (DCMD)**: It is the simplest MD configuration and it is based on maintaining a fluid colder than the feed solution in direct contact with the permeate side of the membrane. In this way, the volatile compounds are evaporated in the liquid-vapor interface originated in the membrane pores, and they are then condensed in the liquid-vapor interface created by the cooling fluid at the other side of the membrane. Its main drawback is the high thermal losses across the membrane which are produced by the low heat transfer resistence provided by the thin membrane layer [34].
- **Air-gap Membrane Distillation (AGMD)**: In this configuration, stagnant air is introduced between the condensation surface and the permeate side of the membrane [35]. This air acts as an isolation layer helping to reduce the thermal losses regarding the DCMD configuration. Nevertheless, this air layer also augments the mass transfer resistance causing the distillate flow to decrease.
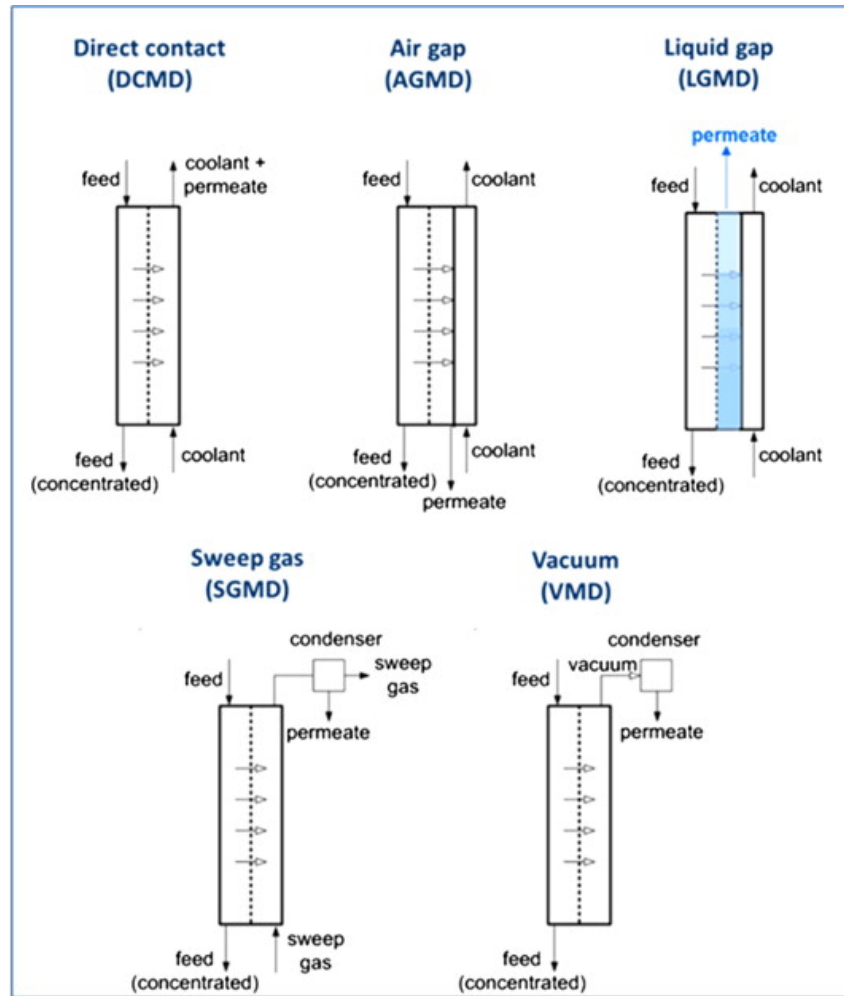
Figure 1.3: MD configurations, obtained from [3].

- **Liquid-Gap Membrane Distillation (LGMD)**: It can be defined as a modification of the AGMD configuration. The main difference among them is that the gap between the membrane and the condensation surface is plenty of liquid instead of stagnant air [36]. This fact improves the mass transfer in comparison to the AGMD configuration, however, the thermal isolation is not as good as in AGMD thus reducing the thermal efficiency [37].
- **Sweeping Gas Membrane Distillation (SGMD)**: In this case, a flow of cold inert gas is used to withdraw the vapor molecules outside of the membrane where the condensation takes place [38]. The gas movement makes the mass transfer to enhance in comparison to the AGMD technique, but it requires additional equipment that increases costs.
- **Vacuum Membrane Distillation (VMD)**: In this configuration, the sweeping gas is replaced by the application of a pressure level lower than the saturation pressure of volatile molecules of feed solution. This pressure level drives the vapor outside of the module where it is condensed. Thus, in VMD modules the thermal losses are almost negligible, and the distillate production is notably improved by the higher partial pressure gradient [39]. However, the additional force can produce pore wetting which can decrease distillate quality.

In any kind of MD configuration, large amounts of heat are required to carry out the evaporation process. For example, the minimum heat requirement in the evaporator channel is defined

by the latent heat of evaporation, which is 655 kWh per m^3 of distillate produced. However, in real MD processes, the heat losses make this figure even higher. To improve this fact, one of the approaches proposed has been to promote internal heat recovery in the MD modules [40]. In the main, the basic operation of an MD module with internal heat recovery can be explained according to Fig. 1.4. The feed solution enters through the feed channel of the module. Along this channel, it is pre-heated with the sensible heat that crosses the condenser channel. Later, the pre-heated solution is driven to the heat exchanger where it is warmed up with fluid coming from the heat generation circuit. Them, the hot solution flows to the evaporation channel of the module where the volatile compounds are evaporated and pass through the membrane while the non-volatile ones are rejected in the form of brine. Finally, the evaporated compounds are condensed obtaining distillated water. Note that apart from the explained solution, other module configurations and designs can be adopted to improve the heat recovery which are described elsewhere [40].
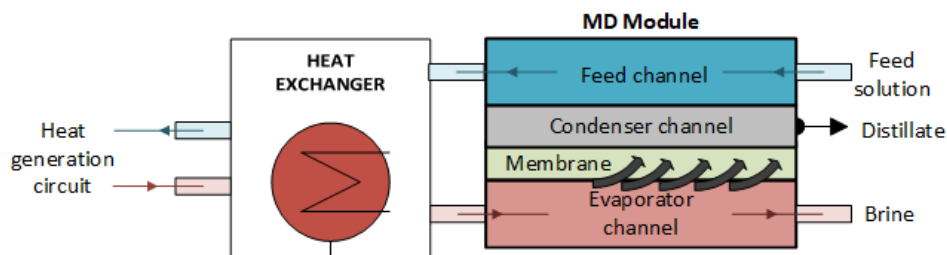
Figure 1.4: Schematic diagram of a MD module (DCMD, AGMD, LGMD) with heat recovery, adapted from [4].

Characteristics

From the process point of view, MD technique has a series of favourable characteristics that place it in the spotlight:

- MD can treat high salinity solutions without pre-treatment requirements [41–43].
- The rejection of solid molecules is theoretically of 100 % [44], being the practical one higher than 99 % [43].
- Its driving force is originated using a temperature difference rather than a mechanic power that increases exergy and costs [45].
- It operates at low pressure (around 0.1 MPa), much lower than the one required by conventional processes as RO (2.5-8.5 MPa) [46].
- It requires a low operating temperature, below 90 ºC, allowing MD processes to be combined with low-grade solar energy [44] and other sources of low enthalpy as waste heat [31].

Potential applications

The latter characteristics, together with the simplicity of the process, make MD technology the most appropriate technique to develop stand-alone desalination plants to be implemented in off-grids areas with small-medium water requirements and good solar irradiance conditions. In fact, this is one of the most promising applications of MD technology as other desalination processes do not allow their down-scaling because their efficiency drastically drops, significantly increasing costs [47]. This was studied in [48] where a Solar Membrane Distillation (SMD) plant was analyzed in economical terms, concluding that the price of desalinated water is around 10-11.30 €/m^3 for a plant with a capacity of 100 m^3/day. These results showed the economic

viability of the MD technology for medium-small size plants when compared to an installation of the same capacity based on RO powered by photovoltaic energy, in which the price amounted to 11.7-15.6 €/m^3. However, it must be noted that similar research works using newer and efficient MD modules are required, since prices discussed above can significantly decrease. Additionally, another problem for conventional desalination processes in this application is that they usually require access to fundamental supply services such as electricity or fuel, which normally are not available in isolated regions.

One more possible application of MD technology is the treatment of concentrated feed solutions. In this sense, MD technology can be used to treat brines from other desalination processes as RO thanks to its high tolerance to salinity in comparison to conventional desalination methods [49]. The brine treatment is a recurring problem that has not yet been solved, as brines cannot be directly dumped into the sea, aquifers, sewage systems or ponds. This problem is notably aggravated on island locations. In this way, the brines can be further concentrated by MD based plants reaching zero liquid discharge [50], thus avoiding the use of expensive methods for its treatment and the environmental problems they can cause.

On balance, MD technology is suitable to be used in fields of application in which other desalination methods cannot be applied. So, the objective of MD technology is not substituting conventional desalination methods (as it is not yet economically competitive at large scale), but extending the variety of possibilities of them. Thus, numerous publications can be found addressing MD technology as a supplementary process to RO [51, 52], or as an alternative water source powered by solar energy to be implemented in remote locations [53, 54].

1.2.2 State of art and development

To understand the work developed in this thesis project it is beneficial to briefly revise the state of art and development of MD technology. MD was first mentioned in a patent published by Bruce Bodell in 1963 [55]. However, even though it is not a new concept or technique today, it has not been fully commercialized yet, being its low thermal efficiency one of the major barriers. Thus, research efforts so far have been dedicated to improve this issue, both designing new modules and configurations and developing effective operating strategies.

Since the emergence of MD technology in 1963, the most exploited research field has been the search for new designs of MD modules. These investigations have been focused on the creation of new membranes, modules and configurations [32], and in comprehend membrane fouling [56], which consists of the deposition of macromolecules, particles, suspensions, emulsions and colloids on or in the membrane, reducing membrane functionality due to pore blocking, cake formation or foulant absorption [57]. The progress carried out in these kinds of works have caused a breakthrough in terms of thermal efficiency as MD modules have gone from an initial thermal consumption of 810 kWh/m^3, thermal consumption of MD modules without heat recovery under the best operating conditions [58], to the current consumption of around 49 kWh/m^3 also in optimal operating conditions but using modules with internal heat recovery [42]. Despite thermal consumption still being high compared for example to that reported before of MSF processes, what makes MD technology especially interesting is that these energy requirements can be provided by solar energy [3] or low enthalphy thermal energy sources. Consequently, several publications propose adequate combinations among MD modules and solar fields [59], as well as integrated compact systems of MD and solar energy [60]. Also, coupling this technique with waste heat is a possibility [61].

Although there is still room for improvement and research in the field of MD modules design, this has been one of the topics more addressed in the literature, and therefore, it is in an advanced state of maturity. This fact is reinforced with the implementation of the first MD pilot plants since 2003, and the appearance of the first technology developer companies since 2005 [55]. That is why MD technology is in a new phase of development in which other research areas mainly focused on the operation of MD modules are gaining interest. These works are aimed at modelling and optimizing the variables involved in the MD process [62], and at developing control and optimization methodologies to improve the MD module's performance in real-time [63].

The development of models in the MD field has become a fundamental tool to predict the behaviour of these processes under different operating conditions. In particular, the existence of different MD modules and configurations makes the development of models based on first principles difficult. Besides, in some cases, MD developer companies do not disclose information about the internal configuration of the module at hand, which also prevents the development of these kinds of models. For this reason, the technique most used in literature is the Response Surface Methodology (RSM), which is a statistical method that employs polynomial functions to adjusts linear or smooth nonlinear processes. Some examples of MD modules modeled by RSM can be found in [5, 62, 64]. It should be remarked that these models not only can be used to analyze and predict the system behavior but also they are a fundamental factor for the development of control and optimization strategies. Thus, most of these works are focused on developing RSM models to find optimal operating conditions of MD modules. The procedure used in these kinds of investigations is the same [65]: i) to design and carry out an experimental campaign in a determined operating range, ii) to characterize the selected outputs of the model by the RSM technique, and iii) to find the optimal operating conditions within the studied operating range by using an optimization method. Nevertheless, although these works show how the thermal efficiency and distillate production of the MD modules are significantly improved by following the optimal static operating conditions they suggest, these conditions are difficult to maintain especially when using an intermittent source like solar energy. Therefore, real-time operating strategies are required to deal with this circumstance.

The development of real-time operating procedures started receiving attention since the last decade, when the first SMD pilot plants began to arise [3, 53, 66–68]. However, there are very few publications in this new research line in the field of MD technology. The first control works appear as a result of the operating difficulties presented in SMD plants, as they usually include solar fields and thermal storage devices that provide these plants with a hybrid nature. So, the main objective of these works was to develop suitable control strategies aimed at maintaining an adequate temperature in the solar field powering the MD module and, at increasing heat storage to carry out night operations. In this sense, several publications can be found in the literature which propose low-level control architectures based on Proportional, Integral and Derivative (PID) controllers or ON/OFF controllers [63, 69, 70]. But these kinds of works are not limited to this objective. More recently, advanced control strategies have begun to be proposed which are tasked with improving metrics related to the MD process, as to maximize the distillate production or the thermal efficiency. These techniques are mainly based on the Model Predictive Control (MPC) methodology and some examples were presented in [71–73].

The works carried out in this thesis project are in the line of the papers referenced above. Thus, the contributions presented encompass the development of models, and control and opti-

mization strategies that help commercialize MD technology. The main aim is to improve the thermal efficiency and the distillate production of the process proposing both optimal operating points and optimal operating procedures in real-time based on advanced control systems. It should be highlighted that these kinds of works are fundamental for the proper development of SMD plants as their operation must be optimized in real-time according to solar energy profile.

1.2.3 Solar membrane distillation plant at Plataforma Solar de Almería

In order to validate the research work carried out, most of the developed algorithms have been tested in the SMD pilot plant at the Plataforma Solar de Almería (PSA, www.psa.es, Southeast of Spain), a dependency of the Centro de Investigaciones Energéticas, Medioambientales y Tecnológicas (CIEMAT). Fig. 1.5 shows some of the fundamental elements of this facility. In general, the facility can be divided in two main parts: the heat generation circuit and the desalination unit.

Figure 1.5: SMD pilot plant at PSA. From top to bottom and from left to right: solar field, Solar Spring module and Aquastill module.

On the one hand, the heat generation circuit includes a solar thermal field of 20 m^2 composed of two parallel rows with five flat-plate collectors (Solaris CP1 Nova, by Solaris, Spain) in series each. This field is connected to a thermal storage tank of 1500 L that can be used for thermal regulation and storage. The solar field has a distribution systems that enables the connection of several MD units simultaneously. Moreover, the facility allows the direct supply of the heat from the solar field or the indirect supply by using the storage tank. The nominal thermal power is 7 kW at about 90 °C. All the facility is controlled and monitored enabling heat flow regulation. A more complete description can be found in [3] and in some publications of this thesis [4, 74].

On the other hand, the desalination unit is linked to the heat generation circuit trough a heat exchanger. This part of the plant has a separate cooling water circuit (about 3.5 kW$_{th}$) that is used as a device for supplying simulated seawater. Moreover, there are several MD modules to be connected to the desalination unit. Among them, the Solar Spring and the Aquastill one have been used in this thesis (see Fig. 1.5). The Solar Spring module consists of a spiral-wound Permeate-Gap Membrane Distillation (PGMD) commercial module, called Oryx 150, with a membrane surface of 10 m^2. Note that the PGMD configuration is equivalent to the LGMD one but using permeate to fill the gap. This module was described and analyzed in [64]. The Aquastill module is a spiral-wound AGMD commercial module with 24 m^2 of membrane surface. More details about this module were presented in [62].

1.3 An overview of systems modelling

Models are effective tools that can be useful to reduce costs and time, and to avoid risk situations through simulations and exhaustive analysis. The models allow the user to be trained to determine how one or more changes in the inputs of the modelled system can partially or globally affect the process without the need to test them in reality. Furthermore, they play a major role in the design of any kind of optimization or control strategy, as they attempt to capture some aspects of the process that are relevant for the development of these types of techniques.

1.3.1 Main idea

To define the concept of a model, it is important to review what a process is. A process or system is a set of elements, components or entities that interact with each other to achieve a common goal. Thus, a model can be defined as a simplified representation of a determined process, with which it is intended to increase its understanding, make predictions of its behavior, or design control and optimization strategies. Note that a system or process can be represented in many different ways, so it can have different models, depending on each perspective [75].

Although models can be classified attending to different criteria, this section only distinguishes between models based on first principles and models based on experimental data because they are the ones used in this thesis project. The first term is referred to models obtained from physical laws, which usually are characterized utilizing differential, difference or partial derivative equations among others [69]. The second term includes the models computed from experimental data which normally are represented by black or grey box models and statistical functions [76].

1.3.2 Models based on first principles

This type of modelling methodologies consists of capturing the dynamics of a real process from the physical-chemical principles that govern its functioning. So, its development requires detailed prior knowledge of the process. The main advantages of these kinds of models are: i) they allow to obtain an approximation with high precision of the real process, ii) they are very useful for simulation tasks, and iii) they facilitate the understanding of the real process and the different sub-processes that compose it as the model is built. However, these models are usually difficult to obtain and sometimes it is impossible due to the lack of knowledge about the physicochemical principles that describe the process.

In MD technology, this modelling methodology is mainly used to characterize the different devices composing the solar field of an SMD facility, which are modelled by well-known models

already presented in literature [77, 78]. Some examples can be found in [4, 69, 74, 79, 80]. Nevertheless, there are also numerous publications addressing the modelling of MD modules. The main objective of these works is to study the dynamical behavior of the modules (especially of the mass and heat transfer mechanisms that occur in the module) based on various design parameters, such as the size of the membrane or its porosity, and operating conditions, such as the temperature at the entrance to both channels of the module, and the concentration and flow of the feed water [69, 81–89]. However, although all the models presented in the aforementioned references were experimentally validated, in most cases the data were obtained with lab-scale MD modules. The validations of this type of models in commercial MD modules are rare, and only a few examples can be found in the literature as the works presented in [40] and [90]. One of the problems preventing this is that some of the physical phenomena that happen within the module are simplified making models less reliable, thereby hindering their validation in commercial MD modules.

1.3.3 Models based on experimental data

Unlike the models based on first principles, the models based on experimental data do not require complete knowledge of the process to be modelled. But in this case, their validity and performance strongly depend on a good selection of the dependent and independent variables, an adequate design of the experiments to be performed in the real facility, and an appropriate selection of the structure of the model. This way, these models are easy to obtain as long as the previous issues are properly addressed and a good set of experimental data is available.

Empirical models are especially suitable for characterizing MD modules as the difficulty in constructing theoretical models is greater because of the different internal design of each module. So, these theoretical models have to be continuously modified to adapt them to the different module configurations and designs [62]. For this reason, the development of empirical models is a good choice to obtain a mathematical expression in a relatively fast and simple way. But it must be taken into account that the experimental campaign necessary to validate it correctly can be extensive. Two of the common modelling techniques employed are the RSM and the Artificial Neural Networks (ANN) methodologies [91]. These techniques are valid to fit multi-variable linear and nonlinear processes. However, it should be noted that they cannot be used to extrapolate the results to other systems and that they are only valid for the range of operation in which they have been obtained. Furthermore, these types of models directly represent the final output of the model and do not allow studying the physical phenomenon that occurs in the system. On the contrary, they are valid to visualize and analyze the operating range of the module and understand the behavior of the system.

Response surface methodology technique

The RSM methodology [92] is a statistical technique that uses quadratic functions to characterize linear or smooth nonlinear processes. In this modeling methodology, design of experiment models are usually employed to plan the experimental campaigns carried out to obtain the experimental data. These models focus on applying changes in steps, called levels, to one of the degrees of freedom while the others remain constant. Afterwards, the polynomial model is adjusted based on the experimental response observed at each level for each independent variable. The steps necessary to develop an RSM model are: i) selection of the dependent and independent variables trough screening studies and based on the researcher experience, and delimitation of the studied region, ii) choice of a design of experiment technique that defines the experiments to be performed in the real plant, and iii) to adjust a polynomial function through a statistical

treatment of the experimental data. It should be noted that a unique polynomial function is used for each of the system outputs. This function, for a case with several input variables, is given by:

$$q = w_0 + \sum_{i=1}^{m} w_i \cdot z_i + \sum_{i=1}^{m} w_{ii} \cdot z_i^2 + \sum_{1 \leq i < k}^{m} w_{ik} \cdot z_i \cdot z_k, \tag{1.1}$$

where m is the number of input variables, w_0 is an offset coefficient (also known as bias b), w_i are the coefficients for the linear terms, z_i and z_k are the input variables of the model, w_{ii} represents the coefficients of the quadratic terms, w_{ik} are the coefficients of the interaction terms, and q is the output of the model. Note that in this modelling methodology the nonlinearity is given by the quadratic terms. Some examples of RSM models in MD technology can be found in [33, 93–99].

Artificial neural networks

ANN is also a mathematical model composed of simple interconnected elements, which process information in response to external inputs mimicking the behavior of biological neural networks [100]. These simple elements are called neurons, and they act as a computational processor in which three main operations are performed (see Fig. 1.6):

1. The input vector $(z_1, z_2, \ldots, z_m)$ is multiplied by the different weights $(w_{1,1}, w_{1,2}, \ldots, w_{1,m})$.
2. In the summing junction, the bias vector b is added to the weighted inputs, so that:

$$a = z_1 \cdot w_{1,1} + z_2 \cdot w_{1,2} + \ldots + z_m \cdot w_{1,m} + b. \tag{1.2}$$

3. The argument a is transformed into a scalar value q through a transfer function f. This function can have different profiles such as linear, sigmoidal or Gaussian.
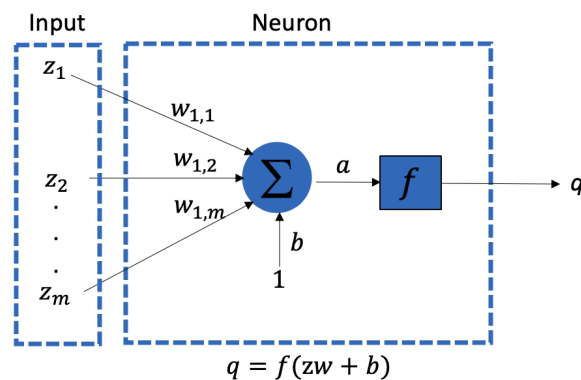
Figure 1.6: Schematic diagram of a neuron, obtained from [5].

The way in which the different neurons composing the net are grouped is known as architecture or topology of the neural network. Normally, they are grouped in different layers called hidden and outputs layers. Besides, the inputs can be considered as an additional layer. Among the different kinds of topologies, one of the most common used to perform function fitting in the MD field is the Multi-Layer feedforward Perceptron (MLP). In this architecture, the number of inputs and outputs of the network is defined according to the number of input and output variables of the system to be modelled. More information about this architecture can be found elsewhere [101].

In this way, the ANN technique has become an emerging tool in recent years in the MD field since, compared to the RSM technique, it is capable of adjusting almost all nonlinear processes.

Thus, it is especially important when independent variables that induce nonlinear behaviors in the system are used, as is the case of the salinity of the MD module feed solution [102]. Some examples of ANN models for MD modules were presented in [63, 76, 102–105]

1.4 An overview of automatic control

Automatic control is a fundamental part of any system or scenario of modern engineering. For instance, it is used in the automotive industry for vehicle controls, in the aerospace industry for decision making, aerial surveillance or control allocation, in energy production systems, and even in biological and medical applications [106]. But also they are present in our daily life since they are employed in many domestic devices as the heating thermostat or the thermostatic tap and in many household appliances. The major part of this thesis project is focused on the application of automatic control strategies to MD plants. For this reason, the present section is aimed at introducing this topic as well as the specific techniques used.

1.4.1 Main idea

To define automatic control, the concept of system or process must be redefined from the point of view of control engineering. A system or process can be seen as an entity that produces a signal transformation [107]. Thus, a system has input signals, that can be manipulated and influence the behavior of the process trough actuators, and output signals, that can be measured by sensors and that are related to the input ones through the transformations performed in the system (see Fig. 1.7). Moreover, the system may also be affected by external and internal stimuli that cannot be manipulated, called disturbances. These disturbances can have a random character (noise) or a deterministic one (interferences). Thus, automatic control systems aim to govern output signals, i.e., to maintain them around desired values, through the adequate manipulation of the inputs ones, regardless of disturbances.
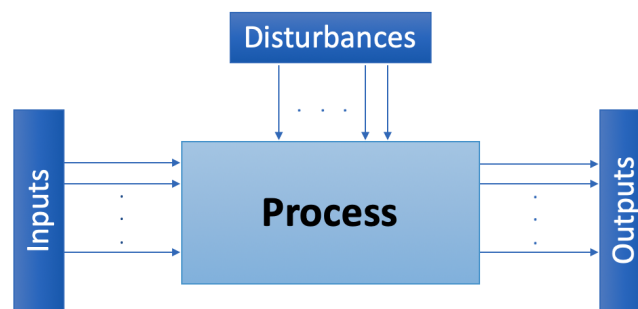
Figure 1.7: Signals flow in a system.

In formal terms, the basis of a control system are: i) to observe the behavior of a real process (i.e., to measure the outputs of the process), ii) to compare it with the desired behavior, and iii) to act on the process (i.e., to manipulate the inputs signals) to modify its behavior and achieve the desired goal. The application of this procedure, which is known as feedback, has given rise to a step forward in control engineering, in fact, many patents have been granted on this principle [6]. The schematic diagram of a simple feedback control loop is shown in Fig. 1.8. As can be observed, the loop is composed of two main components, the controller and the process, which are represented as boxes. Note that the arrows illustrate the relationships among then. On the one

hand, the input of the process, also called control variable, is denoted by u. On the other hand, the output of the process, also known as process variables, is denoted by y. Moreover, the desired value for the process variable, which is called the reference value or set point, is denoted by y_{sp}, and the control error, that is the difference between the process variable and the set point, by e.
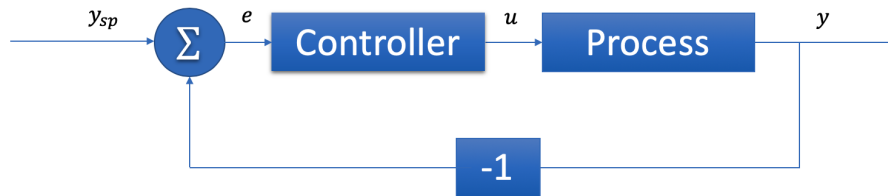
Figure 1.8: Schematic diagram of a unitary feedback control loop, adapted from [6].

To understand the operation of the feedback control loop, it can be assumed a simple process (one input one output) with a behavior such that the process variable increases as the control variable is increased. Consequently, the principle of feedback can be described as: increase the control variable when the error is higher than zero, and decrease it otherwise. In this way, the error will become smaller and smaller, and may be zero in the ideal case. This means that the process variable is going to be very close to the desired operating point regardless of the properties of the process. Apart from this fact, the feedback has a series of beneficial characteristics that make it especially interesting as it can help to reject the effects of the disturbances, and it can make the process insensitive to system variations [6]. Nevertheless, feedback has to be carefully used, mostly in presence of time delay or a high degree of unmodelled dynamics, noise or disturbances; as stability[1] and performance can be compromised. Moreover, any control design has fundamental limitations on achievable performance [8].

Once the concept of feedback is clear, one can observe that there are basic elements required to perform it. Sensors and actuators are fundamental items, but also, an essential part of this method is the controller, which is the mechanism tasked with computing the control actions. Thus, in the following subsections, the control algorithms employed in the different works developed in the framework of this thesis project are briefly introduced.

1.4.2 Proportional integral and derivative control

One of the simplest mechanism to calculate the control actions are the PID controllers. In these kinds of controllers, the control signal, u, is computed as a sum of three terms [6]. Despite this sum can be represented in several ways, the most typical one (ideal configuration) is given by:

$$u(t) = K\left[e(t) + \frac{1}{T_i}\int_0^t e(t)dt + T_d\frac{de(t)}{dt}\right], \tag{1.3}$$

where $e = y_{sp} - y$, K is the proportional gain, T_i is the integral time, and T_d is the derivative time. This way, the first term in Eq. 1.3 is known as proportional action and it is related to the present. The second term represents the past through the integral of the error. The last term is related to the future as it represents a linear extrapolation of the error T_d time units in the future. Therefore, PID controllers have the ability to eliminate the steady-state errors through the integral term, and

---

[1]Here we adopt the bounded-input bounded-output definition of stability, where the system is considered to be stable if its outputs are bounded for any bounded input.

to anticipate the future through the derivative term.

Even though PID control is categorized as a basic control technique, it is appropriate for many control problems, especially for those with favourable dynamics. For this reason, it is one of the control techniques most implemented in industry [6]. Accordingly, it has been one of the first control algorithms implemented in the MD field [63, 69].

1.4.3 Model predictive control

MCP is one of the most generic ways of formulating a control problem in the time domain. This method has expanded notably since it appeared in the late 70s, becoming one of the control techniques more used in both industry and academia [8]. The main advantages of this control procedure are: i) it results in a controller easy to apply even for staff with limited knowledge in control systems, ii) it can deal with a great variety of processes including those with complex or unstable dynamics, dead times, multivariable, etc., iii) it intrinsically includes disturbance compensation on a natural way, iv) it can consider process constraints in the problem formulation, and v) it can use future references if available.

The term MPC is not limited to a single control procedure but it encompasses a family of control techniques that rely on the use of a model of the system to compute a sequence of control signals by optimizing a given criterion. More specifically, the basis of any kind of MPC controller are (see Fig. 1.9) [8]:
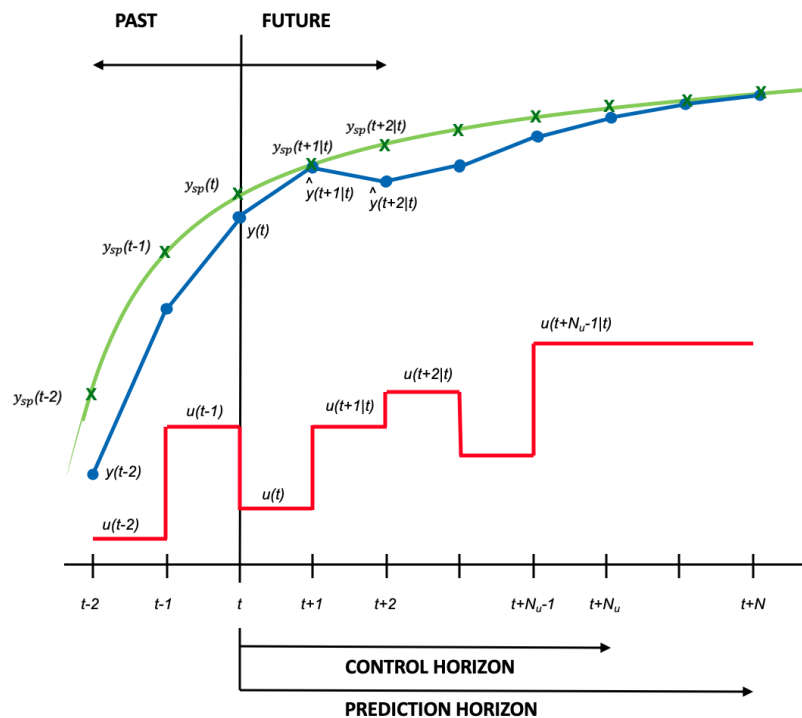
Figure 1.9: MPC strategy, adapted from [7].

1. Use of a process model to predict the future process output, $\hat{y}(t+j|t)$, along a specific o determined prediction horizon N.
2. Minimization of a given objective function to obtain the set of future control actions $(u(t|t), u(t+1|t), \ldots, u(t+N_u-1|t))$, being N_u the control horizon. This objective function

is normally aimed at maintaining the process output as close as possible to a determine reference $y_{sp}(t+j|t)$.

3. Use of a receding horizon strategy, moving at each sampling time the horizon towards the future, and sending to the actual system only the first term, that is $u(t|t)$, of the set of control signals computed at each step.

To implement the above method, the basic architecture presented in Fig. 1.10 is normally used. Hence, to predict the future process outputs, the model of the system is fed by past inputs and outputs and by the future optimal control signals. These signals are computed by the optimizer which considers the objective function, the future tracking errors, and the constraints. Note that the main differences among the family of MPC strategies are both the process and noise model, and the cost function.
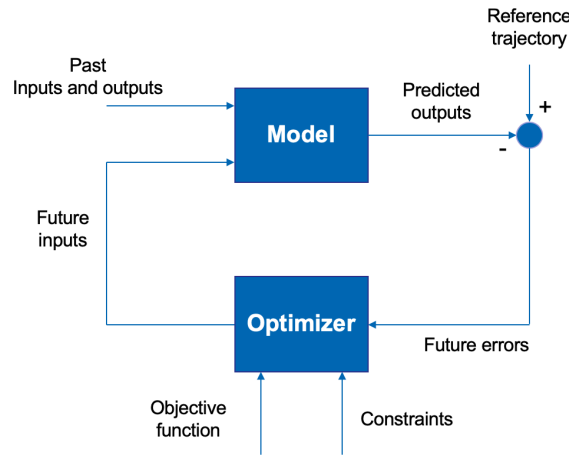
Figure 1.10: Basic MPC architecture, adapted from [8]

The objective function of the optimization problem can be posed as:

$$J = \sum_{j=1}^{N} \alpha \cdot [\hat{y}(t+j|t) - y_{sp}(t+j|t)]^2 + \sum_{j=0}^{N_u-1} \gamma \cdot [\Delta u(t+j)]^2, \tag{1.4}$$

where the predicted system output ($\hat{y}(t+j|t)$) and the desired reference ($y_{sp}(t+j|t)$) are estimated for sampling time $t+j$ using the information available at sampling time t. Moreover, $\Delta u(t+j)$ is the variation in the control signal at sampling time $(t+j)$ whereas α and γ are weighting factors that penalize the future tracking errors and control efforts, respectively, along their horizons (notice that in some cases they can be time-dependent). Regarding the constraints, three types of constraints can be mainly found affecting control actions and process outputs:

$$\Delta u_{min} \leq \Delta u(t) \leq \Delta u_{max}, \forall t \geq 0, \tag{1.5a}$$

$$u_{min} \leq u(t) \leq u_{max}, \forall t \geq 0, \tag{1.5b}$$

$$y_{min} \leq y(t) \leq y_{max}, \forall t \geq 0. \tag{1.5c}$$

In the equations, the first constraint, Eq. (1.5a), is used to limit the control efforts, trying to avoid abrupt changes in the actuator that may cause damages. The second one, Eq. (1.5b), is

involved to the physical hard constraints of the actuator. Finally, the third constraint, Eq. (1.5c), gives the lower (y_{min}) and upper (y_{max}) limits of the output process variable.

It should be noted that MPC has already been tested with successful results in systems including solar thermal fields [108] and also in systems requiring thermal energy management [109], which are two of the main control problems to be addressed in SMD plants. However, it is an emerging technique in the MD field with only few works in the framework of MD facilities [71, 73].

1.4.4 Hierarchical control

In many situations it is difficult, or even impossible, to design a control system as a single entity with centralized decisions, unless the system and control objectives are very simple. In complex industrial processes, such as an SMD plant, different control objectives must be met that normally require different time scales. Besides, in some cases, an overall complex control objective must be met which cannot be directly implemented in a unique controller. The normal way to deal with the design of a controller in such challenging situations is to use hierarchical control architectures. The main idea behind this control methodology is to divide the actual control problem into a sequence of simpler problems hierarchically ordered, which are handled by dedicated control layers. In this way, the design of the controller is easier since simpler control structures are defined requiring different technical and theoretical tools. Moreover, the control reliability and performance are improved [110].

Hierarchical controllers can be formulated according to three basic decomposition methods. The first one is called functional decomposition. This method is used in processes that can be treated as a whole, and it consists of assigning a series of partial control goals in a vertical structure with hierarchical dependency. This structure is known as multilayer structure [110]. The decision unit of each layer calculates control actions concerning the overall system, but each one makes decisions of a different type. The second decomposition method is the spatial decomposition. This methodology is based on the decomposition of the overall control task into several local subtasks, each one with the same objective of the overall one but related to an individual spatially isolated part of the entire process. Note that these subtasks are of smaller dimension and therefore, they have to process less information. This methodology drives to so-called multilevel structures or multilayer-multilevel structures [111]. The last method is called temporal decomposition [112]. This method is applied when the system has a multi-scale behavior in terms of time, i.e., there is a considerable difference among the rate of change of slow and fast state variables (and/or disturbances) of the process. Thus, this method also leads to a multilayer concept, but in this case, each layer has a different time horizon.

Notwithstanding the fact that the three methods described above are the basis of hierarchical control methodology, they can be also mixed. In this way, in this thesis project, a mix between the functional and temporal decomposition methods has been used in most of the developed controllers. An example of the architecture adopted is shown in Fig. 1.11. In this scheme, the two layers involved in the control structure have different objectives. The regulatory layer is usually formed by PID controllers and it is in charge of performing low-level control tasks, i.e., temperature or flow rate control. On the contrary, the upper layer normally includes advanced control methodologies as MPC controllers, and it is tasked with carrying out high-level control tasks. In the case of an SMD plant, it tries to improve metrics related to the distillation process as to enhance the thermal efficiency or distillate production. It should be noted that in this control

structure, the function of the upper layer is to calculate the references for the bottom layer based on the aforementioned criteria. Moreover, it should also be highlighted that the two layers are decoupled in time, since the upper layer normally deals with slow state variables whereas the lower one involves fast state variables.
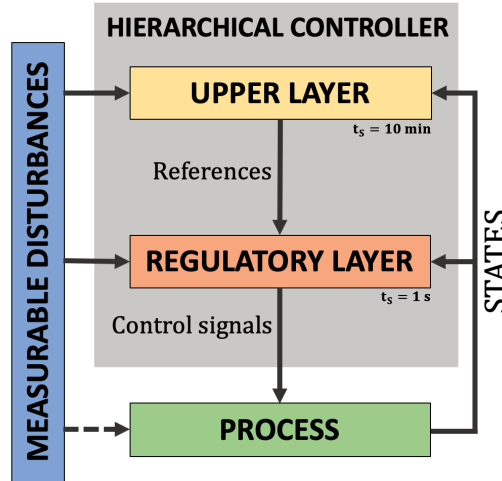
Figure 1.11: Hierarchical control architecture, adapted from [9]. t_s is the sampling time.

1.5 An overview of optimization

As described in the previous section, optimization problems must be solved in some of the control techniques used in this thesis project. For example, in the MPC technique, an optimization problem is solved to compute the optimal control actions. Similarly, in hierarchical controllers, the upper layer aims to provide the follow-up control layer with the optimal values for its references, which also means to formulate and solve an optimization problem. Moreover, optimization algorithms have not only been used in this thesis project for these applications but also they have been used to find optimal operating conditions for the MD module. Therefore, optimization is a fundamental part of the developed works.

This section provides the reader with a general overview of optimization, defining its concept, and presenting a review of strategies to solve these problems. The latter is related to the methods used in this thesis.

1.5.1 Concept and definition

Optimizing means searching for the best way to carry out an activity, and in mathematical terms, finding the maximum or minimum of a certain function defined in some domain. In formal nomenclature, an optimization problem with constraints can be posed as:

$$\min_{x} J(x). \tag{1.6}$$

$$\text{s. t. } \boldsymbol{h}(x) = \boldsymbol{0}, \tag{1.7}$$

$$\boldsymbol{g}(x) \leq \boldsymbol{0}, \tag{1.8}$$

$$x \in X \subseteq \Re^{n_x}, \tag{1.9}$$

where x is a vector of continuous decision variables, J is the objective function, which is defined as a real valued function $J : X \subseteq \Re^{n_x} \to \Re$, X is a non-empty subset in $\Re^{n_x}$, which is known as the feasible or search space. Note that $\Re^{n_x}$ consists of all n-tuples of real numbers in the x-domain, i.e., the real vector space delimiting x-domain. $\boldsymbol{h}(x) = \boldsymbol{0}$ is the set of equality constraints, with $\boldsymbol{h} : X \subseteq \Re^{n_x} \to \Re$, and $\boldsymbol{g}(x) \leq \boldsymbol{0}$ is the set of inequality constraints, with $\boldsymbol{g} : X \subseteq \Re^{n_x} \to \Re$.

To solve the problem formulated above, a minimum objective function value, $J^* \in \Re$ related to every point $\mathbf{x}^* \in X$ of the search space, must be found such that:

$$J^* = J(\mathbf{x}^*) \leq J(\mathbf{x}) \ \forall \mathbf{x} \in X. \tag{1.10}$$

$$\boldsymbol{h}(\mathbf{x}^*) = \boldsymbol{0}, \tag{1.11}$$

$$\boldsymbol{g}(\mathbf{x}^*) \leq \boldsymbol{0}. \tag{1.12}$$

By defining $\mathbf{x}^*$ on this way, it is assumed that $\mathbf{x}^*$ is a global solution of the optimization problem, i.e., it provides the lowest value of the objective function for the entire search space. However, there are also local minima whose definition slightly differ from the global ones. Thus, a local minimum in $\mathbf{x}^* \in X$ exists if there are any value $\varepsilon > 0$ such that:

$$J^* = J(\mathbf{x}^*) \leq J(\mathbf{x}) \ \forall \mathbf{x} \in X \ \text{and} \ ||\mathbf{x} - \mathbf{x}^*|| < \varepsilon. \tag{1.13}$$

$$\boldsymbol{h}(\mathbf{x}^*) = \boldsymbol{0}, \tag{1.14}$$

$$\boldsymbol{g}(\mathbf{x}^*) \leq \boldsymbol{0}. \tag{1.15}$$

The definitions showed above have been performed according to minimization problems. Nevertheless, they can be adapted directly to maximization problems since to maximize a determined objective function $J(x)$ is equivalent as to minimize $-J(x)$.

In what follows, different techniques to solve optimization problems are presented. It should be remarked that optimization problems can be classified taken into account different issues, as the problem nature (linear, quadratic or nonlinear problems), the nature of the decision variables (continuous or binary variables or mixed integer problems), or the taxonomy of optimization methods (exact or heuristic methods). In this thesis, the optimization problems are differentiated according to their nature as is how they have been used in the different works of this thesis.

1.5.2 Linear optimization

In these kinds of problems, also known as Linear Programming (LP) problems, both the objective and all the constraints are linear functions. Thus, a linear optimization problem can be formulated as in Eqs. (1.6)-(1.9) but being $J(x)$, $\boldsymbol{h}(x)$ and $\boldsymbol{g}(x)$ linear functions [113].

LP problems cannot be analytically sorted out; however, the resolution of these problems is in an advanced maturity state and there are a variety of effective techniques to solve them. Some of the most employed resolution techniques are the Simplex algorithm [114] or the Interior Point method [115]. These kinds of solvers can handle problems with hundreds of variables and thousands of constraints being able to solve them in a matter of seconds on a normal desktop computer. Nevertheless, it should be noted that is still a challenge to deal with very large LP problems or to solve them with exact real-time requirements [113].

1.5.3 Quadratic optimization

In quadratic optimization or Quadratic Programming (QP) problems the objective function is quadratic wheres the equality or inequality constraints are linear. So the basic difference with the

definition in Eqs. (1.6)-(1.9) is the objective function which is given by:

$$J(x) = \frac{1}{2}x^T H x + c^T x,$$ (1.16)

where $H \in \mathfrak{R}^{nxn}$ is a symmetric matrix and $c \in \mathfrak{R}^n$ a vector, being $\mathfrak{R}^n$ a sequence of n real numbers. Note that the nomenclature x^T indicates the transpose of variable x.

It should be noted that QP problems have a particularity for the case without constraints since they can be solved analytically as the quadratic function can be transformed is a set of linear functions. Conversely, if the problem has constraints, the difficulty in working out a QP problem has great dependence of the nature of matrix H. On the one hand, in convex QP problems, which are relatively easy to handle, matrix H is positive semidefinite. On the other hand, if H has negative eigenvalues (non-convex QP problems) the objective function can have more than a local minimum [113]. Some of the solvers for these kinds of optimization problems can be found in [116, 117]. Note that most MPC controllers lead to these QP problems [8].

1.5.4 Nonlinear optimization

Although the optimization problems concerning the vast majority of the processes can be formulated simply, i.e., as LP or QP problems, in many applications the objective function or some of the constraints are described by nonlinear functions. These optimization problems are known as Nonlinear Programming (NLP) problems, and they can be posed also as in Eqs. (1.6)-(1.9) but being $J(x)$ or $\boldsymbol{h}(x)$ and $\boldsymbol{g}(x)$ nonlinear functions [118]. In these problems, the behaviour is much different from LP or QP problems as they normally have a set of local minima and a global minimum that can be located in an interior point, on the boundary, or at an extreme point of the search space. Consequently, most of the solvers used in LP or QP problems, which perform derivative-based searches to locate extreme points, may not determine an optimal solution in NLP problems and therefore, other kind of solvers must be employed. Below the two resolution techniques used in this thesis are introduced.

Genetic algorithms

These kinds of solvers are classified as heuristic optimization methods, which are techniques specially designed to explore the entire search space, and with some specific characteristic to escape from local solutions. Particularly, Genetic Algorithms (GA) are population-based methods that work with a set of related candidate solutions, which compete with each other mimicking the processes perceived from biological and natural evolution.

Algorithm 1: Basic GA.

1. Initialize a population of candidate solutions.
2. Evaluate of each candidate solution (or chromosome).
3. Create new candidate solution by using the genetic operators.
4. Evaluate new candidate solutions.
5. Delete some candidate solutions from the augmented population (based on their fitness value) to maintain the size of the population.
6. Evaluate the stopping criteria, if it is met, stop; otherwise, return to step 3.

In general, natural processes can be ordered and structured forming a step-by-step algorithm, which is the basis of GA. In this way, GA is based on the use of a population of chromosomes

(set of candidate solutions) that are created at each generation, i.e., each iteration of the algorithm, through several operations and transformations making by genetic operators. Each candidate solution has an associated fitness value, for example, the objective function value, so that those with better value have more opportunities to survive from one generation to another. The main steps in a basic GA are depicted in Algorithm 1. Note that a more complete description of GA can be found elsewhere [119].

Generalized Benders decomposition

In this thesis project, apart from continuous variables, some of the models include binary ones, leading to Mixed-Integer Nonlinear Programming (MINLP) optimization problems. In these problems, the nonlinear nature can be imposed by: i) nonlinear terms in the integer variables domain, ii) nonlinear terms in the continuous variables domain, and iii) nonlinearities in the joint domain of integer and continuous variables. An MINLP problem can be formulated as:

$$\min_{x,\phi} J(x,\phi). \tag{1.17}$$

$$\text{s. t. } \boldsymbol{h}(x,\phi) = \boldsymbol{0}, \tag{1.18}$$

$$\boldsymbol{g}(x,\phi) \leq \boldsymbol{0}, \tag{1.19}$$

$$x \in X \subseteq \mathfrak{R}^{n_x}, \tag{1.20}$$

$$\phi \in \Phi^{n_y} = \{0,1\}, \tag{1.21}$$

where $\phi \in \Phi^{n_y} = \{0,1\}$ represents binary variables, being Φ^{n_y} the vector space delimiting the ϕ-variables domain. The resolution of an MINLP problem in the form presented in Eqs. 1.17-1.21 has two main types of difficulties to consider. Firstly, as the number of integer variables increases in the problem, a larger and more complex combinatorial problem must be addressed. Secondly, the existence of multiple local solutions due to the non-convex nature of nonlinear problems. Despite these facts, efficient methods for solving these types of problems have been developed in the literature ensuring global or quasi-global convergence to optimal solutions [118]. One of the most used is known as Generalized Benders Decomposition (GBD), and it is based on the use of Lagrange functions and multipliers and duality theory [120].

The basic idea of the GBD technique consists of solving the overall MINLP problem iteratively, calculating in each iteration an upper and lower band in the solution space of the MINLP problem. These bands are obtained by decomposing the MINLP problem into two subproblems: the *master* problem that provides the lower band, and the *primal* problem, which provides the upper one. Thus, the *primal* problem corresponds to the problem defined in Eqs. 1.17-1.21 with the ϕ-variables fixed in a determined solution 0-1, denoted by ϕ^l being l the iteration counter:

$$\min_{x,\phi} J(x,\phi^l). \tag{1.22}$$

$$\text{s.t. } \boldsymbol{h}(x,\phi^l) = \boldsymbol{0}, \tag{1.23}$$

$$\boldsymbol{g}(x,\phi^l) \leq \boldsymbol{0}, \tag{1.24}$$

$$x \in X \subseteq \mathfrak{R}^{n_x}. \tag{1.25}$$

(R) Note that the solution of this *primal* problem is the global solution for problem (1.17)-(1.21).

By finding the solution to the problem above, two different situations can be distinguished: feasible *primal* and infeasible *primal*. On the one hand, the feasible *primal* occurs when the

solution of the *primal* problem is feasible at iteration l. If so, the resolution of the problem provides information of: i) the value of x^l, ii) the value of the upper bound, which is the value of $J(x^l, \phi^l)$, and iii) the value of the optimal Lagrange multipliers vectors λ^l and μ^l related to the set of equality ($\boldsymbol{h}$) and inequality ($\boldsymbol{g}$) constraints respectively. This information can be used to formulate the following Lagrange function, which is called the *optimallity cut*:

$$L^l(x, \phi, \lambda^l, \mu^l) = J(x, \phi) + {\lambda^l}^T \boldsymbol{h}(x, \phi) + {\mu^l}^T \boldsymbol{g}(x, \phi). \tag{1.26}$$

On the other hand, if the *primal* problem at iteration l is detected by the solver to be infeasible, only the constraints of the *primal* problem are considered to identify a feasible point, formulating the infeasible *primal* problem as:

$$\min_{x, \upsilon} \ \upsilon \tag{1.27}$$

$$\text{s.t. } \boldsymbol{h}(x, \phi^l) = \boldsymbol{0}, \tag{1.28}$$

$$\boldsymbol{g}(x, \phi^l) \leq \upsilon, \tag{1.29}$$

$$\upsilon \geq \boldsymbol{0}, \tag{1.30}$$

$$x \in X. \tag{1.31}$$

The resolution of this new problem provides information about the Lagrange multipliers related to the equality and inequality constraints, denoted by $\bar{\lambda}^l$ and $\bar{\mu}^l$ respectively. Thus the feasibility cut can be posed as:

$$\bar{L}^l(x, \phi, \bar{\lambda}^l, \bar{\mu}^l) = {\bar{\lambda}^l}^T \boldsymbol{h}(x, \phi) + {\bar{\mu}^l}^T \boldsymbol{g}(x, \phi). \tag{1.32}$$

> **R** Note that at each iteration only one cut is generated, depending if the *primal* problem is feasible or infeasible. Also, the upper bound is generated only if the *primal* problem is feasible.

The duality theory is used to define the *master* problem, which is based on the projection of the overall MINLP problem in the ϕ-space (see [120] for more details):

$$\min_{\phi, \mu_0} \ \mu_0 \tag{1.33}$$

$$\text{s.t. } \mu_0 \geq L^{l^1}(x^{l^1}, \phi, \lambda^{l^1}, \mu^{l^1}) \quad l^1 = 1, \dots, L^1, \tag{1.34}$$

$$0 \geq \bar{L}^{l^2}(x^{l^2}, \phi, \bar{\lambda}^{l^2}, \bar{\mu}^{l^2}) \quad l^2 = 1, \dots, L^2, \tag{1.35}$$

where L^1 and L^2 are the last iteration counters at which the optimallity and feasibility cuts were updated.

> **R** The master problem is equivalent to the MINLP (1.17)-(1.21). Also, the value of the variable μ_0 is the value of the lower bound.

The whole algorithm is solved on an iterative way according to the method presented in Algorithm 2.

Algorithm 2: Basic GBD algorithm.

1. Initialize a feasible solution for the binary variables and solve the *primal* problem.
2. Solve the *master* problem. Stop if the gap between the upper (UB) and the lower bound (LB) is lower than a given tolerance factor (ε), which is, $UB \leq LB + \varepsilon$.
3. Solve the *primal* problem distinguishing among the two cases: feasible *primal* and infeasible *primal*. Return to step 2.

1.6 Research performed

As described, MD is an emerging separation technology in a pre-commercial phase, with great potential to be employed in applications in which other desalination technologies cannot be used. The current development state of the technology requires the creation of proper operating methods to improve the distillate production and thermal efficiency of the MD modules, two of the main drawbacks of the technology till now. Accordingly, this thesis is focused on developing optimal operating strategies for MD based plants, especially for those powered with solar energy in which the operating management is even more difficult due to the intermittent nature of this source. Thus, several modelling, control, and optimization methodologies are used for the development of the aforementioned operating methods.

The following subsections show an introduction to the different works carried out. These works have been divided and developed in various phases according to the ones of a typical control engineering project. In the first development phase, a model of both the heat generation circuit and the MD module of the SMD plant of the PSA was developed. Also, a direct control layer for the heat generation circuit, mainly aimed at flow and temperature regulation, was proposed. In the second phase, hierarchical control strategies were designed to improve the distillate production and thermal efficiency of the SMD plant as well as to improve the time required in its start-up phase. These strategies were based on the models and regulation controllers developed in the first phase. The third development phase was devoted to the design and creation of advanced control and optimization strategies to improve the operation of commercial MD plants that includes multiple MD modules. In this phase, the models and controllers developed for the heat generation circuit in phases 1 and 2 were also used, and the new strategies were focused on the management of the desalination unit which has not been addressed in the preceding phases. The final phase of the thesis was the elaboration of a tutorial that includes all the knowledge acquired throughout the thesis in the field of modelling and control in MD.

1.6.1 Modelling and low-level control of solar membrane distillation plants
Background

The first work done in the Ph.D. thesis was the development of a model and a regulation control layer for the heat generation circuit of an SMD plant. This work was motivated as the previous proposals in literature have not been validated in real systems [69, 121], so that fundamental dynamics for the development of control systems could be ignored. In addition, the low-level controllers proposed for SMD plants, also presented in [69, 121], were based on simple control loops with ON/OFF controllers and focused on maintaining the temperature in specific parts of the heat generation circuit. However, no work presented a complete control architecture to maintain the temperature at the outlet of the heat generation circuit, which is fundamental for the evaluation of MD modules and the development of higher-level control strategies.

Regarding the MD module modelling, most of the proposals are centered on modelling lab-scale MD modules. In addition, they only take into account as model output the distillate production [94, 97], and only a few works consider also metrics related to the thermal efficiency of the module [62, 64], which is essential to predict its behavior. Besides, very few studies consider the salinity of the feed water as an input of the model [102] which is also fundamental to explore some of the applications of MD technology, as the treatment of brines. On balance, the main gap is the lack of models for commercial MD modules considering both the distillate production and the thermal efficiency as outputs and the salinity of the feed solution as input.

Contributions

The contributions performed in this research area addressed the literature gaps mentioned above. Therefore, a complete dynamic model of the heat generation circuit of an SMD plant was developed and validated in the facility of the PSA. Based on this model, a feedback control architecture was designed and experimentally tested. This control structure was composed of four regulatory control loops and a reference governor that enables to fix suitable operating temperatures in the heat generation circuit to maintain the desired temperature conditions at the entrance of the MD module. This work was successfully published in the journal in [74] (see Section 2.1.1) as an extension of the works in [122–124].

The development and implementation of the controller mentioned in the previous paragraph allowed us to perform an experimental campaign in the SMD plant of the PSA to model a commercial PGMD module. The experimental data obtained were used to develop both an RSM and an ANN model. Unlike most modelling approaches presented in the literature, the distillate production and the thermal energy consumption were considered as predicted performance parameters. In addition, apart from the typical independent variables used in these kinds of models, the salinity of the feed solution was included in a range of 35-140 g/L. This work was published in the journal in [5] (see Section 2.1.2).

1.6.2 Hierarchical controllers for the optimal operation of solar membrane distillation plants

Background

After finishing the previous research tasks, the project was aimed at developing hierarchical controllers for SMD plants. This second development phase is the natural evolution of control engineering projects as first, a regulatory layer is required to perform low-level control tasks, and then, a hierarchical controller can be formulated in which the bottom layer is formed by the regulation controllers and the upper layer by advanced control strategies in charge of carrying out high-level control tasks. In the case of SMD plants, these tasks are aimed at improving both the distillate production and thermal efficiency of the MD module as well as at reducing the operating costs.

Until then, the works focused on improving the metrics mentioned above proposed optimization methods providing static operating points [98, 125]. However, in SMD plants these conditions are difficult to maintain, as they require discontinuous operations and the proper use of specific buffering systems to deal with the unpredictable nature of solar energy. Consequently, real-time operating procedures are more suitable for the management of these plants. From this point of view, the first works published were the approaches presented in [69, 121]. However, as mentioned above, the control methods proposed in those works were based on regulation controllers following static references. A more complete approach was presented in [63], in

which a neural network-based feedforward optimal control system was developed and tested in a real SMD plant. Nevertheless, the objective of this control architecture was to enhance the distillate production without considering other fundamental performance parameters in MD as the thermal energy efficiency. This is the main research gap observed, the lack of real-time procedures to improve both metrics and to reduce the operating costs of the facility.

Moreover, another gap observed was the lack of methodologies for the start-up procedure of these plants. The works referenced above propose control methods for the operation phase, however, another fundamental stage in these facilities is the start-up phase, which was not taken into account on those works. The MD modules cannot be operated at low temperature (i.e., below 60 °C) since they produce very low distillate losing economic profitability. Thus, a nominal operating point must be reached in the heat generation circuit before turning on the MD module. This is not a particular problem of MD processes as most industrial processes powered with solar thermal energy require a nominal operating point to start the operation. To correctly visualize the problem, the reader should take into account that these plants normally include thermal storage devices to improve the dispatchability of solar thermal fields. In this way, if the storage device is unloaded in terms of energy or widely stratified, the transitory regime can take a long time until reaching the operating point. Despite being a common problem, only the work in [126] proposed a methodology to optimally perform this phase. However, the method was based on an off-line dynamical-optimization strategy, in which it was assumed that there were no model uncertainties or process disturbances, which is an ideal situation that does not occur in real operations, particularly if the disturbances are mainly caused by solar irradiance.

Contributions

The research carried out in this area encompasses the two main literature gaps observed. Thus, the first research goal was tasked with the development of a real-time hierarchical control architecture that could be configured with different objective functions allowing to optimize both the distillate production and the thermal efficiency of the MD module and the operating costs of the whole facility. This hierarchical controller was composed of two layers, the bottom layer was based on the controllers presented in [74]. The upper layer was formed by an MPC technique in charge of generating the references for the controllers of the bottom layer by optimizing the aforesaid objectives. Besides, two control modes were proposed for the efficient operation of the SMD plant, as well as a start-stop procedure for the solar field and the MD module. The proposed approach was tested both in simulation and in the SMD pilot plant of the PSA. As a result of this work, several contributions were presented in the conferences in [127, 128] and a journal article was published [4] (see Section 2.2.1).

The second work focused on improving the start-up phase of SMD plants and solar thermal facilities with single-tank storage configuration in general. This work was developed in the framework of a research stay that the Ph.D. candidate made in the Federal University of Santa Catarina (Florianopolis, Brazil). The contributions performed in this area were twofold. First, the use of the mixing valve, see valve 1 in Fig. 1.12, as a control variable. Normally, this valve is used in fixed positions (i.e., opened or closed) and only the water flow rate is used as manipulated variable, which is effective for irradiance disturbances but not when temperature stratification problems appear during the start-up phase due to its physical limits. Second, the development of a real-time procedure for the start-up phase of solar field plants with direct single-tank storage configuration. This procedure was based also in a hierarchical controller composed of two layers.

On the one hand, the bottom layer is composed by one of the direct controllers presented in [74], which is in charge of controlling the outlet solar field temperature by acting on the water flow rate, and a new control loop developed specifically for this work, which is tasked with controlling the inlet solar field temperature by acting on the aperture of the mixing valve. On the other hand, the upper layer included an MPC strategy considering the operating conditions at each sampling time for computing the setpoints for the bottom layer, trying to maximize the temperature in the storage device as fast as possible. The operating strategy was also tested in the pilot SMD plant of the PSA and the results were published in the journal paper in [9] (see Section 2.2.2) as an extension of the conference works in [129, 130]. Besides, a similar control structure but attending also to economic criteria was developed and presented in the conference in [131].
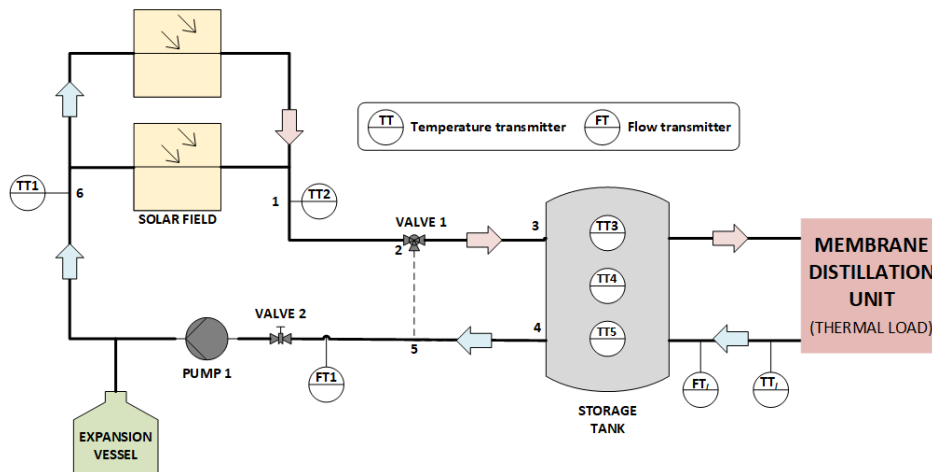
Figure 1.12: Schematic plant diagram obtained from [9].

1.6.3 Control and optimization strategies for membrane distillation industrial applications

Background

In the two previous development phases of the thesis project, as well as in most of the works published in the literature, the proposals were aimed at improving the operation of the solar field, trying to maintain desired temperature operating points at the entrance of the MD module to optimize determined performance metrics. However, not only the temperature affects the performance of MD modules, but also the feed water flow rate [62]. The optimal management of this variable is fundamental as a tradeoff solution must be adopted to maximize both distillate production and thermal efficiency in most of the current commercial-scale MD modules available nowadays [132]. Moreover, the proposed operating strategies were applied to SMD plants including a single MD module and without taking into account a given water demand [4, 63, 121]. This is especially significant since, when designing an SMD plant at industrial scale, it must include multiple MD modules. The reason is that a single commercial MD module produces a relatively low amount of distillate. Note that current commercial MD modules can produce up to 60 L/h in optimal operating conditions [42]. This fact completely alters the control problem, requiring new operating procedures to be posed.

In summary, there is a lack of research works that addressed: i) the optimal real-time management of the feed flow rate of MD modules according to a given water demand and operating conditions, and ii) the management of the multiple MD modules composing an industrial-scale plant.

Contributions

The contributions performed in this field were focused on the management of the desalination unit of an industrial scale SMD plant. With this aim, a case study was adopted combining an SMD plant and a greenhouse. This case study was selected since, to power off-grid greenhouses, is one of the potential application of thermal powered desalination processes [133, 134]. In addition, in the case study the solar field powering the desalination unit was operated with the strategy developed in the previous work [4],

Thus, the first research work was devoted to develop a Distributed MPC (DMPC) strategy in charge of computing the feed flow rates for each of the MD modules included in the SMD plant. The objective of the management technique was to reduce the specific thermal energy consumption of the set of MD modules while ensuring the supply of water for irrigation purposes. The main advantage of the proposed technique was that each of the MD modules included in the desalination unit was considered as an agent of the decentralized controller following the ideas presented in [135]; so, each agent solved a simple MPC problem with the objective mentioned above, only exchanging information with neighboring agents. This fact allowed the controller to considerable reduce the computing time in comparison to centralized approaches, enabling to compute optimal solutions within the required sampling time when considering industrial-scale SMD facilities. The work was published in the journal in [7] (see Section 2.3.1) as extension of the conference contribution in [136]. Also, a preliminary version including the results of the centralized approach was published as a technical report in [137].

In the formulation of the DMPC control system, only continuous variables for the feed water flow rate (within its operating range 400-600 L/h) were considered. In the second work carried out, elaborated also during the research stay of the Ph.D. candidate at the Federal University of Santa Catarina, integer variables were introduced in the problem to manage, apart from the feed flow rate, the number of MD modules turned on at each sampling time according to water needs and operating conditions. The contributions performed were: firstly, the RSM models were adapted to the Mixed Integer Programming (MIP) methodology, in which the binary variables were related to valve apertures that enabled to turn ON/OFF the MD units included in the plant. Based on the MIP model, an MINLP optimization problem was formulated aimed at reducing both the specific thermal energy consumption and the total thermal energy consumption, while assuring the water requirements. Secondly, an efficient algorithm based on the GBD method was developed to solve the MINLP problem. This algorithm allowed us to use simpler optimization solvers (i.e., QP solvers) rather than MINLP for solving the overall problem. This algorithm was then included in an MPC controller to reflect the operational strategy. The work was published in the journal in [138] (see Section 2.3.2). Also, a preliminary version showing the results obtained with the MINLP problem was presented in the conference in [139], and a similar approach but also adding in the problem the possibility of taking water from the public utility network was presented in [140].

1.6.4 Tutorial on modelling and control of membrane distillation technology

Background

Ph.D. thesis projects usually start with a review of the state-of-art of the research field at hand. This step is the basis to identify the research gaps and motivate the thesis framework. In the case of the present project, this review was also performed however, many few works on automatic control in MD were found; basically only the ones in [63, 69, 121]. The main reason behind this is that the application of control techniques is a new research area in the MD field, and almost all

the previous works were aimed at module design or evaluation purposes as mentioned above. This way, the works proposed in the framework of this thesis focus from the outset on developing contributions from the point of view of automatic control, trying to demonstrate how these techniques could be essential for the industrial development of the technology. Nevertheless, along with the project development, the interest in the application of control techniques to MD processes grew up, and other research groups began presenting new proposals [72, 73].

Contributions

Motivated by the emergence of new automatic control approaches and considering the lessons learned throughout the development of the thesis, the last step of the Ph.D. project was to develop a tutorial on modelling and control techniques applied to MD processes. In this work, all the proposals made so far on this topic were revised identifying the different techniques applied and the improvement reached. The objective was to evidence the technological development achieved through the application of these techniques as well as to establish the lines to follow in future works. The work was published in the journal in [141] (see Section 2.4.1) and a preliminary version was published in the conference in [142].

2. Contributions to scientific journals

This Ph.D. thesis is presented as a compendium of publications according to modality A of the normative of the University of Almería (article 24). This normative establishes that any Ph.D. thesis can be presented in the compendium modality as long as it is supported by at least three scientific contributions. Two of them must be included in category A of the rating scale contained in the Research and Transfer Plan from the University of Almería approved in the corresponding year. The third contribution, different from the previous ones and that does not consist of a contribution to a congress, must be included in category B of the rating scale mentioned above. In this rating scale, category A is referred to the journals ranked in the highest position of their subject category, i.e., Q1 in the Journal Citation Report (JCR), and category B to those journals ranked in the second-highest place, i.e., Q2 or Q3 in the JCR.

This thesis project is supported by 7 scientific articles in journals ranked in the JCR, which are classified as shown below:

- **Q1 papers:** 4.
- **Q2 papers:** 2.
- **Q3 papers:** 1.

The articles above have been included in this chapter according to the aforementioned normative. Moreover, they have been ordered as described in Section 1.6. Particularly, Section 2.1 contains the works dealing with the modelling and low-level control of SMD plants. More precisely, Section 2.1.1 includes a work encompassing the modelling of the heat generation circuit and the design of the low-level control structure used for regulating it. Section 2.1.2 contains a work presenting the model of an MD module together with an optimization method for finding its optimal operating conditions.

Then, Section 2.2 shows the works presenting hierarchical control structures for SMD plants. Section 2.2.1 contains a paper presenting the detailed design of a hierarchical controller for the optimal operation of an SMD plant, whereas Section 2.2.2 includes a paper also presenting a

hierarchical controller but in this case for the start-up phase of an SMD plant.

After that, Section 2.3 is devoted to the works proposing control structures for MD plants at an industrial scale. Namely, Section 2.3.1 shows the design of a distributed controller for these kinds of plants. Section 2.3.2 contains the work proposing the MINLP problem for the optimal management of these plants and the design of an efficient algorithm to solve it. Finally, Section 2.4.1 presents the tutorial on modelling and control methodologies for MD plants.

The reader must take into consideration that each of the papers contains its specific bibliography, which is not related to the main bibliography section of the present document. In addition, it should be remarked that apart from the journal papers, the research work developed during the Ph.D. project resulted in the following contributions:

- **Contributions to a general outreach magazine:** 1.
- **Contributions to international conferences:** 6.
- **Contributions to national conferences:** 6.

Each of the aforementioned contributions has been referred to in the corresponding section among the ones described above. Besides, the Ph.D. candidate made two research stays, one at the Federal University of Santa Catarina (Florianopólis, Brazil) and another one in the research center Plataforma Solar de Almería (Almería, Spain).

Aside from the outcomes included in this chapter, the Ph.D. candidate has participated in different contributions directly derived from the activity carried out during the thesis project. However, these publications have been included in Chapter 4 according to the normative of the University of Almería.

2.1 Modelling and low-level control of solar membrane distillation plants

2.1.1 A feedback control system with reference governor for a solar membrane distillation pilot facility

Research in this field is supported by the following journal publication:

Title	A feedback control system with reference governor for a solar membrane distillation pilot facility
Authors	**J. D. Gil**, L. Roca, G. Zaragoza, M. Berenguel
Journal	Renewable Energy
Year	2018
Volume	120
Pages	536-549
DOI	`https://doi.org/10.1016/j.renene.2017.12.107`
IF (JCR 2018)	5.439
Categories	Energy & Fuels (17/103) **Q1**
	Green & Sustainable Science & Technology (7/35) Q1

Contribution of the Ph.D. candidate

The Ph.D. candidate, J. D. Gil, is the main contributor and first author of this paper.

Aside to this publication, it gave rise to the following international conference paper:

- **J. D. Gil**, A. Ruiz-Aguirre, L. Roca, G. Zaragoza, and M. Berenguel, "Solar membrane distillation: A control perspective," in *23th Mediterranean Conference on Control and Automation (MED 2015).* Torremolinos, Spain, 2015, pp. 796–802.

Also, the following contributions to a national conference were presented, which were awarded for the best work in the section of Control Engineering:

- **J. D. Gil**, A. Ruiz-Aguirre, L. Roca, G. Zaragoza, M. Berenguel, and J. L. Guzmán, "Control de plantas de destilación por membranas con apoyo de energía solar–parte 1: Esquemas," in *XXXVI Jornadas de Automática*. Bilbao, España, 2015.
- **J. D. Gil**, A. Ruiz-Aguirre, L. Roca, G. Zaragoza, M. Berenguel, and J. L. Guzmán, "Control de plantas de destilación por membranas con apoyo de energía solar–parte2: Resultados," in *XXXVI Jornadas de Automática*. Bilbao, España, 2015.
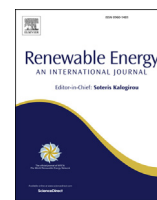
A feedback control system with reference governor for a solar membrane distillation pilot facility

Juan D. Gil [a], Lidia Roca [b], Guillermo Zaragoza [b], Manuel Berenguel [a, *]

[a] Centro Mixto CIESOL, ceiA3, Universidad de Almería, Departamento de Informática, Ctra, Sacramento s/n, Almería 04120, Spain
[b] Centro Mixto CIESOL, CIEMAT-Plataforma Solar de Almería, Ctra, de Senés km. 4,5 Tabernas 04200, Almería 04120, Spain

A B S T R A C T

This work presents the development of a feedback control system for a pilot membrane distillation facility powered with solar energy located at Plataforma Solar de Almería (PSA), Spain. The control system allows to fix a suitable operating temperature at the inlet of the distillation system, improving the operation quality. Four direct control schemes based on Proportional Integral (PI) controllers and Feedforward (FF) are designed as well as a reference governor which generates temperature references for the heat generation circuit direct control layer. Simulations and experimental tests are shown to demonstrate the effectiveness of the proposed scheme.

© 2018 Elsevier Ltd. All rights reserved.

1. Introduction and literature review

Nowadays, water scarcity is one of the main challenges of the World. The demand of fresh water for human use, agriculture and industrial purposes is increasing steadily, reducing the water reservoirs. Consequently, desalination technologies have become a necessity, specially in dry areas with water shortage. Due to the large amount of energy required, desalination technologies must be associated with renewable energy sources for their economical sustainability [1,2]. Using renewable energy for desalination not only sorts out the water problem but also replaces traditional sources like fossil fuels, thus contributing to efficient environment development [3]. Due to the high solar irradiance available in places with lack of water, solar energy is the most suitable renewable source for desalination processes.

In this context, Solar Membrane Distillation (SMD) is an appropriate technology for developing small-scale desalination systems in remote areas with good solar irradiance conditions [4,5]. This technology stands out for its independent features such as easy automation and low thermal energy requirements. It should be noted that SMD has not been yet commercialized due to some technical design

problems and uncertainties associated with economic and energetic costs [6]. Therefore, different kinds of modules and Membrane Distillation (MD) configurations have been evaluated in the recent years in terms of thermal efficiency and distillate production [7,8]. The experimental campaigns carried out in these studies require steady state conditions in the main process variables in spite of changes in the energy source (solar radiation), thus demanding adequate control systems to achieve desired performance [9].

There are a few works in the literature related with control and modeling of SMD processes. In Ref. [10], a review of theoretical models was carried out with a description of the main variables involved in the MD process. A mathematical model was developed in Ref. [11], in order to simulate the daily production of a solar vacuum membrane distillation unit. In Ref. [12] steady-state simulations, using a wide range of operating conditions, were carried out for a direct contact membrane distillation system. A double loop optimization problem was expressed in MATLAB to solve the nonlinear equations.

From an automatic control point of view, the first work published [13], implemented and tested two temperature control loops using PI controllers in a model of a SMD system. Refs. [14,15] also proposed a dynamic mathematical model of a SMD facility to test a control system based on PI and on/off controllers aimed at temperature regulation. A very interesting control approach was presented in Ref. [16], where a control strategy based on a neural network optimization for a SMD unit was developed and experimentally tested.

(a) SMD facility. (b) Aquastill pilot module.

Fig. 1. SMD facility at PSA.
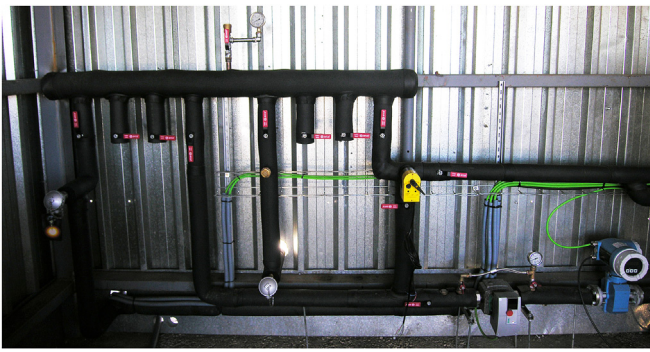
Fig. 2. Distribution system.

The neural network model of the system was employed to identify a range for the feed flow rate, in which optimal operating conditions can be obtained. A control system was implemented to maximize distillate production under variable operating conditions. Besides, a feedforward (FF) controller was used in order to reject irradiance disturbances according to the ideas of [17–21]. The first work which deals with a reference governor for this kind of facilities is [22], where a feedback control system and a reference governor were developed for keeping a desired difference temperature between both sides of the membrane.

In this work a complete feedback control architecture is proposed for an experimental solar powered membrane distillation facility. The use of the developed control scheme which improves the operability and dispatchability of this solar distillation technology could mean a relevant advance for commercial purposes. Thus, a full development of preliminary designs presented in Ref. [9] has been carried out and tested under real operating conditions. The proposed control strategy is complemented with a reference governor which allows us to fix suitable operating temperatures in the heat generation circuit to maintain the desired temperature conditions at the entrance of the membrane module. Additional objectives have been the reduction of both operating costs and non-renewable energy usage by optimizing the solar energy use. Dynamic models of the main variables involved in the process are presented as well as the control system design. Simulation and experimental tests of the control system are also included to evaluate its performance.

2. SMD system

2.1. MD technology

MD is a thermally driven process in which a hydrophobic microporous membrane is used to accomplish the separation of volatile and non-volatile molecules. As result of the difference vapour pressure at the two membrane sides, achieved by a difference in temperature, volatile molecules are evaporated and pass through the membrane, whereas non-volatile components are rejected. The evaporation process allows this technology to treat solutions with high salt concentration rejecting almost all the non-volatile components to produce high quality distillate. MD systems can be classified in several configuration according to the vapour pressure difference across the membrane [23], being Air-Gap Membrane Distillation (AGMD), the one used in this paper, one of the most employed.

2.2. Test-bed facility

The test bed facility (see Fig. 1 (a)) used in this work is located at PSA and it comprises a MD module powered by heat generation circuit that includes a solar field, an air cooler, a storage tank, a distribution system (see Fig. 2) and a heat exchanger [4].

The solar field providing the required thermal energy to the distillation process consists on stationary flat-plate collectors of $2 \, m^2$ (Solaris CP1 Nova by Solaris, Spain) divided into two rows of five collectors each one. The solar field has a nominal thermal power of $7 \, kW$ at about $90 \, °C$, using water with antifreeze as heat transfer medium. An air cooler is located at the outlet of the solar field to avoid temperature excesses at the inlet of the membrane module. The solar field is connected to a thermal storage tank ($1500 \, L$) which can be used as energy buffer in order to work near steady state conditions when needed. As it was presented in Ref. [9], due to the hybrid nature of the facility it can be operated in 14 modes. Nevertheless, only the direct connection (see Fig. 3) between the MD module and the solar field is considered in this work. From a control point of view, direct connection is the most difficult mode since the damping system (storage tank) is not used and transients are spread throughout the plant. Notice that the control algorithms developed in this paper try to be useful for future development of a control algorithm able to cope with all operating modes (following the same approach in Ref. [24] for other kind of installation).

Several MD modules can be coupled to the facility by means of the distribution system (see Fig. 2), including a Liquid Gap Membrane Distillation (LGMD) configuration (built by Solar Spring), a Vacuum Membrane Distillation (VMD) module (built by Aquaver) and two AGMD configurations (built by Aquastill) [4]. Each module is connected to the distribution system by means of its own heat exchanger which is used for heating cold sea water with the circulation fluid coming from the heat generation circuit. One of these Aquastill AGMD modules (see Fig. 1(b)) is used in this work. Its heat exchanger has $1.65 \, m^2$ of exchange surface. The module has an
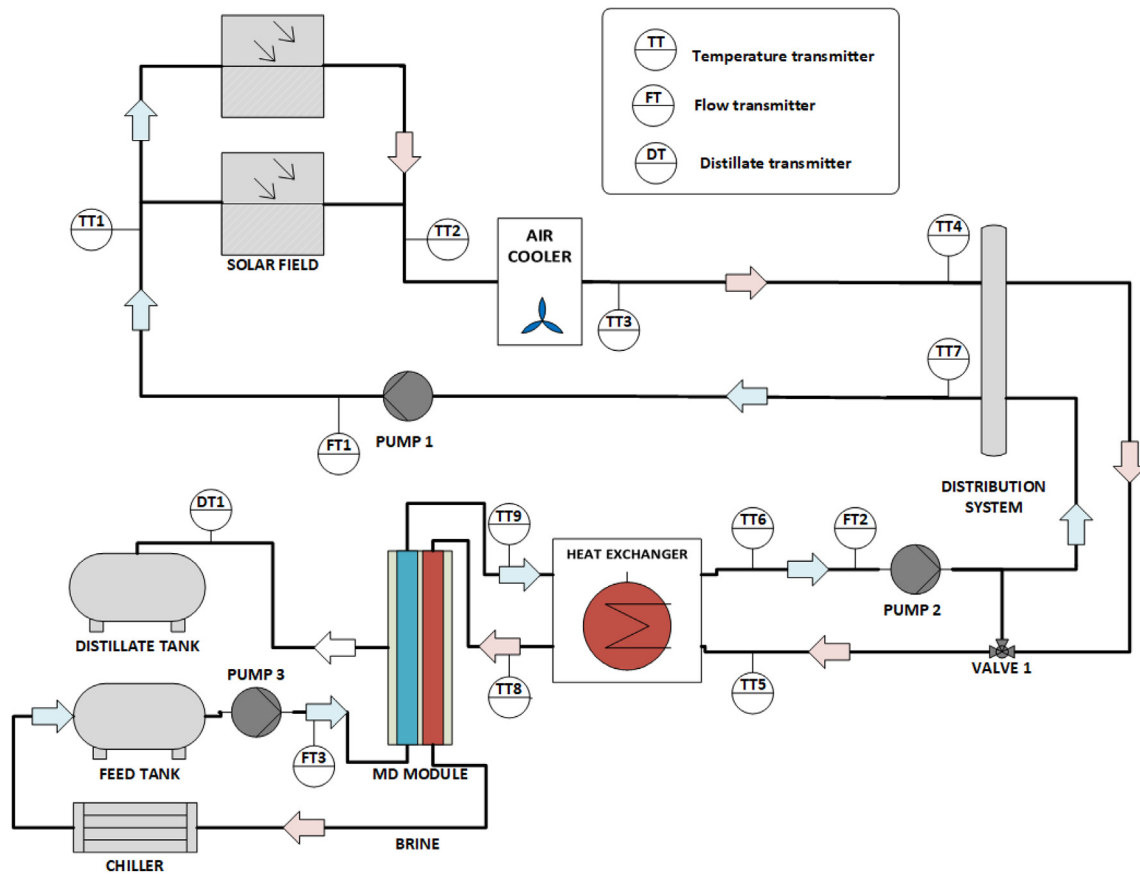
Fig. 3. Schematic diagram of the active components in direct connection mode.

Table 1
Measurement instruments.

Variable	Manufacturer	Model
Flow rate	Endress & Hauser	50P15
Pressure	WIKA	S10
Temperature	–	PT100
Global irradiance	Kipp & Zonen	CM6B

effective area of 24 m² with a length of 5 m, a nominal pore size of 0.3 μm, porosity of 85% and membrane thickness of 76 μm. A productivity analysis of this module was presented by Ref. [25].

The feed tank (2 m³) contains an aqueous solution with a salt concentration of 35 g/L. A compressor chiller is used to keep the feed temperature constant (it is used in this pilot plant to reproduce different seawater temperatures). The temperature inside the module is limited at about 84 °C due to the thermal resistance of the membranes, whereas temperatures lower than 60 °C produce very low distillate. The feed flow rate to the module, FT3, varies from 400 L/h to 600 L/h.

The facility is fully monitored using the instruments detailed in Table 1. Besides, all the system is controlled by means of a Supervisory Control And Data Acquisition (SCADA) which monitors all the variables with a sample time of 1 s through an advanced data acquisition system (National Instruments).

3. System modeling

To develop the control system, a dynamic model of the heat generation circuit in direct connection mode (see Fig. 3) has been

developed, comprising the solar field, air cooler, distribution system, pump 1, pump 2, valve 1 and heat exchanger. Some of these models are based on first principles and some others have been developed from experimental data. A detailed description can be found in the following subsections. The variables and subscripts involved are included in Appendix A.

3.1. Models based on first principles

3.1.1. Solar field model

Following the ideas presented in Ref. [20], a simplified lumped-parameters dynamical equation, based on an energy balance, is used to model the solar field outlet temperature, TT2. This model is developed by considering an equivalent absorber tube, characterized by an equivalent length L_{eq} and an equivalent mass flow rate $\dot{m}_{eq}$, with the same behaviour as the whole solar field. Besides, this model depends on irradiance, I, ambient temperature, T_a and inlet solar field temperature, TT1. The energy balance equation is given by:

$$A_{sf} \cdot \rho \cdot c_p \cdot \frac{\partial TT2(t)}{\partial t} = \beta \cdot I(t) - \frac{H}{L_{eq}} \cdot (\overline{T}(t) - T_a(t))$$
$$- c_p \cdot \dot{m}_{eq} \cdot \frac{TT2(t) - TT1(t)}{L_{eq}}, \quad (1)$$

where:

$$L_{eq} = L_a \cdot n_{cs}, \quad (2)$$

$$\dot{m}_{eq} = \frac{FT1 \cdot \rho}{c_f}, \tag{3}$$

$$\overline{T}(t) = \frac{TT1(t) + TT2(t)}{2}. \tag{4}$$

In this equation β represents the collector efficiency as well as an attenuating factor, whereas H represents the global thermal losses coefficient. Both parameters were calibrated by using real tests with different weather conditions, providing a model which represents the solar field dynamics. The calibration method is presented in Section 3.1.4. Notice that the thermal mass capacity of the solar field material has not been finally considered in Eq. (1) as its effect in the obtained mean quadratic error is almost negligible, while introducing an additional differential equation following the approach in Ref. [26]. So, the model in Eq. (1) represents a good tradeoff between performance and complexity.

3.1.2. Heat exchanger model

The counter-current heat exchanger available at the facility has been modeled using a simple first principles steady state model already tested in other solar systems [27], providing the performance around the selected operating point. Therefore, supposing that there is no phase change and fluid 1 (FT2 in Fig. 3) transfers energy to fluid 2 (FT3 in Fig. 3) without considering heat losses, the outlet temperature in both sides, knowing the inputs, is given by:

$$TT6_m = TT5 - \eta_{he,1} \cdot (TT5 - TT9), \tag{5}$$

$$TT8_m = TT9 + \eta_{he,2} \cdot (TT5 - TT6_m), \tag{6}$$

where:

$$\eta_{he,1} = \frac{1 - e^{\theta_{he}}}{1 - \frac{\dot{m}_1 \cdot c_{p,1}}{\dot{m}_2 \cdot c_{p,2}} e^{\theta_{he}}}, \tag{7}$$

$$\eta_{he,2} = \frac{\dot{m}_1 \cdot c_{p,1}}{\dot{m}_2 \cdot c_{p,2}}, \tag{8}$$

$$\theta_{he} = \alpha_{he} \cdot A_{he} \cdot \left(\frac{1}{\dot{m}_1 \cdot c_{p,1}} - \frac{1}{\dot{m}_2 \cdot c_{p,2}} \right). \tag{9}$$

Three temperature ranges are used inside the module (TT8): 60, 70 and 80 °C, using three flow rates (FT3) in each range: 400, 500 and 600 L/h. Hence, the parameter α_{he} has been calibrated to these operating points and interpolated by polynomial approaches. This model has been also calibrated following the calibration method presented in section 3.1.4.

3.1.3. Distribution system and three-way mixing valve

The distribution system and the mix produced in valve 1 can be modeled by means of static energy balances. Taking into account that the fluid is the same throughout the circuit and that FT1 must be higher than FT2, the equations are:

$$TT5 \cdot FT2 = TT4 \cdot \gamma \cdot FT2 + TT6 \cdot (1 - \gamma) \cdot FT2, \tag{10}$$

$$TT7 = \frac{TT4 \cdot (FT1 - \gamma \cdot FT2) + TT6 \cdot \gamma \cdot FT2}{FT1}, \tag{11}$$

where γ is the aperture of valve 1. Notice that the nonlinear static characteristic curve of the valve relating the position of the valve stem with the fraction of the mass flow γ has been modeled by a

piecewise linear approximation and thus the inverse of this approximation has been used to linearize its behaviour as done in Ref. [28]. Moreover, a low pass filter has been added to the output of equations (10) and (11) with a time constant of 5 and 7 s respectively to fit the simulation curves to the observed step-response tests.

3.1.4. Model calibration and validation

Both solar field and heat exchanger models are classified as gray box models since there is a first-principles based model structure and some unknown parameters. Calibration of the model by identifying these unknown parameters has been done using the Mean Squared Error (MSE) as objective function (using as error the difference between the outputs calculated by the model and the real measurements):

$$MSE = \frac{1}{N} \sum_{k=1}^{N} \left(\widehat{Y}(k) - Y(k) \right)^2, \tag{12}$$

where $\widehat{Y}(k)$ is the value calculated by the model in the discrete time instant k and $Y(k)$ is the real measurements at the same instant. N is the number of measurements used for calibration purposes.

For the solar field model, that is linear in the parameters, the typical least-squares identification method has been used. In the nonlinear case (heat exchanger model), a combination of global and local optimization algorithms has been applied. Genetic Algorithm (GA) has been chosen as global search due to its random nature, and an interior point method as local search algorithm.

The values obtained for solar field model parameters, β and H, are 0.11 m and 5.88 J/s·K respectively. In this case, 15 days with different environmental conditions have been used for calibration purposes, whereas 5 days have been considered for validation. Fig. 4 shows a solar field model illustrative validation tests. The mean error is 1.05 °C, while the maximum error is 2.85 °C.

In the same way, the heat exchanger model has been calibrated using the nonlinear calibration method. The value of the parameter α_{he} is presented in Table 2 and a representative validation result in Fig. 5. For this model, 5 days with variable operation conditions have been considered for calibration and 2 for validation.

A first order filter and a time delay have been added to this static model to fit real step response data. The representative time constant is 40 s and the time delay is 23 s for TT6_m while the time constant is 20 s and the time delay is 15 s for TT8_m. In this case, the mean error is 0.445 °C, being the maximum error 0.895 °C for TT6 whereas the mean error for TT8 is 0.36 °C and the maximum error is 0.82 °C. If the heat transfer coefficient is considered constant ($\alpha_{he} = 670.78$ W/m^2 K) in the full operating range, the mean error for TT6 would be 0.69 °C, being the maximum error 1.15 °C whereas the mean error for TT8 would be 0.51 °C and the maximum error 1.06 °C.

3.2. Models based on experimental data

In addition to the model based on first principles, transfer functions experimentally obtained have been considered to model the relation between the main variables involved in the process to the controlled variables. Open-loop tests have been performed, introducing typical step changes and making use of the State-Variable Filters (SVF) approach and the Generalized Poisson Moment Functions (GPMF) approach [29], to estimate the parameters of the corresponding first order plus dead time (FOPDT) transfer functions. The metric function used to evaluate the percentage of the response reproduced by the model is the Normalized Root Mean Square Error (NRMSE, see MSE definition):
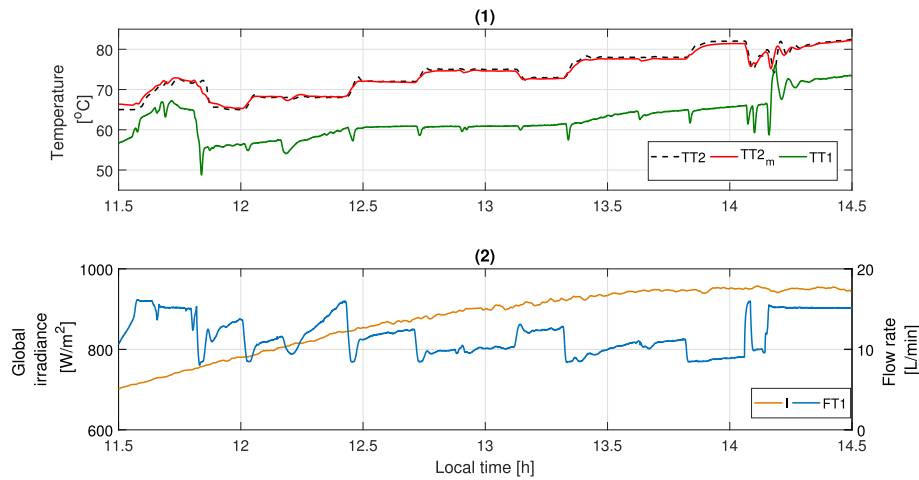
Fig. 4. Solar field model validation. (1) Outlet solar field temperature (TT2), model output (TT2$_m$) and inlet solar field temperature (TT1) and (2) solar field water flow rate (FT1) and global irradiance (I).

Table 2
α_{he} values.

Temperature [°C]	Flow rate [L/h]	α_{he}[W/m² K]
60	400	480.29
	500	582.81
	600	754.05
70	400	530.22
	500	689.30
	600	857.13
80	400	476.44
	500	593.40
	600	670.78

$$\text{NRMSE [\%]} = \sqrt{\frac{\sum\limits_{k=1}^{N}\left(\widehat{Y}(k) - Y(k)\right)^2}{\sum\limits_{k=1}^{N}\left(Y(k)\right)^2}}. \tag{13}$$

Table 3 summarizes the obtained FOPDT transfer functions in the form $G(s) = Y(s)/U(s) = k \cdot e^{-t_d s}/(\tau \cdot s + 1)$, where k is the static gain, τ is the representative time constant and t_d the time delay.

Firstly, to characterize the pumps used in the control system (Pump 1 and Pump 2 in Fig. 3), step changes of 20% in its variable frequency drive were applied each 3 min to obtain $G_1(s)$ and $G_2(s)$ respectively (see Table 3). In the same way, the relationship between FT1 and the outlet solar field temperature TT2 ($G_3(s)$) has been determined by introducing step changes in the flow rate FT1. It was accomplished under quasi-steady conditions in the inlet temperature of the solar field TT1, and around solar midday when the global irradiance is almost constant. The effect of the air cooler has been also modeled through reaction curve method to allow us obtaining $G_4(s)$, relating TT3 with the frequency drive of the air cooler. As in the previous case, this test was carried out around solar midday with quasi-steady conditions in TT1. Finally, the relation between valve 1 and TT5 was obtained ($G_5(s)$) by means of several open loop steps of different values with quasi-steady conditions in TT4. Apart from this relation, the linear range of the valve was identified between 40 and 75%.

3.3. Complete model of the heat generation circuit in the direct connection mode

Using the equations shown in Section 3.1 and the FOPDT models presented in Table 3, a complete model of the heat generation
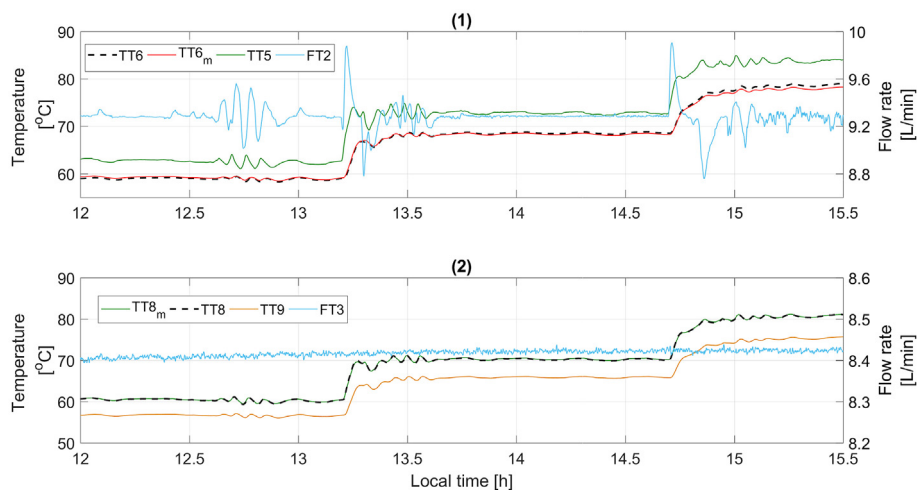
Fig. 5. Heat exchanger model validation using a day with oscillations caused by the chiller operation. (1) Water outlet temperature leaving the hot side of the heat exchanger (TT6), model output (TT6$_m$), inlet temperature to the hot side of the heat exchanger (TT5) and heat exchanger water flow rate (FT2) and (2) water outlet temperature leaving the cold side of the heat exchanger (TT8), model output (TT8$_m$), inlet temperature to the cold side of the heat exchanger (TT9) and MD water flow rate (FT3).

Table 3
Transfer functions obtained from experimental data.

$G(s)$	$Y(s)$	$U(s)$	k	τ [s]	t_d [s]	NRMSE [%]
$G_1(s)$	$FT1(s)$	$F_{P1}(s)$	0.2344	5	1	96.7
$G_2(s)$	$FT2(s)$	$F_{P2}(s)$	0.1345	8.03	3	97.2
$G_3(s)$	$TT2(s)$	$FT1(s)$	−1.37	66.62	16	95.2
$G_4(s)$	$TT3(s)$	$F_{ac}(s)$	−0.1087	27.48	20	96.5
$G_5(s)$	$TT5(s)$	$F_{V1}(s)$	0.1502	14.3	10	86.2

Table 4
Dead time values.

Pipe section	Dead time [s]
TT3-TT4	35
TT7-TT1	65

circuit in the direct connection mode has been developed in *Simulink* (MATLAB). In addition to the models shown in Section 3.1 And 3.2, transport dead times have been added to model delays caused by the interconnection of the pipes and the sensor position. These transport delays have been observed from field data and they do not change significantly with the operating ranges. The dead time values are presented in Table 4. Fig. 6 shows the comparison between real measures and the model outputs. The inputs used are: pump 1, pump 2, air cooler, valve 1, global irradiance, FT3 and TT9.

4. Control system

The main objective of the control system is to maintain a desired operating temperature at the inlet of the MD module. To this purpose, four direct control loops (see Fig. 7) and a reference governor are proposed. The linear models developed in Section 3.2 have been used to design the corresponding control laws. Furthermore, the control scheme includes antiwindup mechanisms to take into account saturation problems. It should be mentioned that, this control architecture is proposed rather than other techniques such as

multivariable control with decoupling, since it can be used in all the operation modes included in Ref. [9].

4.1. Loop 1. Solar field

The transfer functions obtained in Section 3.2 have been used for control design purposes. A cascade control loop with two PI controllers $(PI(s) = K_p(1 + 1/(T_i \cdot s)))$ has been designed to control the outlet solar field temperature TT2. The slave control is in charge of providing the desired water flow rate FT1 by acting on the variable frequency drive of pump 1 and the outer loop calculates the required water flow rate FT1 which allows to obtain the desired outlet solar field temperature TT2. The cascade control loop has been configured with the following parameters:

- Slave PI: $K_p = 2.84$ %/L and $T_i = 0.082$ min (AMIGO method, [28]).
- Outer PI: $K_p = −0.42$ L/°C and $T_i = 1.21$ min (SIMC method, [30]).

Due to the fact that the system is subjected to strong disturbances caused by solar irradiance I and inlet solar field temperature TT1, a FF controller has been included in this loop. This FF is obtained using a static version of the solar field model presented in section 3.1.1 and it provides the nominal operating flow rate ($FT1_{FF}$) taking into account the operating conditions. The static equation making $TT2 = TT2_{SP}$ in Eq. (1) is given by:

$$FT1_{FF} = \left[\frac{\beta \cdot L_{eq}}{c_p \cdot (TT2_{SP}(t) − TT1(t))} \cdot I(t) \right.$$
$$\left. − \frac{H}{c_p} \cdot \frac{(\overline{T}(t) − T_a(t))}{(TT2_{SP}(t) − TT1(t))} \right] \cdot \frac{c_f}{\rho}, \tag{14}$$

$$\overline{T}(t) = \frac{TT1(t) + TT2_{SP}(t)}{2}. \tag{15}$$
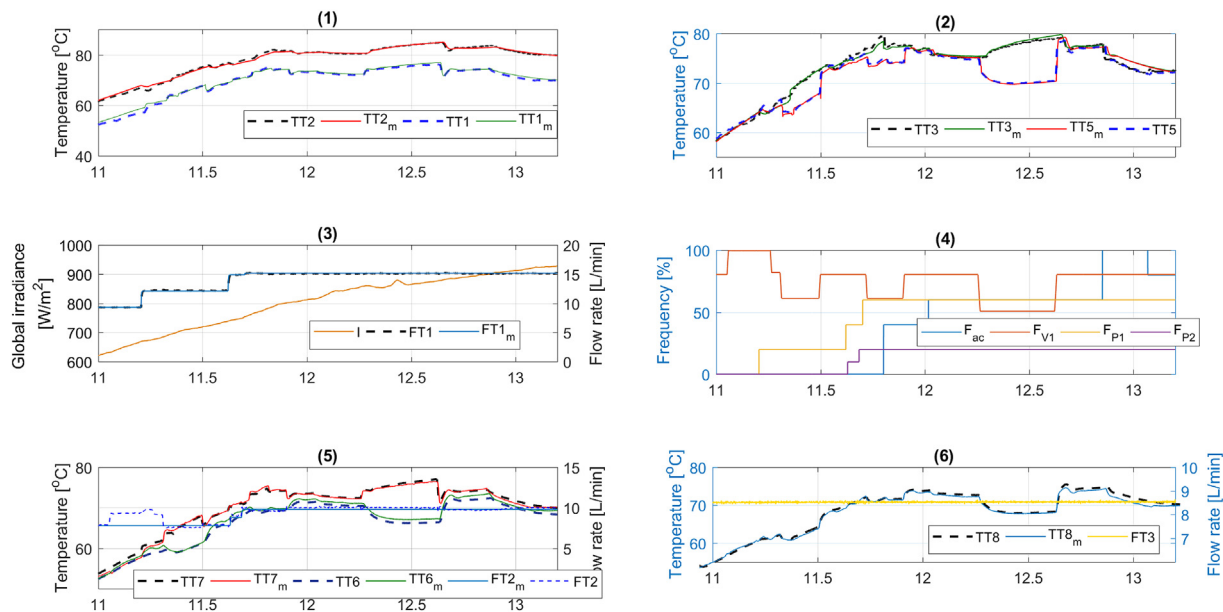
Fig. 6. Comparison between real measurements and model outputs. (1) Inlet and outlet solar field temperature (TT1 and TT2), (2) air cooler water temperature (TT3) and inlet temperature to the hot side of the heat exchanger (TT5), (3) global irradiance (I) and solar field water flow rate (FT1), (4) valve 1 frequency (F_{V1}), air cooler frequency (F_{ac}), pump 1 frequency (F_{P1}) and pump 2 frequency (F_{P2}), (5) outlet distribution system temperature (TT7), water outlet temperature leaving the hot side of the heat exchanger (TT6) and heat exchanger water flow rate (FT2) and (6) water outlet temperature leaving the cold side of the heat exchanger (TT8) and (FT3) MD water flow rate.
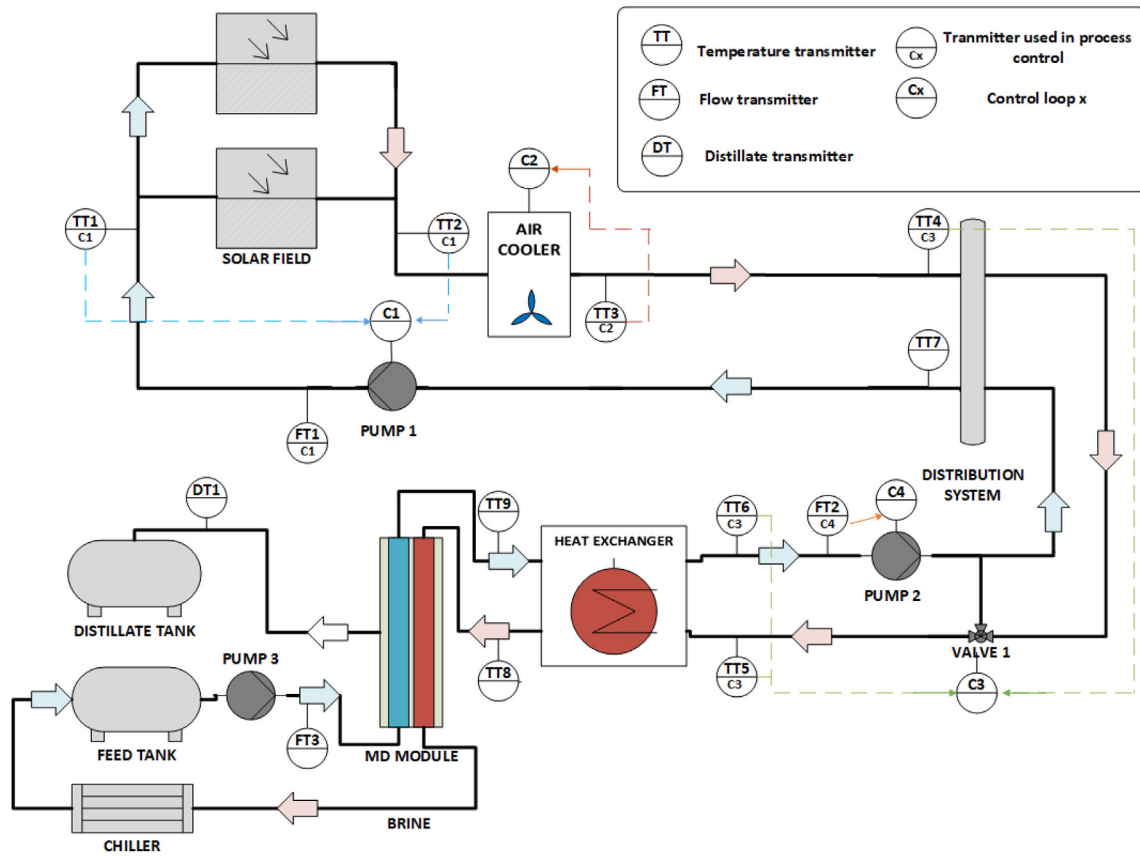
Fig. 7. Schematic diagram of the active components in direct connection mode with control loops.

The nomenclature associated to the equation is presented in Appendix A. A low pass filter (LPF) has been added to this static equation with a representative time constant of 75 s to achieve a better dynamical and smooth response. Finally, a low pass filter of 60 s has been included in the reference signal to find a good tradeoff between reference tracking and disturbances rejection and to reduce overshoots against setpoint step changes. Fig. 8 shows the control scheme.

4.2. Loop 2. Air cooler

This loop is also focused on controlling the outlet solar field temperature and it acts when TT2 is higher than desired outlet solar field temperature, mainly due to flow saturation. Fig. 9 shows the control scheme. The PI controller has been configured with $K_p = -7.48$ %/$^{\circ}$C and $T_i = 0.233$ min (Improved SIMC method, [31]), using the linear model presented in Table 3.

4.3. Loop 3. Valve 1 control loop

Although in direct mode the inlet heat exchanger temperature TT5 could be controlled with loop 2 described previously (if valve 1 is fully open), a temperature control loop using valve 1 is considered to improve the setpoint tracking and to reject disturbances coming from the distribution system (TT4). To this purpose, a PI controller with a FF is developed. Based on the steady-state energy balance obtained from Eq. (10), the FF has been designed such as:

$$F_{V1,FF}(\%) = \frac{TT5_{SP} - TT6}{TT4 - TT6} \cdot 100. \tag{16}$$

In order to achieve a better dynamical and smooth response, a low pass filter has been added to the FF with a representative time constant of 65 s. Fig. 10 shows the control scheme. The parameters of the PI controller are: $K_p = 2.22$ %/$^{\circ}$C and $T_i = 0.5$ min (Improved SIMC method, [31]), using the linear model in Table 3.
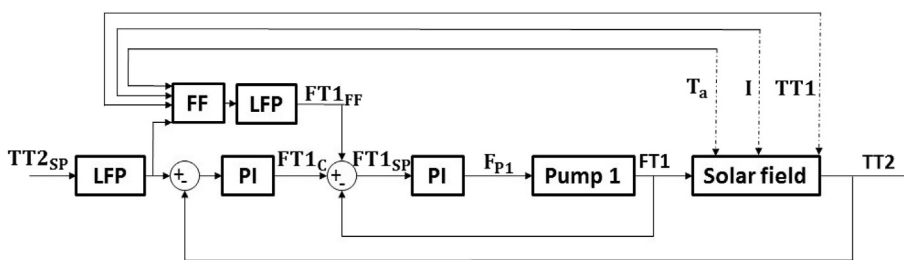
Fig. 8. Solar field control scheme.
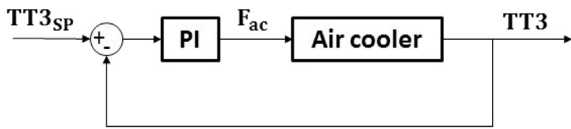
Fig. 9. Air cooler control scheme.
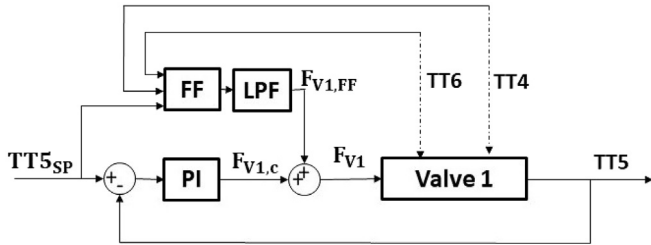
Fig. 10. Valve 1 control scheme.
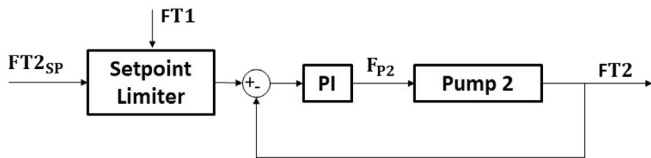
Fig. 11. Heat exchanger water flow rate control scheme.

4.4. Loop 4. Heat exchanger water flow rate

Although the control system is aimed at temperature control purposes, variations in valve 1, cause variations in the flow rate and therefore in the temperature, so it is necessary to fix the water flow rate FT2 by means of a controller. Besides, by fixing FT2 with the same value as FT3, the maximum heat transfer is achieved in the heat exchanger. However, it should be taken into account that FT2 cannot be higher than FT1, due to the fact that the fluid coming from the solar field and the fluid coming from the heat exchanger would be mixed in the hotter side of the distribution system. A PI controller is designed with a setpoint limiter which checks if FT2 setpoint is less than FT1, which varies to maintain the outlet solar field temperature, loop 1. The PI controller has been configured with $K_p = 4.12$ %/L and $T_i = 0.1505$ min (Improved SIMC method, [31]), using the transfer function presented in Table 3. Fig. 11 shows the control scheme.

4.5. Reference governor

The proposed temperature control scheme with the reference governor is shown in Fig. 12. The heat exchanger model presented in section 3.1.2 is used to calculate suitable setpoints for the direct control system, helping to obtain the desired temperature at the inlet of the MD module (TT8).

The equations implemented in the reference governor are the following ones:

$$TT6_m = TT5 - \eta_{he,1} \cdot (TT5 - TT9), \tag{17}$$

$$TT5_{SP} = \frac{TT8_{SP} - TT9 + \eta_{he,2} \cdot TT6_m}{\eta_{he,2}}. \tag{18}$$

Thus, Eq. (18) gives $TT5_{SP}$ and the setpoint for loops 1 and 2 is $TT5_{SP} + \Delta T$. This ΔT must be characterized for each module in order to balance the corresponding energy consumption. The nominal value characterized for Aquastill 24 m²-module, based on experience, is 4 °C. Besides, this ΔT maintains the temperature of the solar field higher than the desired temperature at the inlet of the heat exchanger, allowing valve 1 acting in its linear range.

It is important to emphasize that this system in direct mode requires smooth setpoint changes rather than step ones to avoid oscillations. Therefore, a LPF has been added to each setpoint. The representative time constants for $TT2_{SP}$ and $TT5_{SP}$ are 85 and 75 s respectively.

5. Simulation tests

This section shows two simulation tests carried out in order to analyse the performance of the control system under two different weather profiles, using data from PSA on 21 and 25 September 2016. The model developed in section 3 has been used in this test to simulate the plant behaviour. Notice that TT9 is an input to the control system (see Fig. 12), so this temperature is also required to test the performance. Since TT9 depends on operating conditions (sea water flow rate and temperature and flow rate and temperature of the water coming from the heat exchanger) and the three first inputs are assumed constant (FT3 = 500 L/h, sea water temperature = 20 °C, and FT2 = FT3) in the simulations carried out, only temperature TT8 must be considered to simulate variations in TT9 and test the control system. In the operational range employed in TT8 (60—80 °C), the temperature difference observed during the experimental campaign performed to model the plant varies between 3.5 and 4.5 °C, so that, a fixed value of 4 °C has been used in the simulation tests.
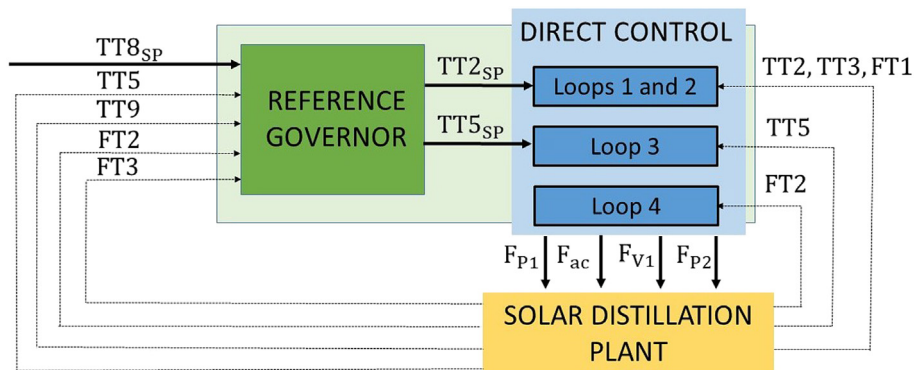
Fig. 12. Reference governor scheme.
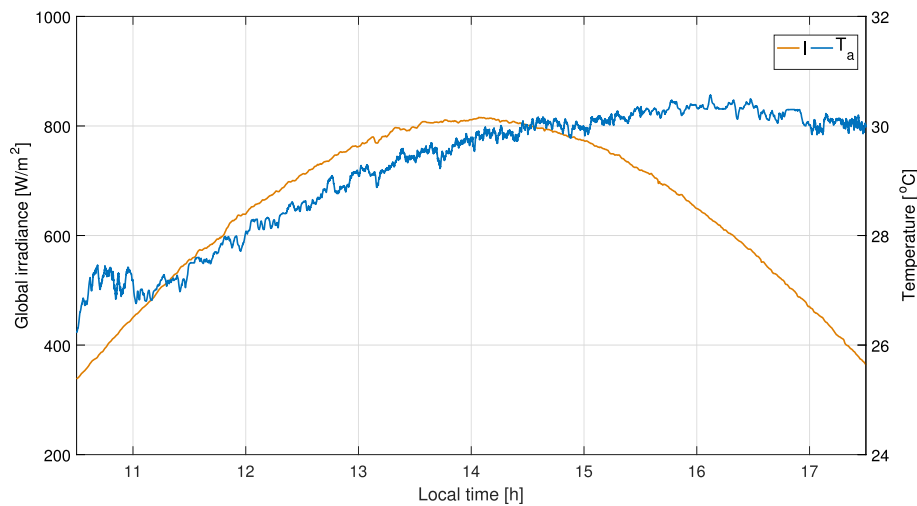
Fig. 13. Meteorological inputs for the simulation test in a sunny day. Global irradiance (I) and ambient temperature (T_a).
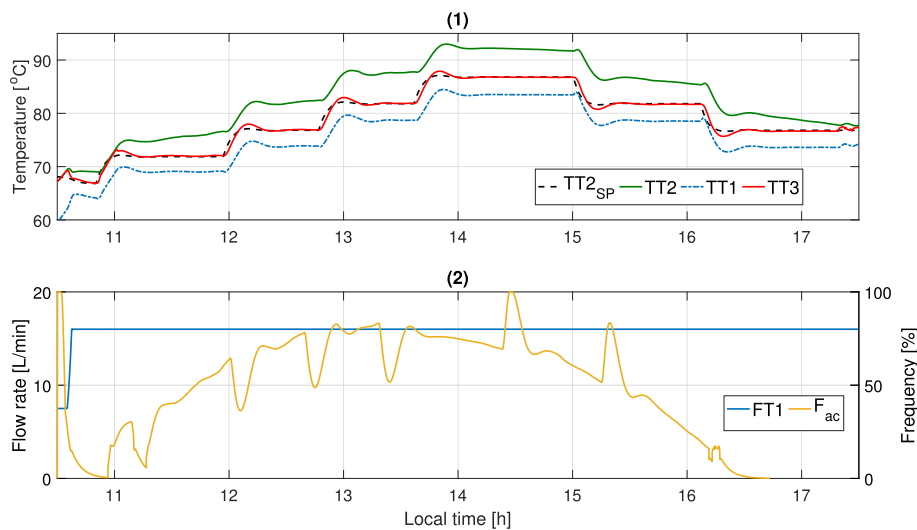
Fig. 14. Simulation results of loops 1 and 2 in a sunny day. (1) Reference ($TT2_{SP}$), outlet solar field temperature (TT2), inlet solar field temperature (TT1) and water air cooler temperature (TT3) and (2) solar field flow rate (FT1) and air cooler frequency (F_{ac}).

5.1. Sunny day

Fig. 13 shows the environmental conditions used for this simulation test. At the beginning, the temperature at the inlet of the MD module is higher than the setpoint fixed, 60 °C (see Fig. 16). Due to this fact the reference governor decreases the setpoints of each direct control loop (see Figs. 14 and 15) on a smooth way, allowing to reach the reference. Then, positive step changes of 5 °C are introduced in $TT8_{SP}$ at times 10.83, 11.94, 12.78 and 13.61 h. In Figs. 14 and 15, it can be observed how the setpoints of each loop are increased by the reference governor to reach the desired temperatures at the inlet of the MD module. The settling times in these changes are around 20 min and the overshoots are around 10−15%. Notice that a tradeoff solution between overshoots and settling times has been reached with this control system configuration. Thus, better results are obtained in comparison with manual operations; settling times are 20−30 min faster and the obtained overshoots are within the allowed range defined by plant operators. At times 15 and 16.11 h two negative steps of 5 °C are applied at $TT8_{SP}$ with similar dynamical results as the positive ones.

In this test, loop 1 is saturated all the time because of irradiance values as well as the low energy consumption of the module and solar field oversizing. Thus, the air cooler is used to control the temperature excess, as can be observed in Fig. 14. Since the references of this loop are 4 °C higher than those of loop 3, valve 1 acts in its linear range (see Fig. 15) getting an accurate control at the inlet of the heat exchanger. It is important to mention that, this fact is essential to get an adequate temperature control at the inlet of the MD module.

5.2. Cloudy day

In this example, the irradiance curve shows fluctuations due to transient clouds (see Fig. 17). At the beginning, the temperature at the inlet of the MD module is higher than the desired value (see Fig. 20), so the reference governor decreases the setpoints of the direct control system (see Figs. 18 and 19). Then, at times 12.22 and 13.89 h, two positive steps of 5 °C at $TT8_{SP}$ are introduced. In this case, the overshoots are around 15% and the settling times are around 25 min. It should be taken into account that in this test, the

Fig. 15. Simulation results of loop 3 in a sunny day. (1) Inlet temperature to the hot side of the heat exchanger (TT5), water outlet temperature leaving the hot side of the heat exchanger (TT6), inlet distribution system temperature (TT4) and reference (TT5$_{SP}$) and (2) valve 1 frequency (F$_{V1}$).
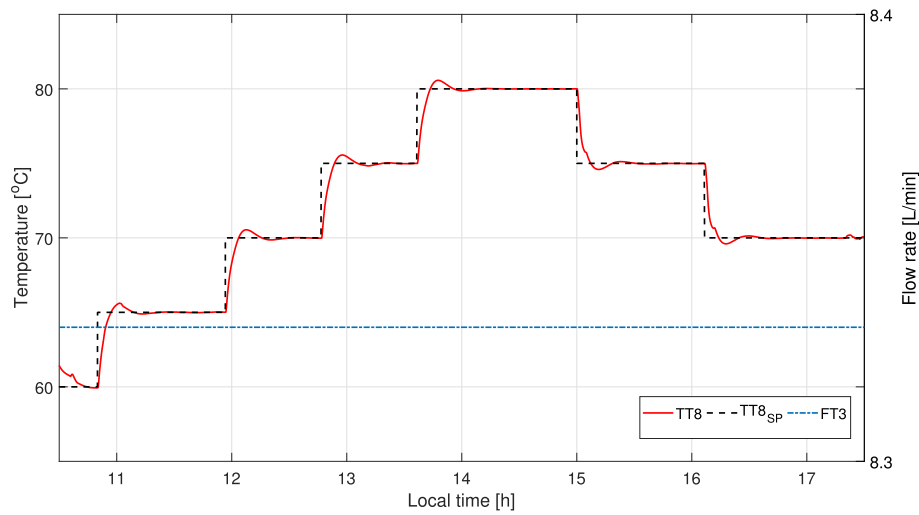
Fig. 16. Simulation results at the inlet of the MD module in a sunny day. Water outlet temperature leaving the cold side of the heat exchanger (TT8), reference (TT8$_{SP}$) and MD module water flow rate (FT3).
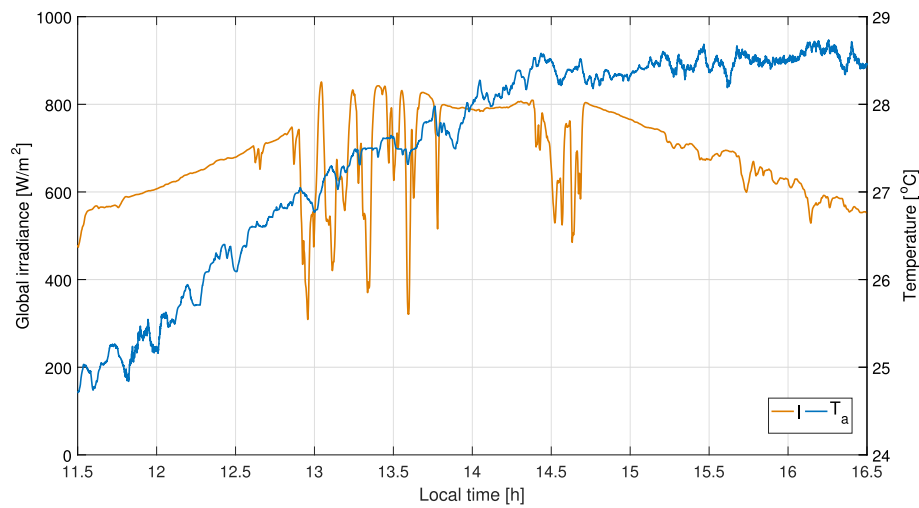
Fig. 17. Meteorological inputs of the simulation test in a partly cloudy day. Global irradiance (I) and ambient temperature (T$_a$).
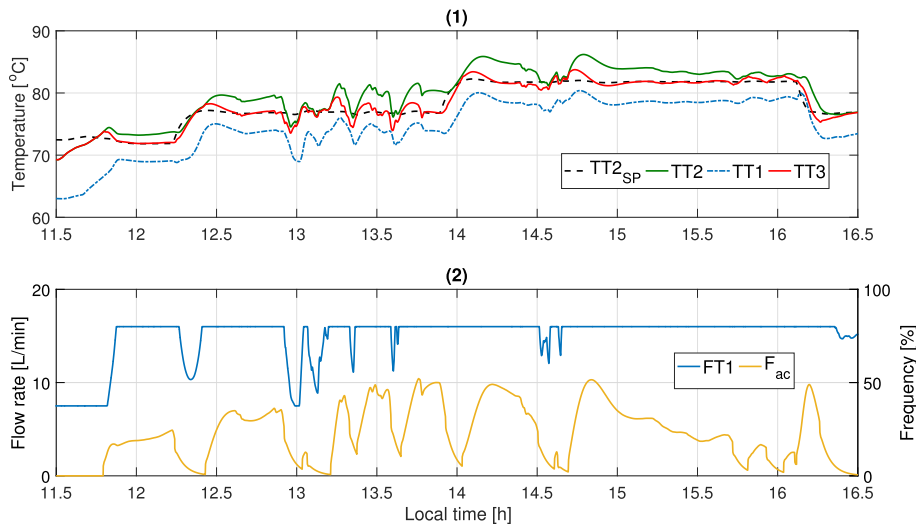
Fig. 18. Simulation results of loops 1 and 2 in a partly cloudy day. (1) Reference ($TT2_{SP}$), outlet solar field temperature (TT2), inlet solar field temperature (TT1) and water air cooler temperature (TT3) and (2) solar field flow rate (FT1) and air cooler frequency (F_{ac}).
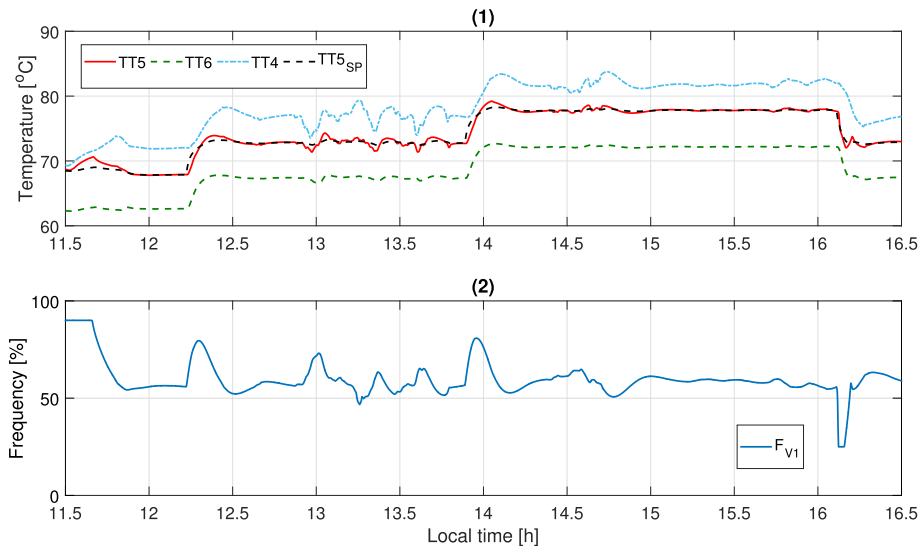
Fig. 19. Simulation results of loop 3 in a partly cloudy day. (1) Inlet temperature to the hot side of the heat exchanger (TT5), water outlet temperature leaving the hot side of the heat exchanger (TT6), inlet distribution system temperature (TT4) and reference ($TT5_{SP}$) and (2) valve 1 frequency (F_{V1}).
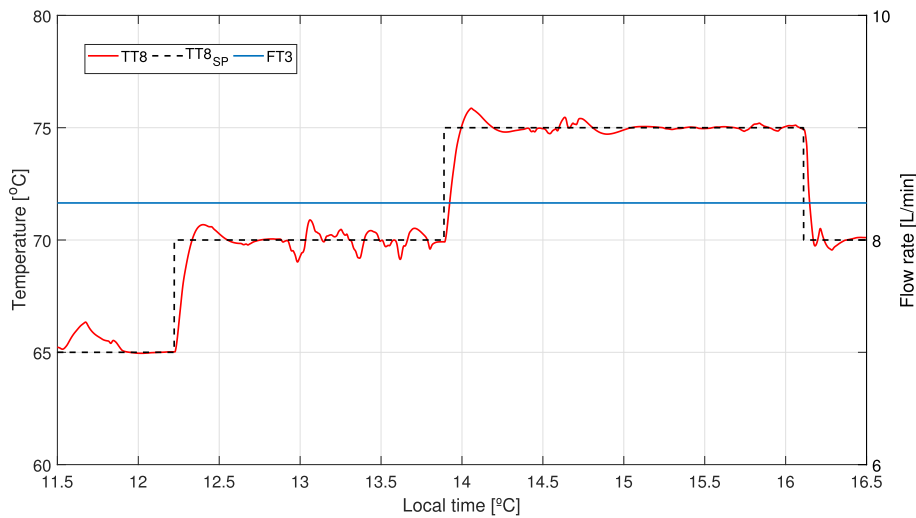
Fig. 20. Simulation results at the inlet of the MD module in a partly cloudy day. Water outlet temperature leaving the cold side of the heat exchanger (TT8), reference ($TT8_{SP}$) and MD module water flow rate (FT3).
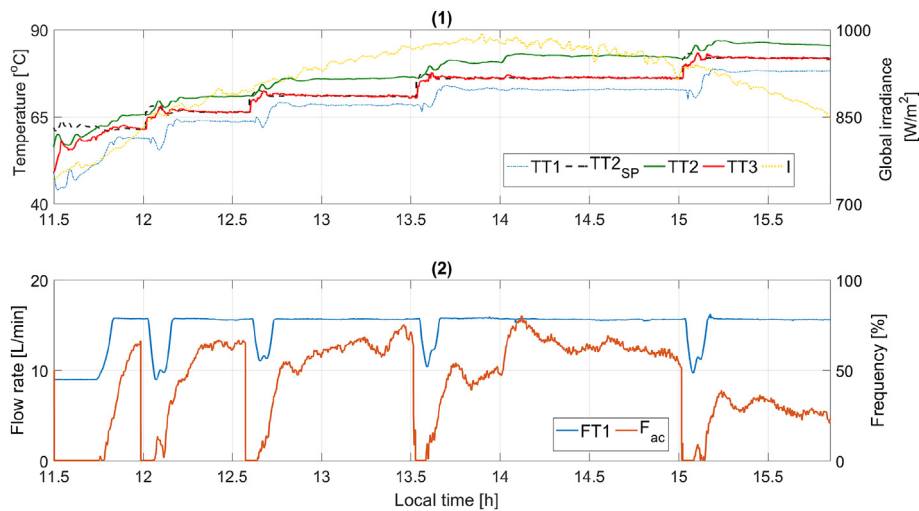
Fig. 21. Experimental results of loops 1 and 2. (1) Reference (TT2$_{SP}$), outlet solar field temperature (TT2), inlet solar field temperature (TT1), water air cooler temperature (TT3) and global irradiance (I) and (2) solar field flow rate (FT1) and air cooler frequency (F$_{ac}$).

tracking errors of the direct control loops are higher than in the test above, due to irradiance fluctuations. A time 16.11 h a negative step of 5 °C at TT8$_{SP}$ is introduced with similar results.

Fig. 18 shows how the solar field water flow rate decreases according to the irradiance level, reducing temperature fluctuations. Besides, these fluctuations are also reduced by loop 3 as can be observed in Fig. 19 by means of the FF, which rejects disturbances coming from the distribution system. Finally, at the inlet of the MD module, the temperature varies in a range less than ±1 °C when there are irradiance disturbances (see Fig. 17). Notice that the tracking error accepted by plant operators in a manual operation with favourable meteorological conditions is ±1 °C.

6. Real experimental test

An experimental campaign has been performed in the solar distillation facility to test the proposed control strategy under different operating and weather conditions. One of these tests (on September 30th, 2016) is presented in this section, clearly

improving (in terms of performance indexes such as overshoot and settling times) preliminary results presented in Ref. [9].

Figs. 21—23 show the experimental results. Firstly, a setpoint of 55 °C is imposed at the inlet of the MD module and FT2 is fixed with the same value as FT3, 8.6 L/min. Since the temperature is lower than the setpoint fixed, the reference governor increases the setpoints for loops 1, 2 and 3 (see Figs. 21 and 22). Once the system reaches the desired temperature, a step change of 5 °C at TT8$_{SP}$ is introduced at time 12.01 h. The setpoints for the direct control loops are increased by the reference governor. As it can be observed in Fig. 21, when the reference changes, the flow rate decreases due to the new setpoint and to the inlet temperature disturbance that modifies the feedforward output. This fact is not only caused by the setpoint changes but also by disturbances in the inlet solar field temperature due to recirculation. The settling time in this change is 19 min, the overshoot is 22% (see Fig. 23) and the steady state error is around 0.4 °C. Then, at time 12.6 h the TT8$_{SP}$ is changed to 65 °C. In this case, the time spent in the change is 18 min, the overshoot is 25% and the steady state error is around 0.3 °C. At times 13.53 and
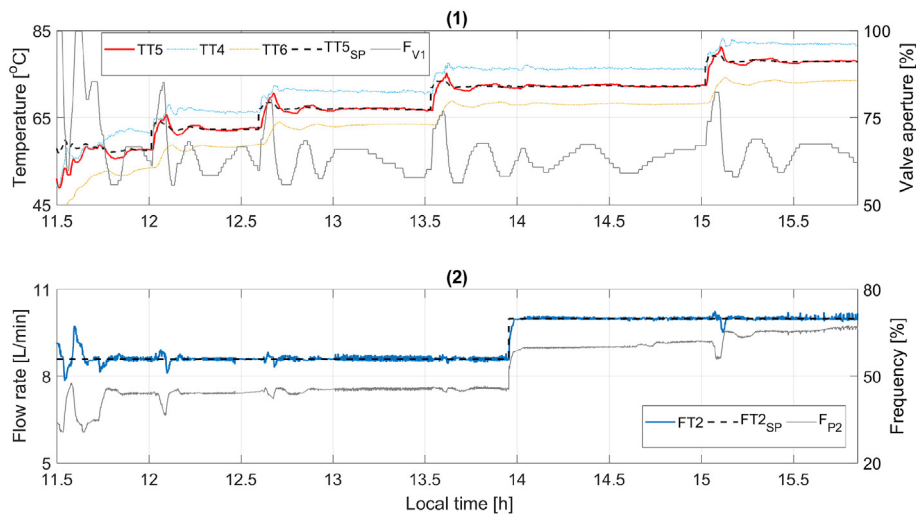
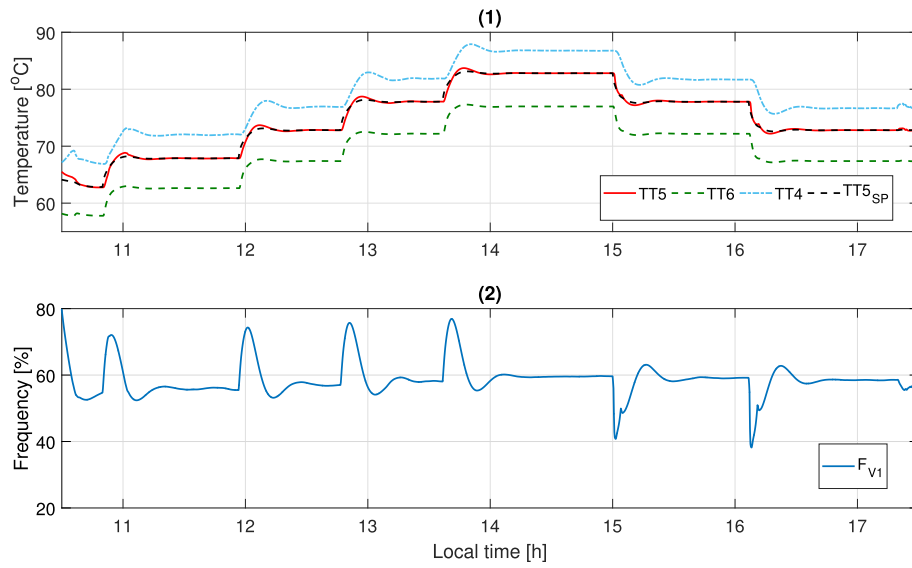**Fig. 22.** Experimental results of loops 3 and 4. (1) Inlet temperature to the hot side of the heat exchanger (TT5), water outlet temperature leaving the hot side of the heat exchanger (TT6), inlet distribution system temperature (TT4) and reference (TT5$_{SP}$) and valve 1 frequency (F$_{V1}$) and (2) heat exchanger water flow rate (FT2), reference (FT2$_{SP}$) and pump 2 frequency (F$_{P2}$).
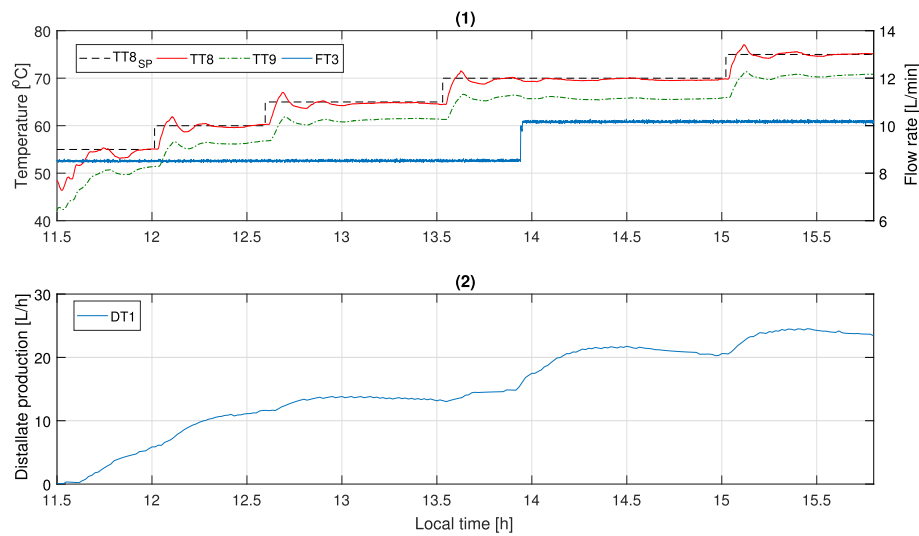
Fig. 23. Experimental results at the inlet of the MD module. (1) Water outlet temperature leaving the cold side of the heat exchanger (TT8), reference (TT8$_{SP}$), inlet temperature to the cold side of the heat exchanger (TT9) and MD module water flow rate (FT3) and (2) distillate production (DT1).

15.02 h, two step changes are introduced with similar results as in the previous cases. At time 13.94 h, both FT2 and FT3 are changed to 10 L/min. This fact produces that the temperature at the inlet of the MD module decreases. Therefore, the reference governor increases the setpoints of the direct controllers to reject this disturbance.

As can be observed in Fig. 21 the outlet solar field temperature is mainly controlled with the air cooler, since loop 1 is saturated due to high irradiance levels. The settling times obtained in the step changes are around 6 min and the steady state error is less than 0.2 °C without overshoots.

As was tested in simulation, when valve 1 works in its linear range, an accurate control at the inlet of the heat exchanger is achieved (see Fig. 22). The settling times in this loop are around 15 min and the mean steady state error is less than 0.2 °C. However, the overshoots are around 20%. This fact is caused by FF actions, because it tries to reject disturbances produced by temperature coming from the distribution system (TT4). These disturbances occur because there is a time period where the outlet solar field temperature varies until it is established in its reference by loops 1 and 2. This situation produces the overshoots inside the module. Although these overshoots are undesirable, a tradeoff solution between settling time and overshoot allowed by plant operators in this operation mode has been reached, as has been pointed out before.

7. Conclusions

This paper has addressed the development of a feedback control system in a solar membrane distillation facility. It has been accomplished using the most difficult operation mode, which is a challenge from a control point of view. Promising results have been obtained which allow us to draw the two following conclusions:

1. Settling times are considerably reduced. In a manual operation the time spent to establish an operating temperature inside the module is around 40—50 min, whereas with the control system is 20 min.
2. A suitable operating temperature at the inlet of the distillation module, in the direct connection mode, can be obtained using the model-based reference governor and the control system in spite of disturbances. This task was highly difficult to follow in experimental campaigns with manual operation.

Future works will include the implementation of a control system able to manage all operating modes, following the approach in Ref. [24], as we can take advantage of all the work developed in this paper, and also testing multivariable-decoupling strategies. Moreover, the developed control layer should be integrated into a hierarchical control architecture aimed at maximizing the efficiency according to different metrics used in distillation processes or maximizing the daily production while reducing operational costs.

Appendix A. Nomenclature

A_{he}	Heat exchanger area, 1.65 m^2
A_{sf}	Collector absorber cross-section area, 0.007 m^2
c_f	Conversion factor to account for connections, number of modules and L/min conversion, $9 \cdot 2 \cdot 6 \cdot 10^4$ (s L)/(min m^3)
c_p	Specific heat capacity, J/(kg °C)
DT1	Distillate production, L/h
F	Input frequency, %
FT1	Solar-field water flow rate, L/min
FT2	Heat exchanger water flow rate, L/min
FT3	MD water flow rate, L/min
H	Global thermal losses coefficient, 5.88 J/(s K)
I	Global irradiance, W/m^2
k	Static gain of FOPDT transfer functions
L_a	Collector absorber tube length, 1.95 m
L_{eq}	Equivalent absorber tube length, 9.75 m
LPF	Low pass filter, —
$\dot{m}$	Mass flow, kg/s
n_{cs}	Number of serie-connections in a collectors group, 5
$\overline{T}$	Equivalent absorber tube mean temperature, °C
T_a	Ambient temperature, °C
t_d	Representative time delay of FOPDT transfer functions, s
TT1	Inlet temperature of the solar field, °C
TT2	Outlet temperature of the solar field, °C

TT3   Air cooler water temperature, °C

TT4   Inlet temperature of the distribution system, °C

TT5   Inlet temperature to the hot side of the heat exchanger, °C

TT6   Water outlet temperature leaving the hot side of the heat exchanger, °C

TT7   Outlet distribution system temperature, °C

TT8   Water outlet temperature leaving the cold side of the heat exchanger, °C

TT9   Inlet temperature to the cold side of the heat exchanger, °C

α_{he} Heat exchanger heat transfer coefficient, W/(m^2·K)

B Irradiance model parameter, 0.11 m

γ V1 aperture, -

η_{he} Heat exchanger auxiliary factor 1, −

τ Representative time constant of FOPDT transfer functions, s

θ_{he} Heat exchanger auxiliary factor 2, −

ρ Water density, 975 kg/m^3

Subscript

ac   Air cooler

C   Feedback control

eq   Equivalent

FF   Feedforward

m   Model output

P1   Pump 1

P2   Pump 2

SP   Setpoint

V1   Valve 1

1   Relative to FT2

2   Relative to FT3

References

[1] M.R. Qtaishat, F. Banat, Desalination by solar powered membrane distillation systems, Desalination 308 (2013) 186—197.

[2] E.S. Mohamed, G. Papadakis, Advances of Renewable Energy Powered Desalination, in: Handbook of Clean Energy Systems, John Wiley Sons, Ltd, 2015, pp. 1—10.

[3] N. Ghaffour, S. Lattemann, T. Missimer, K.C. Ng, S. Sinha, G. Amy, Renewable energy-driven innovative energy-efficient desalination technologies, Appl. Energy 136 (2014) 1155—1165.

[4] G. Zaragoza, A. Ruiz-Aguirre, E. Guillén-Burrieza, Efficiency in the use of solar thermal energy of small membrane desalination systems for decentralized water production, Appl. Energy 130 (2014) 491—499.

[5] A. Cipollina, M. Di Sparti, A. Tamburini, G. Micale, Development of a membrane distillation module for solar energy seawater desalination, Chem. Eng. Res. Des. 90 (2012) 2101—2121.

[6] M. Khayet, Solar desalination by membrane distillation: dispersion in energy consumption analysis and water production costs (a review), Desalination 308 (2013) 89—101.

[7] E. Guillén-Burrieza, J. Blanco, G. Zaragoza, D.-C. Alarcón, P. Palenzuela, M. Ibarra, W. Gernjak, Experimental analysis of an air gap membrane distillation solar desalination pilot system, J. Membr. Sci. 379 (2011) 386—396.

[8] E. Guillén-Burrieza, G. Zaragoza, S. Miralles-Cuevas, J. Blanco, Experimental evaluation of two pilot-scale membrane distillation modules used for solar desalination, J. Membr. Sci. 409 (2012) 264—275.

[9] J.D. Gil, A. Ruiz-Aguirre, L. Roca, G. Zaragoza, M. Berenguel, Solar Membrane Distillation: a Control Perspective, in: 23th Mediterranean Conference on Control and Automation (MED 2015), 2015, pp. 796—802. Torremolinos, Málaga, Spain.

[10] M. El-Bourawi, Z. Ding, R. Ma, M. Khayet, A framework for better understanding membrane distillation separation process, J. Membr. Sci. 285 (2006) 4—29.

[11] S.B. Abdallah, N. Frikha, S. Gabsi, Simulation of solar vacuum membrane distillation unit, Desalination 324 (2013) 87—92.

[12] V. Bui, L.T. Vu, M. Nguyen, Simulation and optimisation of direct contact membrane distillation for energy efficiency, Desalination 259 (2010) 29—37.

[13] J.-S. Lin, H. Chang, G.B. Wang, Modelling and control of the solar powered membrane distillation system, in: AIChE Annual Meeting, Minneapolis, MN, USA, 2011.

[14] H. Chang, G.-B. Wang, Y.-H. Chen, C.-C. Li, C.-L. Chang, Modeling and optimization of a solar driven membrane distillation desalination system, Renew. Energy 35 (2010) 2714—2722.

[15] H. Chang, S.-G. Lyu, C.-M. Tsai, Y.-H. Chen, T.-W. Cheng, Y.-H. Chou, Experimental and simulation study of a solar thermal driven membrane distillation desalination process, Desalination 286 (2012) 400—411.

[16] R. Porrazzo, A. Cipollina, M. Galluzzo, G. Micale, A neural network-based optimizing control system for a seawater-desalination solar-powered membrane distillation unit, Comput. Chem. Eng. 54 (2013) 79—96.

[17] E.F. Camacho, M. Berenguel, F.R. Rubio, D. Martínez, Control of Solar Energy Systems, Springer, 2012.

[18] L. Roca, M. Berenguel, L.J. Yebra, D.C. Alarcón-Padilla, Solar field control for desalination plants, Sol. Energy 82 (2008) 772—786.

[19] C.O. Ayala, L. Roca, J.L. Guzmán, J.E. Normey-Rico, M. Berenguel, L.J. Yebra, Local model predictive controller in a solar desalination plant collector field, Renew. Energy 36 (2011) 3001—3012.

[20] L. Roca, J.L. Guzmán, J.E. Normey-Rico, M. Berenguel, L.J. Yebra, Robust constrained predictive feedback linearization controller in a solar desalination plant collector field, Contr. Eng. Pract. 17 (2009) 1076—1088.

[21] M. Beschi, M. Berenguel, A. Visioli, L. Yebra, On reduction of control effort in feedback linearization GPC strategy applied to a solar furnace, Optim. Contr. Appl. Meth. 37 (2016) 521—536.

[22] F. Eleiwi, I. N'Doye, T.-M. Laleg-Kirati, Feedback control for distributed heat transfer mechanisms in direct-contact membrane distillation system, in: 2015 IEEE Conference on Control Applications (CCA), Sydney, Australia, 2015, pp. 1624—1629.

[23] A. Alkhudhiri, N. Darwish, N. Hilal, Membrane distillation: a comprehensive review, Desalination 287 (2012) 2—18.

[24] M. Pasamontes, J.D. Álvarez, J.L. Guzmán, M. Berenguel, E.F. Camacho, Hybrid modeling of a solar-thermal heating facility, Sol. Energy 97 (2013) 557—590.

[25] A. Ruiz-Aguirre, D.-C. Alarcón-Padilla, G. Zaragoza, Productivity analysis of two spiral-wound membrane distillation prototypes coupled with solar energy, Desalination and Water Treatment 55 (2015) 2777—2785.

[26] J. Alvarez, L. Yebra, M. Berenguel, Adaptive repetitive control for resonance cancellation of a distributed solar collector field, Int. J. Adapt. Contr. Signal Process. 23 (2009) 331—352.

[27] A. de la Calle, L. Roca, J. Bonilla, P. Palenzuela, Dynamic modeling and simulation of a double-effect absorption heat pump, Int. J. Refrig. 72 (2016) 171—191.

[28] K.J. Åström, T. Hägglund, Advanced PID Control, ISA-The Instrumentation, Systems, and Automation Society, Research Triangle Park, NC, 2005, 27709.

[29] L. Ljung, Experiments with identification of continuous time models, in: IFAC Proceedings Volumes, vol. 42, 2009, pp. 1175—1180.

[30] S. Skogestad, Simple analytic rules for model reduction and PID controller tuning, J. Process Contr. 13 (2003) 291—309.

[31] S. Skogestad, C. Grimholt, The SIMC method for smooth PID controller tuning, in: PID Control in the Third Millennium, Springer, 2012, pp. 147—175.

2.1.2 Prediction models to analyse the performance of a commercial-scale membrane distillation unit for desalting brines from reverse osmosis plants

Research in this field is supported by the following journal publication:

Title	Prediction models to analyse the performance of a commercial-scale membrane distillation unit for desalting brines from RO plants
Authors	**J. D. Gil**, A. Ruiz-Aguirre, L. Roca, G. Zaragoza, M. Berenguel
Journal	Desalination
Year	2018
Volume	445
Pages	15-28
DOI	`https://doi.org/10.1016/j.desal.2018.07.022`
IF (JCR 2018)	6.035
Categories	Water Resources (2/91) **Q1**
	Engineering, Chemical (10/138) Q1

Contribution of the Ph.D. candidate
The Ph.D. candidate, J. D. Gil, is the main contributor and first author of this paper.
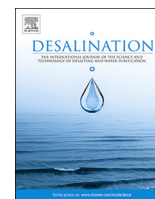
Prediction models to analyse the performance of a commercial-scale membrane distillation unit for desalting brines from RO plants

Juan D. Gil[a], Alba Ruiz-Aguirre[a,c], Lidia Roca[b], Guillermo Zaragoza[b,*], Manuel Berenguel[a]

[a] Centro Mixto CIESOL, ceiA3, Universidad de Almería, Ctra. Sacramento s/n, Almería 04120, Spain
[b] CIEMAT-Plataforma Solar de Almería, Ctra. de Senés s/n, Tabernas 04200, Almería, Spain
[c] Dipartimento dell'Innovazione Industriale e Digitale (DIID), Ingegneria Chimica, Gestionale, Informatica, Meccanica, Università di Palermo (UNIPA), viale delle Scienze Ed. 6, 90128 Palermo, Italy

ARTICLE INFO

ABSTRACT

Desalting brines from Reverse Osmosis (RO) plants is one of the most promising applications of Membrane Distillation (MD) systems. The development of accurate models to predict MD system performances plays a significant role in the design of this kind of industrial applications. In this paper, a commercial-scale Permeate-Gap Membrane Distillation (PGMD) module was modelled by means of two different approaches: Response Surface Methodology (RSM) and Artificial Neural Networks (ANN). Condenser inlet temperature, evaporator inlet temperature, feed flow rate and feed water salt concentration were selected as inputs of the model, while permeate flux and Specific Thermal Energy Consumption (STEC) were chosen as responses. The prediction abilities of both RSM and ANN models were compared with further experimental data by using the Analysis of Variance (ANOVA) and the Root Mean Squared Error (RMSE). The results show that the ANN model is able to predict in a more precise way the behaviour of the module for the whole range of input variables. Thus, ANN model was used to find the optimal operating conditions, for the module operating at feed water salinity of 70 and 105 g/L, concentrations that can be reached when desalting RO brines.

1. Introduction

Due to the high tolerance of MD systems to high salinity feeds, one of the possible industrial applications of this technology consists of desalting seawater RO brines. Integrating MD technology in RO plants could be an essential factor to obtain efficient desalination lines in terms of recovery [1-4]. However, the uncertainty associated with the performance of MD technology at large scale has prevented the development of this kind of applications so far [5-8]. Therefore, investigating the performance of large scale MD systems, under the operating conditions imposed by RO brine, is required for assessing the energy efficiency which is one of the main barriers of the MD technology [6]. In this context, the development of accurate theoretical (first principles-based) or empirical models, to predict the performance of MD processes is fundamental. Models not only allow designers to simulate and analyse MD systems under the required operating conditions [9-12], but can also be used for developing real time optimization strategies [13,14], or to develop optimization algorithms aimed at obtaining optimal designs of the application at hand [15].

The construction of first principles based models requires a total knowledge of the process to be modelled, and it is usually a laborious task. On the contrary, this knowledge is not as necessary to elaborate empirical models, but in this case a good selection of the dependent and independent variables, and a good design of experiments are needed. Additionally, in the case of MD systems, the difficulty in constructing theoretical models is greater as the different internal design of each module influences its performance. So, internal modifications of this theoretical models have to be done to adapt them to the different module designs, which in many cases are non-disclosed information. For that reason, the use of empirical models is a good option to obtain a mathematical expression in a relatively fast and simple way. Two of the most common empirical models used in the field of membrane sciences to visualize the operational space and to understand the system behaviour are RSM and ANN [16,17]. These models, also known as *black blox* models, are able to fit both linear and nonlinear multi-variable problems. It should be remarked that these kind of empirical models cannot be used to extrapolate the results to other systems, and they are only valid for the range of operation in which they have been

---

Table 1

Existing RSM modelling approaches in MD systems. AGMD is the Air-Gap membrane Distillation configuration, DCMD is the Direct Contact Membrane Distillation configuration, VMD is the Vacuum Membrane Distillation one, and SGMD is the Sweeping Gas Membrane Distillation configuration.

Reference	MD configuration	Inputs and ranges	Outputs
[30]	VMD	Feed inlet temperature (30–70 °C) NaCl concentration in feed solution (1–9%) Feed velocity (1–17 m/min) Module packing density (5–45%) Length-diameter ratio of module (3.3–16.7)	Water permeate flux (kg/(h·m²)) Water productivity per unit volume of module (kg/(h·m³)) Gained Output Ratio (GOR) Comprehensive index
[31]	-	Feed solution (0.4–0.9 L/min) Flow rate draw solution (0.3–0.7 L/min) Feed solution salt concentration (3–5 M)	Permeate salt concentration (g/L)
[12]	PGMD	Feed flow rate (400–600 L/h) Condenser inlet temperature (20–30 °C) Evaporator inlet temperature (60–80 °C)	Permeate flux (L/(h·m²)) STEC (kWh/m³)
[32]	AGMD	Hot feed inlet temperature (40–80 °C) Cold feed inlet temperature (10–50 °C) Feed conductivity (500–10000 μS/cm) Feed flow rate (4–8 L/min)	Permeate flux (kg/(h·m²)) Specific performance ratio
[18]	AGMD	Feed flow rate (1–5 L/min) Feed temperature (60–80 °C) Coolant temperature (60-80 °C) Coolant flow rate (1–3 L/min) Air gap width (3–7 mm)	Permeate flux (L/(h·m²))
[19]	DCMD	Feed temperature (46.6–63.4 °C) Permeate temperature (6.6–23.4 °C) Feed flow rate (199–451 L/h) Permeate flow rate (199–451 L/h)	Permeate flux (kg/(h·m²))
[25]	DCMD	Feed inlet temperature (40–80 °C) Permeate inlet temperature (15–35 °C) Flow velocity of feed solution (6–54 m/min) Module packing density (5–45 %) Length-diameter ratio of module (2.9–8.35)	Average permeate flux (kg/(h·m²)) Production per unit volume of module (kg/(h·m³)) Production per unit energy consumption (kg/kJ) Comprehensive index
[20]	VMD	Feed temperature (25–55 °C) Vacuum pressure (10–90 mbar) Feed flow rate (15–60 mL/s) Feed concentration (100–300 g/L)	Permeate flux (kg/(h·m²))
[26]	AGMD	Cold feed inlet temperature (23.2–56.8 °C) Hot feed inlet temperature (58.5–91.8 °C) Feed inlet flow rate (23.7–84.3 L/h)	Permeate flux (L/(h·m²)) GOR
[21]	DCMD	Vapor pressure difference (3.5–35.5 10³Pa) Permeate flow rate (5.2–28.8 L/h) Feed flow rate (6.4–73.6 L/h) Feed ionic strength (21.4–338 mM)	Permeate flux (L/(h·m²))
[22]	AGMD	Cooling inlet temperature(13.9–26.1 °C) Feed inlet temperature(59–71 °C) Feed flow rate (145–205 L/h)	Specific performance index (kg/kWh)
[9]	SGMD	Water inlet temperature (58–72 °C) Air inlet temperature (17.2–22.8 °C) Water circulation velocity (0.16–0.25 m/s) Air circulation velocity (1.03–2.13 m/s)	Permeate flux (kg/(s·m²))
[23]	DCMD	Hot fluid flow rate (1–4 10⁻²kg/s) Hot fluid temperature (45.2–84.74 °C) Cold fluid flow rate (1.5–4 10⁻²m³/s) Membrane thickness (30–150 μm)	Recovery ratio (%)
[23]	AGMD	Hot fluid flow rate (1.72–4.17 10⁻²kg/s) Hot fluid temperature (45–75 °C)	Recovery ratio (%)
[24]	DCMD	Stirring velocity (88.2–786.8 rpm) Feed temperature (22.3–52.7 °C) NaCl concentration (0.007–2.193 M)	Permeate flux (m/s)

calculated.

RSM is a statistical method extensively used for characterizing membrane distillation systems. This methodology is an efficient modelling tool providing quadratic functions to fit responses in linear or smooth nonlinear processes. As can be seen in Table 1, most works presented until now in the literature use RSM in order to optimize MD systems in terms of two of the most important parameters in this technology: permeate production and thermal energy efficiency. However, not all works treat these two parameters in a simultaneous way [9, 18-24]. In addition, in most papers the feed water salt concentration, one of the most important parameters influencing the performance of MD systems, is not taken into account as an input of the model [9,12,18,19,22,23,25,26].

ANN is an emerging modelling tool in the field of MD systems. The main advantage of this methodology is that it is able to fit almost all nonlinear processes. Besides, the way in which the model is built allows retraining the model with further experimental data for improving predictions. Table 2 summarizes the proposals made up to now in the literature for modelling MD systems by means of ANN based models. As can be seen, almost all the works use ANN for characterizing only the permeate production of a MD unit [10,11,14,27,28], and only Shibazian and Alibabaei [29] consider also the thermal energy. Furthermore, the feed water salt concentration is only considered by Cao et al. [27] and Tavakolmoghadam and Safavi [28].

The goal of this work is to develop empirical models able to predict, in a precise way, the performance of a commercial-scale PGMD module

Table 2

Existing ANN modelling approaches in MD systems. All the approaches used Multi-Layer feedforward Perceptron Networks.

Reference	MD configuration	Inputs and ranges	Outputs	Topology
[29]	AGMD	Cold inlet temperature (23.2–56.8 °C) Hot feed inlet temperature (65–91.8 °C) Feed-in flow rate (36–84.3 L/h)	Permeate flux (L/(h·m^2)) Cold outlet temperature (°C) GOR	-
[27]	VMD	Feed inlet temperature (60–70.44 °C) Vacuum pressure (0.037–0.089 MPa) Feed flow rate (69.89–111 L/h) Feed water salt concentration (30–45 g/kg)	Permeate flux (kg/(s·m^2))	4:3:1
[14]	PGMD	Feed flow rate (L/h) Cold inlet temperature (°C) Irradiance (W/m^2)	Permeate flow rate (L/h)	3:5:1
[11]	SGMD	Feed inlet temperature (54–68 °C) Air flow rate (0.966–2.028 m/s) Feed flow rate (0.140–0.206 m/s)	Permeate flux (kg/(s·m^2))	3:9:1
[10]	AGMD	Air gap thickness (3.0–7.4 mm) Cold inlet temperature (13.9–26.1 °C) Feed inlet temperature (30–71 °C) Feed flow rate (145–205 L/h)	Permeate flux (kg/(s·m^2))	4:10:1
[28]	VMD	Vacuum pressure (10–80 mbar) Feed temperature (25–55 °C) Salt concentration (50–300 g/L) Feed flow rate (15–60 mL/s)	Permeate flux (kg/(s·m^2))	4:3:1

for desalting RO brines. For this purpose, three main objectives are developed: i) obtaining empirical forecasting models based on RSM and ANN, under the required operating conditions, ii) comparing the prediction abilities of the two modelling approaches, and iii) finding the optimal operating conditions of this module for two of the salinity concentrations that can be reached when desalting RO brines, 70 and 105 g/L. Compared to most modelling approaches presented until now in the literature (see Tables 1 and 2), in this work, both the permeate production and the thermal energy consumption were selected as predicted performance parameters. In addition, apart from the typical independent variables considered in this technology (condenser inlet temperature, evaporator inlet temperature, and feed flow rate), the feed water salt concentration (35–140 g/L) has been used as an input, in order to visualize the effect of this parameter in the responses. It should be pointed out that most of the studies presented in the literature use bench-scale modules, whereas this study has been performed using a commercial-scale module, which can be very relevant to commercial purposes.

2. Methodology

2.1. Test-bed facility

In this study, a spiral wound MD commercial module called Oryx 150 was evaluated (see Fig. 1-b). The module was designed by the Fraunhofer Institute for Solar Energy systems and is marketed by the company Solar Spring (Freiburg, Germany). It had a Permeate Gap Membrane Distillation (PGMD) configuration. The location of the different channels of the module was placed to minimize heat losses to the environment. All inlets and outlets were located at the top of the module. The permeate outlet was located on the outer perimeter of the coil to facilitate the recovery of sensible heat from the permeate. This module had a length, a height and a channel width of 7 m, 0.7 m and 3.2 mm respectively. The membrane surface area was 10 m^2. The membrane used in the module was a commercial membrane of W. L. Gore Associates. The membrane was constituted by an active Polytetrafluoroethylene (PTFE) layer with a nominal pore size of 0.2 μm, a thickness of 70 μm and a porosity of 80% and a support of Polypropylene (PP) with a thickness of 280 μm and a porosity of 50%. The spacers were made of Low-Density Polyethylene (LDPE) and the condensation foil was made of Ethylene Tetrafluoroethylene (ETFE). The permeate gap was created by a PP spacer of 1 mm. The Oryx 150 module was integrated into a structure that was formed by a feed tank (475 L), a filter of 300 μm placed after the outlet of the feed tank and before the inlet of the MD module, the pump to circulate the feed solution, a deaerator and the heat exchanger. Four PT100 temperature sensors were placed directly at the inlet of the evaporator and condensation channels and at the outlets of them (see Fig. 2). The fifth temperature sensor was located at the inlet of the heat exchanger on the side of the heating fluid (see Fig. 2). The volumetric flow rate (F in Fig. 2) was measured with a flow meter placed before the inlet of the condenser channel. A pressure sensor (WIKA) was located at the inlet of

(a) SMD facility. (b) Solar Spring pilot module.

Fig. 1. Test-bed facility at Plataforma Solar de Almería (PSA).
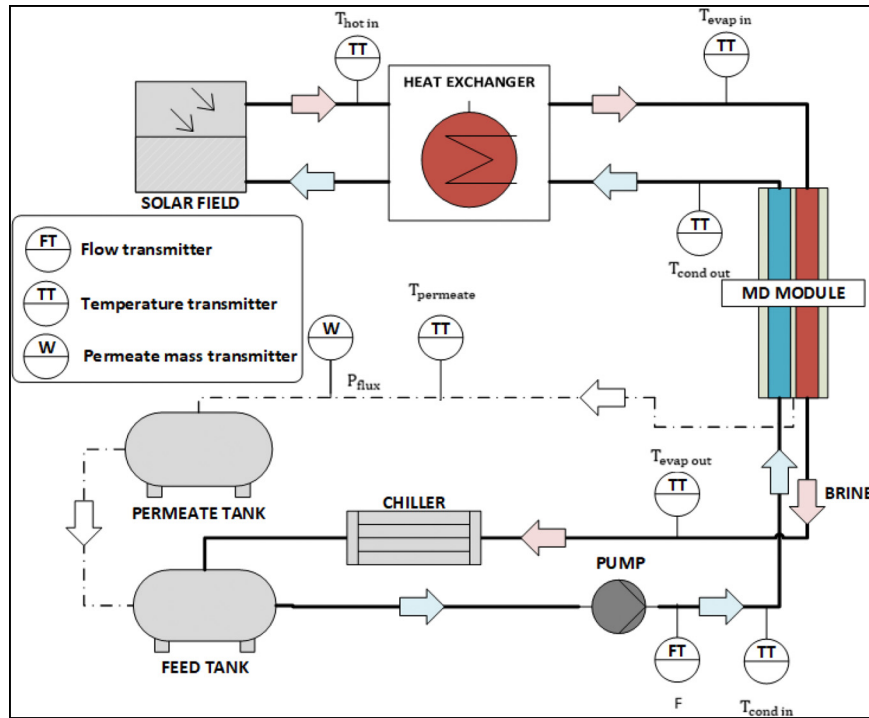
Fig. 2. Schematic diagram of the test-bed facility.

the condenser channel to avoid overpressure. The permeate was measured with a weight (W in Fig. 2), using a tank to collect the permeate, and then, returning it to the feed tank. All the temperature and pressure measurements were monitored and registered by a Supervisory Control And Data Acquisition (SCADA) system connected through a Programmable Logic Controller (PLC).

The MD module was tested in the Solar Membrane Distillation (SMD) pilot facility of Plataforma Solar de Almería (PSA, www.psa.es) (see Fig. 1-a). In this facility, the module was connected to a solar field through a heat exchanger. The solar field was formed by 10 flat plate collectors (Solaris CP1 Nova, Solaris, Spain) divided into two files with 5 collectors each one. The nominal thermal power supplied was 7 kW$_{th}$ at a temperature of 90 °C. The heat rate supplied to the heat exchanger was controlled by means of the feedback control structure presented in [33].

The operation of the MD system consisted of pumping the cold feed solution to the condenser inlet. The low temperature of the feed solution helped the condensation of the permeate. The circulation of the feed solution along the condensation channel allowed preheating the solution thanks to the latent heat of condensation and to the sensible heat that crossed the membrane. After leaving the condensation channel, the solution passed to the deaerator to eliminate the non-condensable gases from the feed solution and later it was circulated towards the inlet of the heat exchanger. Afterwards, the hot feed went into the evaporator channel and circulated countercurrent with respect to the circulation in the condensation channel. As the feed circulated along the evaporator channel, the vapour passed through the pores of the membrane driven by the vapour pressure difference created on both sides of the membrane due to the temperature difference. The concentrated feed solution (brine) left the module through the outlet of the evaporator channel and was poured into the feed tank for recirculation. Since the brine had a temperature above that of the feed solution, it was cooled down with a chiller.

2.2. Thermal energy performance metric

The thermal efficiency of the distillation process can be evaluated

by means of several metrics, being the Specific Thermal Energy Consumption (STEC), the one adopted in this work, one of the most employed [12,34-36]. This metric provides the thermal energy required per volume unit of distillate, and it can be calculated as follows:

$$STEC(kWh/m^3) = \frac{F \cdot \rho_{feed} \cdot c_p \cdot (T_{evap\,in} - T_{cond\,out})}{c \cdot D},$$

(1)

where c is a conversion factor (3.6· 10^6 s·W/(h·kW)), ρ_{feed} is the feed water density (kg/m^3), c_p is the heat water capacity (J/(kg·°C)), D is the permeate flow rate (L/h), and the rest of variables are according to Fig. 2.

2.3. Response Surface Methodology (RSM)

RSM is a set of mathematical and statistical techniques based on the fitting of empirical models to the experimental data obtained through an experimental design. The RSM procedure consists of the development of a linear or quadratic polynomial function that adjusts the response (permeate production, energy efficiency and so on) depending on the operating conditions (temperatures, flow rates and so on). Therefore, polynomial functions are used to describe the studied system and consequently, to explore (model and displace) the experimental conditions up to their optimization to achieve the best performance of the system [37].

The development of a RSM has several steps: (i) selection of the main variables that exert the highest effect on the system through the screening studies and the delimitation of the experimental region, in accordance with the goal of the study and the experience of the researcher; (ii) choice of an experimental design that defines which experiments should be carried out in the experimental region and conduction of the experiments according to the selected experimental matrix; (iii) mathematical-statistical treatment of the experimental data by adjusting a polynomial function (see Eq. (2)); (iv) evaluation of the validity of the model.

$$y = \beta_0 + \sum_{i=1}^{k} \beta_i \cdot x_i + \sum_{i=1}^{k} \beta_{ii} \cdot x_i^2 + \sum_{1 \le i < j}^{k} \beta_{ij} \cdot x_i \cdot x_j,$$

(2)

where k is the number of variables, β_0 is the offset term coefficient, β_i represents the coefficients of the linear effects, x_i and x_j represent the variables, β_{ij} represents the coefficients of the interaction of effects, and β_{ii} represents the coefficients of the quadratic parameters. To estimate the coefficients of the equation, the experimental design must ensure that all the studied variables are carried out for at least three levels of each variable. Among the most used second order designs are the three-level factorial design, the Box-Behnken design and the central composite design. These designs differ from each other in their selection of experimental points, number of levels for the variables and number of executions. In particular, central composite design is a fractional factorial or factorial design with extended central points with a group of axial points also called star points. So, for example, to optimize a process with three variables ($k = 3$), the first block is a factorial 2^3, the second block is a set of 2×3 tests and the third blocks are repetitions in the center [38]. There are three types of central composite design, specifically, circumscribed, inscribed and face-centred central composite. In the last one, the star points are the centre of each face of the vector space, so this variety requires only three levels of each factor. After the experimental plan proposed by the design has been carried out and the values of the responses have been obtained for each experimental point, it is necessary to evaluate the quality of the adjusted model by applying the ANOVA [39]. With the ANOVA, the variation due to the treatment (change in the combination of the levels of the variables) is compared with the variation due to the random errors inherent in the measurements of the generated responses. From this comparison, it is possible to evaluate the significance of the regression used to predict the answer.

2.4. Artificial Neural Network (ANN)

An ANN is also a mathematical model which is composed of simple interconnected elements, that process information in response to external inputs, trying to imitate the behaviour of biological neural networks. These simple elements, called neurons, are computational processors in which three main operations (see Fig. 3) are carried out [40,41]:

1. The n-element input vector (z_1, z_2, ...z_n) is multiplied by weights ($w_{1,1}$, $w_{1,2}$, ...$w_{1,n}$).
2. In the summing junction, the weighted inputs are added together with the bias vector b, obtaining the argument a:

$$a = z_1 \cdot w_{1,1} + z_2 \cdot w_{1,2} + ... + z_n \cdot w_{1,n} + b. \tag{3}$$

3. Finally, the argument a is converted into a scalar value *Out* by means of the transfer function f (see Fig. 3):

$$Out = f(\mathbf{zW} + b). \tag{4}$$
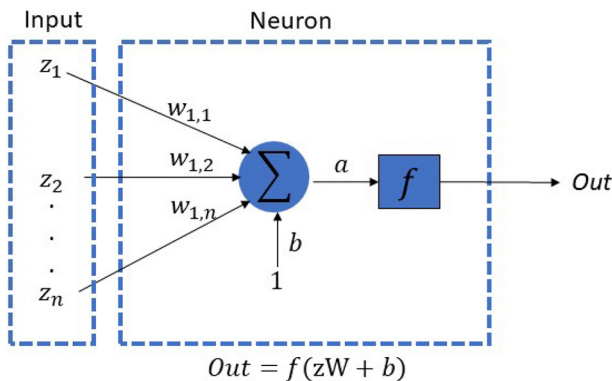
Fig. 3. Schematic diagram of an artificial neuron.

In the transfer function block (f in Fig. 3), several functions can be employed, two of the most adopted being the linear (*purelin*) and the log-sigmoid (*logsig*) transfer functions [40,41]. Thus, the outputs of neurons calculated by these transfer functions can be expressed as:

$$\text{Purelin} \quad : Out = f(a) = a, \tag{5}$$

$$\text{Logsig} \quad : Out = f(a) = \frac{1}{1 + e^a}. \tag{6}$$

The form in which neurons are grouped and connected is known as topology or architecture of the neural network. In general, neurons are grouped in different layers such as hidden and output layers. Moreover, the inputs can be treated as an additional layer. Between the different kinds of architectures, one of the most used to perform function fitting is the Multi-Layer feedforward Perceptron (MLP) [42]. In this architecture, the number of inputs and outputs of the network is defined according to the number of input and output variables of the system to be modelled. On the other hand, the optimal selection of the number of layers, and the number of neurons required in each layer, is still an active research area and it is usually obtained by trial and error. In practice, most neural networks have only two or three hidden layers [42].

Once the architecture of the network is chosen, the weights and biases are adjusted by means of a training algorithm. Back Propagation (BP) algorithm is the most commonly employed for training MLP networks [10,11,17,42]. This algorithm tries to minimize a performance function by iteratively adjusting network weights and biases. The index used as performance function in this work is the Root Mean Square Error (RMSE):

$$\text{RMSE} = \sqrt{\frac{\sum_{i=1}^{M} \sum_{j=1}^{N} (Y_{i,j} - \hat{Y}_{i,j})^2}{M \cdot N}}, \tag{7}$$

where M is the number of network outputs, N is the number of data used for training, and $Y_{i,j}$ and $\hat{Y}_{i,j}$ are the experimental and predicted responses respectively. Thus, in each iteration BP algorithm modifies weights and biases in the direction in which RMSE decreases. One iteration of this algorithm is given by [42]:

$$\lambda_{k+1} = \lambda_k - \delta \Delta_k, \tag{8}$$

where λ_k is a vector containing current network weights and biases, δ is the learning rate, Δ_k is the current gradient of RMSE function, and k being the iteration number.

2.5. Multi-objective optimization

The space of solutions of the RSM model can be easily explored by a conventional gradient-based optimization method, as it is quadratic. However, the ANN model does not guarantee a linear or smooth nonlinear solution space to be explored. Therefore, other global techniques such as genetic-based algorithms should be considered. In this work, a multi-objective evolutionary algorithm NSGA-II was employed to carry out the optimization. NSGA-II is a fast and elitist optimizing approach which stands out for obtaining spread solutions near the optimal Pareto Front. In general, the algorithm can be roughly divided in the following steps:

1. Creation of an initial population randomly selected according to the problem and constraints
2. Non-dominated sorting of the population initialized previously
3. Calculation of the crowding-distance
4. Selection of individuals based on a crowded-comparison operator
5. Use crossover and mutation operators to generate a new population

All the steps are widely explained in [43]. The optimization was

Table 3
Input model variables.

Variable	Nomenclature	Range
Evaporator inlet temperature (°C)	T_{evap}	60–80
Condenser inlet temperature (°C)	T_{cond}	20–30
Feed flow rate (L/h)	F	400–600
Feed water salt concentration (g/L)	S	35–140

carried out with Matlab R2018a (the Mathworks, USA). The population size of the algorithm was fixed at 10, the maximum number of iterations at 500, and the convergence tolerance was 1e-100.

3. Results and discussion

3.1. Response Surface Methodology based model

RSM was used to characterize the performance of MD module through the specific thermal energy consumption (STEC) and permeate flux (P_{flux}), as a function of the main parameters that affect the performance in this technology, which are summarized in Table 3. Notice that the variables have been selected according to the allowed operational limits of the module [12], since the objective is to perform a realistic study in commercial-scale. After choosing the variables, the Design of the Experiment (DoE) was carried out with Statgraphics centurion, a highly specific multivariate analysis package. The chosen design to obtain the experimental campaign was the Face-centred Central Composite (CCF) design which required three levels of each of the variables. The data proposed by the CCF design for modelling are presented in Appendix A.

After carrying out the experimental campaign and introducing the experimental values of the responses of interest, the experimental design was analysed. The ANOVA analysis was used to verify if the regression equations were statistically valid. The statistical parameters used to evaluate the goodness of the fit was the p-value, the coefficient of determination (R^2) and the adjusted coefficient of determination (adjusted-R^2). Specifically, the p-value was used to determine which terms of the equation were statistically significant. For that, the p-value was compared with the level of significance to decide which terms were excluded from the final model. A value of 0.05 was used for the level of significance, meaning that if the p-value was lower than 0.05, the coefficient was significantly different from zero with a confidence level of 95%. Therefore, the coefficients with a p-value higher than 0.05 were not included in the final equations. Table 4 shows the p-values of the coefficients for both responses (STEC and P_{flux}). Thus T_{evap}, T_{cond}, F, S, T_{evap}·F, T_{evap}·S, T_{cond}·S, F·S and S^2 were significant for Pflux while for

Table 4
Values of the regression coefficients and their statistical significance.

Terms	$P_{flux}(L/(h·m^2))$		STEC(kWh/m³)	
	Coefficient	P-value	Coefficient	P-value
T_{evap}	0.039820	0.0000	−75.525	0.0006
T_{cond}	−0.000171	0.0000	105.672	0.0505
F	0.002683	0.0000	−6.079	0.1223
S	-0.010709	0.0000	26.804	0.0000
T_{evap}^2	−0.000065	0.7800	0.613	0.5504
T_{evap}·T_{cond}	−0.000063	0.7383	−1.365	0.1147
T_{evap}·F	0.000062	0.0000	0.059	0.1651
T_{evap}·S	−0.000208	0.0000	−0.273	0.0042
T_{cond}^2	−0.000181	0.8463	0.613	0.8804
T_{cond}·F	0.000006	0.7383	−0.113	0.1838
T_{cond}·S	−0.000107	0.0104	0.368	0.0336
F^2	−0.000004	0.1374	0.005	0.5966
F·S	−0.000009	0.0002	−0.014	0.0758
S^2	0.000132	0.0000	−0.024	0.5127

Table 5
Goodness of the adjustment of the simplified models of P_{flux} and STEC.

Statistical estimator	Condition for a good fit	P_{flux}	STEC
P-value	≤ 0.05	≤ 0.01	≤ 0.02
R^2	Closed to 1	0.998	0.704
Adjusted-R^2	In agreement with R^2	0.996	0.664

STEC, only T_{evap}, S and T_{evap}·S were statistically significant. Non-significant terms were removed from the model to obtain the simplified equations for both Pflux and STEC:

$$P_{flux} = -0.8868 + 0.0291·T_{evap} - 0.0104·T_{cond} - 0.0008·F$$
$$- 0.0087·S + 0.000061·T_{evap}·F - 0.0002·T_{evap}·S$$
$$- 0.0001·T_{cond}·S - 0.000009·F·S + 0.0001·S^2 \quad (9)$$

$$STEC = -317.712 + 5.874·T_{evap} + 24.296·S - 0.273·T_{evap}·S \quad (10)$$

The simplified equations were also subjected to an analysis of variance. Table 5 shows the values of the statistics for the simplified models for P_{flux} and STEC. The p-value and the coefficients of determination determined a good fit for Pflux but the R^2 and adjusted-R^2 were low for the STEC. The comparison between the observed values and the adjusted values by the models is shown in Fig. 4. An excellent fit can be observed between the experimental and predicted responses for P_{flux} (see Fig. 4-1). On the other hand, the adjustment in the STEC response is not so good (see Fig. 4-2), as expected in view of the results of the ANOVA. Notice that the RSM model is composed of linear, interaction and quadratic terms, which are good at adjusting linear or quadratic behaviours, however it provides unsuccessful fitting when it comes to nonlinear behaviour, as the one obtained by the feed water salt concentration influence on the STEC. When the feed water salt concentration is not taken into account as an input of the model, RSM provides satisfactory adjustments [12].

3.2. Neural Network based model

The Neural Network based model was developed considering as inputs S, T_{cond}, T_{evap} and F (see Table 3), and as outputs P_{flux} and STEC. In this case, the data used in the RSM method were complemented with more samples. It should be remarked that, although DoE ensures data well distributed throughout all the input data range, the ANN model, which is exclusively data-based, can present abrupt nonlinearities in the responses if the amount of data is not large enough, and if the data set is not well distributed. This fact can be especially significant when the range of the input data is large, and some of these parameters have a clear nonlinear influence on the responses, as is the case of feed water salt concentration in this study. Thus, Appendix A shows all the experimental data. Besides, it should be commented that, as in the case of experimental data used in RSM model, four measurements were taken for each experimental point.

The experimental data set was divided in 3 subsets: i) training subset (75% of samples), ii) validation subset (20% of samples), and iii) test subset (5% of samples). Moreover, in order to avoid overfitting during the training process, both the input and output variables were normalized in the range 0.1–0.9 by means of the following expression [10]:

$$y_n = (1 - U - L)·\frac{y_k - y_{min}}{y_{max} - y_{min}} + L, \quad (11)$$

where y_n is the normalized sample, y_k is the actual sample, y_{max} and y_{min} are the maximum and minimum values of the variable to be normalized, and U and L are the upper and lower bounds considered to define the output network range ($U = L = 0.1$).

The training process was accomplished in the Neural Network Toolbox of MATLAB, using the Lavenberg-Marquardt BP algorithm

Fig. 4. Comparison between predicted values by RSM model ($STEC_{pred}$ and $P_{flux,pred}$) and experimental data ($STEC_{exp}$ and $P_{flux,exp}$).

[40]. Several ANN architectures were tested varying the number of hidden layers between 1 and 3 and the number of neurons in each layer between 1 and 10. The transfer function adopted in the hidden layers was the *logsig*, whereas the one employed in the output layer was the *purelin*. The optimal architecture was selected according to the performance function (RMSE).

The optimal ANN model (see Fig. 5) is composed of 4 inputs, two hidden layers containing 7 and 2 neurons respectively, and two outputs. This feedforward neural network topology can be described as MLP (4:7:2:2). Notice that the training process was iteratively performed (as was mentioned in Section 2.4) until reaching a RMSE sufficiently small, according to the imposed goal for the training subset ($RMSE \leq 5 \cdot 10^{-4}$, normalized value according to Eq. (11)). In the optimal network case, the training process was stopped after 13 iterations obtaining a $RMSE = 2.61 \cdot 10^{-4}$ for the training data subset, while the RMSE of the validation and test subsets was lower than $1 \cdot 10^{-3}$. Table 6 summarizes the optimal values of network weights and bias in a matrix-vector format. The ANN model can be expressed as:

$$\widehat{Y} = \Phi^{(3)}(\mathbf{LW}^{(3,2)}\Phi^{(2)}(\mathbf{LW}^{(2,1)}\Phi^{(1)}(\mathbf{IW}^{(1,1)}\mathbf{x} + \mathbf{b}^{(1)}) + \mathbf{b}^{(2)}) + \mathbf{b}^{(3)}), \quad (12)$$

where $\Phi^{(i)}$ is the transfer function correspondent to layer i ($i = 1$-3), $\mathbf{L}$ $\mathbf{W}^{(2,1)}$ and $\mathbf{L}$ $\mathbf{W}^{(3,2)}$ are the layer weight matrices, where the superscripts

indicate the destination and source connections, $\mathbf{I}$ $\mathbf{W}^{(1,1)}$ is the input weight matrix, $\mathbf{x}$ is the network input, and $\widehat{Y}$ is the network output. It should be commented that the same notation has been employed in Table 6 and Fig. 5.

The fit between the experimental data used in the training and validation processes, and the predicted values by the ANN model are shown in Fig. 6. Besides, Table 7 shows the analysis of variance (ANOVA) for these two subsets. As can be observed, the obtained p-values (lower than 0.05) and coefficients of determination (close to 1) evidence the good fit obtained by ANN model in both cases P_{flux} and STEC. Notice that in the next subsection more experimental data will be used to test the performance of the ANN model.

3.3. Comparison between the prediction abilities of the two modelling approaches

In order to compare in the same conditions the prediction abilities of the RSM and ANN models, additional experimental data were employed (see Table 8). The comparisons were performed based on the Root Mean Square Error (RMSE), the coefficient of determination (R^2) and the adjusted-R^2.

Fig. 7 shows the correlation between the additional experimental

Fig. 5. Schematic diagram of the optimal network architecture. x_1, x_2, x_3 and x_4 are S, T_{cond}, T_{evap} and F, while $\widehat{Y}_1$ and $\widehat{Y}_2$ are STEC and P_{flux}.

Table 6
Optimal network weights and bias.

Input weight matrix	$\mathbf{IW}^{(1,1)} = \begin{vmatrix} -1.441 & 0.890 & 0.372 & -2.015 \\ -1.528 & 1.047 & 0.516 & -2.105 \\ -0.831 & -0.541 & 0.926 & 0.213 \\ 2.115 & 1.427 & 0.796 & 0.612 \\ -1.957 & 0.117 & 0.139 & -0.472 \\ 0.023 & -0.053 & 0.177 & 0.210 \\ -0.698 & 0.842 & 1.351 & -0.953 \end{vmatrix}$
Hidden layer 1 bias vector	$\mathbf{b}_{(1)} = \begin{vmatrix} 2.148 \\ 2.269 \\ 2.840 \\ -0.788 \\ -1.478 \\ -0.042 \\ -4.384 \end{vmatrix}$
Hidden layer 2 weight matrix	$\mathbf{LW}^{(2,1)T} = \begin{vmatrix} -0.610 & -0.593 \\ 0.450 & 0.461 \\ -1.086 & -0.257 \\ -0.011 & 0.049 \\ -0.593 & -0.408 \\ -0.974 & -1.613 \\ -0.280 & 0.467 \end{vmatrix}$
Hidden layer 2 bias vector	$\mathbf{b}_{(2)} = \begin{vmatrix} -0.680 \\ 1.162 \end{vmatrix}$
Output layer weight matrix	$\mathbf{LW}^{(3,2)} = \begin{vmatrix} 1.860 & -0.030 \\ -0.094 & -1.518 \end{vmatrix}$
Output layer bias vector	$\mathbf{b}_{(3)} = \begin{vmatrix} 0.844 \\ 0.398 \end{vmatrix}$

Table 7
Goodness of the adjustment of ANN model.

	P_{flux}		STEC	
	Training	Validation	Training	Validation
P-value	≤ 0.01	≤ 0.01	≤ 0.01	≤ 0.01
R^2	0.994	0.991	0.993	0.990
Adjusted-R^2	0.993	0.990	0.992	0.989

Table 8
Additional experimental data used to compare the two modelling approaches.

S (g/L)	T_{cond}(°C)	T_{evap}(°C)	F(L/h)	STEC(kWh/m^3)	P_{flux}(L/(h·m^3))
35	20	75	600	297.563	2.303
35	25	75	400	246.323	1.568
35	30	65	500	286.500	1.311
60	20	65	600	506.388	1.141
60	25	65	500	535.293	0.756
60	30	65	400	453.794	0.580
60	30	75	600	368.303	1.524
140	20	75	500	499.528	1.054
140	25	65	600	678.193	0.736
140	30	65	400	1172.35	0.214

data and the predicted values, and Table 9 shows the performance metrics. On the one hand, in the case of the permeate flux (P_{flux}), the R^2 and the adjusted-R^2 values obtained with both models were similar (very close to 1, see Fig. 7), whereas the obtained RMSE error was 0.06 and 0.10 (L/(h·m^2)) for the ANN and RSM model respectively, which

evidences the good results obtained with both models. On the other hand, in the STEC case, the R^2 and the adjusted-R^2 values obtained with the ANN model were 0.982 and 0.981 respectively, whereas the ones obtained with the RSM model were 0.770 and 0.742 respectively. The RMSE of the ANN model was 27.01 (kWh/m^3) while the RMSE of the
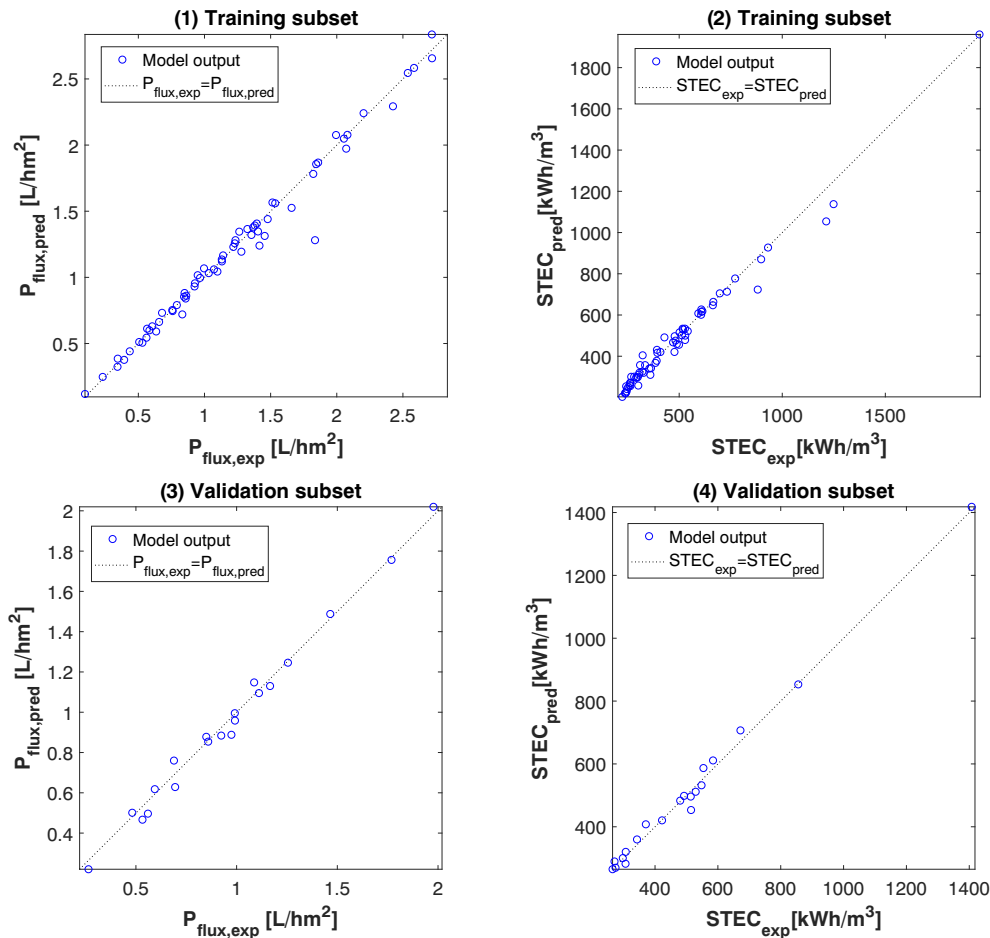
Fig. 6. Comparison between predicted values by ANN model (STEC$_{pred}$ and P$_{flux,pred}$) and experimental data (STEC$_{exp}$ and P$_{flux,exp}$).
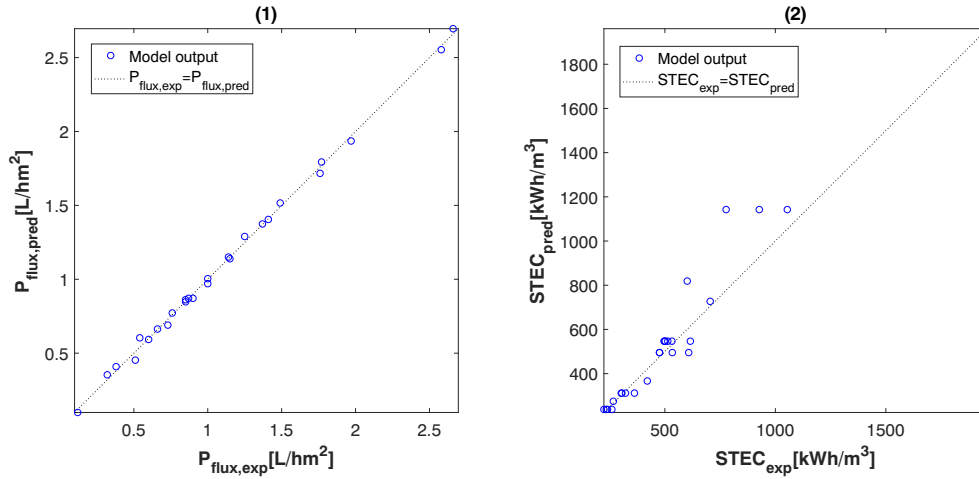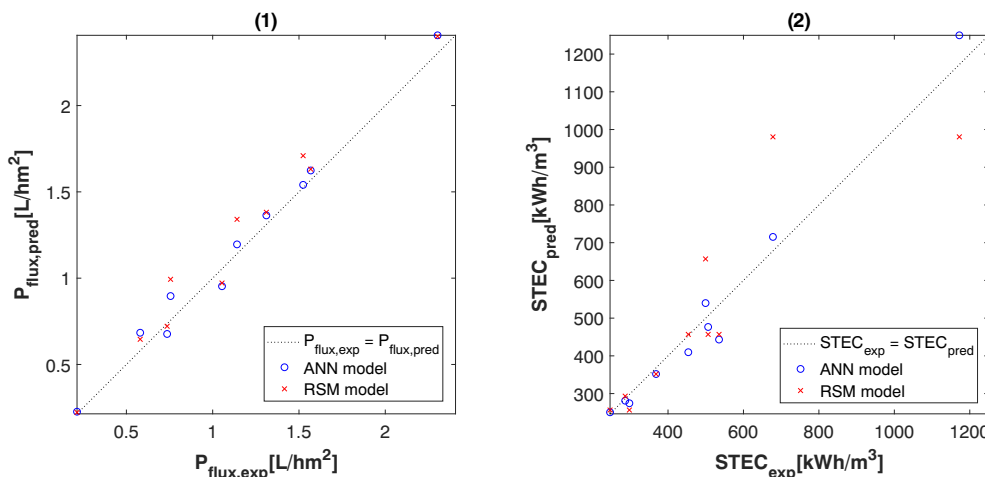
Fig. 7. Comparison between predicted values of both models ($STEC_{pred}$ and $P_{flux,pred}$) and experimental data ($STEC_{exp}$ and $P_{flux,exp}$).

Table 9
Comparison of predictive abilities of RSM and ANN.

	RSM		ANN	
	STEC	P_{flux}	STEC	P_{flux}
RMSE	85.70	0.10	27.01	0.06
R^2	0.770	0.985	0.982	0.988
Adjusted-R^2	0.742	0.984	0.981	0.987

RSM model was 85.70 (kWh/m³). It should be taken into account that the low grade of adjustment obtained by the RSM model in the STEC case can be explained for two main reasons: (1) the nonlinear behaviour of STEC with respect to feed water salt concentration, and (2) the simplified equation modelling STEC does not consider the influence of T_{cond} and F in the responses, hence it adds uncertainty to the model (see Eq. (10)). Thus, it can be concluded that the ANN model is more suitable for predicting STEC, especially when working at high feed water salt concentration.

In addition to the comparison carried out previously, 3D response surfaces were displayed to observe the influence of the feed water salt concentration in both P_{flux} and STEC, and also to compare the surfaces provided by RSM and ANN models. It should be taken into account that the influence of the rest of input variables was studied in [12]. Thus, Figs. 8 and 9 show the 3D response surfaces for RSM and ANN models respectively.

On the one hand, the influence of the feed water salt concentration and the other input variables (T_{evap}, T_{cond} and F) in the P_{flux} predicted by the RSM and ANN models respectively can be observed in Fig. 8-1, 3 and 5, and in Fig. 9-1, 3 and 5. It can been seen that P_{flux} decreases significantly with increasing feed water salt concentration. Notice that, the 3D response surfaces obtained by the two models were similar, due to P_{flux} being almost linear in all the input data range.

On the other hand, in Fig. 8-2, 4 and 6, and in Fig. 9-2, 4 and 6 the effects of S, T_{evap}, T_{cond} and F on the STEC predicted by the RSM and ANN models are shown. In this case, the opposite behaviour than in P_{flux} can be observed, STEC augments when increasing feed water salt concentration. Therefore, an increase in the salinity implies a decrease in thermal efficiency. Besides, some differences can be seen in the 3D response surfaces of both models. RSM model provides almost linear surfaces for the whole input data range, whereas ANN model provides nonlinear surfaces which represent in a more accurate way the behaviour of STEC observed from experimental data (see Appendix A). In addition, ANN model takes into consideration the influence of T_{cond} and F in the response (see Fig. 9-4 and 6), whereas RSM model does not consider these variables (see Eq. (10)) as was commented before.

According to the results obtained, different interaction effects can be seen among the input variables. Considering T_{evap} and S, the increase of T_{evap} yields to an increase of the performance, namely, an increase of P_{flux} and a decrease of STEC, and this effect is stronger the higher the S values. The increase of S leads to a decrease of the performance and this effect is stronger for smaller T_{evap}. Regarding the interaction effect between F and S, an increase of F at different S values causes an enhancement of P_{flux}. However, the effect of increasing F on STEC depends on S. For a salinity value of 35 g/L, an increase of F causes a negative effect on STEC, while for high S values, an increase of F produces the contrary effect. This is because at high S and low F, the permeate production decreases at a higher rate than the decrease of the external heat necessary by working with a low F. Finally, the effect of T_{cond} on the P_{flux} is negative. An increase of this variable, yields to a decrease of the driving force, diminishing P_{flux} and this effect is stronger for high S. Regarding the STEC, at a salinity of 35 g/L, an increase of T_{cond} favours the decline of the STEC, however, at high S values, the increase of T_{cond} leads to an increase of STEC because the decrease of P_{flux} at high S is more pronounced.

From an optimization point of view, two interesting conclusions can be drawn. Firstly, in Fig. 9-6 it can be observed how STEC decreases at low F when S is in a low-medium range, and then, at high S, STEC has an almost curvilinear behaviour with respect to F where the minimum value is located around 500 L/h. Secondly, it can be observed that the STEC does not present large variations with respect to T_{evap} at low S, around 80 kWh/m³ at 500 L/h (see Fig. 9-1). However, at high salinity concentrations (i.e. 140 g/L), the influence is remarkable, around 500 kWh/m³ at 500 L/h (see Fig. 9-1). This fact can be very relevant in solar powered batch operations since the result of an optimization problem with a time horizon of 1 day could be: working at low T_{evap} at low salinity concentrations and storing thermal energy to be able to operate at high temperature, significantly improving performance, when high salinity ranges are reached.

3.4. Multi-objective optimization

Once the models were developed, validated and compared, a multi-objective optimization was carried out using NSGA-II algorithm. The objective was to find a set of solutions that ensure a trade-off between the two performance parameters (maximizing P_{flux} and minimizing STEC), that require contrary operating conditions in some variables such as T_{cond} and F. This set of optimal solutions is known as *Pareto Front* or *nondominant solutions*. Thus, two optimization cases were proposed according to the levels of feed water salt concentration that can be reached when performing batch operation for desalting RO brines. In the first optimization problem, the feed water salt
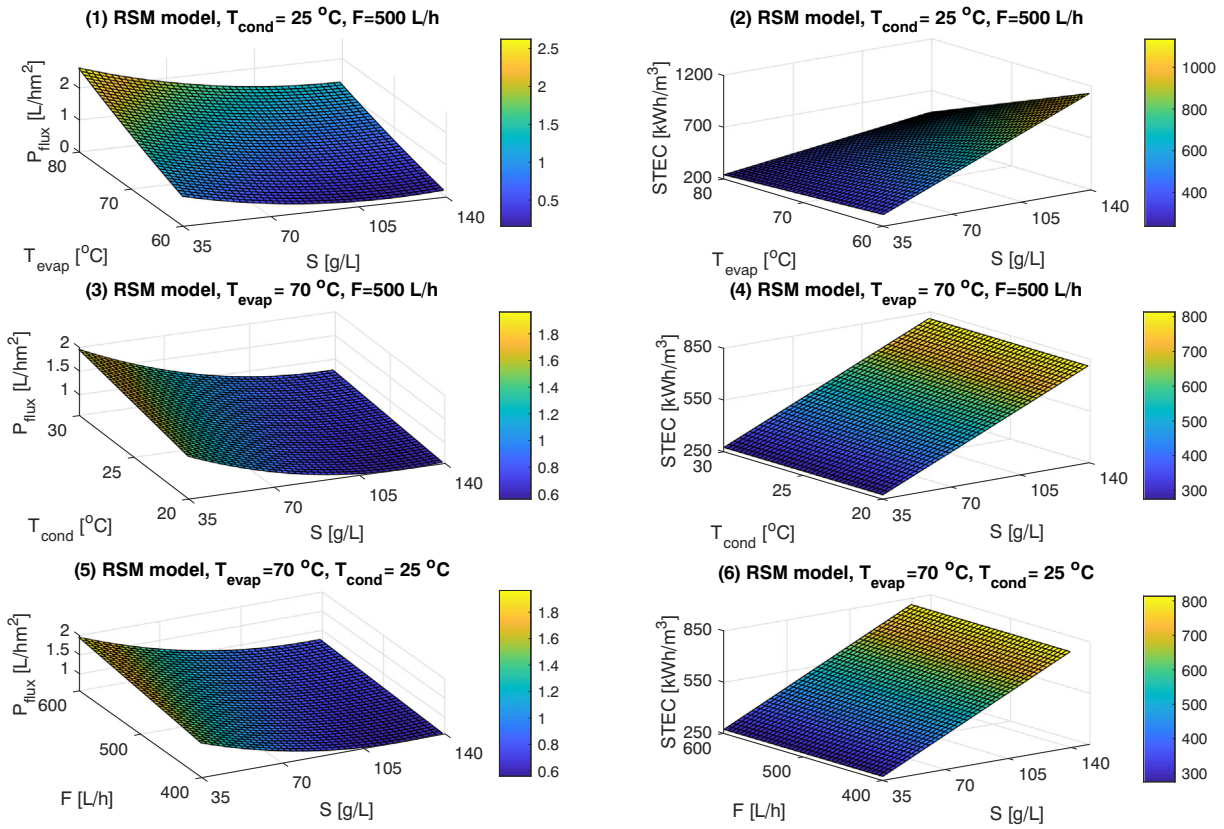
Fig. 8. 3D response surfaces obtained by RSM model.
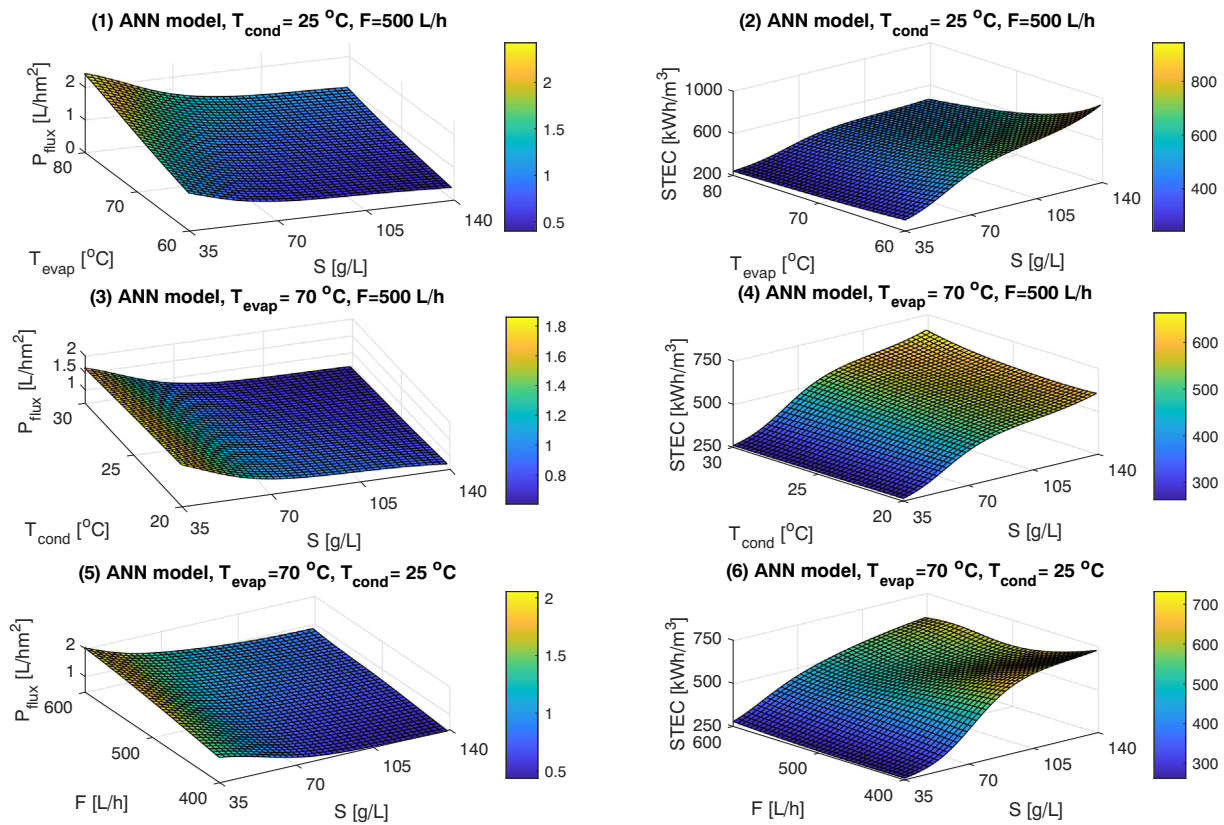
Fig. 9. 3D response surfaces obtained by ANN model.
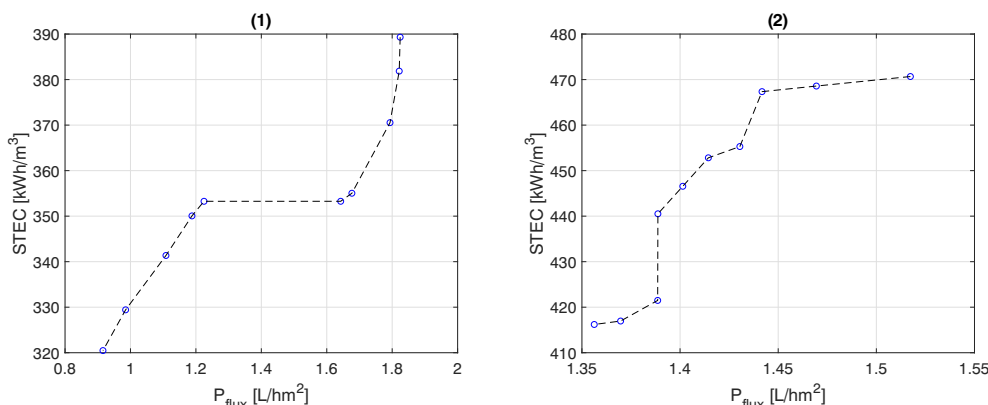
Fig. 10. Pareto fronts of the two optimization cases. (1) Results related to optimization problem 1, and (2) results related to optimization problem 2.

Table 10

Values of the Pareto fronts obtained by ANN model for both optimization problems.

Run	T_{cond}(°C)	T_{evap}(°C)	F(L/h)	$STEC_{pred}$ (kWh/m^3)	$P_{flux,pred}$ (L/(h·m^2))
Pareto front values of optimization problem 1					
1	20.00	80.00	600.00	389.31	1.83
2	20.31	80.00	577.04	381.85	1.82
3	21.09	80.00	557.45	370.53	1.79
4	28.81	80.00	599.86	355.03	1.67
5	30.00	80.00	597.49	353.26	1.64
6	26.64	80.00	436.35	353.26	1.22
7	26.84	80.00	426.97	350.05	1.18
8	26.85	80.00	401.38	341.36	1.10
9	29.67	80.00	412.29	329.42	0.98
10	30.00	80.00	400.00	320.47	0.91
Pareto front values of optimization problem 2					
1	20.00	80.00	600.00	470.67	1.51
2	21.02	80.00	598.73	468.58	1.46
3	21.49	80.00	595.28	467.35	1.44
4	20.62	80.00	556.64	455.28	1.43
5	21.11	80.00	557.07	452.81	1.41
6	21.40	80.00	548.95	446.56	1.40
7	21.33	80.00	532.78	440.51	1.38
8	30.00	80.00	600.00	421.48	1.38
9	29.86	80.00	585.48	416.96	1.36
10	30.00	80.00	580.10	416.20	1.35

Table 11

Validation of the optimal operating points.

Run in the optimization	$STEC_{pred}$ (kWh/m^3)	$P_{flux,pred}$ (L/(h·m^2))	$STEC_{exp}$ (kWh/m^3)	$P_{flux,exp}$ (L/(h·m^2))
Confirmation runs of optimization problem 1				
3	370.53	1.79	361.50	1.79
6	353.26	1.22	360.10	1.18
8	341.36	1.10	357.15	1.02
Confirmation runs of optimization problem 2				
1	470.67	1.51	474.97	1.48
4	455.28	1.43	456.08	1.46
5	452.81	1.41	454.38	1.40

concentration was fixed at 70 g/L, whereas in the second optimization problem, the feed water salt concentration was fixed at 105 g/L. Notice that the optimized variables in both cases are T_{cond}, T_{evap}, and F, since they can be easily manipulated to achieve the desired performance. The optimization was carried out using only the ANN model as it takes into account all the input variables for the two performance parameters, as was commented in the previous section. The results obtained for both optimization cases are reported in Fig. 10 and Table 10. In addition, three experimental runs randomly selected were performed in order to

validate the optimal points obtained in the two optimization problems (see Table 11).

Attending to the results, Table 10 shows that different operating conditions are required in some of the parameters depending on the level of feed water salinity. Notice that the pareto fronts must be analysed by assigning different importance for responses, according to the specific desirability of the application. In general, it can be seen that in the two studied cases, for applications that require higher distillate production it is better to operate with larger F and smaller T_{cond}. However, if the thermal efficiency is the decisive factor in the application, it is better to operate with smaller F and larger T_{cond} at the feed water salinity of 70 g/L. On the other hand, at the feed water salinity of 105 g/L, larger T_{cond} and larger F are required. It is also important to remark that in the two optimization problems, the inlet evaporator channel temperature is at the maximum (80 °C) for all the pareto solutions. Nevertheless, in real solar powered operations, this temperature will be limited by the irradiance conditions at every moment and, therefore, the optimal operating conditions can be obtained by modifying only T_{cond} and F. It should be pointed out that T_{cond} steadily increases when performing batch operations, but it could be manipulated using cooling devices in order to work in the optimal operating points, thus increasing MD module performance.

Moreover, Table 12 shows the salt rejection factor (SRF) for three of the studied salinities. For the three salinities, the SRF was close to 100%, confirming that in this case, in accordance with the MD fundamentals, the operating conditions do not affect the salinity of permeate [44].

4. Conclusion

Response Surface Methodology (RSM) and Artificial Neural Networks (ANN) were used for modelling the performance of a commercial-scale PGMD module, under the operating conditions required by one of its possible potential industrial implementation: desalting brines from RO plants. The independent variables chosen for the models were the condenser inlet temperature (20–30 °C), the evaporator inlet temperature (60–80 °C), the feed flow rate (400–600 L/h) and the feed water salt concentration (35–140 g/L), while permeate flux (L/(h·m^2)) and Specific Thermal Energy Consumption (STEC, kWh/m^3) were selected as predicted variables. The prediction abilities of the two

Table 12

Salt rejection factor for each salinity.

S (g/L)	T_{cond}(°C)	T_{evap}(°C)	F(L/h)	SRF (%)
35	20.00	80.00	583.00	99.99%
60	21.10	80.00	558.00	99.99%
140	20.60	80.00	557.45	99.99%

modelling tools were compared with further experimental data. In addition, the optimal operating conditions (maximizing and minimizing P_{flux} and STEC respectively) for two of the feed salinity concentrations (70 and 105 g/L) that can be reached when performing batch operation for desalting RO brines were determined.

Regarding the models, the ANN model achieved higher accuracy in predicting the responses, especially in the STEC case. This fact can be explained since the feed water salt concentration affects the STEC on a nonlinear way, which cannot be well represented by a quadratic equation. Therefore, ANN model is shown to be more adequate than RSM for developing models in which the feed water salt concentration is considered as an input. However, it should be also commented that it required more experimental data.

The multi-objective optimization carried out revealed that, depending on the level of feed water salinity, different operating conditions are required in some of the parameters. Therefore, real time multi-objective optimization could be essential for performing batch operations aimed at desalting RO brines, especially when the MD facility is powered by solar energy.

In the future works, the models presented in this paper will be used for developing optimization algorithms able to perform optimal designs of a solar powered MD facility to be integrated in a RO plant. In the same way, models will be used for optimizing the solar powered operation of the MD module in batch mode operation.

Acknowledgements

Appendix A. Experimental data

Table 13
Experimental data used for RSM and ANN modelling.

Run	ANN subset	Used in RSM	S (g/L)	T_{cond}(°C)	T_{evap}(°C)	F(L/h)	STEC(kWh/m^3)	P_{flux} (L/(h·m^2))
1	Validation	Yes	35	20	60	400	300.305	0.995
2	Training	No	35	20	70	400	369.411	1.440
3	Training	Yes	35	20	80	400	222.526	1.973
4	Training	No	35	20	60	500	356.991	1.257
5	Training	No	35	20	70	500	300.350	1.867
6	Training	No	35	20	80	500	229.492	2.545
7	Validation	Yes	35	20	60	600	359.706	1.487
8	Training	No	35	20	70	600	298.275	2.077
9	Training	Yes	35	20	80	600	260.154	2.656
10	Training	No	35	25	60	400	298.676	0.954
11	Training	No	35	25	70	400	255.285	1.378
12	Training	No	35	25	80	400	222.468	1.856
13	Validation	No	35	25	60	500	320.154	1.130
14	Validation	Yes	35	25	70	500	264.936	1.756
15	Training	No	35	25	80	500	254.171	2.293
16	Training	No	35	25	60	600	356.744	1.391
17	Training	No	35	25	70	600	300.857	2.048
18	Training	No	35	25	80	600	250.845	2.306
19	Validation	Yes	35	30	60	400	282.328	0.854
20	Training	No	35	30	70	400	271.258	1.281
21	Training	Yes	35	30	80	400	202.907	1.320
22	Training	No	35	30	60	500	319.819	1.043
23	Training	No	35	30	70	500	271.653	1.525
24	Training	No	35	30	80	500	219.481	2.241
25	Training	Yes	35	30	60	600	319.630	1.365
26	Validation	No	35	30	70	600	269.584	2.019
27	Training	Yes	35	30	80	600	240.578	2.583
28	Validation	No	60	20	60	400	483.201	0.618
29	Validation	No	60	20	70	400	407.835	0.888
30	Training	No	60	20	80	400	257.824	1.560
31	Training	No	60	20	60	500	515.713	0.745
32	Training	No	60	20	70	500	416.734	1.230
33	Training	No	60	20	80	500	404.528	1.281
34	Training	No	60	20	60	600	521.765	1.016
35	Training	No	60	20	70	600	491.363	1.313
36	Training	No	60	20	80	600	309.722	2.076
37	Training	No	60	25	60	400	420.777	0.612
38	Training	No	60	25	70	400	342.163	0.931
39	Training	No	60	25	80	400	294.926	1.240
40	Test	No	60	25	60	500	545.728	0.654
41	Training	No	60	25	70	500	378.013	1.166
42	Test	No	60	25	80	500	305.985	1.620

Table 13 (continued)

Run	ANN subset	Used in RSM	S (g/L)	T_{cond}(°C)	T_{evap}(°C)	F(L/h)	STEC(kWh/m^3)	P_{flux} (L/(h·m^2))
43	Validation	No	60	25	60	600	453.292	0.884
44	Training	No	60	25	70	600	420.574	1.347
45	Test	No	60	25	80	600	334.478	1.978
46	Validation	No	60	30	60	400	498.438	0.466
47	Training	No	60	30	70	400	340.396	0.840
48	Validation	No	60	30	80	400	289.640	1.095
49	Training	No	60	30	60	500	533.780	0.591
50	Training	Yes	60	30	70	500	367.792	1.032
51	Training	No	60	30	80	500	310.756	1.566
52	Training	No	60	30	60	600	529.871	0.720
53	Training	No	60	30	70	600	430.971	1.194
54	Training	No	60	30	80	600	325.401	1.782
55	Training	Yes	87.5	25	60	500	705.05	0.506
56	Training	Yes	87.5	20	70	500	501.44	0.996
57	Training	Yes	87.5	25	70	400	615.29	0.544
58	Training	Yes	87.5	25	70	500	500.06	0.882
59	Training	Yes	87.5	25	70	600	496.07	1.148
60	Training	Yes	87.5	30	70	500	532.01	0.760
61	Training	Yes	87.5	25	80	500	420.44	1.246
62	Training	Yes	140	20	60	400	927.252	0.324
63	Validation	No	140	20	70	400	706.733	0.496
64	Training	Yes	140	20	80	400	478.825	0.853
65	Validation	No	140	20	60	500	853.079	0.501
66	Training	No	140	20	70	500	626.960	0.790
67	Training	No	140	20	80	500	459.124	1.120
68	Training	Yes	140	20	60	600	777.253	0.663
69	Validation	No	140	20	70	600	611.118	0.958
70	Training	Yes	140	20	80	600	475.667	1.407
71	Training	No	140	25	60	400	1137.747	0.147
72	Training	No	140	25	70	400	713.008	0.441
73	Validation	No	140	25	80	400	586.875	0.628
74	Test	No	140	25	60	500	960.347	0.396
75	Training	Yes	140	25	70	500	601.207	0.732
76	Training	No	140	25	80	500	467.379	1.060
76	Training	No	140	25	60	600	870.252	0.511
78	Training	No	140	25	70	600	618.107	0.861
79	Training	No	140	25	80	600	455.628	1.345
80	Training	Yes	140	30	60	400	1960.897	0.118
81	Training	No	140	30	70	400	723.315	0.385
82	Training	Yes	140	30	80	400	607.823	0.600
83	Validation	No	140	30	60	500	1418.157	0.220
84	Training	No	140	30	70	500	647.301	0.630
85	Training	No	140	30	80	500	497.021	1.068
86	Training	Yes	140	30	60	600	1054.110	0.376
87	Training	No	140	30	70	600	663.802	0.753
88	Training	Yes	140	30	80	600	533.632	1.135

References

[1] J.P. Mericq, S. Laborie, C. Cabassud, Vacuum membrane distillation of seawater reverse osmosis brines, Water Res. 44 (18) (2010) 5260–5273.

[2] D. Qu, J. Wang, B. Fan, Z. Luan, D. Hou, Study on concentrating primary reverse osmosis retentate by direct contact membrane distillation, Desalination 247 (1-3) (2009) 540–550.

[3] C.R. Martinetti, A.E. Childress, T.Y. Cath, High recovery of concentrated RO brines using forward osmosis and membrane distillation, J. Membr. Sci. 331 (2009) 31–39.

[4] J. Sanmartino, M. Khayet, M. García-Payo, H. El-Bakouri, A. Riaza, Treatment of reverse osmosis brine by direct contact membrane distillation: chemical pretreatment approach, Desalination 420 (2017) 79–90.

[5] A. Alkhudhiri, N. Darwish, N. Hilal, Membrane distillation: a comprehensive review, Desalination 287 (2012) 2–18.

[6] M. Khayet, Solar desalination by membrane distillation: dispersion in energy consumption analysis and water production costs (a review), Desalination 308 (2013) 89–101.

[7] E. Drioli, A. Ali, F. Macedonio, Membrane distillation: recent developments and perspectives, Desalination 356 (2015) 56–84.

[8] N. Thomas, M.O. Mavukkandy, S. Loutatidou, H.A. Arafat, Membrane distillation research & implementation: lessons from the past five decades, Sep. Purif. Technol. 189 (2017) 108–127.

[9] M. Khayet, C. Cojocaru, A. Baroudi, Modeling and optimization of sweeping gas membrane distillation, Desalination 287 (2012) 159–166.

[10] M. Khayet, C. Cojocaru, Artificial neural network modeling and optimization of desalination by air gap membrane distillation, Sep. Purif. Technol. 86 (2012) 171–182.

[11] M. Khayet, C. Cojocaru, Artificial neural network model for desalination by sweeping gas membrane distillation, Desalination 308 (2013) 102–110.

[12] A. Ruiz-Aguirre, J. Andrés-Mañas, J. Fernández-Sevilla, G. Zaragoza, Modeling and optimization of a commercial permeate gap spiral wound membrane distillation module for seawater desalination, Desalination 419 (2017) 160–168.

[13] J.D. Gil, L. Roca, A. Ruiz-Aguirre, G. Zaragoza, M. Berenguel, Optimal operation of

a solar membrane distillation pilot plant via nonlinear model predictive control, Comput. Chem. Eng. 109 (2018) 151–165.

[14] R. Porrazzo, A. Cipollina, M. Galluzzo, G. Micale, A neural network-based optimizing control system for a seawater-desalination solar-powered membrane distillation unit, Comput. Chem. Eng. 54 (2013) 79–96.

[15] Y.-H. Chen, Y.-W. Li, H. Chang, Optimal design and control of solar driven air gap membrane distillation desalination systems, Appl. Energy 100 (2012) 193–204.

[16] I. Hitsov, T. Maere, K. De Sitter, C. Dotremont, I. Nopens, Modelling approaches in membrane distillation: a critical review, Sep. Purif. Technol. 142 (2015) 48–64.

[17] M. Khayet, C. Cojocaru, M. Essalhi, Artificial neural network modeling and response surface methodology of desalination by reverse osmosis, J. Membr. Sci. 368 (2011) 202–214.

[18] A.E. Khalifa, D.U. Lawal, Application of response surface and Taguchi optimization techniques to air gap membrane distillation for water desalination: a comparative study, Desalin. Water Treat. 57 (2016) 28513–28530.

[19] S.T. Bouguecha, A. Boubakri, S.E. Aly, M.H. Al-Beirutty, M.M. Hamdi, Optimization of permeate flux produced by solar energy driven membrane distillation process using central composite design approach, Water Sci. Technol. 74 (2016) 87–98.

[20] T. Mohammadi, P. Kazemi, M. Peydayesh, Optimization of vacuum membrane distillation parameters for water desalination using Box-Behnken design, Desalin. Water Treat. 56 (2015) 2306–2315.

[21] A. Boubakri, A. Hafiane, S.A.T. Bouguecha, Application of response surface methodology for modeling and optimization of membrane distillation desalination process, J. Ind. Eng. Chem. 20 (2014) 3163–3169.

[22] M. Khayet, C. Cojocaru, Air gap membrane distillation: desalination, modeling and optimization, Desalination 287 (2012) 138–145.

[23] H. Chang, J.-S. Liau, C.-D. Ho, W.-H. Wang, Simulation of membrane distillation modules for desalination by developing user's model on Aspen Plus platform, Desalination 249 (2009) 380–387.

[24] M. Khayet, C. Cojocaru, C. García-Payo, Application of response surface methodology and experimental design in direct contact membrane distillation, Ind. Eng. Chem. Res. 46 (2007) 5673–5685.

[25] D. Cheng, W. Gong, N. Li, Response surface modeling and optimization of direct contact membrane distillation for water desalination, Desalination 394 (2016) 108–122.

[26] Q. He, P. Li, H. Geng, C. Zhang, J. Wang, H. Chang, Modeling and optimization of air gap membrane distillation system for desalination, Desalination 354 (2014) 68–75.

[27] W. Cao, Q. Liu, Y. Wang, I.M. Mujtaba, Modeling and simulation of VMD desalination process by ANN, Comput. Chem. Eng. 84 (2016) 96–103.

[28] M. Tavakolmoghadam, M. Safavi, An optimized neural network model of desalination by vacuum membrane distillation using genetic algorithm, Procedia Eng. 42 (2012) 106–112.

[29] S. Shirazian, M. Alibabaei, Using neural networks coupled with particle swarm optimization technique for mathematical modeling of air gap membrane distillation (AGMD) systems for desalination process, Neural Comput. & Applic. 28 (2017) 2099–2104.

[30] D. Cheng, N. Li, J. Zhang, Modeling and multi-objective optimization of vacuum membrane distillation for enhancement of water productivity and thermal efficiency in desalination, Chem. Eng. Res. Des. 132 (2018) 697–713.

[31] Y. Zhou, M. Huang, Q. Deng, T. Cai, Combination and performance of forward osmosis and membrane distillation (FO-MD) for treatment of high salinity landfill leachate, Desalination 420 (2017) 99–105.

[32] N.U. Kumar, A. Martin, Experimental modeling of an air-gap membrane distillation module and simulation of a solar thermal integrated system for water purification, Desalin. Water Treat. 84 (2017) 123–134.

[33] J.D. Gil, L. Roca, G. Zaragoza, M. Berenguel, A feedback control system with reference governor for a solar membrane distillation pilot facility, Renew. Energy 120 (2018) 536–549.

[34] H.C. Duong, P. Cooper, B. Nelemans, T.Y. Cath, L.D. Nghiem, Evaluating energy consumption of air gap membrane distillation for seawater desalination at pilot scale level, Sep. Purif. Technol. 166 (2016) 55–62.

[35] E. Guillén-Burrieza, G. Zaragoza, S. Miralles-Cuevas, J. Blanco, Experimental evaluation of two pilot-scale membrane distillation modules used for solar desalination, J. Membr. Sci. 409 (2012) 264–275.

[36] G. Zaragoza, A. Ruiz-Aguirre, E. Guillén-Burrieza, Efficiency in the use of solar thermal energy of small membrane desalination systems for decentralized water production, Appl. Energy 130 (2014) 491–499.

[37] W.J. Hill, W.G. Hunter, A review of response surface methodology: a literature survey, Technometrics 8 (1966) 571–590.

[38] G.E. Box, K.B. Wilson, On the experimental attainment of optimum conditions, Breakthroughs in Statistics, Springer, 1992, pp. 270–310.

[39] L. Stahle, S. Wold, et al., Analysis of variance (ANOVA), Chemom. Intell. Lab. Syst. 6 (1989) 259–272.

[40] M.H. Beale, M.T. Hagan, H.B. Demuth, Neural Network Toolbox: User's Guide (Version 10.0), (2017).

[41] M.T. Hagan, H.B. Demuth, Neural networks for control, American Control Conference, 1999. Proceedings of the 1999, vol. 3, IEEE, 1999, pp. 1642–1656.

[42] H.B. Demuth, M.H. Beale, O. De Jess, M.T. Hagan, Neural Network Design, PWS Publishing Co., 2014.

[43] K. Deb, A. Pratap, S. Agarwal, T. Meyarivan, A fast and elitist multiobjective genetic algorithm: NSGA-II, IEEE Trans. Evol. Comput. 6 (2002) 182–197.

[44] D. Winter, J. Koschikowski, M. Wieghaus, Desalination using membrane distillation: experimental studies on full scale spiral wound modules, J. Membr. Sci. 375 (2011) 104–112.

2.2 Hierarchical controllers for the optimal operation of solar membrane distillation plants

2.2.1 Optimal operation of a solar membrane distillation pilot plant via nonlinear model predictive control

Research in this field is supported by the following journal publication:

Title	Optimal operation of a solar membrane distillation pilot plant via nonlinear model predictive control
Authors	**J. D. Gil**, L. Roca, A. Ruiz-Aguirre, G. Zaragoza, M. Berenguel
Journal	Computers & Chemical Engineering
Year	2018
Volume	109
Pages	151-165
DOI	`https://doi.org/10.1016/j.compchemeng.2017.11.012`
IF (JCR 2018)	3.334
Categories	Computer Science, Interdisciplinary Applications (28/106) **Q2**
	Engineering, Chemical (36/138) Q2

Contribution of the Ph.D. candidate
The Ph.D. candidate, J. D. Gil, is the main contributor and first author of this paper.

Apart from the main work, the research on this topic led to the following contributions to international conferences:

- **J. D. Gil**, L. Roca, A. Ruiz-Aguirre, G. Zaragoza, J. L. Guzmán, and M. Berenguel, "Using a nonlinear model predictive control strategy for the efficient operation of a solar-powered membrane distillation system," in *2017 25th Mediterranean Conference on Control and Automation (MED)*. IEEE, pp. 1189–1194, 2017.
- **J. D. Gil**, P. R. Mendes, G. Andrade, L. Roca, J. E. Normey-Rico, and M. Berenguel, "Hybrid NMPC applied to a solar powered membrane distillation system," *IFAC-Papers OnLine*, vol. 52, no. 1, pp. 124–129, 2019.
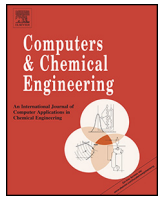
Optimal operation of a Solar Membrane Distillation pilot plant via Nonlinear Model Predictive Control

Juan D. Gil [a], Lidia Roca [b], Alba Ruiz-Aguirre [a], Guillermo Zaragoza [b], Manuel Berenguel [a,*]

[a] Centro Mixto CIESOL, ceiA3, Universidad de Almería, Ctra. Sacramento s/n, Almería 04120, Spain
[b] CIEMAT-Plataforma Solar de Almería, Ctra. de Senés s/n, Tabernas, 04200 Almería, Spain

ABSTRACT

Solar Membrane Distillation (SMD) is an under-investigation desalination process suitable for developing self-sufficient small scale applications. The use of solar energy considerably reduces the operating costs, however, its intermittent nature requires a non-stationary optimal operation that can be achieved by means of advanced control strategies. In this paper, a hierarchical control system composed by two layers is used for optimizing the operation of a SMD pilot plant, in terms of thermal efficiency, distillate production and cost savings. The upper layer is formed by a Nonlinear Model Predictive Control (NMPC) scheme that allows us to obtain the optimal operation by optimizing the solar energy use. The lower layer includes a direct control system, in charge of attaining the variable references provided by the upper layer. Simulation and experimental tests are included and commented in order to demonstrate the benefits of the developed control system.

© 2017 Elsevier Ltd. All rights reserved.

1. Introduction

Desalination technologies require intensive generation energy processes for the production of fresh water. For this reason, most of the costs depend directly on the way the energy is obtained and managed. The conventional use of non-renewable energy resources, like fossil fuels, represents a non-sustainable solution from an economic and environmental point of view. Recent research focuses on combining renewable energy sources and desalination processes, as a way of developing efficient and sustainable systems.

In this context, Membrane Distillation (MD) is a thermally driven desalination process that can be powered with low grade solar thermal energy (Zaragoza et al., 2014; Cipollina et al., 2012). The main drawback of using solar energy as source is its unpredictable nature that requires discontinuous operation and the use of specific energy buffering systems. Hence, to develop sustainable SMD commercial systems it is necessary to combine a good technical design and adequate control techniques able to optimize the system operation according to the solar energy behaviour.

There exist numerous examples of the use of offline optimization techniques in the literature aimed at finding optimum operating parameters in terms of thermal efficiency and distillate production. In He et al. (2014), the response surface methodology is used to model an Air Gap Membrane Distillation (AGMD) module. Then, a non-dominated sorting genetic algorithm II was employed to determinate the optimum operating conditions that maximize both distillate production and thermal efficiency. In Khayet and Cojocaru (2012), regression models are proposed to predict the energy module consumption as function of different variables. An optimization problem using Monte-Carlo stochastic methodology was applied in order to maximize the thermal efficiency. However, the optimal operating conditions presented in these works require steady state conditions around the defined points, which are difficult to achieve under real solar-powered operation. As suggested in Gil et al. (2015a,b,c), specific control systems can be used to maintain the main variables of SMD facilities near steady state conditions. From this automatic control point of view, two interesting control approaches are described in Chang et al. (2010, 2012), where a control system formed by conventional Proportional Integral (PI) controllers is employed in order to track optimal operating conditions calculated by means of an offline optimization study focused on maximizing the distillate production. This control system was tested in simulation, obtaining results near the optimum only for clear sky operation. Nevertheless, for coupling desalination processes and solar energy, real time optimization techniques

can provide better results in terms of energy efficiency, distillate production and cost savings, since these techniques take into consideration the plant conditions at each sample time. In Karam and Laleg-Kirati (2015) a Newton-based extremum seeking controller is proposed to optimize the permeate flux and the inlet feed according to the variance of the temperature. A dynamic model of the system was used to test the control architecture. The use of a real time optimization system for a real SMD facility has been only addressed by Porrazzo et al. (2013), in which a neural network-based feedforward optimal control system is proposed to maximize the daily production of distillate.

This paper presents a hierarchical control architecture with two layers, focused on optimizing the solar-powered operation of a MD pilot plant. The upper layer includes a Practical Nonlinear Model Predictive Control (PNMPC) strategy (Plucenio et al., 2007) which provides temperature and flow rate setpoints for the heat generation SMD circuit. Besides, a double Exponential Smoothing (DES) technique (NIST, 2016; Pawlowski et al., 2011) combined with the application of Lagrange interpolation method for signal reconstruction (Pawłowski et al., 2014) has been used to perform irradiance estimation. On the other hand, the lower layer (Gil et al., 2015a,b,c) is formed by PI and feedforward controllers which are in charge of tracking the references calculated by the upper layer. Moreover, two control modes are proposed for the efficient operation of the facility, as well as a start-stop procedure for the solar field and the MD module. In comparison with the work in Porrazzo et al. (2013), the proposed approach has several differences. Whereas in Porrazzo et al. (2013) the feedforward-based controller is used to maximize the distillate production, in the proposed hierarchical control approach different objective functions have been tested (using the same control architecture) allowing to optimize, apart from distillate production, thermal efficiency and cost savings. Additionally, instead of using a complete nonlinear model of the system to determine the optimal operation, the PNMPC strategy calculates an approximated linear model at each sample time. Although this fact can cause a small loss of accuracy, the complexity to solve the optimization problem as well as the computational effort are decreased. The proposed control approach has been tested in the MD-solar pilot plant located at Plataforma Solar de Almería (PSA, www.psa.es), Spain. Simulation and experimental tests are included, showing that the adoption of the proposed control scheme could represent a significant advance towards the development of autonomous commercial SMD systems.

2. MD-solar pilot plant

2.1. The MD technology

MD consists on a thermally-driven desalination process that uses a hydrophobic micro-porous membrane to separate the water vapour from sea or brackish water. The driving force of the process is the pressure gradient originated at both membrane sides, which is achieved by a temperature difference. In consequence, volatile molecules are evaporated and transported through the porous membrane whereas non-volatile compounds are rejected. The vapour can then be condensed inside the module or outside in an external condenser, depending of the MD configuration employed (Alkhudhiri et al., 2012). The most adopted configurations are Direct Contact Membrane Distillation (DCMD), Permeate Gap Membrane Distillation (PGMD) and AGMD, in which condensation takes place inside the module, and Sweeping Gas Membrane Distillation (SGMD) and Vacuum Membrane Distillation (VMD), where condensation occurs outside the module in an external device.

Table 1
Variables monitored in the SMD facility.

Variable	Description	Units
DT1	Distillate production	L/min
FT1	Solar field water flow rate	L/min
FT2	Water flow rate between the tank and the distribution system	L/min
FT3	Heat exchanger water flow rate	L/min
FT4	Feed water flow rate	L/min
I	Global irradiance measured at 36° tilted	W/m^2
T_a	Ambient temperature	°C
TT1	Solar field inlet temperature	°C
TT2	Solar field outlet temperature	°C
TT3	Temperature at the top of the tank	°C
TT4	Distribution system inlet temperature	°C
TT5	Heat exchanger inlet temperature, hot side	°C
TT6	Heat exchanger outlet temperature, hot side	°C
TT7	Distribution system outlet temperature	°C
TT8	Temperature at the bottom of the tank	°C
TT9	Heat exchanger inlet temperature, cold side	°C
TT10	Heat exchanger outlet temperature, cold side	°C
TT11	Feed water temperature	°C

MD systems have several advantages that make this technology specially suitable for developing self-sufficient small scale desalination applications. Among the several advantages, the main ones are: (1) an intensive pre-treatment of the feed water is not required, just a simple filtration process; (2) the simplicity of the process reduces the maintenance requirements and enables easy automation; (3) it can be operated under intermittent conditions without damaging the membrane; (4) the operating temperature is low, between 60 and 85 °C. Particularly, the last two make possible the use of solar energy as source, thus enabling the development of efficient autonomous systems (Zaragoza et al., 2014; Cipollina et al., 2012).

2.2. The SMD pilot plant

The SMD pilot plant at PSA (Zaragoza et al., 2014; Ruiz-Aguirre et al., 2017b) is formed by an AGMD module and a heat generation circuit which comprises a solar thermal field, a storage tank and a distribution system (see Fig. 1).

The MD commercial unit (built by Aquastill) consists on a spiral wound module based on the AGMD technology (Alkhudhiri et al., 2012). The effective surface area is 24 m^2 with a length of 5 m. Productivity tests and a full characterization of the AGMD module were presented in (Ruiz-Aguirre et al., 2015). The unit has its own heat exchanger, which is used to warm up the feed water, which is preheated after acting as a coolant in the condenser channel of the module, with the fluid coming from the heat generation circuit.

The required thermal energy is provided by a solar field formed by stationary flat-plate collectors Solaris CP1 Nova purchased from Solaris (Spain), which are set in two rows of five collector each one. A complete description of the solar field was presented in (Zaragoza et al., 2014). The facility is also equipped with a thermal storage tank (1500 L) that is used as energy buffer device to store and manage the thermal energy coming from the solar field. The storage tank permits the operation of the plant in several modes, as it was described in Gil et al. (2015a). In this paper the MD module is fed by the storage tank, which is heated by recirculating the fluid through the solar field (see Section 2.3). Finally, a distribution system is available to connect the heat generation circuit and the MD module. Notice that the distribution system enables the simultaneous connection of several MD units.

The plant is completely monitored and controlled trough a Programmable Logic Controller (PLC) and a Supervisory Control And Data Acquisition (SCADA) system with a sample time of 1 s. All the monitored variables are presented in Table 1. Details about
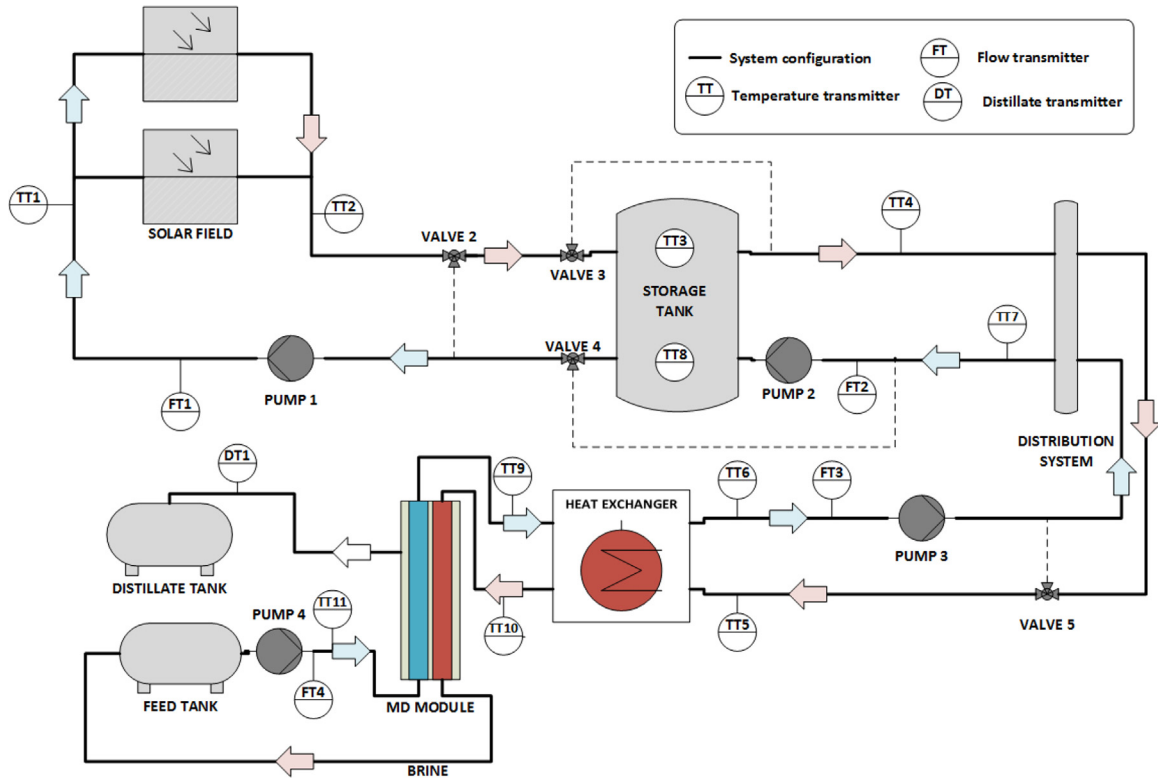
Fig. 1. Schematic diagram of the plant.

instrumentation can be found in Zaragoza et al. (2014), Gil et al. (2015a).

2.3. System configuration and nominal operating ranges

As it has been highlighted before, the SMD plant can be operated in different modes (Gil et al., 2015a). In this case, the fluid coming from the solar field flows directly to the tank, which is used to feed the module. By using this operating mode, the continuity of the operation is improved, since most of the transients caused by irradiance disturbances are attenuated by the buffer system. In addition, in this paper, only the solar-powered operation is investigated, assuming that there are not other thermal sources.

On the other hand, pump 4 (see Fig. 1) drives feed water into the condenser channel of the module (see Fig. 2). This feed flow rate varies between 400 and 600 L/h, that is the maximum allowed by the module. Moreover, the feed tank temperature is kept at 20 °C and the salinity is 35 g/L, representing mean values of the seawater conditions adopted in this work. Once the feed water reaches the heat exchanger, it is heated with the recirculating fluid coming from the heat generation circuit. Then, the hot feed water flows into the evaporator channel of the module. The inlet evaporator temperature varies from 60 to 84 °C, since temperatures lower than 60 °C produce very low distillate flow, and 84 °C is the maximum allowed by membrane materials. The volatile molecules of the hot feed water are evaporated in the evaporator channel and pass trough the membrane, whereas the non-volatile components exit from the evaporator channel as brine. The volatile molecules are then condensed in contact with the condensation foil of the membrane, thus transferring some of the heat to the feed water that circulates in the condensation channel, which is pre-heated before reaching the heat exchanger. It should be noted that both the brine and the distillate are returned to the feed tank, which causes an increase of the temperature during the operation. Thus,

an auxiliary tank equipped with a chiller is used to keep the desired feed tank conditions.

3. System modeling

In order to achieve a successful implementation of the PNMPC control system, it is necessary to develop a model which accurately represents the behaviour of the facility. According to the SMD plant configuration, the model has to include the solar field, thermal storage tank, distribution system, heat exchanger, pump 1, pump 2, pump 3 and MD module. It should be taken into account that the model of the heat generation circuit has been already presented and validated in (Gil et al., 2015a,b,c). The definition of all the parameters used in Eqs. (1)–(13) is presented in Table 2 (those not included in Table 1).

Thus, the solar field was modeled using the lumped-parameters model included in Roca et al. (2009), that is given by:

$$A_{sf} \cdot \rho \cdot c_p \cdot \frac{\partial \mathrm{TT2}(t)}{\partial t} = \beta \cdot \mathrm{I}(t) - \frac{H}{L_{eq}} \cdot$$
$$(\bar{T}(t) - \mathrm{T}_a(t)) - c_p \cdot \dot{m}_{eq} \cdot \frac{\mathrm{TT2}(t) - \mathrm{TT1}(t)}{L_{eq}}, \tag{1}$$

where:

$$L_{eq} = L_a \cdot n_{cs}, \tag{2}$$

$$\dot{m}_{eq} = \frac{\mathrm{FT1} \cdot \rho}{c_1}, \tag{3}$$

$$\bar{T}(t) = \frac{\mathrm{TT1}(t) + \mathrm{TT2}(t)}{2}. \tag{4}$$
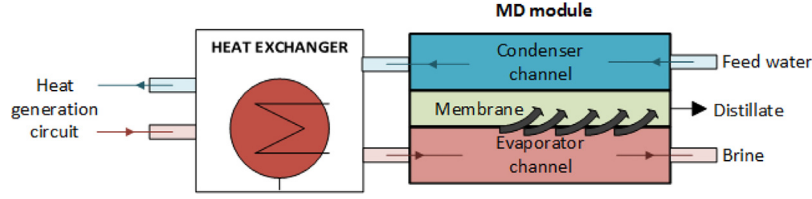
Fig. 2. Schematic diagram of the MD module.

Table 2
Model parameters.

Variable	Description	Units
A_{he}	Heat exchanger area	$1.65\,m^2$
A_{sf}	Collector absorber cross-section area	$0.007\,m^2$
c_1	Conversion factor to account for connections, number of modules and L/min conversion	$9 \cdot 2 \cdot 6 \cdot 10^4\ (s\,L)/(min\,m^3)$
c_2	Conversion factor to kWh	$3.6 \cdot 10^6\,J/kWh$
c_p	Specific heat capacity of demineralized water	$J/(kg\,^\circ C)$
$c_{p,sw}$	Specific sea water heat capacity	$J/(kg\,^\circ C)$
F	Input frequency	%
H	Solar field global thermal losses coefficient	$5.88\,J/(s\,K)$
k	Static gain of FOPDT transfer functions	
L_a	Collector absorber tube length	$1.95\,m$
L_{eq}	Equivalent absorber tube length	$9.75\,m$
$\dot{m}_{ds}$	Water mass flow rate between the tank and the distribution system	kg/s
$\dot{m}_{eq}$	Equivalent solar-field mass flow rate	kg/s
$\dot{m}_{sf}$	Water mass flow rate between the tank and the solar field	kg/s
$\dot{m}_1$	Heat generation circuit mass flow rate	kg/s
$\dot{m}_2$	MD module circuit mass flow rate	kg/s
n_{cs}	Number of series-connections in a collectors group	5
$\bar{T}$	Equivalent absorber tube mean temperature	$^\circ C$
$TT6_m$	TT6 estimated by the model	$^\circ C$
$TT10_m$	TT10 estimated by the model	$^\circ C$
t_d	Representative time delay of FOPDT transfer functions	s
UA_1	Tank thermal losses coefficient, lower part	$3.6\,J/(s\,K)$
UA_2	Tank thermal losses coefficient, upper part	$3.8\,J/(s\,K)$
V	Tank volume	$1.5\,m^3$
α_{he}	Heat exchanger heat transfer coefficient	$670.80\,W/(m^2\,K)$
β	Irradiance model parameter	$0.11\,m$
ΔT	Temperature difference between TT10 and TT9	$^\circ C$
η_{he}	Heat exchanger auxiliary factor	–
τ	Representative time constant of FOPDT transfer functions	s
θ_{he}	Heat exchanger auxiliary factor	–
ρ	Demineralized water density	kg/m^3
ρ_{feed}	Feed water density	kg/m^3

A two-nodes stratified dynamic model was employed for the storage tank, as suggested in Duffie and Beckman (1980):

$$\frac{\partial TT3(t)}{\partial t} = \frac{1}{\rho \cdot V} \cdot \left(\dot{m}_{sf} \cdot TT2(t) + \dot{m}_{ds} \cdot TT8(t) - \dot{m}_{sf} \cdot TT3(t) \right.$$
$$\left. - \dot{m}_{ds} \cdot TT3(t) - \frac{UA_1 \cdot (TT3(t) - T_a(t))}{c_p} \right), \tag{5}$$

$$\frac{\partial TT8(t)}{\partial t} = \frac{1}{\rho \cdot V} \cdot \left(\dot{m}_{sf} \cdot TT3(t) + \dot{m}_{ds} \cdot TT7(t) - \dot{m}_{sf} \cdot TT8(t) \right.$$
$$\left. - \dot{m}_{ds} \cdot TT8(t) - \frac{UA_2 \cdot (TT8(t) - T_a(t))}{c_p} \right). \tag{6}$$

Table 3
Transfer functions obtained from experimental data.

$G(s)$	$Y(s)$	$U(s)$	k	τ [s]	t_d [s]
$G_1(s)$	$FT1(s)$	$F_{P1}(s)$	0.2344	5	1
$G_2(s)$	$FT2(s)$	$F_{P2}(s)$	0.1674	7.65	3.01
$G_3(s)$	$FT3(s)$	$F_{P3}(s)$	0.1345	8.03	3

A first principles-based static model was used to characterize the heat exchanger, according to the ideas presented in de la Calle et al. (2016):

$$TT6_m = TT5 - \eta_{he,1} \cdot (TT5 - TT9), \tag{7}$$

$$TT10_m = TT9 + \eta_{he,2} \cdot (TT5 - TT6_m), \tag{8}$$

where:

$$\eta_{he,1} = \frac{1 - e^{\theta_{he}}}{1 - \frac{\dot{m}_1 \cdot c_p}{\dot{m}_2 \cdot c_{p,sw}} e^{\theta_{he}}}, \tag{9}$$

$$\eta_{he,2} = \frac{\dot{m}_1 \cdot c_p}{\dot{m}_2 \cdot c_{p,sw}}, \tag{10}$$

$$\theta_{he} = \alpha_{he} \cdot A_{he} \cdot \left(\frac{1}{\dot{m}_1 \cdot c_p} - \frac{1}{\dot{m}_2 \cdot c_{p,sw}} \right). \tag{11}$$

Moreover, a first order filter and a time delay have been added to this static model to fit real response data. The representative time constant is 40 s and the time delay is 23 s for $TT6_m$, whereas the time constant is 20 s and the time delay is 15 s for $TT10_m$.

The distribution system was modeled by means of a static energy balance, taking into account that in a normal operation, with FT2 higher than FT3, a mixture is produced between the fluid coming from the tank and the cold fluid coming from the heat exchanger:

$$TT7 = \frac{TT4 \cdot (FT2 - FT3) + TT6 \cdot FT3}{FT2}. \tag{12}$$

Besides, as in the previous case, a low pass filter has been added to the output of Eq. (12) with a representative time constant of 7 s based on experimental results.

Pumps were modeled trough First Order Plus Dead Time (FOPDT) transfer functions obtained from experimental data, see Table 3.

Finally, an experimental campaign was carried out to obtain a static model of the AGMD module distillate production (DT1) and ΔT, that is the difference between the inlet evaporator channel temperature (TT10) and the outlet condensation channel temperature (TT9). More details about the experimental procedure were shown in (Ruiz-Aguirre et al., 2015).

$$\begin{aligned} DT1 = {} & 24 \cdot (0.135 + 0.003 \cdot TT10 - 0.0204 \cdot TT11 - 0.001 \cdot FT4 \\ & + 0.00004 \cdot TT10 \cdot FT4), \end{aligned} \tag{13}$$

$$\Delta T = -0.739 + 0.078 \cdot TT10 - 0.067 \cdot TT11 + 0.0019 \cdot FT4. \tag{14}$$

Fig. 3. 3D response surface plot of distillate flow rate.
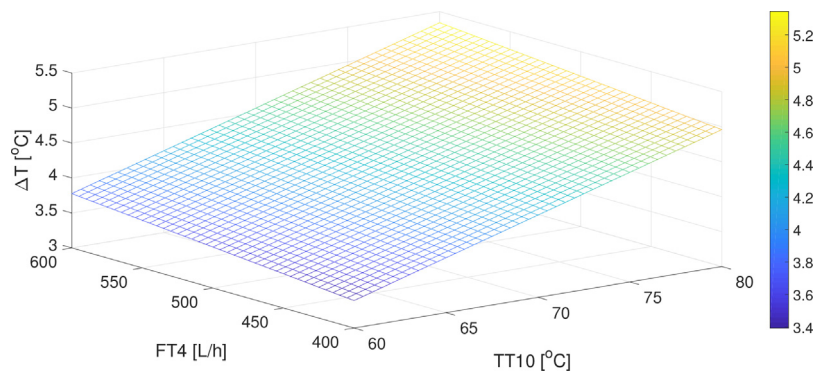
Fig. 4. 3D response surface plot of ΔT.

4. Optimal operation of the MD module

When coupling a thermal desalination process with solar energy, the plant thermal efficiency is an essential factor. It should be noted that the thermal efficiency varies according to the MD configuration and module design. Thus, the optimal operation strategy in terms of energy efficiency as well as distillate production should be characterized for each MD module. Several performance indices can be adopted to evaluate thermal efficiency, being the Specific Thermal Energy Consumption (STEC), which is widely employed in the literature to evaluate the energy consumption of MD systems (Duong et al., 2016; Guillén-Burrieza et al., 2012; Zaragoza et al., 2014,b; Ruiz-Aguirre et al., 2017a,b), the one used in this work:

$$STEC[kWh/m3] = \frac{FT4 \cdot \rho_{feed} \cdot c_{p,sw} \cdot \Delta T}{c_2 \cdot DT1}, \tag{15}$$

this index provides the thermal energy required per volume unit of distillate produced.

In order to observe the influence of each variable in the STEC value and to assess the optimal operation of the AGMD module employed in this work, 3D response surface plots have been displayed. The performance of STEC, ΔT and DT1 have been evaluated with respect to the inlet evaporation channel temperature (TT10) and the feed water flow rate (FT4), maintaining TT11 fixed at 20 °C (mean seawater temperature considered in this work).

Fig. 3 shows the 3D distillate flow rate response surface plot. It can be seen that the distillate production flow rate augments when FT4 and TT10 increase. Nevertheless, TT10 affects more significantly than FT4. Moreover, in accordance with Eq. (15), STEC is a function of FT4, DT1 and ΔT. Fig. 4 and 5 show the effects of TT10 and FT4 in ΔT and STEC. It should be taken into account that TT10 has more influence than FT4 in both parameters. Besides, although ΔT increases when high TT10 is applied (see Fig. 4), DT1 increases

more significantly (see Fig. 3). This fact reduces STEC, which implies a greater thermal efficiency in the operation.

Hence, to obtain an optimal operation in terms of thermal efficiency and distillate production, the temperature should be the highest reachable one by the heat generation circuit at each instant, taking into account that this temperature varies in accordance with the operating conditions. On the other hand, the minimum STEC and the maximum distillate production is achieved with low and high FT4, respectively. Nevertheless, the distillate flow rate production difference achieved when the maximun and minimum FT4 is applied, is much greater than the STEC one, from 17.8 to 28.44 L/h for the distillate flow rate and from 117.2 to 119.6 kWh/m³ for the STEC. Therefore, FT4 will be operated at 600 L/h in order to achieve the maximum flow rate of distillate.

5. Control system architecture

After the previous analysis, it has been concluded that the key for the optimal operation of the SMD facility is the proper management of temperature TT10, by means of the heat generation circuit. For this purpose, the two chosen controlled variables are TT2 and FT2, which enable to control the thermal power to load and unload the tank. It should be considered that FT2 has a significant influence in the inlet solar field temperature as well as in the outlet distribution system temperature, due to the mix produced in the distribution system and in the lower part of the tank. This fact produces that its operation is not trivial, thus justifying its inclusion in the control system.

On the other hand, to obtain a profitable economic balance of the plant, pump 2, 3 and 4 should not be operated when TT10 is lower than 60 °C, since the MD module produces very low distillate flux in comparison with the electric consumption of pumps. In this way, two different control modes are proposed. The first one

Fig. 5. 3D response surface plot of STEC.

consists on a tank fast heating mode, in which the PNMPC strategy optimizes the solar field outlet temperature (TT2) in order to warm up the tank quickly, until reaching a temperature that allows us to operate the MD module with 60 °C. The second 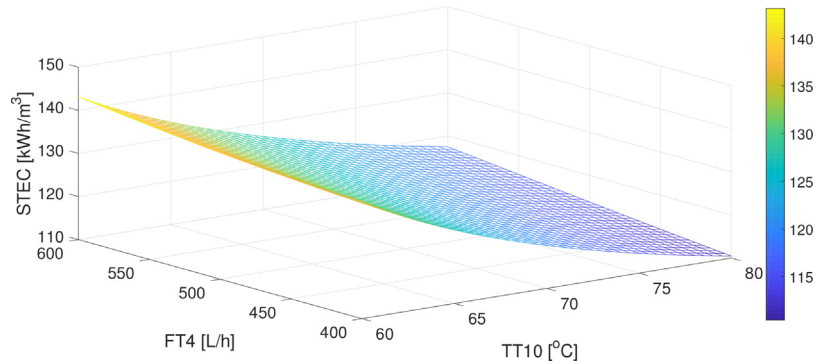one is the normal operating mode, which is used as long as the MD module is operated. When this mode is selected, the control system acts on TT2 and FT2 setpoints (TT2$_{SP}$ and FT2$_{SP}$) according to the two different objective functions proposed for this mode. The switching mechanism (decision maker in Fig. 6) between both modes is based on the start-stop procedure explained in Sections 5.4 and 5.5.

Therefore, the proposed control architecture (see Fig. 6) consists on a classical hierarchical control system, in which the optimization layer, the top one, acts as reference governor, by using a PNMPC strategy (Plucenio et al., 2007) providing temperature and flow rate references. Besides, a DES technique (Pawlowski et al., 2011) is used to predict the irradiance and to improve the system behaviour estimation. The inner layer, which is composed by a direct control system, manipulates the input frequency of pump 1 and 2 (F$_{P1}$ and F$_{P2}$) to maintain the setpoints calculated by the upper layer in spite of irradiance disturbances.

5.1. Lower layer: direct control system

The direct control layer includes two loops, and all the details about its configuration were presented in Gil et al. (2015a,b,c). The aim of this control layer is to maintain the two controlled variables, TT2 and FT2, near steady state conditions despite disturbances, which mainly are ambient temperature (T$_a$), inlet solar field temperature (TT1) and global irradiance (I). Firstly, TT2 is controlled using a cascade control loop (see Fig. 7), acting in the input frequency of pump 1 (F$_{P1}$). Besides, a feedforward (FF) that uses a static version of the solar field model (see Section 3), provides the nominal flow rate FT1 in accordance with irradiance disturbances and operating conditions. A Low Pass Filter (LPF) has been added to this static FF to achieve a better dynamical behaviour and a smooth response. In the same way, a LPF has been also included in the reference signal to find a good tradeoff between reference tracking and disturbances rejection and to reduce overshoots against setpoint step changes. The representative closed-loop time constant of this controller is 72 s.

Secondly, a classical feedback loop with a PI controller (see Fig. 8) is employed to control the feed flow rate FT2 by means of the input frequency of pump 2 (F$_{P2}$). In this occasion, the representative closed-loop time constant is 6.5 s.

Notice that an antiwindup scheme was added to each control loop. Pump 1 values range from 7.5 to 16 L/min and the pump 2 one from 15 to 25 L/min. This direct control layer has been implemented with a sample time of 5 s, allowing the solar field control loop detecting irradiance changes quickly. It should be mentioned that the original control architecture presented in Gil et al. (2015a,b,c)
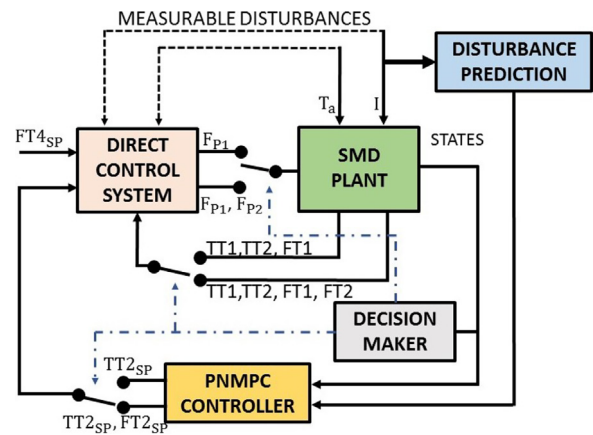
Fig. 6. Hierarchical control strategy scheme.

also includes a temperature control loop aiming at controlling the temperature at the inlet of the heat exchanger, by acting on valve 5. However, in this work, instead of using this control loop, valve 5 is kept fully open and it acts only commanded by means of a security mechanism that closes the valve when the temperature coming from the distribution system is higher than 95 °C, avoiding damages in the membrane.

5.2. Upper layer: PNMPC strategy

As it has been pointed out before, the optimization layer manages the thermal energy storage in the tank by generating appropriate setpoints to the outlet solar field temperature (TT2$_{SP}$) and to the feed flow rate FT2 (FT2$_{SP}$), according to the selected control mode and the objective function employed in the normal operating mode. For this purpose, a PNMPC strategy has been adopted (Plucenio et al., 2007), which has already been successfully tested in other nonlinear systems (Castilla et al., 2014; Álvarez et al., 2013), being also possible to increase robustness of the approach by filters shown in Andrade et al. (2013).

PNMPC algorithms are identified by the use of a vector $\hat{Y}$ that includes predictions of the future system outputs in a determined prediction horizon N, as a function of the future movements of the control signal ΔU:

$$\hat{Y} = F + G \cdot \Delta U, \tag{16}$$

where F is the free response and $G \cdot \Delta U$ is the forced response. In linear MPC algorithms, $\hat{Y}$ is estimated using a linear model of the system at hand. However, in the PNMPC control approach, $\hat{Y}$ is calculated using the nonlinear SMD plant model presented in Section 3. It should be mentioned that, in order to save computational time,
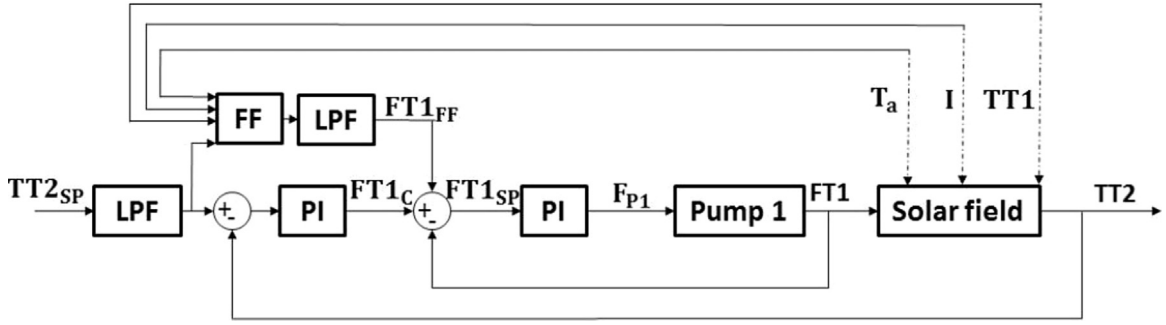
Fig. 7. Solar field control scheme. FT1$_{FF}$ is the FF control signal and FT1$_c$ is the feedback control signal.

difference equations have been employed for the solar field and tank models instead of the differential ones.

Firstly, in the tank fast heating mode (related with J1, see Section 5.2.1), the input used for the PNMPC technique ($\mathbf{U}_{J1}$) are the actual and future values of TT2$_{SP}$, whereas the output ($\hat{Y}_{J1}$) includes the future predicted values of TT3. Thus, the PNMPC formulation for the first control mode is given by:

$$\hat{\mathbf{Y}}_{J1} = \mathbf{F} + \mathbf{G}_{PNMPC} \cdot \boldsymbol{\Delta}\mathbf{U}, \tag{17}$$

where

$$\boldsymbol{\Delta}\mathbf{U} = \boldsymbol{\Delta}\mathbf{U}_{J1}, \tag{18}$$

$$\mathbf{F} = f(\mathbf{y}_{J1,p}, \boldsymbol{\Delta}\mathbf{u}_{J1,p}, \boldsymbol{\Delta}\mathbf{v_p}), \tag{19}$$

$$\mathbf{G}_{PNMPC} = \left[\frac{\partial \hat{\mathbf{Y}}_{J1}}{\partial \mathbf{U}_{J1}} \right], \tag{20}$$

$\mathbf{y}_{J1,p}$, $\boldsymbol{\Delta}\mathbf{u}_{J1,p}$ and $\boldsymbol{\Delta}\mathbf{v_p}$ are sets of past values of outputs, inputs and disturbances respectively.

Secondly, the two chosen input vectors of actual and future control actions, $\mathbf{U_1}$ and $\mathbf{U_2}$, for the normal operating mode (related with J2 and J3, see Section 5.2.1) are TT2$_{SP}$ and FT2$_{SP}$ respectively, whereas the predicted output vector, $\hat{\mathbf{Y}}$, is TT10. Thus, the PNMPC formulation is:

$$\hat{\mathbf{Y}} = \mathbf{F} + \mathbf{G}_{PNMPC} \cdot \Delta\mathbf{U}, \tag{21}$$

$$\mathbf{F} = f(\mathbf{y_p}, \boldsymbol{\Delta}\mathbf{u_p}, \boldsymbol{\Delta}\mathbf{v_p}), \tag{22}$$

$$\boldsymbol{\Delta}\mathbf{U} = \left[\boldsymbol{\Delta}\mathbf{U_1}; \boldsymbol{\Delta}\mathbf{U_2} \right], \tag{23}$$

$$\mathbf{G}_{PNMPC} = \left[\frac{\partial \hat{\mathbf{Y}}}{\partial \mathbf{U_1}} \quad \frac{\partial \hat{\mathbf{Y}}}{\partial \mathbf{U_2}} \right], \tag{24}$$

$\mathbf{y}_p$, $\boldsymbol{\Delta}\mathbf{u_p}$ and $\boldsymbol{\Delta}\mathbf{v_p}$ are sets of past values of outputs, inputs and disturbances respectively.

It should be taken into account that this technique provides only an approximation of the predictions, nevertheless it reproduces better the system performance than a linear model, due to $\mathbf{G}_{PNMPC}$ being computed using linearized models at each instant, while $\mathbf{F}$ is estimated with the nonlinear model, maintaining the future control movements constants and using the prediction of the measurable disturbances (see Section 5.3). Thus, to calculate $\mathbf{F}$ and $\mathbf{G}_{PNMPC}$ for each control mode at each sample time, the algorithm presented in Algorithm 1 and described in Plucenio et al. (2007) should be used. Additionally, as pointed out in Plucenio et al. (2007), Andrade et al. (2013), for the treatment of disturbances, prediction errors and noises, the implementation of the PNMPC algorithm in this work uses an explicit form of generalized predictive control where the integral of the filtered prediction error is added to the predicted system output to correct open loop predictions (not explicitly included in Algorithm 1 for the sake of simplicity).
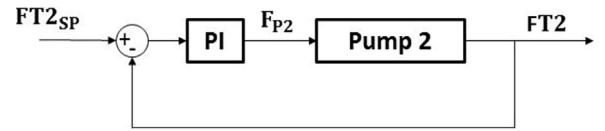
Fig. 8. FT2 control scheme.

Algorithm 1. Procedure to estimate $\mathbf{F}$ and $\mathbf{G}_{PNMPC}$

1.	To obtain $\hat{\mathbf{Y}}^0$, which is a vector of N elements, where N is the prediction horizon, the model should be executed using past inputs, outputs and the prediction of the measurable disturbances (see Section 5.3), with[a] $\boldsymbol{\Delta}\mathbf{U} = [0\,0\ldots0]^t$. So that, $\mathbf{F} = \hat{\mathbf{Y}}^0$.
2.	To calculate the first column of $\mathbf{G}_{PNMPC}$. $\hat{\mathbf{Y}}^1$ is obtained as it has been detailed in the previous step, but in this case $\boldsymbol{\Delta}\mathbf{U} = [\epsilon\,0\ldots0]^t$, where ε is a small increment in the control signal, e.g. $\frac{u(k-1)}{1000}$. $\mathbf{G}_{PNMPC}(:,1) = \frac{\hat{\mathbf{Y}}^1 - \hat{\mathbf{Y}}^0}{\epsilon}$.
3.	The second column of the $\mathbf{G}_{PNMPC}$, is estimated by calculating $\hat{\mathbf{Y}}^2$ with $\boldsymbol{\Delta}\mathbf{U} = [0\,\epsilon\ldots0]^t$. $\mathbf{G}_{PNMPC}(:,2) = \frac{\hat{\mathbf{Y}}^2 - \hat{\mathbf{Y}}^0}{\epsilon}$.
4.	Continue with the remaining columns of $\mathbf{G}_{PNMPC}$ using the same procedure as in the two previous steps. Notice that number of column of $\mathbf{G}_{PNMPC}$ is determined by the control horizon N_u, so the last column is given by: $\mathbf{G}_{PNMPC}(:,N_u) = \frac{\hat{\mathbf{Y}}^{N_u} - \hat{\mathbf{Y}}^0}{\epsilon}$.

5.2.1. Cost functions

In PNMPC controllers, the control signal is calculated by minimizing a cost function. In this case, three different cost functions have been formulated. It should be taken into account that the control architecture includes two control modes. Thus, the first cost function is the one used by the PNMPC strategy in the tank fast heating mode, whereas the other two are the ones proposed for the normal operating mode.

The tank fast heating mode cost function is aimed at finding out the actual and future control changes ($\boldsymbol{\Delta}\mathbf{U}_{J1} = $TT2$_{SP}$) maximizing **TT3** ($\hat{\mathbf{Y}}_{J1}$):

$$J1 = -\sum_{j=1}^{N_1} \hat{Y}_{J1}(k+j|k), \tag{25}$$

where N_1 is the prediction horizon and $\hat{Y}_{J1}(k+j|k)$ is the prediction of TT3 at instant $k+j$, calculated with the information available at instant k.

The first cost function proposed for the normal operating mode tries to maximize **TT10** ($\hat{\mathbf{Y}}$) in order to increase the thermal efficiency and the distillate production, in accordance with the analysis presented in Section 4. This cost function also penalizes the future

control changes $\Delta \mathbf{U}$ ($\mathbf{U_1} = \mathbf{TT2}_{SP}$ and $\mathbf{U_2} = \mathbf{FT2}_{SP}$) by means of a weight factor λ_i:

$$J2 = -\sum_{j=1}^{N} \hat{Y}(k+j|k) + \sum_{i=1}^{2}\sum_{j=1}^{N_u} \lambda_i [\Delta U_i(k+j-1)]^2, \tag{26}$$

where N is the prediction horizon, N_u is the control horizon, $\hat{Y}(k+j|k)$ is the prediction of TT10 estimated at sample time $k+j$ with the information acquired up to discrete-time instant k, $\Delta U(k+j-1)$ is the future increment in the control variable i, where U_1 is $TT2_{SP}$ and U_2 is $FT2_{SP}$, and λ_1 and λ_2 are weighting factors affecting $\mathbf{U_1}$ and $\mathbf{U_2}$ respectively.

The second cost function proposed for the normal operating mode provides the actual and future control changes $\Delta \mathbf{U}$ ($\mathbf{U_1} = \mathbf{TT2}_{SP}$ and $\mathbf{U_2} = \mathbf{FT2}_{SP}$) minimizing the relation between the distillate production ($\hat{D}$) [m^3] and its associated electric costs ($\hat{E}_{Cost}$) [ ]:

$$J3 = \sum_{j=1}^{N} \frac{\hat{E}_{Cost}(k+j|k)}{\hat{D}(k+j|k)}. \tag{27}$$

In this cost function, $\hat{D}_{Flux}(k+j|k)$ is estimated using the MD module model (Eq. (13)), with the prediction of TT10 ($\hat{\mathbf{Y}}$) provided by the PNMPC strategy:

$$\hat{D}_{Flux}(k+j|k) = 24 \cdot (0.135 + 0.003 \cdot \hat{Y}(k+j|k) - 0.0204 \cdot TT11$$
$$-0.001 \cdot FT4 \tag{28}$$
$$+0.00004 \cdot \hat{Y}(k+j|k) \cdot FT4),$$

where TT11 and FT4 are constant at 20 °C and 600 L/h, respectively.

The electric costs associated to the operation can be divided in two parts, a fixed part that is not included in the cost function, produced by pumps which are operated with constant references (pump 3 and 4), and a variable part, included in the cost function, produced by pumps which are in charge of controlling TT2 and FT2 (pump 1 and 2). The electric power consumed by pumps is estimated with the characteristic pump curves provided by the manufacturer:

$$P_{Pump1}(k+j|k) \ [kW] = \frac{34.91 \cdot FT1(k+j|k) \cdot 0.06 + 120}{1000}, \tag{29}$$

$$P_{Pump2}(k+j|k) \ [kW] = \frac{22.72 \cdot U_2(k+j|k) \cdot 0.06 + 39.54}{1000}. \tag{30}$$

Notice that the electric power consumption of pump 2 can be included directly in the optimization problem because it depends on one of the outputs (FT2$_{SP}$). However, Eq. (29) depends on FT1 which is the control variable used to reach the other optimization output (TT2$_{SP}$), so this equation must be rewritten in terms of TT2$_{SP}$:

$$FT1(k+j|k) = \left[\frac{\beta \cdot L_{eq}}{c_p \cdot (U_1(k+j|k) - TT1(k+j|k))} \cdot I(k+j|k) \right.$$
$$\left. - \frac{H}{c_p} \cdot \frac{(\bar{T}(k+j|k) - T_a(k+j|k))}{(U_1(k+j|k) - TT1(k+j|k))} \right] \cdot \frac{c_1}{\rho}, \tag{31}$$

with

$$\bar{T}(k) = \frac{TT1(k+j|k) + U_1(k+j|k)}{2}, \tag{32}$$

where TT1 and T_a are considered constants in the ahead instant times, whereas I is predicted with the method showed in Section 5.3. Finally, $\hat{E}_{Cost}$ is calculated as the product of the electric power consumed by pumps during N and the mean electricity price in Spain (0.14 /kWh).

To solve the optimization problem, the *fmincon* solver of MAT-LAB has been chosen. This algorithm is based on the interior-point method, and it has been selected due to the problem being subjected to linear constraints (see next section) and it presents a smooth nonlinear behaviour.

5.2.2. Constraints

The cost functions presented in the previous section are subjected to three different kind of constraints. The first one, Eq. (33), limits the maximum and minimum changes allowed in the control signals (slew rate ones) at each sample time. These limits are imposed in order to obtain small setpoint movements trying to avoid security problems caused by transients. Thus, outlet solar field temperature steps are limited to 5 °C, whereas the steps in FT2 are limited to 1 L/min.

$$\boldsymbol{\Delta U}_{min} \leq \boldsymbol{\Delta U}(k+j|k) \leq \boldsymbol{\Delta U}_{max}$$
$$j = 0, \ldots, N_u - 1. \tag{33}$$

The second constraint, Eq. (36), defines the physical limits of the controlled variables. Pump 2 reachable ranges are 15–25 L/min. On the other hand, the maximum and minimum temperatures (T$_{max}$ and T$_{min}$) reachable by the solar field are not constants and vary in accordance with the operational conditions. To address this problem, these limits are calculated at each sample time, using a static version of the solar field model:

$$T_{min}(k) = TT1(k) + \frac{\beta \cdot L_{eq} \cdot I(k) \cdot}{c_p} - H \cdot \frac{(\bar{T}(k) - T_a(k) \cdot c_1}{FT1_{max} \cdot c_p \cdot \rho}, \tag{34}$$

$$T_{max}(k) = TT1(k) + \frac{\beta \cdot L_{eq} \cdot I(k) \cdot}{c_p} - H \cdot \frac{(\bar{T}(k) - T_a(k) \cdot c_1}{FT1_{min} \cdot c_p \cdot \rho}, \tag{35}$$

where FT1$_{min}$ is 7.5 L/min and FT1$_{max}$ is 16 L/min.

$$\mathbf{U}_{min} \leq \mathbf{U}(k+j|k) \leq \mathbf{U}_{max}$$
$$j = 0, \ldots, N_u - 1. \tag{36}$$

Finally, the third constraint limits the output vector **TT10** to 80 °C that is the maximum temperature allowed by materials of the membranes. It should be taken into account that it is not necessary to limit **TT3** ($\hat{\mathbf{Y}}_{J1}$) when the fast heating tank mode is used, since it is switched before reaching a high temperature (see Section 5.5).

$$Y_{min} \leq Y(k+j|k) \leq Y_{max}$$
$$j = 0, \ldots, N. \tag{37}$$

5.3. Irradiance estimation

To complete the PNMPC strategy and to improve its performance, the irradiance behaviour is estimated by means of the DES technique (Pawlowski et al., 2011). Notice that ambient temperature could be also estimated with the same technique, however, it does not suffer significant changes along the sample time adopted. In this manner, the irradiance estimation is given by:

$$S_k = \alpha \cdot I_k + (1-\alpha) \cdot (S_{k-1} + b_{k-1}), \tag{38}$$

$$b_k = \theta \cdot (S_k - S_{k-1}) + (1-\theta) \cdot b_{k-1}, \tag{39}$$

where S is the estimated series value, and b is the estimated trend, which are calculated using actual and past series values. The constants α and $\theta \in (0,1)$ have been characterized by means of optimization techniques using experimental irradiance values. Thus, the estimation of m periods is given by:

$$\hat{I}_{k+m} = S_k + m \cdot b_k. \tag{40}$$

Several methods can be employed to set the initial values for S and b according to NIST (2016). In this case:

$$S_o = I_k, \tag{41}$$

$$b_o = \frac{1}{3}\sum_{j=0}^{2} I_{k-j} - I_{k-j-1} \qquad (42)$$

It should be considered that this forecasting irradiance method calculates N future values according to the prediction horizon of the PNMPC controller. Hence, to reconstruct the signal according to the sample time of the lower layer, the Lagrange interpolation method has been employed, in consonance with the ideas presented in (Pawłowski et al., 2014). Thus, supposing that the discrete data set is composed by N samples, such as $\{(t_0, I_0), \ldots (t_N, I_N)\}$, the Lagrange polynomial applied to this problem is given by:

$$L(t) = \sum_{j=0}^{k} I_j \cdot l_j, \qquad (43)$$

where

$$l_j(t) = \prod_{i=0, i \neq j}^{k} \frac{t - t_i}{t_j - t_i} = \frac{t - t_0}{t_j - t_0} \cdots \frac{t - t_{j-1}}{t_j - t_{j-1}} \frac{t - t_{j+1}}{t_j - t_{j+1}} \cdots \frac{t - t_k}{t_j - t_k}. \qquad (44)$$

5.4. Start-stop procedure

Based on the facility configuration and in the MD module operating limits (see Section 2.3), a start-stop procedure has been developed for the solar field and the MD module.

Due to irradiance conditions, TT2 can be lower than the tank temperature, causing the tank to cool down. To avoid this situation, the static model of the solar field is used to estimate the global irradiance value which ensures that TT2 is going to be higher that the tank temperature:

$$I(k) = \left[\frac{FT1(k) \cdot \rho}{c_1} - \frac{H}{c_p} \cdot \frac{(\bar{T}(k) - T_a(k))}{TT2(k) - TT1(k)} \right] \cdot$$
$$\frac{c_p \cdot (TT2(k) - TT1(k))}{\beta \cdot L_{eq}}, \qquad (45)$$

where TT2 is fixed at the same value as the top tank temperature and TT1 at the same value as the bottom tank temperature. Therefore, pump 1 is tuned on or off if the real irradiance value is higher or lower than the calculated one. This condition is evaluated each 5 min, in accordance with the sample time of the PNMPC strategy (see Section 6). Furthermore, to avoid chattering problems, a mean irradiance value of the last 10 min sampled each second is used.

In the same way, as it has been previously commented, it does not makes sense to operate the MD module with temperatures lower than 60 °C. To tackle this problem, the heat exchanger model has been used to calculate if the tank temperature allows to operate the MD module over 60 °C:

$$TT6_m(k) = TT5(k) - \eta_{he,1} \cdot (TT5(k) - TT9(k)), \qquad (46)$$

$$TT5_m(k) = \frac{TT10_{min}(k) - TT9(k) + \eta_{he,2} \cdot TT6_m(k)}{\eta_{he,2}}. \qquad (47)$$

where it is assumed that TT5 has the same value as the top tank temperature and $TT10_{min}$ is equal to 60 °C. TT9 is calculated with ΔT model (Eq. (14)). Hence, pump 2, 3 and 4 are turned on or off whether $TT5_m$ is respectively higher or lower than the tank temperature. This condition is also executed with a sample time of 5 min.

5.5. Decision maker

The aim of this block (see Fig. 6) is to switch between the two proposed control modes. Thus, this block selects the fast heating tank mode or the normal operating mode according to the following situations:

1. The tank temperature does not allow to operate the MD module over 60 °C. Thus, the start-stop procedure is in charge of turning on pump 1 according to the irradiance level, and this block selects the fast heating tank mode, which activates the optimization problem related to J1 (see Eq. (25)).
2. The global irradiance level permits to obtain an outlet solar field temperature higher than the tank temperature, and the tank temperature allows to operate the MD module over 60 °C. In this situation, the start-stop procedure turns on pumps 1, 2, 3 and 4 and the decision maker selects the normal operating mode, cost functions J2 or J3 (see Eq. (26, 27)).
3. The solar field cannot be operated with a temperature higher than the tank temperature, but the tank temperature allows to operate the MD module over 60 °C. Consequently, the start-stop procedure only turns on pump 2, 3 and 4, and the decision maker selects the normal operating mode. It should be stressed that, in this situation, the PNMPC strategy only provides setpoint for FT2, maintaining $TT2_{SP}$ equal to 0.

6. Simulation results

This section presents the simulation results obtained with the proposed control system, during a week with variable weather profiles. Fig. 9 shows the meteorological data from PSA used in the tests, corresponding to the days of March 6–12, 2017. Firstly, the control system performance is analyzed, making a comparison between the performance of the two control objective functions formulated for the normal operating mode. Secondly, the results obtained with the proposed control architecture are compared with a case in which only the direct control layer is employed with constant references. In addition, two potential industrial applications are suggested in order to evidence the benefits achieved with the proposed hierarchical control system in terms of thermal efficiency and cost savings.

The tests have been carried out with a sample time of 5 min in the upper layer and 5 s in the lower one. The control and prediction horizon in both modes, the fast heating tank mode and the normal operating mode, were 2. These values have been selected taking into account the closed-loop characteristic time constant of the solar field controller, the characteristic time constant of the intermediate buffer (tank) and the heat exchanger, and chattering problems observed in pump 1 when small values of the sample time are used and the start-stop procedure is evaluated. On the other hand, the use of a larger prediction horizon implies higher errors in the irradiance prediction, leading to inaccurate control actions. Besides, lower sample times have been tested without improving the results obtained with a sample time of 5 min. The weighting factor values adopted in J2 were $\lambda_1 = 0.1$ and $\lambda_2 = 1.1$, decided after simulating different combinations, while the DES technique parameters were $\alpha = 0.1$ and $\theta = 0.9$. Besides, FT4 has been fixed at 600 L/h, according to the study presented in Section 4, and FT3 is operated at the same value in order to achieve a maximum heat transfer in the heat exchanger.

6.1. Control system performance

In order to compare the performance of the hierarchical control system with the two objective functions proposed for the normal operating mode, the last simulation day is shown in Fig. 10 and 11 for J2 and J3 respectively.

The start-stop procedure enables that, at the beginning of the operation, the initial tank temperature is similar all the days, since
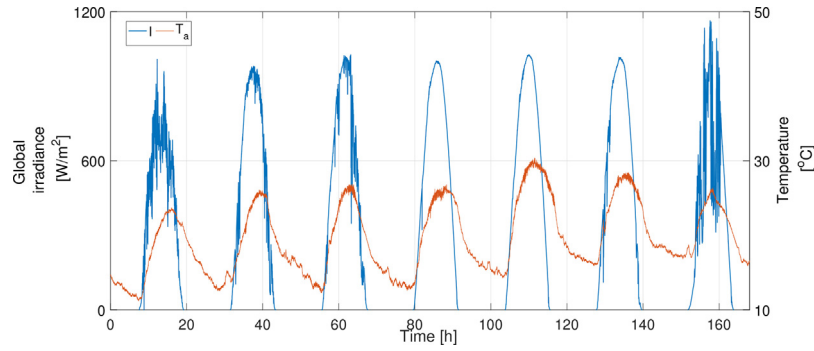
Fig. 9. Meteorological data from PSA.

Fig. 10. Control system performance with J2. (a) meteorological conditions, (b) solar field variables, (c) tank and distribution system variables and (d) MD module variables.

the start and stop conditions are the same, as it has been previously mentioned in Section 5.4. Thus, the operation in both cases starts at instant time 153.9 h. As the tank temperature is not high enough to operate the MD module, the decision maker selects the fast heating tank mode. Initially, this mode provides $TT2_{SP}$ close to the lower optimization temperature limit (normal behaviour in clear sky days), when FT1 is close to the maximum, to increase the water flow rate and increase the thermal power delivered to the tank. However, this operation is subjected to strong irradiance disturbances, so that, $TT2_{SP}$ and therefore FT1 vary according to disturbances. At instant 154.4 h, the start-stop procedure turns off pump 1 because the irradiance level is too low. After 12 min, pump 1 is turned on and the control system uses the fast heating tank mode to continue augmenting the tank temperature. It must be kept in mind that, in this kind of days, if the condition to turn on and off pump 1 was checked with instant irradiance values rather than mean ones, chattering problems might occur. In this way, even though the outlet solar field temperature is lower than the top tank temperature (TT3) in short time periods, the operation is more efficient and continuous.

At instant 155 h, the tank temperature reaches 62.4 °C which is high enough to operate the MD module over 60 °C. From this

moment the operation is different in both cases, due to the fact that decision maker selects the normal operating mode. Notice that in a clear sky day, when using J2, $TT2_{SP}$ is operated as in the fast heating mode (close to the T_{min} curve) whereas $FT2_{SP}$ is almost constant at the minimum when the solar field is used, and it is smoothly increased when the solar field is turned off. This increase is justified because, when the solar field is turned off and the tank temperature is high, the control system tries to keep the thermal energy stored in the tank, by maintaining as much as possible the temperature of the mixture produced in the distribution system (TT7). This procedure is displayed in Fig. 10 and 11.

On the other hand, when using J3, $TT2_{SP}$ is operated close to the upper limit (which causes FT1 to be close the minimum). Thus, the electric energy consumption of pump 1 is lower. Conversely, $FT2_{SP}$ is not operated at the minimum when the solar field is operating, as happens when using J2, since it varies in accordance with the operational conditions trying to increase the thermal energy stored in the tank. It should be taken into account that the electric consumption of pump 1 is higher than that of pump 2 (see Eq. (29 and 30)), in this way, the control system mainly acts over $FT2_{SP}$ to increase the distillate production. Then, when the solar field is not operated, $FT2_{SP}$ is smoothly increased again, as when J2 is used.
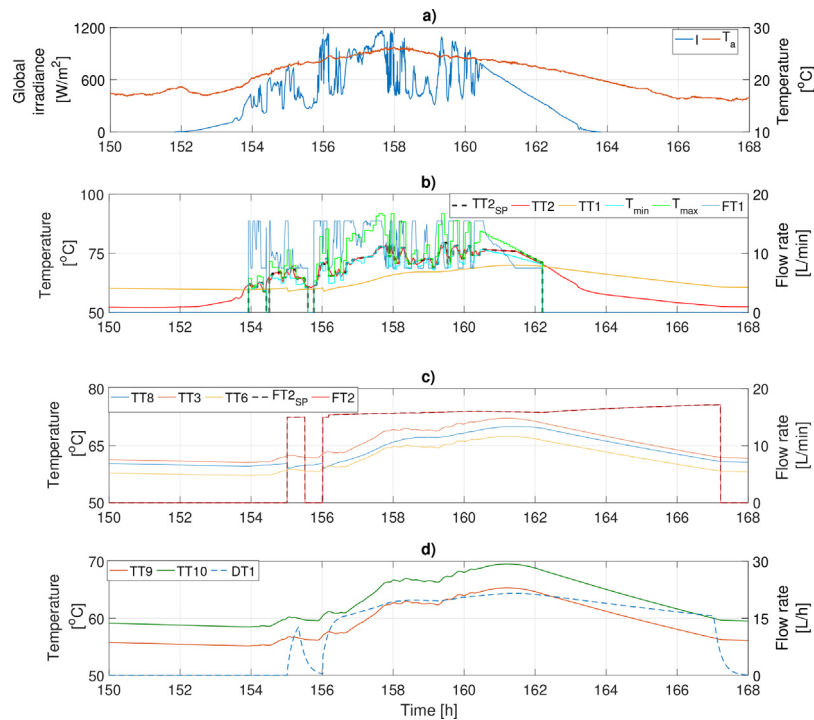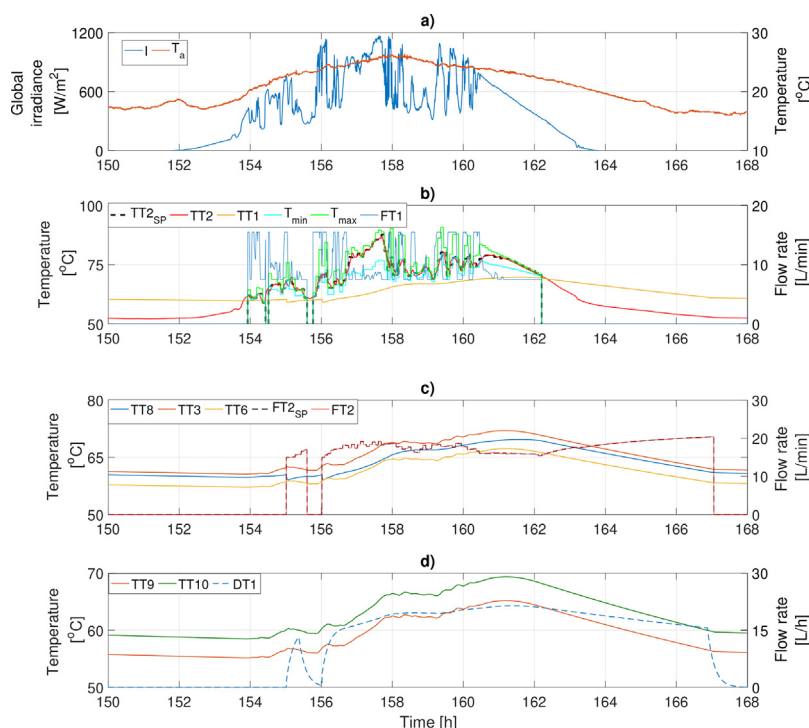
Fig. 11. Control system performance with J3. (a) meteorological conditions, (b) solar field variables, (c) tank and distribution system variables and (d) MD module variables.

Table 4
Comparison of simulation results.

PNMPC	N	MD-OH [h]	Distillate [L]	STEC [kWh/m³]	Costs [/m³]
No	–	97.49	1945	140.17	1.48
J2	2	102.50	2082	138.96	1.36
	3	102.47	2073	139.01	1.37
	4	102.42	2074	138.99	1.35
J3	2	100.50	2043	139.31	1.34
	3	100.83	2021	139.52	1.35
	4	101.33	2018	139.76	1.35

The operational procedure described previously can be observed in Fig. 10 and 11, but in this occasion the references experiment more changes due to irradiance variation. At instant 155.56 h and 155.55 h in Fig. 10 and 11 respectively, the solar field and the MD module are turned off because of strong disturbances. After 16 min, the operation is reestablished carrying on with the normal control operating procedure.

6.2. Comparison of results and discussion

Table 4 shows the comparison between the results obtained with the hierarchical control architecture, adopting different prediction horizons in the normal operating mode, and the ones obtained using only the direct control layer with TT2$_{SP}$ equal to 85 °C and FT2$_{SP}$ equal to 25 L/min. The stored distillate production during the seven days, supposing that it is not removed at the end of the operation, the mean STEC and the mean electric costs per volume unit of distillate in the seven days have been employed as performance indexes. Besides, the MD module operating hours (MD-OH) are also reported.

As can be observed in Table 4, all the performance parameters are improved by using the proposed hierarchical control system. One of the main advantages is that the PNMPC strategy permits to operate the MD module for longer time, between 30 and 40 min each day, depending on the objective function used in the nor-

mal operating mode. This fact, together with the increase of the evaporator inlet temperature, causes the distillate production to augment between 14 and 20 L each day. Notice that, in terms of distillate production, the results obtained with J2 are the best, as was expected.

Moreover, the mean STEC is also diminished in all the cases. It should be considered that STEC is an index that varies in accordance with the temperature. In this manner, although the optimum operation point is achieved working at the maximum temperature, when operating only with solar energy, the STEC tendency varies according to the irradiance behaviour. Thus, at the beginning of the operation the STEC value is high, around the solar midday when the thermal energy of the tank is maximum, STEC reaches its minimum value, and at the end of the operation when the thermal energy of the tank drops, STEC increases. It should be also taken into account that, as the PNMPC strategy makes the operation longer, working at low temperature during more time, the mean STEC value is penalized. Nevertheless, the STEC value is clearly improved, obtaining the best result by using J2 with N = 2 as expected, that provides a mean value of 1.21 kWh/m³ less than the case without the PNMPC strategy, which means that the proposed technique requires 1.21 kWh of thermal energy less to produce a volume unit of distillate.

In order to highlight STEC improvements and to compare in the same conditions both cases, a simulation has been carried out using the second day of meteorological data (see Fig. 9), establishing as stopping condition a distillate production of 200 L. Fig. 12 shows the variables affecting STEC for the case with PNMPC strategy (the ones with the subscript J2) using J2 with N = 2, and for the case without PNMPC strategy. As it has been discussed in Section 4, an increase in the evaporator inlet temperature (TT10) causes an augment in ∆T and the distillate production. According to Eq. (15), the increase of ∆T produces higher values of STEC, however, this increase is almost insignificant in comparison with the one achieved in the distillate production, thus minimizing STEC as can be observed in Fig. 12. Therefore, the use of the PNMPC strategy enables the STEC to be almost 3 kWh/m³ lower than the case without PNMPC while the solar field is used, and around 0.8 kWh/m³ when the solar field is
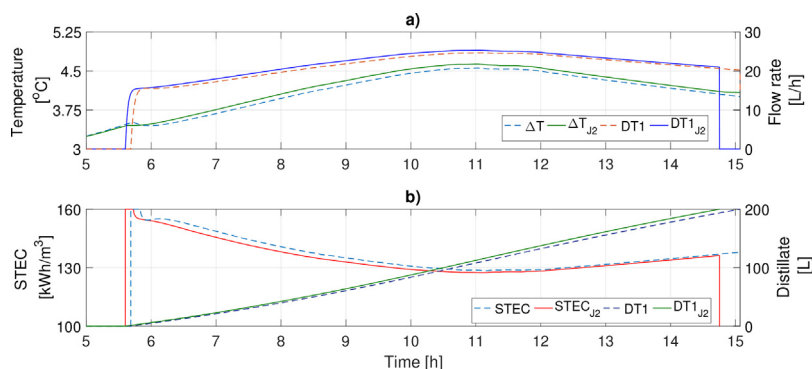
Fig. 12. STEC calculation. (a) variables affecting STEC, and (b) STEC and accumulative distillate production.

not operative. This fact evidences that the PNMPC strategy manages properly the solar energy, obtaining the maximum temperature reachable at each moment, and enabling the MD module to operate with a high thermal efficiency.

In addition, Fig. 12 highlights how the PNMPC strategy allows starting operation before, thanks to the fast heating tank mode, and reaches the desired distillate production before, thanks to the solar energy management produced by normal operating mode.

From an economic point of view, the results obtained are quite significant. Notice that to calculate the cost index, the fixed costs associated to the operation of pump 3 and 4 have not been taken into account. In the same way, it should be pointed out that, in the pilot facility pumps are oversized, so the absolute value of the electric costs presented in Table 4 are high, however the relative ones are valid. Thus, when J3 is used with $N = 2$ in the normal operating mode, 0.14 €/m³ of distillate produced can be saved.

At this point, it is important to mention that the SMD facility is a small-scale pilot plant one. In potential industrial cases the improvements in terms of thermal efficiency and economic costs can be very relevant. Consider the following two potential applications of MD technology:

1. Offgrid areas water supply. One of the main future application of SMD processes is the fresh water supply in offgrid areas with sea or brackish water access. In Spain, an inhabitant has an average water consumption of 142 L/day (Instituto Nacional de Estadística, 2013). In this way, in a small area of 3654 inhabitants, population of Tabernas (Almería) where the pilot facility is located, the use of the proposed control system, with J3 and $N = 2$, can save around 26514.15 € each year in comparison with an operation without PNMPC. In addition, the plant would require around 627.83 kWh less thermal energy each day, by using J2 with $N = 2$.

2. Crops water supply. An other potential application is to use MD technology to fulfil the irrigation water demand of cultivation areas close to the coast. According to the studio presented in Becerra and Bravo (2010), tomato crop growth, one of the most extended in the south of Spain, has a water demand of 4.11 m³/ha. Assuming a cultivation area of 20 ha (typical of small-medium size farmers in Almería, south of Spain), the use of the proposed control architecture, with J3 and $N = 2$, can save around 4200.42 € each year, requiring around 99.46 kWh less thermal energy each day if J2 with $N = 2$ is employed.

7. Experimental results

An experimental campaign has been carried out to evaluate the performance of the hierarchical control system in the SMD plant at PSA during March 2017. Figs. 13, 14 and 15 show the most representative results. The control system configuration employed in these tests is the same that the one used in the simulation tests (Section 6.1).

Firstly, Fig. 13 presents a test using J2 in a clear sky day. The operation starts at 10.85 h, using the normal operating mode since the tank temperature and irradiance level permit to operate the MD module and the solar field. As happened in simulation when using J2, $TT2_{SP}$ is close to the lower limit, thus maintaining FT1 at maximum and augmenting the thermal power delivered from the solar field to the tank (see Fig. 13b and c). On the other hand, $FT2_{SP}$ is kept close to the minimum. As there are not disturbances in the global irradiance, the operating evaporator temperature inside the module (TT10) increases over the course of the operation. At instant 14.8 h, TT10 reaches 79 °C, as can be observed in Fig. 13d, close to the temperature limit (80 °C) which can cause damage in the module membrane. Due to the fact that this limit is included in the optimization problem constraints, the algorithm increases $TT2_{SP}$, so that, FT1 decreases and the tank temperature is almost constant around 15.5 h. This action helps controlling the evaporator inlet temperature TT10, thus preventing it to reach 80 °C, as can be seen in Fig. 13d. Notice that in this test, the maximum distillate production (see Fig. 13d) reached is 30 L/h.

Secondly, Fig. 14 shows another test using J2 in the normal operating mode, but in this occasion there are irradiance disturbances caused by passing clouds. The operation starts at 9.85 h, using the fast heating tank mode because the tank temperature is not high enough to operate the MD module over 60 °C. As the tank temperature at the beginning is too low, the algorithm generates references close to T_{min}, thus maximizing the tank temperature working with FT1 close to the maximum. At instant 10.5 h, $TT2_{SP}$ begins to approach the lower limit, thus augmenting FT1, however, at 10.7 h irradiance disturbances cause the control algorithm to increase $TT2_{SP}$ again (see Fig. 14b).

At 11.26 h, the tank temperature reaches 63 °C and the MD module is turned on. In this moment, the inlet solar field temperature decreases due to cold recirculating fluid being introduced in the lower part of the tank, so that, FT1 decreases to maintain the desired reference $TT2_{SP}$. Then, from 11.4 to 12 h, $TT2_{SP}$ and FT1 vary according to irradiance disturbances (see Fig. 14b). In the same way, during this time period, $TT2_{SP}$ approaches the lower limit, thus increasing FT1, as expected in a normal operation (clear sky conditions). Until 15 h, the operation continues with this procedure, nevertheless, it should be remarked that FT1 experiments variations because of irradiance disturbances. Finally, at 15 h the irradiance level varies strongly, therefore FT1 decreases until saturating. As the strong irradiance disturbances lasts more than 10 min (see Fig. 14b), the mean irradiance value during this period abruptly decreases, thereby, the start-stop procedure turns off the solar field. Notice that, although the solar field is turned off, the MD module is kept operating (see Fig. 14c and d) since the tank temperature enables the module to operate over 60 °C.

Fig. 13. Experimental results with J2 in a clear sky day. (a) meteorological conditions, (b) solar field variables, (c) tank and distribution system variables and (d) MD module variables.

Fig. 14. Experimental results with J2 in a cloudy day. (a) meteorological conditions, (b) solar field variables, (c) tank and distribution system variables and (d) MD module variables.

Thirdly, Fig. 15 shows a test using J3 in the normal operating mode. As in the previous case, at the beginning of the operation the tank temperature is low, so the decision maker selects the fast heating tank mode. In this way, as there are not irradiance disturbances and the tank temperature is not as low as in the previous case, the algorithm keeps TT2$_{SP}$ close to the lower limit as expected in a clear sky operation day. Then, at 12.4 h, the decision maker changes to the normal operating mode, at this point, the inlet solar field temperature strongly decreases, due to the fact that cold fluid coming from the distribution system is introduced in the lower part of the tank. In this way, according to Eq. (34 and 35) the optimization temperature limits, and therefore TT2$_{SP}$, decrease (see Fig. 15b). Then, according
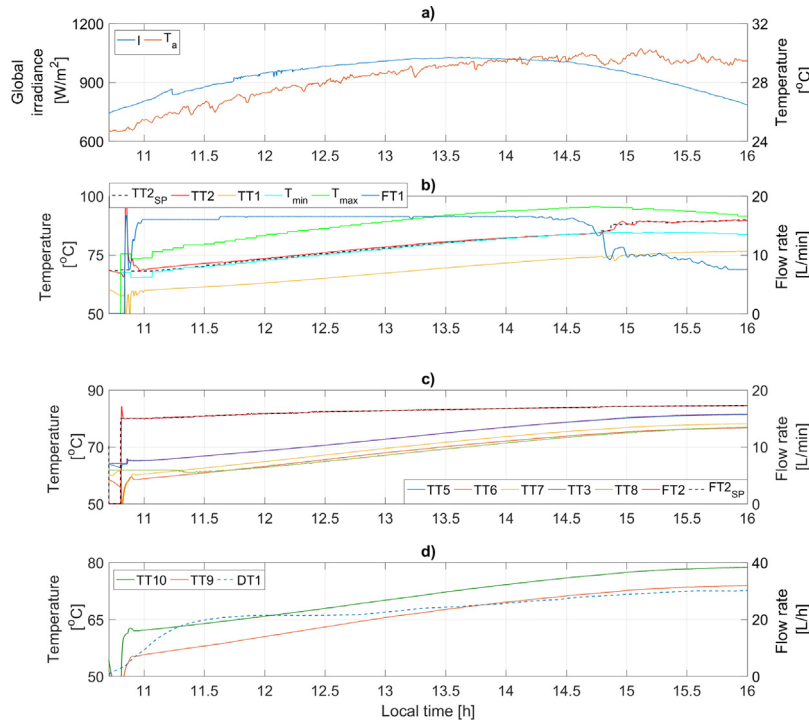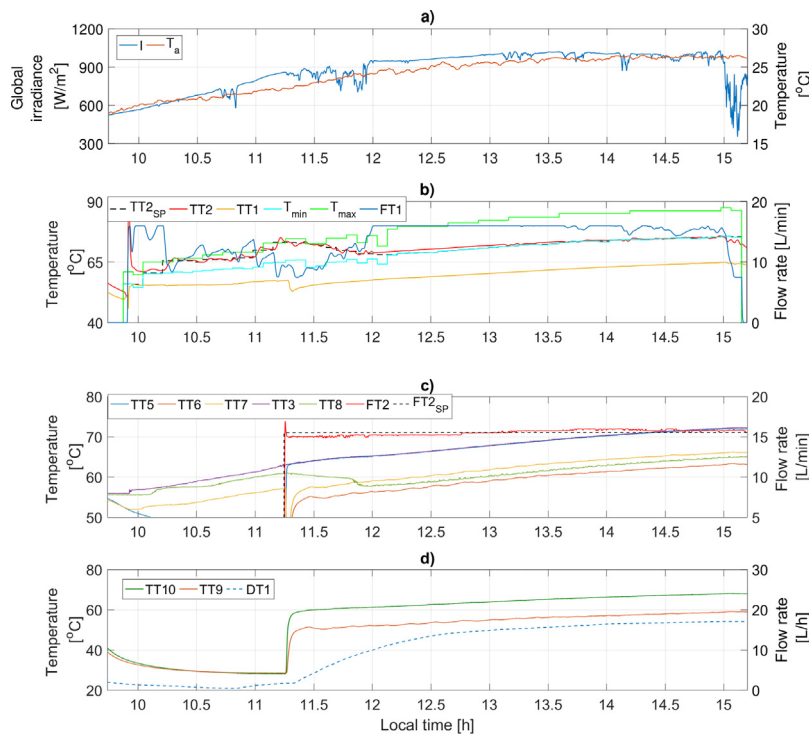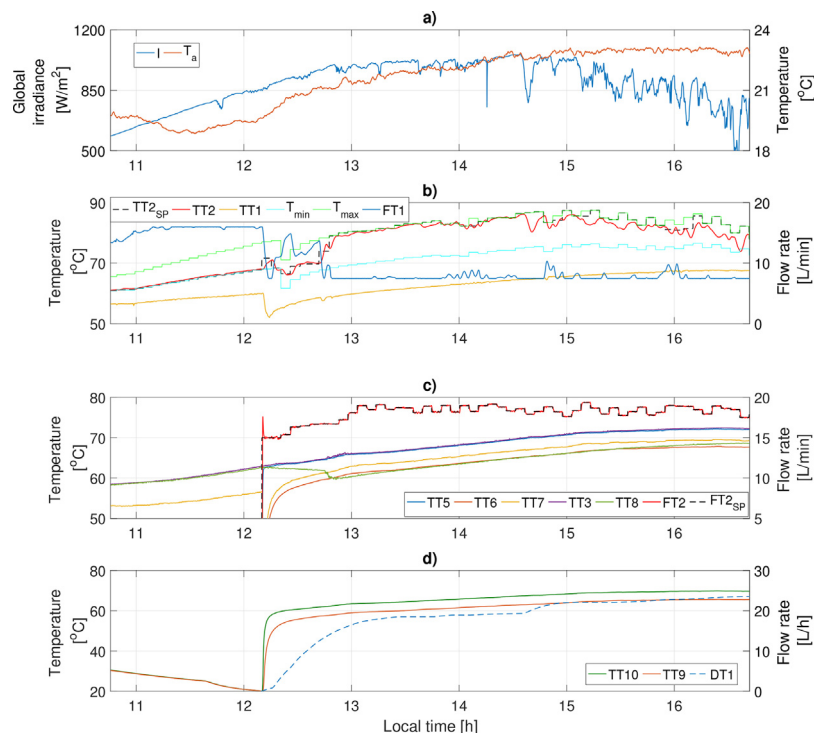
Fig. 15. Experimental results with J3 in a cloudy day. (a) meteorological conditions, (b) solar field variables, (c) tank and distribution system variables and (d) MD module variables.

to the simulation tests with J3, the control algorithm varies $FT2_{SP}$ in accordance with disturbances and $TT2_{SP}$, trying to maximize the thermal energy stored in the tank, as it can be observed in Fig. 15c. It should be mentioned that, in this kind of days with large irradiance variations, there are some periods in which the references calculated by the upper layer cannot be reached by the lower one, as can be observed in Fig. 15 from 14.5 h. Although the method presented in Section 5.2.2 to calculate the maximum and minimum temperatures reachable by the solar field provides reliable results, it is based on a static model and some errors are obtained when sudden disturbances occur such as in the case of irradiance in cloudy days. This fact is specially remarkable when using J3, since this objective function tries to maintain FT1 close to the lower limit to minimize the costs, and the solar field controller is saturated or close to saturation, so it is not able to reach or regulate around the setpoint.

8. Conclusions

This work focuses on optimizing the solar-powered operation of a MD facility in terms of distillate production, thermal energy and economic costs, taking into account the intermittent availability of energy caused by the use of solar energy as source. To deal with this problem, a hierarchical control system composed by two layers is proposed. The upper layer is based on a PNMPC controller that includes an optimization problem, whereas the inner one consists on a direct control system formed by PI plus feedforward controllers. In addition, two control modes and a start-stop procedure have been developed to complete the hierarchical control system.

The proposed control system has been tested in simulation, in the nonlinear test-bed model, and experimentally, in the solar-MD pilot plant at PSA. The results obtained in the pilot plant, show that the proposed control system is able to improve the daily distillate production in 14–20 L, reduce the thermal energy demand in 0.41–1.21 kWh/m^3 and diminish the costs in 0.11–0.14 $€/m^3$,

depending on the objective function adopted in the PNMPC strategy. These results have been extrapolated to two real potential applications of MD technology, evidencing that the control system can save around 26514 $€$/year and 627.83 kWh/m^3 in the supply of a small representative area of 3654 inhabitants, and 4200.42 $€$/year and 99.46 kWh/m^3 in the supply of a greenhouse tomato growth area of 20 ha.

In future works, the proposed control architecture will be extended to the non renewable resources, in order to undertake the night operation of the facility. Then, the full control strategy will be integrated in an optimization problem that allows to obtain an optimal design of a SMD facility, according to the water demand of the application scenario.

References

Alkhudhiri, A., Darwish, N., Hilal, N., 2012. Membrane distillation: a comprehensive review. Desalination 287, 2–18.
Álvarez, J., Redondo, J., Camponogara, E., Normey-Rico, J., Berenguel, M., Ortigosa, P., 2013. Optimizing building comfort temperature regulation via model predictive control. Energy Build. 57, 361–372.
Andrade, G., Pagano, D., Álvarez, J., Berenguel, M., 2013. A practical NMPC with robustness of stability applied to distributed solar power plants. Solar Energy 92, 106–122.
Becerra, A.T., Bravo, X.L., 2010. La agricultura intensiva del poniente almeriense. diagnóstico e instrumentos de gestión ambiental. M+ A. Rev. Electrón. Medioambiente, 18–40.
de la Calle, A., Roca, L., Bonilla, J., Palenzuela, P., 2016. Dynamic modeling and simulation of a double-effect absorption heat pump. Int. J. Refrig. 72, 171–191.
Castilla, M., Álvarez, J., Normey-Rico, J., Rodríguez, F., 2014. Thermal comfort control using a non-linear MPC strategy: a real case of study in a bioclimatic building. J. Process Control 24, 703–713.

Chang, H., Lyu, S.-G., Tsai, C.-M., Chen, Y.-H., Cheng, T.-W., Chou, Y.-H., 2012. Experimental and simulation study of a solar thermal driven membrane distillation desalination process. Desalination 286, 400–411.

Chang, H., Wang, G.-B., Chen, Y.-H., Li, C.-C., Chang, C.-L., 2010. Modeling and optimization of a solar driven membrane distillation desalination system. Renew. Energy 35, 2714–2722.

Cipollina, A., Di Sparti, M., Tamburini, A., Micale, G., 2012. Development of a membrane distillation module for solar energy seawater desalination. Chem. Eng. Res. Des. 90, 2101–2121.

Duffie, J.A., Beckman, W.A., 1980. Solar Engineering of Thermal Processes. John Wiley and Sons, New York, NY.

Duong, H.C., Cooper, P., Nelemans, B., Cath, T.Y., Nghiem, L.D., 2016. Evaluating energy consumption of air gap membrane distillation for seawater desalination at pilot scale level. Sep. Purif. Technol. 166, 55–62.

Gil, J.D., Ruiz-Aguirre, A., Roca, L., Zaragoza, G., Berenguel, M., 2015a. Solar membrane distillation: a control perspective. In: 23th Mediterranean Conference on Control and Automation (MED, Torremolinos, Málaga, Spain, pp. 796–802.

Gil, J.D., Ruiz-Aguirre, A., Roca, L., Zaragoza, G., Berenguel, M., Guzmán, J.L., 2015b. Control de plantas de destilación por membranas con apoyo de energía solar-parte 1: Esquemas (Control of membrane distillation plants with solar energy support – part 1: Schema). In: XXXVI Jornadas Autom’atica, Bilbao, España.

Gil, J.D., Ruiz-Aguirre, A., Roca, L., Zaragoza, G., Berenguel, M., Guzmán, J.L., 2015c. Control de plantas de destilación por membranas con apoyo de energía solar-parte 2: resultados (control of membrane distillation plants with solar energy support – part 2: results). In: XXXVI Jornadas Autom’atica, Bilbao, España.

Guillén-Burrieza, E., Zaragoza, G., Miralles-Cuevas, S., Blanco, J., 2012. Experimental evaluation of two pilot-scale membrane distillation modules used for solar desalination. J. Membr. Sci. 409, 264–275.

He, Q., Li, P., Geng, H., Zhang, C., Wang, J., Chang, H., 2014. Modeling and optimization of air gap membrane distillation system for desalination. Desalination 354, 68–75.

2013. Instituto Nacional de Estadística. http://www.ine.es/prensa/np807.pdf.

Karam, A.M., Laleg-Kirati, T.M., 2015. Real time optimization of solar powered direct contact membrane distillation based on multivariable extremum seeking. In: 2015 IEEE Conference on Control Applications (CCA), IEEE, pp. 1618–1623.

Khayet, M., Cojocaru, C., 2012. Air gap membrane distillation: desalination, modeling and optimization. Desalination 287, 138–145.

NIST, 2006. Engineering Statistics Handbook. http://www.itl.nist.gov/div898/handbook/.

Pawłowski, A., Guzmán, J.L., Berenguel, M., Dormido, S., 2014. Lagrange interpolation for signal reconstruction in event-based GPC. In: Emerging Technology and Factory Automation (ETFA), 2014 IEEE, IEEE, pp. 1–7.

Pawlowski, A., Guzmán, J.L., Rodríguez, F., Berenguel, M., Normey-Rico, J.E., 2011. Predictive control with disturbance forecasting for greenhouse diurnal temperature control. IFAC Proc. Vol. 44, 1779–1784.

Plucenio, A., Pagano, D., Bruciapaglia, A., Normey-Rico, J., 2007. A practical approach to predictive control for nonlinear processes. IFAC Proc. Vol. 40, 210–215.

Porrazzo, R., Cipollina, A., Galluzzo, M., Micale, G., 2013. A neural network-based optimizing control system for a seawater-desalination solar-powered membrane distillation unit. Comput. Chem. Eng. 54, 79–96.

Roca, L., Guzman, J.L., Normey-Rico, J.E., Berenguel, M., Yebra, L.J., 2009. Robust constrained predictive feedback linearization controller in a solar desalination plant collector field. Control Eng. Pract. 17, 1076–1088.

Ruiz-Aguirre, A., Alarcón-Padilla, D.C., Zaragoza, G., 2015. Productivity analysis of two spiral-wound membrane distillation prototypes coupled with solar energy. Desalin. Water Treat. 55, 2777–2785.

Ruiz-Aguirre, A., Andrés-Mañas, J., Fernández-Sevilla, J., Zaragoza, G., 2017a. Comparative characterization of three commercial spiral-wound membrane distillation modules. Desalin. Water Treat. 61, 152–159.

Ruiz-Aguirre, A., Andrés-Mañas, J., Fernández-Sevilla, J., Zaragoza, G., 2017b. Modeling and optimization of a commercial permeate gap spiral wound membrane distillation module for seawater desalination. Desalination 419, 160–168.

Zaragoza, G., Ruiz-Aguirre, A., Guillén-Burrieza, E., 2014. Efficiency in the use of solar thermal energy of small membrane desalination systems for decentralized water production. Appl. Energy 130, 491–499.

2.2.2 Hierarchical control for the start-up procedure of solar thermal fields with direct storage

Research in this field is supported by the following journal publication:

Title	Hierarchical control for the start-up procedure of solar thermal fields with direct storage
Authors	**J. D. Gil**, L. Roca, G. Zaragoza, J. E. Normey-Rico, M. Berenguel
Journal	Control Engineering Practice
Year	2020
Volume	95
Pages	-
DOI	`https://doi.org/10.1016/j.conengprac.2019.104254`
IF (JCR 2018)	3.232
Categories	Automation & Control Systems (22/62) **Q2**
	Engineering, Electrical & Electronic (81/266) Q2

Contribution of the Ph.D. candidate

The Ph.D. candidate, J. D. Gil, is the main contributor and first author of this paper.

Aside to the main contribution, the following contributions were published in international conferences:

- **J. D. Gil**, L. Roca, M. Berenguel, and J. L. Guzmán, "A multivariable controller for the start-up procedure of a solar membrane distillation facility," *IFAC–PapersOnLine,* vol. 51, no. 4, pp. 376–381, 2018.
- **J. D. Gil**, L. Roca, and M. Berenguel, "Starting-up strategies for solar thermal fields attending to time and economic criteria: Application of hierarchical control," *IFAC–PapersOnLine (In press).*

Besides, it resulted also in the following contribution to a national conference:

- **J. D. Gil**, L. Roca, M. Berenguel, and J. L. Guzmán, "Optimización del arranque de una planta de destilación por membranas solar," in *Actas IV Simposio CEA de Modelado, Simulación y Optimización.* Valladolid (Spain), 2018.

Hierarchical control for the start-up procedure of solar thermal fields with direct storage

Juan D. Gil [a], Lidia Roca [a,b], Guillermo Zaragoza [b], Julio E. Normey-Rico [c], Manuel Berenguel [a,*]

[a] *Centro Mixto CIESOL, ceiA3, Universidad de Almería, Ctra. Sacramento s/n, Almería 04120, Spain*
[b] *CIEMAT-Plataforma Solar de Almería, Ctra. de Senés s/n, Tabernas 04200, Almería, Spain*
[c] *Federal University of Santa Catarina, Department of Automation and Systems, Florianópolis, Brazil*

ARTICLE INFO

ABSTRACT

Thermal energy storage tanks are habitually combined with solar thermal fields to improve the dispatchability of these facilities. From the dynamical point of view, the start-up phase is relevant since if the storage device is unloaded in terms of energy or widely stratified, the transitory regime can take long time until reaching the operating point. In this paper, an optimal real-time procedure based on a hierarchical controller for improving the start-up phase is proposed. The hierarchical controller is composed of two layers based on a Model Predictive Control (MPC) technique and Proportional Integer Derivative (PID) controllers. Real experimental tests were performed in a pilot facility located at Plataforma Solar de Almería (Almería, Spain). In addition, a comparison in simulation with the typical manual procedure and with two techniques proposed previously in the literature for the same plant is provided. The results demonstrate the benefits obtained by using the proposed method; since it reduces the start-up phase in 34 [min] in comparison with the manual operation, and in 26 and 6 [min] with respect to the two previous techniques.

1. Introduction

In recent decades, the depletion of non-renewable energy resources such as fossil fuels, as well as the growing concern for atmospheric pollution, have led to an intensive search for alternative energy solutions, among which, solar thermal energy stands out. This technology plays a major role in any scenario of sustainable and efficient development with adequate conditions of solar irradiance, both to generate electricity and to feed thermal powered processes. Although the installation of solar thermal plants is spread throughout the world, there is still room for investigating and improving aspects that range from the design to the operation of these kind of plants (Kumar, Prakash, & Dube, 2018).

From the design point of view, as solar energy is an intermittent source, the integration of thermal storage systems in these kind of facilities has become a key factor to increase the performance of the technology (Gibb et al., 2018; Pelay, Luo, Fan, Stitou, & Rood, 2017; Rovira, Montes, Valdes, & Martínez-Val, 2011). Considering the solar field, the storage device, and the power block or the thermal load (depending of the kind of process powered), several layout configurations can be found in the literature attending to the number of storage tanks used in the facility, and the way in which they are connected to the system (Biencinto, Bayón, Rojas, & González, 2014). These layouts mainly are (see Fig. 1 (a)–(d)): (i) two-tank with indirect storage, as the

ANDASOL 3 plant which is described in Dinter and Gonzalez (2014), (ii) single-tank with indirect storage, as the facility analysed in Kolb (2011) and most of the low concentration solar plants (Abid, Yousef, Assad, Hepbasli, & Saeed, 2018), (iii) two-tank with direct storage, as the GEMASOLAR plant (Casella, Casati, & Colonna, 2014), and (iv) single tank with direct storage as the ACUREX plant (Camacho & Gallego, 2013). It should be remarked that this last layout is also used in most of low concentration applications (Artur, Neves, Cuamba, & Leão, 2018). These configurations are the most used in the literature but not the only ones, since this is an open research field in which there are many authors proposing new designs (Sebastián, Abbas, Valdés, & Casanova, 2018) and connection modes between the different devices (Li et al., 2019; Rovira et al., 2011).

Even though the use of storage devices enables longer or continuous operations of the powered systems, and helps to balance transients caused by irradiance disturbances, only around 50% of the concentrated solar power facilities currently in operation include these kind of devices (Pelay et al., 2017). However, the continuous progress in thermal energy storage technology (Kuravi, Trahan, Goswami, Rahman, & Stefanakos, 2013), and the necessity of using it to make solar thermal energy competitive, have caused around 70% of the facilities in construction to include storage systems (Pelay et al., 2017). In this way,
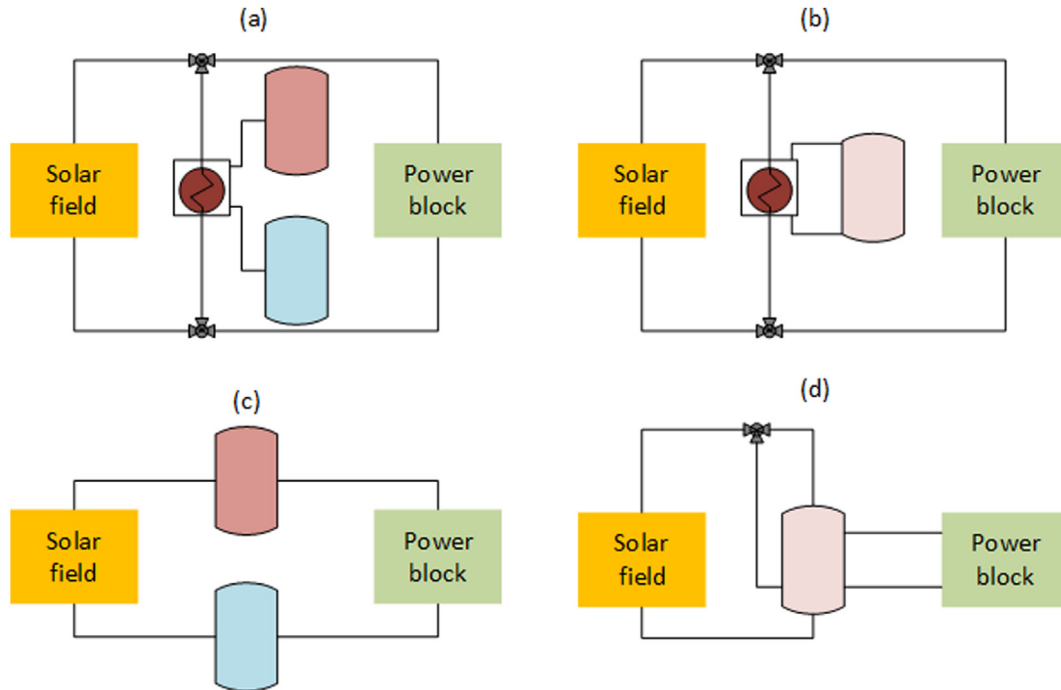
Fig. 1. Simplified schematic diagrams of the main thermal solar fields described in the literature. (a) Two-tank with indirect storage, adapted from Dinter and Gonzalez (2014), (b) single tank with indirect storage, adapted from Kolb (2011), (c) two-tank with direct storage, adapted from Casella et al. (2014), and (d) single tank with direct storage, adapted from Camacho and Gallego (2013).

the development of accurate operation strategies aimed at maximizing the performance of these facilities is essential.

Various works have been presented in the literature proposing operating methodologies for the plant configurations shown in Fig. 1. For the case of two-tank with indirect storage, in Relloso and Delgado (2009) the operating modes for the day and night times of ANDASOL 1 plant were described. In the same way, the operation of the ANDASOL 3 plant was documented in Dinter and Gonzalez (2014), presenting several operating modes to maximize the economic benefits. In Biencinto et al. (2014), different modes for charging and discharging the tanks were presented and analysed using a simulation environment, and in Guédez, Spelling, and Laumert (2015), an operating mode for minimizing the number of turbine starts was proposed. The operating strategy can be a solution of an optimization problem such as that presented in Usaola (2012); with the aim of maximizing the revenues and taking into consideration the daily electricity prices. Besides, an optimal-control framework was proposed in Rubio, Navas, Ollero, Lemos, and Ortega (2018) to maximize the thermal power supplied by the solar field. Regarding the single-tank with indirect storage configuration, an operating mode aimed at minimizing the thermocline degradation was presented in Biencinto et al. (2014), and compared with the operation of a two-tank with indirect storage based plant. Similarly, in Kolb (2011), the operating modes of these two configurations were compared. In the case of two-tanks with direct storage, in Casella et al. (2014), an optimal control procedure was presented for the operation of these kind of plants according to the variable electricity tariffs. A more extended control algorithm was proposed in Casati, Casella, and Colonna (2015) with the same aim. Moreover, optimal start-up policies were presented in Lopez-Alvarez, Flores-Tlacuahuac, Ricardez-Sandoval, and Rivera-Solorio (2018) which were obtained by means of a dynamical-optimization problem. Finally, in the case of single-tank with direct connection, a hierarchical control architecture was proposed in Berenguel et al. (2005); with the objective of maximizing the electricity production by optimizing in real-time the operation of the facility. A similar approach was proposed in Camacho and Gallego (2013), but in this case aimed at reducing thermal losses in the solar field.

Although all these works present optimal operating methodologies, the start-up procedure has hardly been addressed. A suitable start-up policy is essential not only for the first operation days, but also for the daily operation, especially in configurations with direct storage. In these kind of plants, the start-up procedure is usually performed using heuristic-rules, which are formulated according to the storage device states (Cirre, 2007). However, these rules can be inefficient since they do not explicitly take into consideration the operating constraints and the process disturbances. In facilities with two tanks with direct storage (see Fig. 1-(c)), the start-up problem has been already addressed by Lopez-Alvarez et al. (2018). In that work, an off-line dynamical-optimization problem was proposed for computing the optimal flow rate according to the states of the hot and cold tanks and irradiance conditions, trying to achieve full operation from shut-down as fast as possible. Nevertheless, in this off-line dynamical-optimization method, it was assumed that there were no process disturbances or model uncertainties, which is an ideal situation that does not happen in real operations, particularly if the disturbances are mainly caused by irradiance.

Motivated by the previous literature review, the main contributions of this work are: first, the use of the mixing valve as control variable, apart from the water flow rate (typical control variable in solar thermal fields), which allows the controller to cope with both the irradiance disturbance and temperature stratification problems during the start-up phase. It should be commented that there is no works in the literature that use this valve as control variable. Second, the development of a real-time procedure for the start-up phase of solar field plants with direct single-tank storage configuration. Note that this question has not been well discussed in literature as most published works proposed offline optimization techniques or rule-based procedures. The proposed technique is based on hierarchical controller composed by two layers. The upper layer includes a Model Predictive Control (MPC) strategy, which takes into account the operating conditions at each sampling time for computing the setpoints for the lower layer; trying to maximize the temperature in the storage device as fast as possible. The lower one is formed by Proportional Integral Derivative (PID) controllers which are in charge of tracking the setpoints provided by the upper
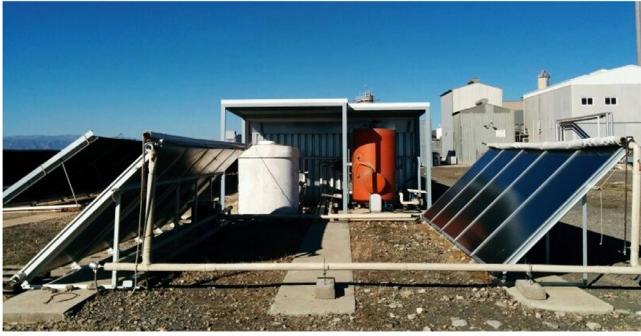
Fig. 2. Real facility at PSA.

layer by acting on the two aforementioned actuators: the flow rate and valve aperture (see Fig. 1-(d)). Third, the proposed method has been tested in a real facility located at Plataforma Solar de Almería (PSA). It should be remarked that the previous published works were only tested in simulation. Moreover, a comparative simulation study with two start-up methods previously proposed for the same facility and with a manual operation is provided in order to evidence the benefits achieved by the application of the proposed technique.

2. Plant description

The facility used as reference in this paper (see Fig. 2) is located in PSA (www.psa.es), and it is a test-bed for evaluating solar membrane distillation modules (Zaragoza, Ruiz-Aguirre, & Guillén-Burrieza, 2014). The layout of the system is shown in Fig. 3, and it includes a solar thermal field, a storage device and a membrane distillation module (thermal load).

The solar field of the facility is based on stationary flat-plate collectors Solaris CP1 Nova of 2 m^2, commercialized by Solaris (Spain). The collectors are disposed in two rows including five collectors each one. The nominal thermal power at about 90 °C is 7 kW, using water with antifreeze as heat transfer medium. In addition, the solar field is equipped with an expansion vessel and a cut valve (valve 2 in Fig. 3), which are used to absorb circuit pressure increases and protect the flat-plate collectors from evaporations. In particular, the valve is closed when the facility is not in operation, so if the temperature of the solar fluid increases and vapour is produced inside the absorber pipes, it flows to the expansion vessel. When the solar pump is turned on, the valve is opened and the water inside the expansion vessel is pushed again towards the collectors.

The solar field is directly linked with a thermal storage tank with a volume of 1.5 m^3. This device is used to balance transients and irradiance disturbances, as well as a buffer system to store thermal energy. The other side of the tank is connected with the thermal load which in this case is a membrane distillation unit, as was previously mentioned. Note that this connection is made through a heat exchanger, which is included in the membrane distillation unit. This technology, as most solar powered processes, requires a minimum operating temperature which in this case is 60 °C (Gil, Roca, Ruiz-Aguirre, Zaragoza and Berenguel, 2018). This fact implies that the storage tank must be at a certain operating point in terms of temperature before feeding the membrane distillation unit.

A Supervisory Control And Data Acquisition (SCADA) system is in charge of monitoring and controlling the installation with a 1 s sampling time. This system is coupled to the plant by means of an advanced data acquisition system manufactured by National Instruments. The measured and controlled variables of interest for this work are summarized in Table 1.

Table 1
Variables measured at the facility.

Variable	Description	Unit
FT$_l$	Water flow rate coming from the load to the tank	[L/min]
F$_{P1}$	Pump 1 input frequency percentage	[%]
FT1	Solar field water flow rate	[L/min]
T$_a$	Ambient temperature	[°C]
TT$_l$	Temperature coming from the load to the tank	[°C]
TT1	Inlet solar field temperature	[°C]
TT2	Outlet solar field temperature	[°C]
TT3	Temperature at the top of the tank	[°C]
TT4	Temperature around the middle of the tank	[°C]
TT5	Temperature at the bottom of the tank	[°C]
V1	Valve 1 aperture	[%]

3. System modelling

The facility was completely modelled in order to design the control system and perform simulation tests. Notice that the calibration and validation procedures of the models were already presented in Gil, Roca, Zaragoza and Berenguel (2018).

Firstly, the outlet solar field temperature was modelled using a lumped-parameter model as the one described in Roca, Berenguel, Yebra, and Alarcón-Padilla (2008). In this model, the outlet solar field temperature (TT2) is calculated based on the main variables that affect its performance: (i) global irradiance (I), (ii) inlet solar field temperature (TT1), (iii) ambient temperature (T$_a$), and (iv) solar field water flow rate (FT1). The model is formulated as follows:

$$A_c \cdot \rho \cdot c_p \cdot \frac{d\text{TT2}(t)}{dt} = \beta \cdot \text{I}(t) - \frac{H}{L_{eq}} \cdot (\bar{\text{T}}(t) - \text{T}_a(t)) - c_p \cdot \dot{m}_{eq}(t) \cdot \frac{\text{TT2}(t) - \text{TT1}(t)}{L_{eq}},$$

(1)

where:

$$L_{eq} = L \cdot n_{cs}, \quad \dot{m}_{eq}(t) = \frac{\text{FT1}(t) \cdot \rho}{c_f}, \quad \bar{\text{T}}(t) = \frac{\text{TT1}(t) + \text{TT2}(t)}{2}.$$

(2)

Notice that all the variables are defined in Tables 1 and 4, and the fluid considered in the model was water without antifreeze. It should be noted that this model is one of the most used to model solar thermal fields, especially for control purposes (Camacho, Berenguel, Rubio, & Martínez, 2012).

Secondly, TT1 was computed according to the mix produced in the three way mixing valve (Valve 1 in Fig. 3), which was modelled by means of a static mass balance:

$$\text{TT1}(t) = \text{TT2}(t) \cdot \frac{\text{V1}_m(t)}{100} + \text{TT5}(t) \cdot (1 - \frac{\text{V1}_m(t)}{100}),$$

(3)

where V1$_m$ was calculated according to the nonlinear static characteristic curve of the valve, which relates the fraction of the mass flow with the position of the valve stem. For modelling this nonlinear behaviour, several experimental tests were carried out, introducing positive and negative steps in the valve aperture, observing the static values of TT1, TT2 and TT5, and calculating with Eq. (3) the value of V1$_m$. Then, the experimental points were fitted by five order polynomials. Thereby, V1$_m$ for positive variations of the valve aperture was calculated as:

$$\text{V1}_m(t) = 1.6562 \cdot 10^{-7} \cdot \text{V1}(t)^5 - 4.1953 \cdot 10^{-5} \cdot \text{V1}(t)^4$$
$$+ 0.0033 \cdot \text{V1}(t)^3 - 0.0664 \cdot \text{V1}(t)^2 + 0.3292 \cdot \text{V1}(t),$$

(4)

whereas for the negative ones it was calculated as:

$$\text{V1}_m(t) = -3.3958 \cdot 10^{-7} \cdot \text{V1}(t)^5 + 7.2667 \cdot 10^{-5} \cdot \text{V1}(t)^4$$
$$- 0.0053 \cdot \text{V1}(t)^3 + 0.1719 \cdot \text{V1}(t)^2 - 1.8433 \cdot \text{V1}(t).$$

(5)

Moreover, both equations were limited between 0 and 100, which is the operating range of V1. Fig. 4 shows the adjustment between the experimental points and the polynomials.

Thirdly, the storage tank was modelled using a three-nodes stratified dynamic model, following the ideas presented in Duffie and Beckman
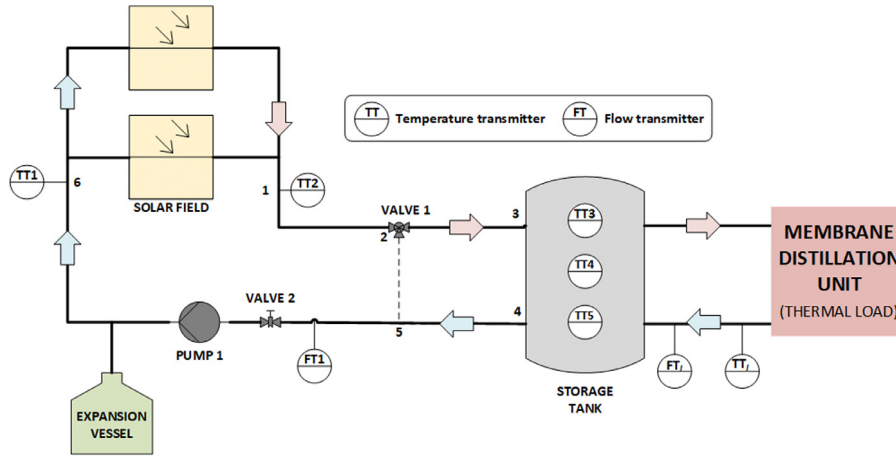
Fig. 3. Schematic diagram of the facility.
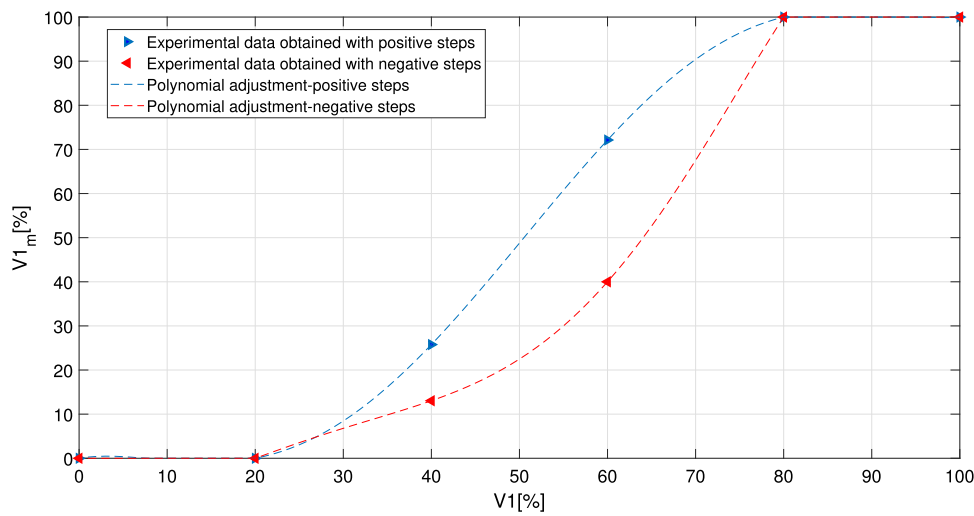
Fig. 4. Valve aperture fitting.

(2013). Thus, the temperature of each node was calculated by means of an energy balance as:

$$\frac{d\text{TT3}(t)}{dt} = \frac{1}{\rho \cdot V_a} \cdot \left[\dot{m}_{sf}(t) \cdot (\text{TT2}(t) - \text{TT3}(t)) \right.$$
$$\left. + \dot{m}_l(t) \cdot (\text{TT4}(t) - \text{TT3}(t)) - \frac{\alpha_1 \cdot (\text{TT3}(t) - \text{T}_a(t))}{c_p} \right], \quad (6)$$

$$\frac{d\text{TT4}(t)}{dt} = \frac{1}{\rho \cdot V_b} \cdot \left[\dot{m}_{sf}(t) \cdot (\text{TT3}(t) - \text{TT4}(t)) \right.$$
$$\left. + \dot{m}_l(t) \cdot (\text{TT5}(t) - \text{TT4}(t)) - \frac{\alpha_2 \cdot (\text{TT4}(t) - \text{T}_a(t))}{c_p} \right], \quad (7)$$

$$\frac{d\text{TT5}(t)}{dt} = \frac{1}{\rho \cdot V_c} \cdot \left[\dot{m}_{sf}(t) \cdot (\text{TT4}(t) - \text{TT5}(t)) \right.$$
$$\left. + \dot{m}_l(t) \cdot (\text{TT}_l(t) - \text{TT5}(t)) - \frac{\alpha_3 \cdot (\text{TT5}(t) - \text{T}_a(t))}{c_p} \right]. \quad (8)$$

All the variables and parameters are also defined in Tables 1 and 4. It should be remarked that, although the stratification volumes vary with respect to the time, constant volumes according to the actual position of the temperature transmitters in the tank were identified. Besides, the parameters modelling the thermal losses were obtained by using real data and characterization techniques as presented in Gil, Roca, Ruiz-Aguirre et al. (2018) and Gil, Roca, Zaragoza et al. (2018).

Fourthly, as the solar field water flow rate was varying during the daily operation due to the control system performance, the residence time of the fluid in the pipes was not constant. Therefore, there were variable transport delays which had to be estimated and included in the model to perform accurate simulations of the system, especially to test the controller (as control loops were affected by varying delays). These transport delays were estimated as flow-dependent delays as proposed in Normey-Rico, Bordons, Berenguel, and Camacho (1998). Taking into account that the flow rate changes at each sampling time t_s, the transport delay, $t_{r,i-j}$, can be estimated as integer multiples, n_{i-j}, of the sampling time, that is $n_{i-j} \cdot t_s \approx t_{r,i-j}$. Thus, the value of n_{i-j} was computed at each sampling time as:

$$l_{i-j} = \int_0^{t_{r,i-j}} v_{i-j}(t)dt \rightarrow l_{i-j} = \frac{t_s}{A_p} \sum_{h=0}^{h=n_{i-j}-1} f_{i-j}(k-1), \quad (9)$$

where i and j are referred to the points 1, 2, ..., 6 presented in Fig. 3, with $i-j \in \{1-2, 2-3, 2-5, 4-5, 5-6\}$, k is the actual sampling time, and the rest of parameters are defined in Tables 2 and 4. It should be noted that the temperature transmitters TT1 and TT2 are located right at the inlet and at the outlet of the solar field respectively, and therefore, the flow-dependent delays between these transmitters and the solar field were not significant.

Finally, several transfer functions of the First Order Plus Dead Time (FOPDT) were employed to model the effect of the control variables and actuators involved in the system with respect to the controlled variables. These transfer functions were experimentally obtained, performing open-loop tests with step changes in the actuators,

Table 2
Distance between points.

Distance between points (l_{i-j})	Value
l_{1-2}	15.30 [m]
l_{2-3}	1.73 [m]
l_{2-5}	0.77 [m]
l_{4-5}	1.69 [m]
l_{5-6}	12.12 [m]

Table 3
Transfer functions experimentally obtained.

$G(s)$	$Y(s)$	$U(s)$	K	$\tau[s]$	$t_d[s]$
$G_1(s)$	FT1(s)	$F_{P1}(s)$	0.234 [L/min %]	5	1
$G_2(s)$	TT2(s)	FT1(s)	−1.37 [°C min/L]	66.62	16
$G_3(s)$	TT1(s)	V1(s)	0.102 [°C/%]	43	79

Table 4
Definition of the parameters involved in the model.

Parameter	Description	Unit
A_c	Cross-section area of one fluid inside the flat-plate collector	$1.539 \cdot 10^{-4}$ [m^2]
A_p	Pipe cross-section area	$7.068 \cdot 10^{-4}$ [m^2]
c_f	Conversion factor to account for connections, number of modules and L/min conversion	$3.6 \cdot 10^6$ [s L/min m^3]
c_p	Specific heat capacity of water	[J/kg °C]
f_{i-j}	Water flow rate between points i and j	[m^3/s]
H	Solar field global losses coefficient	5.88 [J/s °C]
K	Static gain	
l_{i-j}	Distance between points i and j	[m]
L	Collector absorber tube length	1.95 [m]
L_{eq}	Equivalent absorber tube length	[m]
$\dot{m}_{eq}$	Equivalent solar-field mass flow rate	[kg/s]
$\dot{m}_l$	Load mass flow rate	[kg/s]
$\dot{m}_{sf}$	Solar field mass flow rate	[kg/s]
n_{cs}	Number of series-connections in a collectors group	5
n_{i-j}	Integer multiple for estimating the delay between point i and j	[–]
t_d	Time delay	[s]
$t_{r,i-j}$	Transport delay between points i and j	[s]
t_s	Sampling time	[s]
$\bar{T}$	Equivalent absorber tube mean temperature	[°C]
v_{i-j}	Velocity rate between points i and j	[m/s]
V_a	Volume, first stratification	0.4 [m^3]
V_b	Volume, second stratification	0.3 [m^3]
V_c	Volume, third stratification	0.8 [m^3]
$V1_m$	Variable modelling the nonlinear behaviour of valve 1	[%]
α_1	Thermal losses coefficient, first stratification	3.3 [J/s K]
α_2	Thermal losses coefficient, second stratification	2.9 [J/s K]
α_3	Thermal losses coefficient, third stratification	3.3 [J/s K]
β	Irradiance model parameter	0.134 [m]
ρ	Water density	[kg/m^3]
τ	Representative time constant	[s]

and using the reaction curve method to obtain the parameters of the FOPDT transfer functions as done in Gil, Roca, Zaragoza et al. (2018). In Table 3 the transfer functions, $G(s) = Y(s)/U(s) = K \cdot e^{-t_d s}/(\tau \cdot s + 1)$, for the mean operating range of each of the control variables are shown, where K is the static gain, τ the representative time constant, and t_d the delay time.

4. Control system

The goal of the proposed hierarchical controller consists on improving the start-up procedure of the plant used as test-bed. The thermal load of the facility, as most solar-powered processes, requires

a determined operating temperature to start the operation, which in this case is 60 [°C]. Moreover, it should be remarked that the thermal load is connected to the fluid coming from the tank through a heat exchanger, so the temperature at the top of the tank must be even higher. Therefore, if the temperature in the tank does not allow operating the membrane distillation unit, a start-up procedure must be implemented, in which the solar field is used to increase the temperature of the tank.

Traditionally, qualified operators perform this procedure in a manual way attending to heuristic rules as the ones presented in Cirre (2007). First, when the global irradiance reaches values between 500–600 [W/m^2], normal range in which most solar thermal facilities are turned on Dinter and Gonzalez (2014) and Kolb (2011), pump 1 is started, and the fluid is recirculated only through the solar field (i.e. with valve 1 close to the solar field). Afterwards, when a high temperature (such as 80 [°C]) is reached at the outlet of the solar field, valve 1 is opened towards the tank, circulating the fluid through it until reaching the required temperature to operate the thermal load. However, this manual procedure presents two main problems. The first one is related to the irradiance disturbances, since the operator must close valve 1 when there are severe irradiance disturbances to avoid loading the tank with cold fluid, which could be hard to perform in a manual way, especially when the disturbances are caused by passing clouds. The second problem is associated to the stratification of the storage tank. This kind of tanks are usually operated with several degrees of stratification (Duffie & Beckman, 2013), that means that the temperature at the top of the tank is higher than in the bottom. So, depending on the degree of stratification, when performing the manual start-up procedure and opening the valve 1 to recirculate the fluid through the tank, the temperature at the outlet of the solar field can drop drastically until the tank reaches a certain degree of homogeneity. For these reasons, the manual procedure can take long time, and it requires the full attention of an operator to ensure that the tank is not being loaded with cold fluid.

The first automatic approach for improving this manual start-up procedure was developed in the previous paper (Gil, Roca, Ruiz-Aguirre et al., 2018). In that work, the steady-state model of the solar field was used to estimate the value of irradiance required to turn the solar field on for heating the tank. In addition, a predictive controller was used to calculate the setpoints at the outlet of the solar field, trying to maximize the temperature in the tank, and a cascade controller was proposed for tracking these setpoints by acting in pump 1. Thus, the problem related to the irradiance disturbances was improved, and the solar field was turned on in a more deterministic way. However, the problem related to the stratification of the tank was not considered. A second step towards the improvement of the start-up procedure was presented in Gil, Roca, Berenguel and Guzmán (2018), in which valve 1, which was fixed in open position to feed the tank in the work mentioned above, was used as control variable allowing to obtain a proper temperature at the entrance of the solar field that guarantees a minimum temperature for heating the tank. The control structure proposed in that work was composed of a reference governor and a multivariable controller. On the one hand, the reference governor solved an optimization problem, using the steady-state model of the solar field, aimed at maximizing the temperature at the top of the tank, guaranteeing that the temperature of the fluid flowing to the tank was higher than the one at the top of the tank. On the other hand, the multivariable controller was tasked with tracking the setpoints computed by the reference governor by acting on both pump 1 and valve 1. Therefore, the irradiance disturbance and tank stratification problems were improved with this approach.

In the present work, the idea for improving the start-up procedure is the same that the one presented in Gil, Roca, Berenguel et al. (2018), which consists on using valve 1 as a control variable for heating the tank faster. However, the control structure has been considerably improved by using a hierarchical control system composed of two layers (see Fig. 5): (i) an upper layer based on a predictive controller, and (ii) a regulatory layer based on PID controllers. We have opted
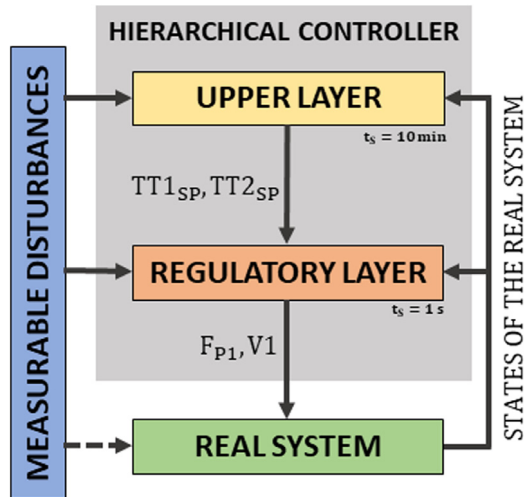
Fig. 5. Schematic diagram of the hierarchical control system.

for a hierarchical control structure (where the top layer calculates the setpoints to be tracked by the lower layer) instead of a classical optimal control structure (where the optimization directly calculates the control signals that are sent to the actuators) for two fundamental reasons: firstly, it is a more intuitive structure for the operators of the installation, allowing to maintain classic PID controllers in the regulation layer; secondly, because optimal control strategies provide very aggressive control signals, which are not adequate for this type of installation. The schematic diagram of the hierarchical structure is shown in Fig. 6. In the upper layer, the predictive controller uses the nonlinear model of the system presented in Section 3 for making the predictions and calculating the setpoints for the regulatory layer. In this way, a prediction horizon and a nonlinear model are considered in the control procedure, allowing to calculate the setpoints more accurately than in the approach proposed in Gil, Roca, Berenguel et al. (2018), in which a steady-state model and static values are used for calculating the references. The regulatory layer comprises a cascade control scheme for controlling the outlet solar field temperature by acting on pump 1, and a Filtered Smith Predictor (FSP) structure for controlling the inlet temperature of the solar field by using valve 1. These two control systems were also used in the two loops of the multivariable controller proposed in Gil, Roca, Berenguel et al. (2018). However, in this work, the multivariable approach has not been considered due to the low interaction between the variables involved in the process, as was analysed in Gil, Roca, Berenguel et al. (2018). Moreover, the FSP controller has been improved by adding the nonlinear model of valve 1 (see Fig. 5).

4.1. Regulatory layer

The PID based regulatory layer includes two loops, and its objective consists on tracking the setpoints computed by the upper layer for the two controlled variables, i.e. TT1 and TT2, as well as maintaining them near steady state conditions around these references despite temperature or irradiance disturbances.

In order to control TT2, a cascade control loop is employed (see Fig. 6). The design and test of this loop were already presented in Gil, Roca, Zaragoza et al. (2018). According to Fig. 6, the slave controller (PI-2) is tasked with controlling the flow rate (FT1) by using the input frequency of pump 1 (F_{P1}), whereas the outer one (PI-1) is responsible for maintaining the desired temperature at the outlet of the solar field (TT2$_{SP}$) by acting on the flow rate (FT1$_{PID}$). In addition, a feedforward (FF) including the steady-state model of the solar field is used for improving the disturbance rejection of the loop. Notice that

Table 5
Parameters of controller blocks of the regulatory layer. k_c and T_i are the proportional gain and integral time of the Proportional Integral (PI) controller, and τ_F the characteristic time constant of the low pass filters. Notice that the PI controllers have been implemented using the ideal PID transfer function.

Block	k_c	T_i [s]	τ_F [s]
LPF-1	–	–	75
LPF-2	–	–	60
LPF-3	–	–	40
LPF-4	–	–	43
LPF-5	–	–	39.50
PI-1	−0.42 [L/min °C]	72.60	–
PI-2	2.84 [% min/L]	4.92	–
PI-3	14.01 [% °C]	43	–

at the outlet of the feedforward, a low pass filter (LPF-1) is added to achieve a better dynamical behaviour. In this way, the setpoint for the slave loop (FT1$_{SP}$), is calculated taking into account the contributions of the feedforward (FT1$_{FF}$) and the outer loop (FT1$_{PID}$), as well as the feedback. Finally, a low pass filter (LPF-2) is also included in the reference for reducing overshoots against reference step changes. The parameters of each of the blocks of this loop are shown in Table 5.

The second loop is used for controlling TT1 by acting on the Valve 1 aperture (V1). In this loop, a FSP structure is adopted (Normey-Rico & Camacho, 2007). This structure is appropriate for the problem at hand, since the nominal delay of the process (79 [s]) is dominant with respect to the characteristic time constant (43 [s]), see Section 3. In addition, there are modelling dead-time errors due to the transport delays caused by the variations of the flow rate, which degrades performance and can cause instability. In this way, the FSP approach adds robustness to the controller (Normey-Rico & Camacho, 2007), enabling to achieve the desired performance. The schematic diagram of the controller is shown in Fig. 7. Notice that the configuration of this loop was presented in Gil, Roca, Berenguel et al. (2018). However, in the present approach, a modification is introduced by including the nonlinear model of valve 1 and the mix produced in it, Eqs. (3), (4), and (5), in the fast model of the FSP structure. These static equations allow us to calculate TT1 taking into account the nonlinear characteristics of Valve 1, thus improving the control performance. Besides, a low pass filter (LPF-4) with the dynamic obtained at the medium operating range of V1 is used to complete the fast model and compute the predicted value of inlet temperature after the delay $\hat{TT}1(t + t_d)$. For modelling the time delay (t_d), the nominal error model shown in Table 3 has been used. Moreover, the filter of the SP structure (LPF-5) has been designed taking into account the variations between the maximum and minimum dead times observed in the system and the selected nominal dead time. These differences are around ±25 [%], so the time constant of the filter can be computed as $\tau_F = 0.5 \cdot t_d$, according to the recommendations given in Normey-Rico and Camacho (2007). It should be remarked that the reference (TT1$_{SP}$) is filtered by means of a low pass filter (LPF-3). The parameters of the controller are also presented in Table 5.

Finally, it should be remarked that an antiwindup scheme is included in each of the control loops. The operating limits of each of the control variables are 10–90 [%], 7.5-20 [L/min], and 20–80 [%] for pump 1 (F_{P1}), water flow rate (FT1) and valve 1 (V1) respectively. Notice that with frequencies lower than 10 [%] the pump is turned off. Both controllers have been implemented with a sampling time of 1 [s], which was chosen according to the fastest representative time constant of the variables involved in the loops, which is the one of the transfer function relating the flow rate and the pump frequency (see Table 3).

4.2. Upper layer

This layer is in charge of calculating the setpoints, TT1$_{SP}$ and TT2$_{SP}$, for the regulatory layer, trying to increase TT3 faster, so that the operational time of the facility is maximized. The control methodology
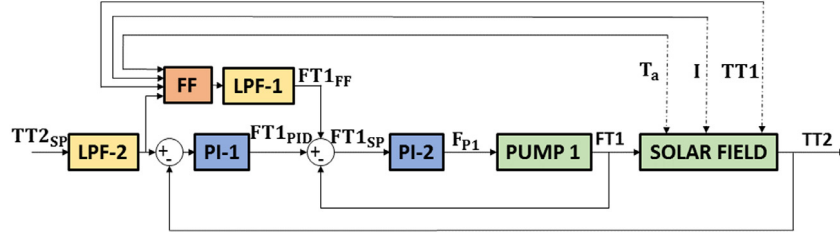
Fig. 6. Schematic diagram of the outlet solar field temperature controller.
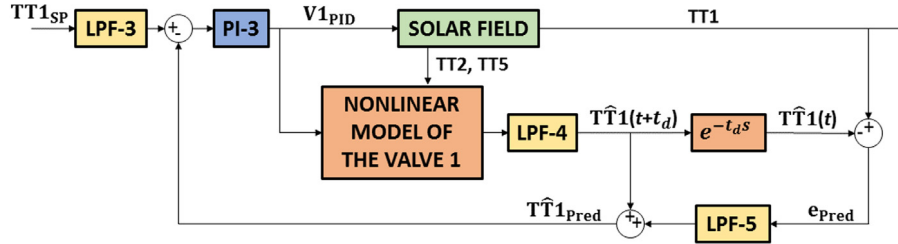

Fig. 7. Schematic diagram of the inlet solar field temperature controller.

chosen for developing this layer is the MPC technique. This advanced control strategy is one of the most generic ways of formulating a control problem, and it has been selected because it intrinsically deals with the main problems presented in the facility used in this work, mainly long time delays and disturbances (Camacho & Bordons, 2004). Besides, this control technique has been already applied in solar thermal fields with satisfactory results (De Andrade, Álvarez, Pagano, & Berenguel, 2015; Gallego, Merello, Berenguel, & Camacho, 2019).

There are different algorithms in the family of MPC controllers, however, the basis of all of them are the same:

1. use of a system model to compute the prediction of the process output in a prediction horizon;
2. formulation of an optimization problem to calculate the control sequence along the control horizon; and
3. use of a receding strategy, displacing at each sampling time the horizon towards the future, and applying in the actual system only the first control signal of the set computed at each step.

Their differences are due to the model that they use for representing the system and the noises, as well as the cost function that must be minimized. In this work, as the model of the facility is nonlinear, an MPC algorithm able to cope with this kind of models must be chosen. Thus, the Practical Nonlinear Model Predictive Control (PNMPC) algorithm is used due to the several advantages that it presents with respect to other nonlinear MPC techniques (Plucenio, Pagano, Bruciapaglia, & Normey-Rico, 2007) as: (i) it can cope with different nonlinear model structures, (ii) it is simple to compute, and (iii) it does not use iterative algorithms for linearizing the process model. In addition, it has been already tested in other nonlinear processes with successful results (Andrade, Pagano, Álvarez, & Berenguel, 2013; Castilla, Álvarez, Normey-Rico, & Rodríguez, 2014; Gil, Roca, Ruiz-Aguirre et al., 2018).

4.2.1. PNMPC algorithm

In MPC techniques, the prediction of the output process variable $\hat{Y}$, in a determined prediction horizon N, is calculated in a vectorial form as:

$$\hat{Y} = f + G \cdot \Delta u, \tag{10}$$

where $\hat{Y}=[\hat{Y}(t+1|t), \hat{Y}(t+2|t) \ldots \hat{Y}(t+N|t)]^T$,[1] $f=[\hat{f}(t+1|t), \hat{f}(t+2|t) \ldots \hat{f}(t+N|t)]^T$, $\Delta u=[\Delta u(t|t), \Delta u(t+1|t) \ldots \Delta u(t+N_u-1|t)]^T$, N_u being the control

horizon. f is known as free response whereas $G \cdot \Delta u$ is called forced response and Δu is the future control increment. As was previously mentioned, one of the differences among MPC algorithms is the way in which the free response f and the step response matrix G are calculated. In linear systems, they can be easily computed based on the superposition principle (Camacho & Bordons, 2004). However, in nonlinear processes, the superposition principle does not hold, and an approximation for calculating $\hat{Y}$ must be performed. The strategy for estimating $\hat{Y}$ using the PNMPC algorithm (Plucenio et al., 2007) is given by:

$$\hat{Y} \approx f + G_{PNMPC} \cdot \Delta u, \tag{11}$$

$$f = f(\overline{Y}, \Delta\overline{u}, \Delta\overline{v}), \tag{12}$$

$$G_{PNMPC} = \frac{\partial \hat{Y}}{\partial \Delta u}, \tag{13}$$

where $f(\cdot)$ is a function of its arguments, $\overline{Y}$ is a set of past and present process outputs, $\Delta\overline{u}$ is a set of past increments in the inputs, $\Delta\overline{v}$ is a set of past increments in the measurable disturbances, f is the vector of predictions provided by the nonlinear model obtained with $\Delta u = 0$, and G_{PNMPC} is the Jacobian matrix computed in the current point u. To compute both f and G_{PNMPC}, the procedure presented in Plucenio et al. (2007) and described in Algorithm 1 must be used. Note that, although this technique is only an approximation, it provides better results than if a linear model were used, since f is directly calculated with the nonlinear model of the process, while G_{PNMPC} is computed by linearizing the model around the trajectory, thus allowing this technique to consider the nonlinearity along the prediction horizon (Plucenio et al., 2007).

Following the formulation of the proposed control system, the PNMPC strategy is employed in this work to make the prediction of the top tank temperature, $\hat{Y}_{TT3}$, as a function of the increments in the setpoints of the loops included in the regulatory layer ($\Delta TT1_{SP}$ and $\Delta TT2_{SP}$), which are the actual manipulated variables involved in the upper layer. According to the PNMPC procedure the prediction is given by:

$$\hat{Y}_{TT3} \approx f_{TT3} + [G_{PNMPC-1} \; G_{PNMPC-2}] \cdot [\Delta TT1_{SP}; \Delta TT2_{SP}], \tag{14}$$

$$f_{TT3} = f(\overline{Y}_{TT3}, \Delta\overline{TT1}_{SP}, \Delta\overline{TT2}_{SP}, \Delta\overline{v}), \tag{15}$$

$$G_{PNMPC-1} = \frac{\partial \hat{Y}_{TT3}}{\partial \Delta TT1_{SP}}, \tag{16}$$

$$G_{PNMPC-2} = \frac{\partial \hat{Y}_{TT3}}{\partial \Delta TT2_{SP}}, \tag{17}$$

---

[1] The nomenclature $\hat{x}(t+k|t)$ refers to the value of x at discrete instant time $t+k$, computed with the information acquire up to instant t.

Algorithm 1: Method to compute $\mathbf{F}$ and $\mathbf{G_{PNMPC}}$

---

1. To calculate $\hat{\mathbf{Y}}^0$, which is a vector of length N, the model must be executed with past measurable disturbances, outputs, and inputs with $\mathbf{\Delta u}=[0\ 0\ldots 0]^T$. So that, $\mathbf{F}=\hat{\mathbf{Y}}^0$.

2. To calculate the first column of $\mathbf{G_{PNMPC}}$. $\hat{\mathbf{Y}}^1$ is computed as stated in the step above, but with $\mathbf{\Delta u}=[\epsilon\ 0\ldots 0]^T$, where ϵ is a little increment in the control action, i.e. $\frac{u(k-1)}{1000}$.

   $\mathbf{G_{PNMPC}}(:,1)=\frac{\hat{\mathbf{Y}}^1-\hat{\mathbf{Y}}^0}{\epsilon}$.

3. To compute the second column of the $\mathbf{G_{PNMPC}}$, $\hat{\mathbf{Y}}^2$ is calculated with $\mathbf{\Delta U}=[0\ \epsilon\ldots 0]^t$. $\mathbf{G_{PNMPC}}(:,2)=\frac{\hat{\mathbf{Y}}^2-\hat{\mathbf{Y}}^0}{\epsilon}$.

4. The same method as in the two previous steps must be repeated until completing the remaining columns of matrix $\mathbf{G_{PNMPC}}$. It should be remarked that the number of columns of $\mathbf{G_{PNMPC}}$ is given by the control horizon N_u, so the last column is computed as: $\mathbf{G_{PNMPC}}(:,N_u)=\frac{\hat{\mathbf{Y}}^{N_u}-\hat{\mathbf{Y}}^0}{\epsilon}$.

---

where $\overline{\mathbf{Y}}_{\mathbf{TT3}}$ is a set of past and present values of TT3, $\Delta\overline{\mathbf{TT1}}_{\mathbf{SP}}$ is a set of past values of input $\Delta TT1_{SP}$, and $\Delta\overline{\mathbf{TT2}}_{\mathbf{SP}}$ is a set of past values of input $\Delta TT2_{SP}$. It should be remarked that the main disturbances that affect to the facility are the irradiance and the ambient temperature ones, so that $\Delta\overline{\mathbf{v}}$ is composed by a set of past increments of these two variables.

4.2.2. Treatment of the disturbances and prediction errors

As in other MPC techniques, the PNMPC strategy completes the predictions including a model for taking into account disturbances and prediction errors. This model is given by:

$$\Lambda = \mu(t)\cdot \mathbf{1}_{N\times 1}, \tag{18}$$

$$\Delta\mu(t) = \frac{\phi}{\Omega}(Y(t)-\hat{Y}(t)), \tag{19}$$

where $\mathbf{1}$ is a vector of length $N\times 1$, ϕ and Ω (which includes an integrator) are the numerator and denominator respectively of a discrete time filter, and $Y(t)-\hat{Y}(t)$ is the error between the actual output value and the predicted one. This method is comparable to the *CARIMA* model (Camacho & Bordons, 2004). The intention is to add the integral of the filtered prediction error to each predicted process output. (Eq. (18)). The numerator and denominator of the discrete time filter are normally considered as design parameters. The most popular structure of this filter is $\phi(q^{-1})/\Omega(q^{-1}) = 1/(1-q^{-1})$, where q^{-1} is the backwards shift operator. However, the robustness of the disturbance model can be improved by considering the numerator as $\phi(q^{-1}) = 1-a\cdot q^{-1}$, with $0\ll a\leq 1$ (De Keyser & Ionescu, 2003). In this way, the structure used in this work is given by $\phi(q^{-1})/\Omega(q^{-1}) = (1-a\cdot q^{-1})/(1-q^{-1})$.

4.2.3. Objective function

The set of control actions is computed by minimizing an objective function (J). In this case, the aim of the control procedure is to maximize the temperature at the top of the storage tank (TT3). Therefore, the first term of the objective function is aimed at maximizing the predictions of this variable, $\hat{Y}_{TT3}(t+k|t)$ along the prediction horizon N, which means $\forall k\in 1,\ldots,N$. Besides, a second term has been added to penalize the variations in the control actions, $\Delta TT1_{SP}(t+k-1)$ and $\Delta TT2_{SP}(t+k-1)$, along the control horizon N_u, that is $\forall k\in 1,\ldots,N_u$ (to avoid aggressive control actions):

$$J = -\sum_{k=1}^{k=N}\hat{Y}_{TT3}(t+k|t)+\lambda\cdot\sum_{k=1}^{k=N_u}(|\Delta TT1_{SP}(t+k-1)|+|\Delta TT2_{SP}(t+k-1)|), \tag{20}$$

where λ is a weighting factor. In the problem at hand, the two control actions have the same importance in the optimization problem, thus only one λ was used in J.

4.2.4. Constraints

The optimization problem is subjected to several constraints which are defined according to the process requirements. As the fluid flowing through the pipes of the solar field is water, the temperature must be lower than 100 [°C] to avoid vapour formation during the operation:

$$TT2(t+k-1) < 100\ \forall k\in 1,\ldots,N_u, \tag{21}$$

In addition, TT2 cannot be lower than TT1, neither lower than TT3 to avoid cooling down the tank:

$$TT2(t+k-1) > TT1(t+k-1)\ \forall k\in 1,\ldots,N_u, \tag{22}$$

$$TT2(t+k-1) > \hat{Y}_{TT3}(t+k|t)\ \forall k\in 1,\ldots,N_u, \tag{23}$$

Finally, the outlet temperature of the solar field can vary between the maximum and minimum temperature reachable at each instant, $TT2_{max}$ and $TT2_{min}$ respectively. These limits can be calculated using the model of the solar field (Eq. (1)) in steady-state conditions as was done in Gil, Roca, Ruiz-Aguirre et al. (2018), according to the operating conditions (i.e global irradiance level, ambient temperature, inlet solar field temperature) and the maximum and minimum water flow rate, $FT1_{max}$ and $FT1_{min}$ respectively:

$$TT2_{min}(t+k-1|t) = f(I(t),T_a(t),TT1(t+k-1),FT1_{max})$$
$$\forall k\in 1,\ldots,N_u, \tag{24}$$
$$TT2_{max}(t+k-1|t) = f(I(t),T_a(t),TT1(t+k-1),FT1_{min})$$
$$\forall k\in 1,\ldots,N_u. \tag{25}$$

Note that the irradiance and ambient temperature are kept constant along the prediction horizon to compute the equations formulated above. It was tested that maintaining irradiance constant, the results obtained are comparable to those obtained if a prediction technique such as the one proposed in Pawlowski, Guzmán, Rodríguez, Berenguel, and Normey-Rico (2011) were applied, due to the low reliability of these kind of techniques. Thus, the constraint can be formulated as:

$$TT2_{min}(t+k-1|t) \leq TT2(t+k-1) \leq TT2_{max}(t+k-1|t)\ \forall k\in 1,\ldots,N_u. \tag{26}$$

4.3. Procedure to turn on the hierarchical controller

The procedure to turn on the hierarchical controller is divided in two phases. In the first one, as it was done in Gil, Roca, Ruiz-Aguirre et al. (2018), the steady-state model of the solar field is used to calculate the value of global irradiance required to start-up the solar field. By using this model, the value of global irradiance can be calculated as:

$$I_{th}(t) = f(FT1_{max}(t),TT1(t),TT2(t),T_a(t)). \tag{27}$$

To consider the operating conditions of the tank when calculating this value, $TT2(t)$ has been fixed at the same value than the top tank temperature $TT3(t)$. In the same way, as the fluid is initially recirculated only through the solar field when starting the operation (see the second phase to turn on the solar field), $TT1(t)$ is set to a degree below $TT2(t)$ to consider thermal losses in the pipes. In addition, the water flow rate was fixed at its maximum operating range. To choose this value several simulation tests were carried out checking this procedure with the maximum and minimum water flow rate. These tests showed that by using the minimum range, the required global irradiance is lower, however, if there is cold fluid in the pipes, the time that the fluid must be recirculated through the solar field for reaching the tank temperature is higher.

In the second phase, once the actual global irradiance value reaches the calculated one, i.e. $I_{th}(t) \leq I(t)$, the fluid is only recirculated through the solar field until reaching the tank temperature, time instant in which the hierarchical control system is turned on. Also note that, in order to avoid chattering problems, the conditions are checked with mean values of the last five minutes instead of instant ones.
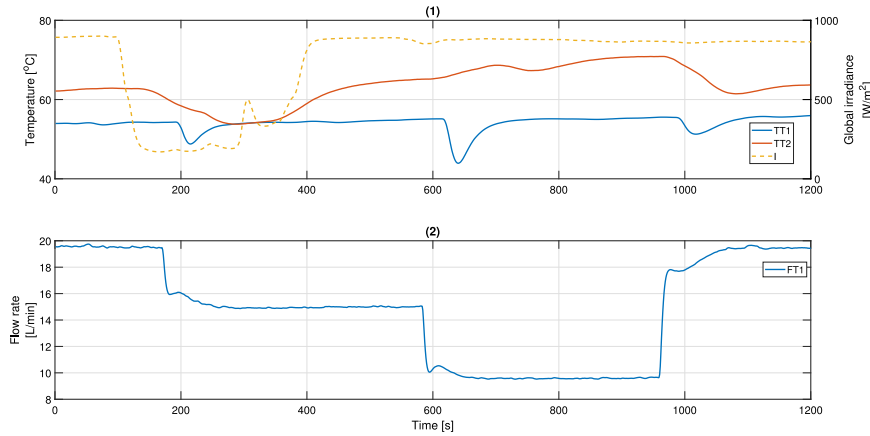
Fig. 8. Illustrative open loop test. (1) Inlet temperature of the solar field (TT1), outlet temperature of the solar field (TT2), and global irradiance (I), and (2) solar field water flow rate (FT1).

5. Results and discussion

A simulation and an experimental campaign were carried out for evaluating the proposed approach. The controller was implemented in MATLAB 2018a, using the YALMIP toolbox (Löfberg, 2004) and the *fmincon* solver (MATLAB, 2018). Regarding the controller set-up, the sampling time of the lower layer was fixed at 1 s, which was chosen taken into account the fastest representative time constant of the variables involved in the loops, as mentioned above. The sampling time of the upper layer was fixed at 10 min, which was selected according to the settling time of the lower layer controllers (around 8 min). The prediction horizon N and the control horizon N_u were set to 5 and 1, respectively. These values were selected taking into account traditional recommendations in MPC controllers, N large enough to contemplate the transient part of the response, and $N_u \ll N$. Finally, λ and a were fixed at 0.2 and 0.8 respectively, which were selected after exhaustive simulations until obtaining the desired closed loop response.

In what follows: (i) the implementation of the approach in the real facility and the results obtained with the application of the controller are presented, and (ii) a comparison among the results obtained in simulation with the approach presented in this paper, with a manual operation, and with the strategies proposed in Gil, Roca, Berenguel et al. (2018) and Gil, Roca, Ruiz-Aguirre et al. (2018) is shown.

5.1. Implementation of the algorithm in the real facility and experimental results

Due to an anomalous behaviour in the operation of the expansion vessel of the solar field, the control algorithm had to be slightly modified for doing the experimental tests. Note that this behaviour should not occur, and it is an exception that happens only in this plant. So that, for applying the algorithm in other facilities, it must be implemented as has been described above.

An open-loop test is shown in Fig. 8 to visualize the effect that gives rise to this anomalous behaviour. As can be seen, when a positive or a negative change is applied in the flow rate, the inlet temperature of the solar field drastically drops, and then, it is quickly restored, causing an undesired transient in TT1 that can produce oscillations and even instability during the automatic operation. Conversely, it can be observed that this transient is filtered by the solar field, and therefore, it does not affect TT2. Note that when the flow rate is decreased the pressure also decreases, and part of the water remaining in the expansion vessel comes out momentarily cooling the entrance of the circuit. When the flow rate is increased and due to the underdamped behaviour of the pump (see the last change in Fig. 8), there is also a small pressure drop, and again, water from the expansion vessel comes out. It should be remarked that an attempt has been made to model
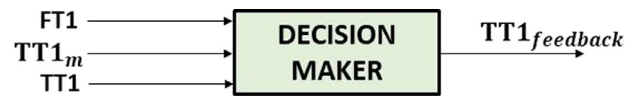
Fig. 9. Decision maker.

this phenomenon, but it has been impossible both with models based on first principles and with empirical models, since the temperature drop has no recognizable patterns.

Thus, to avoid feeding back the controllers with the actual TT1 during these transients, experimental tests were carried out to find both the maximum duration of this transitory effect when a change in the flow rate is applied, and the minimum ramp change in the flow rate that causes them. In this way, it was experimentally tested that, in the worst case, the maximum time was 140 [s], whereas flow rates with slopes lower than 8 [%] do not affect the inlet temperature.

Once these two issues were characterized, a decision maker was designed to decide if the control loops that require TT1, see Figs. 6 and 7, are fed back with the real temperature or with an estimated temperature calculated with the model (see Eq. (3)). The schematic diagram of the decision maker is presented in Fig. 9. The inputs of the block are the solar field water flow rate (FT1), the actual inlet solar field temperature (TT1), and the temperature calculated by Eq. (3) (TT1$_m$). If the slope of the flow rate is less than 8 [%], the output of the block (TT1$_{feedback}$) is the actual TT1, whereas if the slope is higher than this value, the output is TT1$_m$ during 140 [s]. It should be remarked that for doing the transitions between TT1 and TT1$_m$, a low pass filter is used with a characteristic time constant of 15 [s], thus avoiding discontinuities.

Next step was to test the control system in the real facility. Several experiments with different temperature initial conditions in the storage tank were performed in order to evaluate the hierarchical controller. Fig. 10 shows one representative test carried out on the day 15 March, 2019. In this test, the initial temperatures in the tank were 58, 50.6, and 47.6 [°C] for TT3, TT4 and TT5 respectively. It should be remembered that the temperature at the top of the tank must be higher than 60 [°C] for operating the thermal load. So, with these conditions, the tank was unloaded in terms of thermal energy, and therefore, the start-up procedure had to be carried out. In addition, it should be remarked that the degree of stratification was high, what made the automatic operation even more difficult.

The operation was started around 9.00 pm. As stated in Section 4.3, first, the algorithm calculated the value of global irradiance that allowed to start-up the solar field for heating the tank. Then, the algorithm verified at each sample time the actual value of irradiance, and

when it reached the calculated one, the second phase was initialized. In the second phase, pump 1 was turned on with valve 1 closed towards the solar field, i.e., the fluid was recirculated through the solar field. This phase was used to avoid turning on the hierarchical controller during the temperature transients produced by the cold fluid stored in the pipes. Finally, when the outlet temperature of the solar field reached the one at the top of the tank, the hierarchical controller was turned on. Thus, in the test, the calculated value of irradiance was 407.9 [W/m^2], which was reached around 9.28 [h], time instant in which the second phase was started. As can be seen in Fig. 10-(2), this second phase was prolonged around 12 [min], until TT2 reached the value of TT3 around 9.49 [h].

When the second phase was completed, the hierarchical controller was turned on. The first setpoints calculated by the upper layer for each of the control loops were 60.34 and 56.54 [°C], for TT2$_{SP}$ and TT1$_{SP}$ respectively. As TT2 was below its reference, the lower layer controller decreased the flow rate. It is important to observe that flow decrease caused TT1 to drop as a result of the anomalous behaviour of the expansion vessel commented before. Nevertheless, thanks to the performance of the decision maker, the controllers were fed back with an estimated value obtained with the model during this period, see Fig. 10-(2).

As can also be seen in Fig. 10-(2), to maximize TT3, the upper layer maintained the setpoint of TT1 around the same value, while increased TT2 setpoint according to the irradiance conditions. This fact was specially significant for the inlet solar field temperature control loop, since if TT2 increases, for maintaining TT1 around a determined value, the controller has to gradually open valve 1 to mix the fluid coming from the solar field with the one in the bottom of the tank, which is colder. In the test, this procedure can be observed in Fig. 10-(3) between 9.49 and 11.50 [h]. This gradual opening of the valve allowed to extract cold fluid from the tank, heating it through the solar field, and introducing it at the upper part of the tank in a controlled way, thus decreasing the stratification of the tank and increasing its temperature, see Fig. 10-(1).

Regarding the lower layer controllers, first, the TT1 controller tracked the references correctly, performing the operation mentioned in the previous paragraph until instant time 11.50 [h], moment in which the valve was totally opened (see Fig. 10-(3)). Second, the TT2 controller also tracked the references properly, and as can be seen, the feedforward was in charge of providing the nominal flow rate, what caused the PID signal to be always around zero except in some transients. Note that from 11.50 [h], the actuators were saturated and small tracking errors can be observed.

5.2. Comparison with other control strategies and a manual operation

In order to evaluate the benefits achieved by using the proposed hierarchical control approach, its performance was compared with an operation using the manual procedure and the strategies proposed in Gil, Roca, Berenguel et al. (2018) and Gil, Roca, Ruiz-Aguirre et al. (2018). Note that, it is not compared with the approach presented in Lopez-Alvarez et al. (2018) as it was proposed to be applied only to direct two-tank storage configurations, and therefore, it cannot be adapted to the facility used as reference in this paper. The comparison was carried out in simulation so that all methodologies have the same operating conditions. Real meteorological data from PSA (see Fig. 11) were used on the day March 8, 2017. In addition, the initial temperatures of the tank were 58, 50.6, and 47.6 [°C] for TT3, TT4 and TT5 respectively, as in the experimental test shown in the previous section.

For doing the comparison, the time taken to reach 65 [°C] from the beginning of the simulation was measured for each one of the start-up methodologies. As can be seen in Fig. 11 the simulations started at 7.00 am. However, each methodology turned on the solar field according to its start-up policy. The strategies proposed (Gil, Roca, Berenguel et al., 2018; Gil, Roca, Ruiz-Aguirre et al., 2018) and the

Table 6
Time in reaching 65 [°C] at the top of the tank with each one of the approaches.

Starting-up method	Time [min]
Manual	331.08
Approach presented in Gil, Roca, Ruiz-Aguirre et al. (2018)	322.66
Approach presented in Gil, Roca, Berenguel et al. (2018)	302.61
Hierarchical controller	296.36

hierarchical controller turned on the solar field when the irradiance reached 408.2 [W/m^2]. Note that the level is almost the same that in the experimental test shown in the previous section since the tank temperature conditions, which have higher influence in this calculation, are the same. Conversely, the level for turning on the solar field in the manual procedure was fixed at 550 [W/m^2], medium level of the range in which qualified operators turn on the solar field in this kind of plants (see Section 4). It should be remarked that the manual operation was programmed as described in Section 4.

Thus, the results can be analytically and graphically seen in Table 6 and Fig. 11 respectively. The operation that takes more time to reach the determined temperature was the manual one, with a time of 331.08 [min]. This is due to the difficulty in performing this operation when the tank has a high degree of stratification, and also when there are disturbances in the irradiance during the start phase as happened in this test. The operation carried out with the strategy presented in Gil, Roca, Ruiz-Aguirre et al. (2018) took a time of 322.66 [min]. Note that in this strategy the flow rate is used to control TT2 and therefore it is able to reject irradiance disturbances, thus improving the results obtained with the manual operation. However, this operation has problems if the tank is stratified since the valve is not used as control variable. In this way, it can be seen that the time is clearly less with the strategies that use the valve as control variable, since they can cope with both the irradiance disturbance and the tank stratification problems. The strategy proposed in Gil, Roca, Berenguel et al. (2018) required 302.61 [min] for reaching the reference temperature in the tank, whereas the proposed hierarchical controller took 296.36 [min]. This improvement is mainly due to the fact of taking into account a prediction horizon in the upper layer instead of using a static optimization problem. In addition, it should be remarked that this improvement is achieved without adding much calculation effort, as there is not much difference between solving the optimization problem formulated in Gil, Roca, Berenguel et al. (2018) and the proposed in this paper; which is based on a PNMPC controller.

6. Conclusions

This paper shows an optimal real-time predictive control methodology for starting-up solar thermal fields with direct storage configuration. The methodology is based on a hierarchical controller including an MPC based layer and a regulatory one composed of PID controllers. Real experimental tests in a pilot plant with single-tank with direct storage configuration located at PSA are shown. In addition, a simulated comparative analysis with other techniques already proposed in the literature and with a manual operation is presented.

The results evidence how the proper use of a control algorithm that: (i) takes into consideration irradiance disturbances and operating conditions at each sampling time, and (ii) uses a receding control strategy to consider the future tank states to calculate the control signals, can considerably reduce the time spent in the start-up procedure. This fact is especially notable when there is a big degree of stratification in the storage tank. The comparison carried out shows how the proposed controller can reduce the start-up procedure in 34 min with respect to a manual operation, and in 26 [min] if a controller that acts only over the flow rate were used. This improvement is due to the use of the mixing valve as control variable apart from the water flow rate (typical control variable in solar thermal fields), which allows the controller to cope
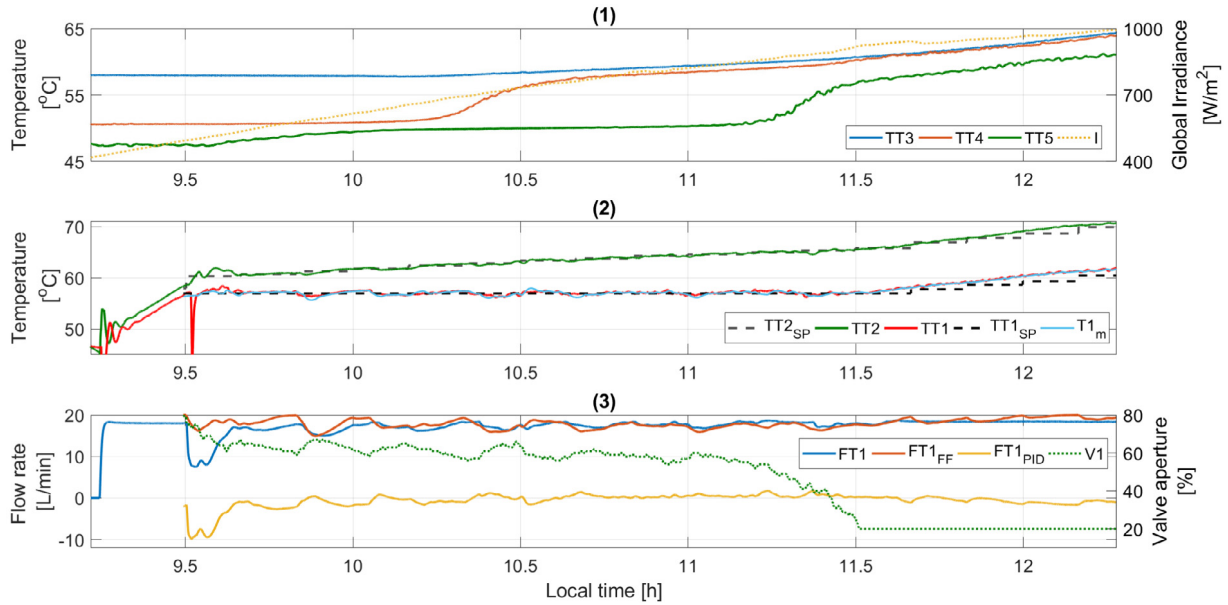
Fig. 10. Experimental tests. (1) Tank temperatures (TT3, TT4 and TT5) and global irradiance (I), (2) inlet and outlet temperatures of the solar field (TT1 and TT2), setpoints (TT1$_{SP}$ and TT2$_{SP}$) and temperature calculated by the decision maker TT1$_m$, and (3) control signals of the outlet solar field temperature control loop (FT1, FT1$_{FF}$ and FT1$_{PID}$) and control signal of the inlet solar field temperature control loop (V1).
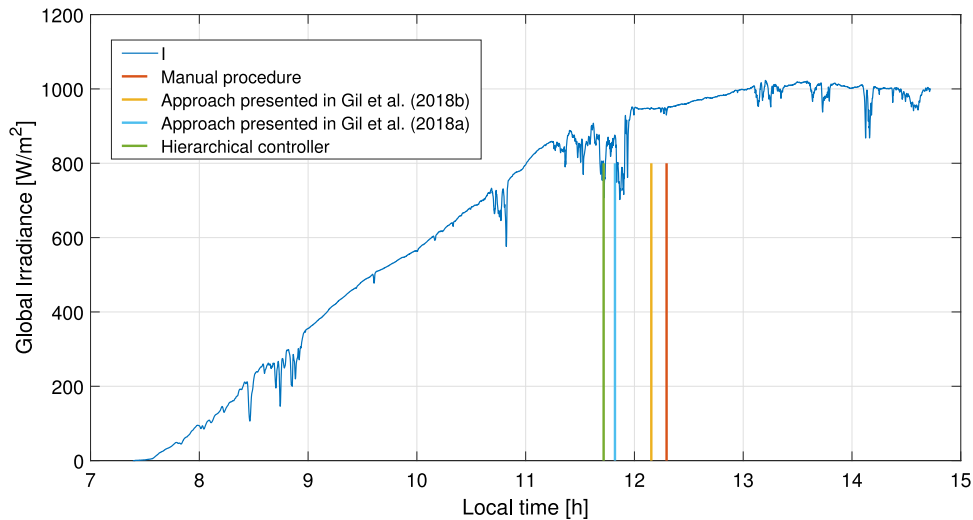
Fig. 11. Global irradiance data used in the simulations, and time in which the temperature 65 [°C] was reached at the top of the tank with each one of the start-up procedures.

with both the irradiance disturbance and temperature stratification problems during the start-up phase.

Note that although the procedure has been tested in a low-temperature solar field design, it could also be used in medium and high concentration solar thermal plants (with parabolic trough collectors or solar towers) using a similar layout as the one of the plant used as reference in this work, including the thermal storage and the mixing valve. However, it must be mentioned that the obtained results cannot be directly extrapolated to plants that use different heat transfer media due to the difference in thermal properties and transport delays. For this reason, future works will focus on evaluating the performance of the proposed technique in this kind of plants.

Declaration of competing interest

The authors declare that they have no known competing financial interests or personal relationships that could have appeared to influence the work reported in this paper.

References

Abid, M., Yousef, B., Assad, M., Hepbasli, A., & Saeed, K. (2018). An experimental study of solar thermal system with storage for domestic applications. *Journal of Mechanical Engineering and Sciences*, *12*(4), 4098–4116.

Andrade, G., Pagano, D., Álvarez, J., & Berenguel, M. (2013). A practical NMPC with robustness of stability applied to distributed solar power plants. *Solar Energy*, *92*, 106–122.

Artur, C., Neves, D., Cuamba, B. C., & Leão, A. J. (2018). Comparison of two dynamic approaches to modelling solar thermal systems for domestic hot water. *Sustainable Energy Technologies and Assessments, 30*, 292–303.

Berenguel, M., Cirre, C. M., Klempous, R., Maciejewski, H., Nikodem, M., Nikodem, J., et al. (2005). Hierarchical control of a distributed solar collector field. In *International conference on computer aided systems theory* (pp. 614–620). Springer.

Biencinto, M., Bayón, R., Rojas, E., & González, L. (2014). Simulation and assessment of operation strategies for solar thermal power plants with a thermocline storage tank. *Solar Energy, 103*, 456–472.

Camacho, E. F., Berenguel, M., Rubio, F. R., & Martínez, D. (2012). *Control of solar energy systems*. Springer.

Camacho, E. F., & Bordons, C. (2004). *Model predictive control*. London: Springer-Verlag Ltd.

Camacho, E., & Gallego, A. (2013). Optimal operation in solar trough plants: A case study. *Solar Energy, 95*, 106–117.

Casati, E., Casella, F., & Colonna, P. (2015). Design of CSP plants with optimally operated thermal storage. *Solar Energy, 116*, 371–387.

Casella, F., Casati, E., & Colonna, P. (2014). Optimal operation of solar tower plants with thermal storage for system design. *IFAC Proceedings Volumes, 47*(3), 4972–4978.

Castilla, M., Álvarez, J., Normey-Rico, J., & Rodríguez, F. (2014). Thermal comfort control using a non-linear MPC strategy: A real case of study in a bioclimatic building. *Journal of Process Control, 24*(6), 703–713.

Cirre, C. R. M. (2007). Control jerárquico de la producción de energía mediante plantas de colectores solares distribuidos (Ph.D. thesis), Universidad de Almería.

De Andrade, G., Álvarez, J., Pagano, D., & Berenguel, M. (2015). Nonlinear controllers for solar thermal plants: A comparative study. *Control Engineering Practice, 43*, 12–20.

De Keyser, R., & Ionescu, C. M. (2003). The disturbance model in model based predictive control. In *CCA 2003: vol. 1, Proceedings of 2003 IEEE conference on control applications, 2003* (pp. 446–451). IEEE.

Dinter, F., & Gonzalez, D. (2014). Operability, reliability and economic benefits of CSP with thermal energy storage: first year of operation of ANDASOL 3. *Energy Procedia, 49*, 2472–2481.

Duffie, J. A., & Beckman, W. A. (2013). *Solar engineering of thermal processes*. John Wiley & Sons.

Gallego, A. J., Merello, G. M., Berenguel, M., & Camacho, E. F. (2019). Gain-scheduling model predictive control of a Fresnel collector field. *Control Engineering Practice, 82*, 1–13.

Gibb, D., Johnson, M., Romaní, J., Gasia, J., Cabeza, L. F., & Seitz, A. (2018). Process integration of thermal energy storage systems–evaluation methodology and case studies. *Applied Energy, 230*, 750–760.

Gil, J. D., Roca, L., Berenguel, M., & Guzmán, J. L. (2018). A multivariable controller for the start-up procedure of a solar membrane distillation facility. *IFAC-PapersOnLine, 51*(4), 376–381.

Gil, J. D., Roca, L., Ruiz-Aguirre, A., Zaragoza, G., & Berenguel, M. (2018). Optimal operation of a solar membrane distillation pilot plant via nonlinear model predictive control. *Computers & Chemical Engineering, 109*, 151–165.

Gil, J. D., Roca, L., Zaragoza, G., & Berenguel, M. (2018). A feedback control system with reference governor for a solar membrane distillation pilot facility. *Renewable Energy, 120*, 536–549.

Guédez, R., Spelling, J., & Laumert, B. (2015). Reducing the number of turbine starts in concentrating solar power plants through the integration of thermal energy storage. *Journal of Solar Energy Engineering, 137*(1), 011003.

Kolb, G. J. (2011). Evaluation of annual performance of 2-tank and thermocline thermal storage systems for trough plants. *Journal of Solar Energy Engineering, 133*(3), 031023.

Kumar, A., Prakash, O., & Dube, A. (2018). A review on technology and promotional initiatives for concentrated solar power in world. *International Journal of Ambient Energy, 39*(3), 297–316.

Kuravi, S., Trahan, J., Goswami, D. Y., Rahman, M. M., & Stefanakos, E. K. (2013). Thermal energy storage technologies and systems for concentrating solar power plants. *Progress in Energy and Combustion Science, 39*(4), 285–319.

Li, J., Gao, G., Kutlu, C., Liu, K., Pei, G., Su, Y., et al. (2019). A novel approach to thermal storage of direct steam generation solar power systems through two-step heat discharge. *Applied Energy, 236*, 81–100.

Löfberg, J. (2004). Yalmip : A toolbox for modeling and optimization in matlab. In *Proceedings of the CACSD Conference*, Taipei, Taiwan.

Lopez-Alvarez, M., Flores-Tlacuahuac, A., Ricardez-Sandoval, L., & Rivera-Solorio, C. (2018). Optimal start-up policies for a solar thermal power plant. *Industrial and Engineering Chemistry Research, 57*(3), 1026–1038.

MATLAB (2018). *MATLAB optimization toolbox release 2018a*. Natick, MA, USA: The MathWorks.

Normey-Rico, J. E., Bordons, C., Berenguel, M., & Camacho, E. F. (1998). A robust adaptive dead-time compensator with application to a solar collector field. *IFAC Proceedings Volumes, 31*(19), 93–98.

Normey-Rico, J. E., & Camacho, E. F. (2007). *Control of dead-time processes*. Springer Science & Business Media.

Pawlowski, A., Guzmán, J. L., Rodríguez, F., Berenguel, M., & Normey-Rico, J. E. (2011). Predictive control with disturbance forecasting for greenhouse diurnal temperature control. *IFAC Proceedings Volumes, 44*(1), 1779–1784.

Pelay, U., Luo, L., Fan, Y., Stitou, D., & Rood, M. (2017). Thermal energy storage systems for concentrated solar power plants. *Renewable & Sustainable Energy Reviews, 79*, 82–100.

Plucenio, A., Pagano, D., Bruciapaglia, A., & Normey-Rico, J. (2007). A practical approach to predictive control for nonlinear processes. *IFAC Proceedings Volumes, 40*(12), 210–215.

Relloso, S., & Delgado, E. (2009). Experience with molten salt thermal storage in a commercial parabolic trough plant. andasol-1 commissioning and operation. In *Proceedings of 15th International SolarPACES Symposium, Sept* (pp. 14–18).

Roca, L., Berenguel, M., Yebra, L. J., & Alarcón-Padilla, D. C. (2008). Solar field control for desalination plants. *Solar Energy, 82*(9), 772–786.

Rovira, A., Montes, M. J., Valdes, M., & Martínez-Val, J. M. (2011). Energy management in solar thermal power plants with double thermal storage system and subdivided solar field. *Applied Energy, 88*(11), 4055–4066.

Rubio, F. R., Navas, S. J., Ollero, P., Lemos, J. M., & Ortega, M. G. (2018). Control óptimo aplicado a campos de colectores solares distribuidos. *Revista Iberoamericana de Automática e Informática industrial, 15*(3), 327–338.

Sebastián, A., Abbas, R., Valdés, M., & Casanova, J. (2018). Innovative thermal storage strategies for fresnel-based concentrating solar plants with east-west orientation. *Applied Energy, 230*, 983–995.

Usaola, J. (2012). Operation of concentrating solar power plants with storage in spot electricity markets. *IET Renewable Power Generation, 6*(1), 59–66.

Zaragoza, G., Ruiz-Aguirre, A., & Guillén-Burrieza, E. (2014). Efficiency in the use of solar thermal energy of small membrane desalination systems for decentralized water production. *Applied Energy, 130*, 491–499.

2.3 Advanced control and optimization strategies for membrane distillation industrial applications

2.3.1 Optimal thermal energy management of a distributed energy system comprising a solar membrane distillation plant and a greenhouse

Research in this field is supported by the following journal paper:

Title	Optimal thermal energy management of a distributed energy system comprising a solar membrane distillation plant and a greenhouse
Authors	**J. D. Gil**, J. D. Álvarez, L. Roca, J. A. Sánchez-Molina M. Berenguel, F. Rodríguez
Journal	Energy Conversion and Management
Year	2019
Volume	198
Pages	-
DOI	https://doi.org/10.1016/j.enconman.2019.111791
IF (JCR 2018)	7.181
Categories	Thermodynamics (2/60) Q1
	Energy & Fuels (12/103) **Q1**
	Mechanics (3/134) Q1

Contribution of the Ph.D. candidate
The Ph.D. candidate, J. D. Gil, is the main contributor and first author of this paper.

In addition, it derived in a publication as technical report in the outreach magazine Era Solar:

- **J. D. Gil**, L. Roca, M. Berenguel, and G. Zaragoza, "Destilación por membranas. Aportaciones de la desalación solar térmica y el control automático en el suministro de agua en invernaderos," *Era solar: Energías renovables*, no. 201, pp. 16–25, 2017.

It also resulted in a contribution to a national conference:

- **J. D. Gil**, L. Roca, M. Berenguel, A. Ruiz-Aguirre, and A. Giménez, "Control predictivo para la operación eficiente de una planta formada por un sistema de desalación solar y un invernadero," in *XXXVIII Jornadas Automática*. Gijón, España, 2017.
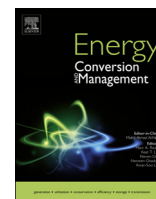
Optimal thermal energy management of a distributed energy system comprising a solar membrane distillation plant and a greenhouse

Juan D. Gil[a], J.D. Álvarez[a,*], Lidia Roca[a,b], J.A. Sánchez-Molina[a], Manuel Berenguel[a], F. Rodríguez[a]

[a] Centro Mixto CIESOL, ceiA3, Universidad de Almería, Ctra. Sacramento s/n, Almería 04120, Spain
[b] CIEMAT-Plataforma Solar de Almería, Ctra. de Senés s/n, Tabernas, 04200 Almería, Spain

ARTICLE INFO

ABSTRACT

The scarcity of water experienced in Almería (south-eastern Spain), and in Mediterranean countries generally, has the potential to compromise one of its main economic drivers – agriculture. A possible solution is to combine thermal desalination technologies with crop cultivation. Accordingly, this paper proposes a distributed model predictive controller for the efficient operation of a distributed energy system comprising a solar-powered membrane distillation facility and a greenhouse, which is the most widespread type of crop cultivation in this region. The controller is in charge of calculating the optimal feed flow rates for each of the membrane distillation modules included in the desalination facility, according to the water requirements of the greenhouse and the thermal energy consumption of the membrane distillation plant (one of the main weak points of the technology). Simulation results using models for two real facilities located in Almería are presented; they show how the proposed distributed approach is able to manage industrial-scale plants in an optimal way. In addition, automatic operation is compared with manual operation (a non-optimal one), showing that the operation's thermal efficiency can be improved by 5 % when applying the proposed technique, while satisfying the water demand. This means important thermal energy savings of around 50 MWh/season less thermal energy consumption for an 8 ha cultivation area.

1. Introduction

Almería is located in the southeast of Spain, a semi-desertic zone with a severe water scarcity problem. Nevertheless, agriculture is one of the economic drivers for this dry region covering a surface area of more than 29035 ha of effective greenhouse production [1]. This is made possible thanks to the availability of untapped water resources, rivers or aquifers, and the use of drip irrigation and efficient control systems combined with the area's great agricultural potential due to its favourable climatic conditions.

The development of water-intensive agriculture has led to this region becoming highly competitive in international markets; however, the intensification of irrigation and the required infrastructure (reservoirs, dams, canals, wells and pools) have had ecological and social impacts which, in some cases, are already irreversible [2]. The development of irrigation in the southeast of Spain is associated with the overexploitation of major river aquifers, which urgently demands solutions to mitigate the problem and make the economy sustainable with

regard to water use. As pointed out by [3], the horticultural sector is on the right path towards a green economy; for this, desalinated and reclaimed water should be used for irrigation demand, thus ensuring aquifer sustainability [4]. In fact, Spain is the leader in using desalinized water for agricultural purposes [5]. Reverse Osmosis (RO) is the most commonly employed technology and the most commercially extended [6], mainly due to its competitive costs compared to other desalination techniques [7]. Despite this, membrane distillation (MD) is a potential technology which is becoming increasingly attractive [8]. Its principal advantages are: it only requires low-grade thermal energy so it can be easily coupled to solar thermal systems [9] and low electricity consumption; it does not usually require chemical pretreatment; the product quality is excellent and insensitive to the feed-water salinity, feed flow rate and temperature, making it suitable for zero-liquid discharge schemes. Given this last advantage, MD can be used not only for desalting seawater but also for producing clean water from contaminated feedwater [10]; thus, it is useful for improving the treated water quality for irrigation.

Nomenclature

Symbol	Description(Units)
A	Surface area (m²)
c_f	Conversion factor ($3.6 \cdot 10^6$ s·W/(h·kW))
c_p	Specific heat capacity (J/(kg·°C))
D	Distillate production (L/h)
F	Feed flow rate (L/h)
H	Absolute humidity (kg water/kg air)
$\dot{m}$	Mass flow rate kg/s
$\dot{M}$	Mass flow rate per square meter (kg/(s·m²))
Q	Heat flux (W/m²)
T	Temperature (°C)
V	volume (m³)
α	Heat exchanger transfer coefficient (689.30 W/(m²·K))
δ	Weighting factor for the tracking error (-)
ΔT	Temperature difference (°C)
ε	Convergence factor (–)
ζ	Weighting factor for the STEC (–)
η	Auxiliary factor for the calculation of the outlet heat exchanger temperatures (–)
θ	Heat exchanger auxiliary factor (–)
λ	Weighting factor for the control action
ρ	Density (kg/m³)
σ	Maximum number of iterations (–)
Subscript	Description
a	Air

AQ	Aquastill module
cnv	Convective
cr	Crop
cs, in	Input at the cold side of the heat exchanger
cs, out	Output at the cold side of the heat exchanger
cv	Cover
dehum	Dehumidification
ext	Exterior
feed	Feed MD water
g	Greenhouse
he	Heat exchanger
hs, in	Input at the hot side of the heat exchanger
hs, out	Output at the cold side of the heat exchanger
hum	Humidification
i	ith MD module in the plant
int	Interior
m	Model output
sol	Solar
ss	Soil surface
SS	Solar Spring module
trp	Transpiration
ven	Ventilation
1	Relative to the hot side of the heat exchanger (demineralized water fluid)
2	Relative to cold side of the heat exchanger (sea water fluid)

Even though Solar-powered MD (SMD) processes are currently relatively expensive compared to other desalination technologies [8], they could provide a feasible solution for small applications in places with high solar irradiance and water scarcity. Moreover, due to the low working temperature, their operation and maintenance is simple, and they can easily be coupled to small production plants such as greenhouses. Nonetheless, in order to combine these successfully and to reduce the cost of the water produced, adequate optimization and control techniques are required to manage SMD facilities according to the solar energy dynamics [11].

Various control approaches for SMD plants have been presented in the literature, of which the ones posited in [12,13] stand out. In the first paper, a neural network-based control system was proposed to maximize the SMD facility's distillate production based on the irradiance conditions. In the second paper, a real-time hierarchical controller was presented which aimed to optimize not only the plant's distillate
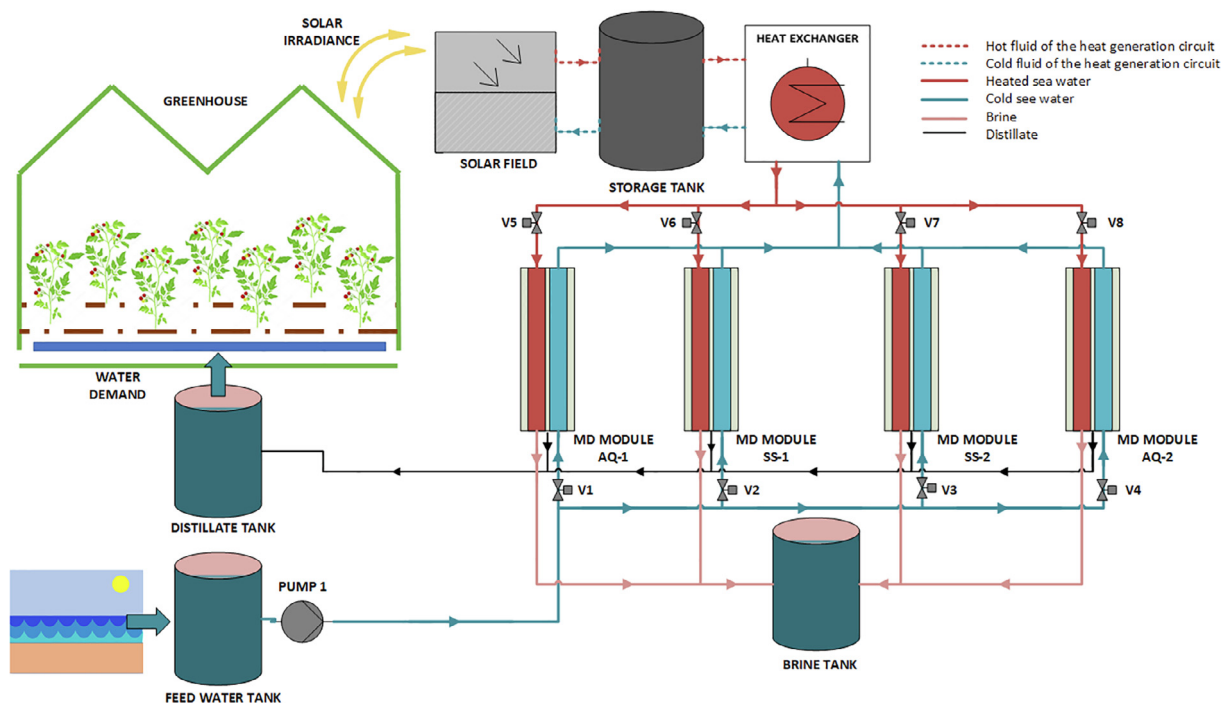

Fig. 1. Schematic diagram of the facility simulated for the case study.

production but also the cost savings related to the pumping system and the MD module's thermal efficiency, which is one of the technology's main drawbacks, as reported in [14] and analysed in [15]. Nevertheless, these strategies were applied to stand-alone pilot plants, which considered the SMD facility as having only one MD module, and did not consider a particular water demand. This is especially relevant since, when designing a potential industrial SMD plant application, such as proposed in this paper, the SMD facility must contain multiple MD modules to satisfy the water requirements. This is because a single commercial MD module has a relatively low distillate production, around 30 L/h under the best operating conditions [16]. This scenario completely alters the control problem, requiring new approaches to be formulated.

To the best of our knowledge, only [17] has addressed the issue of optimally connecting a solar-powered desalination process to a greenhouse. In that work, a Multi-Effect Distillation (MED) unit was evaluated for the desalination plant. To optimally connect both facilities, a centralized Model Predictive Control (MPC) technique was used to control the distillate volume that the desalination plant had to produce to meet the greenhouse water demand. However, the control system did not take into consideration other objectives such as minimizing the thermal energy consumption, which is equally essential for this thermal-powered desalination technology, as analysed in [18,19]. Furthermore, a single MED unit was considered for the solar desalination plant, thus invalidating the centralized control approach for industrial SMD plants.

In our paper, a Distributed MPC (DMPC) strategy is proposed to optimally manage a distributed energy system made up of an SMD plant and a greenhouse. The DMPC technique is in charge of computing the feed flow rates for each of the MD modules in the SMD facility, tasked with reducing the specific thermal energy consumption of the MD modules while maintaining the necessary water level for irrigation purposes. In formulating the DMPC technique proposed, each of the MD modules included in the SMD facility is considered as an agent of the decentralized controller; thus, each agent solves a simple MPC problem with the objective mentioned above, only exchanging information with neighbouring agents following the ideas presented in [20]. This allows us to considerably reduce the computational power required by a centralized approach such as the one proposed in [17], making it possible to compute optimal solutions within the required sampling time when considering industrial-scale SMD plants. The simulation results presented show that the proposed DMPC technique is able to optimally manage an industrial SMD plant in real time, assuring the water requirements of the consumer agent, while reducing the MD modules' thermal energy consumption; an issue not addressed in the literature to date.

The paper is organized as follows: in Section 2 presents the case study. The models are described in Section 3. The control algorithms are formulated in Section 4. The performance of the controller is depicted and analysed in Section 5. Finally, the conclusions are summarized in Section 6.

2. Case study

The facility studied in this work basically consists of a distributed energy system comprising an SMD plant and a greenhouse (see Fig. 1). In this plant, the greenhouse acts as the consumer, requiring fresh water for crop irrigation, while the desalination plant acts as the producer, providing the required fresh water. In addition, a water storage tank ($3 \, \text{m}^3$) is used to connect both facilities. It should be noted that the plant is a simulation based on two real facilities, which are presented in the following subsections.

2.1. Solar distillation plant

The SMD plant (see Fig. 2) is located at the Plataforma Solar de

Almería (PSA, www.psa.es, southeast Spain). It is one of the few MD plants that is fully described in the literature [21]. In this facility, the thermal energy required for the distillation process is provided by a solar field made up of flat-plate collectors. This solar field is directly connected to a storage tank ($1.5 \, \text{m}^3$), which is used as an energy buffer system. Finally, the distillation module is coupled to the heat generation circuit through a heat exchanger.

There are several commercial MD modules available at PSA, using different MD configurations. The two modules used in this work (see Fig. 2) are the Aquastill unit, which is based on Air–gap Membrane Distillation technology, comprehensively described in [16], and Solar Spring technology, which has a Permeate-gap Membrane Distillation configuration, and was described and analysed in [22]. In the case study (see Fig. 1), four MD units (two of each commercial module) were used in order to scale the desalination plant's distillate production to the greenhouse water requirements.

Inside the MD unit (see Fig. 3) the sea water is first pumped through the module's condenser channel. Due to the module's design constraints, the feed flow rate has a limited operating range between 400 and 600 L/h. After this, the feed fluid passes through the heat exchanger, where it is heated using the recirculating fluid coming from the solar field. It is then circulated through the module's evaporator channel. The evaporator inlet temperature varies between 60 and 80 °C; the upper limit being imposed by the membrane materials while the lower is set because, below this temperature, the module produces very little distillate. The temperature difference created on both sides of the channels produces a pressure difference that forces the vapour molecules from the evaporator channel to the condenser channel. Finally, in the evaporator channel, the volatile components of the heated solution pass through a hydrophobic, microporous membrane (becoming distillate following a condensation process) whereas the non-volatile molecules are rejected in the form of brine.

2.2. Greenhouse

The greenhouse (see Fig. 4) used as the reference in this work is located at the Experimental Station of the Cajamar Foundation, also in south-eastern Spain (40 km from the PSA). The structure comprises a multi-span "Almeria-type" greenhouse (E-W orientation), with an

Fig. 2. SMD pilot plant at the PSA. From top to bottom and from left to right: the solar field, the Solar Spring module and the Aquastill module.
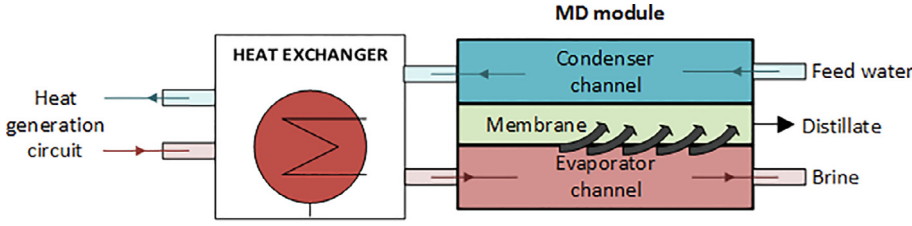
Fig. 3. Schematic diagram of a single MD unit.

Fig. 4. Greenhouse facilities. From left to right and from top to bottom: the greenhouse, the dropper and the tomato crop lines.

$821\ m^2$ surface and a cultivation area of $616\ m^2$. The greenhouse has a polyethylene cover equipped with an automatic ventilation system with side windows on the north and south walls, a biomass-fuelled heating system, a diesel aerothermal system, LED lights, and a humidification/dehumidification system from condensation with a water extraction capacity of $900\ L/day$.

The crop grows in N-S-oriented rows, inside coconut coir bags, with three droppers and six plants each. Throughout the crop season, several internal and external measurements are monitored continuously. Outside the greenhouse, a weather station measures air temperature and relative humidity with a ventilated sensor, solar radiation, photosynthetic active radiation, rain detection, CO_2, wind direction, and wind speed. During the trials, several greenhouse climate variables were measured, especially air temperature, relative humidity, solar radiation, PAR, soil and cover temperature, and CO_2 concentration.

Irrigation was periodically applied throughout each day to the crop. The irrigation frequency was controlled using a demand tray system; fixed volumes were applied. The demand tray system, which uses water-level sensors, is the most commonly used system for automatically activated irrigation of soilless crops in SE Spain. A water-level sensor is installed in a small water reservoir in which the water volume (and therefore the surface level) is in equilibrium with the substrate water content. When the water level in the reservoir drops to the physical level of the sensor, as a result of crop uptake, irrigation is activated. The physical height of the sensor is adjusted by the grower based on measured drainage volumes and experience. This method can be used once the crop root system is established. A microlysimeter was chosen to measure the transpiration, drainage and crop water loss measurements. The device consists of two electronic weighing scales connected to a personal computer. The first ($150\ kg\ 1\ g$, Sartorius) records the weight of a bag with six plants plus a support structure. The second weighing scale ($20\ kg\ 0.5\ g$, Sartorius), which follows the first, measures the drainage weight from the substrate bag. A more detailed description of the greenhouse has been presented elsewhere [23].

3. System modelling

The case study presented in the previous section was used to evaluate the performance of a DMPC technique which manages the optimal operation of the desalination plant to meet the crop's water requirements while reducing the MD modules' thermal energy consumption. Consequently, a model capable of accurately representing the behaviour of both facilities is required.

3.1. SMD facility model

The SMD facility model can be divided into two different components linked by a heat exchanger: (1) the heat generation system, comprising the solar field and the storage tank, and (2) the desalination unit. The model for the heat generation system has already been presented in [11] (the solar field, pipes and heat exchanger) and [13] (the storage tank). To simplify the simulations in this work, temperature profiles at the hot side inlet of the heat exchanger have been employed. These temperature profiles were obtained by simulating a model of the heat generation circuit (the solar field and thermal storage tank) with real meteorological data from PSA, similar to those used in this work, and using the operational strategy proposed in [13].

The heat exchanger was modelled using a first principles-based static model following the ideas proposed in [24]:

$$T_{hs,out-m} = T_{hs,in} - \eta_1 \cdot (T_{hs,in} - T_{cs,in}), \tag{1}$$

$$T_{cs,out-m} = T_{cs,in} + \eta_2 \cdot (T_{hs,in} - T_{hs,out-m}), \tag{2}$$

where:

$$\eta_1 = \frac{1 - e^{\theta}}{1 - \frac{\dot{m}_1 \cdot c_{p,1}}{\dot{m}_2 \cdot c_{p,2}} e^{\theta}}, \tag{3}$$

$$\eta_2 = \frac{\dot{m}_1 \cdot c_{p,1}}{\dot{m}_2 \cdot c_{p,2}}, \tag{4}$$

$$\theta = \alpha \cdot A_{he} \cdot \left(\frac{1}{\dot{m}_1 \cdot c_{p,1}} - \frac{1}{\dot{m}_2 \cdot c_{p,2}} \right). \tag{5}$$

All variables and constants are defined in the Nomenclature table in the appendices. The surface area of the heat exchanger (A_{he}) is $3.15\ m^2$. The surface area of the heat exchanger (A_{he}) is $3.15\ m^2$. Moreover, as was presented in [13], a time delay and a first-order filter have been added to each model output so as to include the required dynamics to fit the experimental data. For the case of $T_{cs,out-m}$, the time delay is $23\ s$ and the representative time constant is $40\ s$, whilst for $T_{cs,out-m}$, the time delay is $15\ s$ and the time constant is $20\ s$.

As was mentioned in Section 2.1, two kinds of MD modules have been used in this work. The models for the MD units consist of static equations obtained from the experimental data, employing the Response Surface Methodology (RSM). The model for the first module, Solar Spring (SS-1 and SS-2 in Fig. 1), was presented in [22] and is given by:

$$D$$
$$= A_{SS} \cdot (-1.088 + 0.024 \cdot T_{cs,out} - 0.018 \cdot T_{feed} - 0.001 \cdot F + 0.00006 \cdot T_{cs,out} \cdot F), \tag{6}$$

$$\triangle T = -0.201875 + 0.1385 \cdot T_{cs,out} - 0.158 \cdot T_{feed} + 0.0049 \cdot F, \tag{7}$$

where A_{SS} is the surface area of the Solar Spring module membrane,

$10 \, \text{m}^2$. The units for each term in Eq. (6) are L/hm^2, whereas the ones for Eq. (7) are in °C.

The model for the Aquastill module (AQ-1 and AQ-2 in Fig. 1) was developed in [16] and is described by the following equations:

$$D = A_{AQ} \cdot (0.135 + 0.003 \cdot T_{cs,out} - 0.0204 \cdot T_{feed} - 0.001 \cdot F + 0.00004 \cdot T_{cs,out} \cdot F), \tag{8}$$

$$\triangle T = -0.739 + 0.078 \cdot T_{cs,out} - 0.067 \cdot T_{feed} + 0.0019 \cdot F. \tag{9}$$

As in the previous model, A_{AQ} is the surface area of the Aquastill module membrane, which in this case is $24 \, \text{m}^2$. The units for the terms in Eq. (8) are L/hm^2 whereas the ones for Eq. (9) are in °C. It should be pointed out that in Eqs. (7) and (9), $\triangle T$ is the temperature difference between the evaporator channel inlet temperature and the condenser channel outlet temperature of the MD module, and D is the distillate production. Static models are used here because the MD modules have fast dynamics when compared to the other facility systems. However, one can observe that they are affected by the temperature coming from the heat generation circuit ($T_{cs,out}$) and, therefore, by its dynamics.

Finally, the feed flow rate is controlled by pump 1, supplying flow rates between 1600 and 2000 L/h. This feed flow rate is a shared resource between the four modules; it is not enough to feed all the modules working at the maximum flow rate (the maximum flow rate of each module is 600 L/h). This limitation might be a design decision based on the cost of pumping the sea water and because maximum thermal efficiency is achieved when the MD modules are run at the minimum feed flow rate, as will be shown in Section 4.1. Then, valves V1, V2, V3 and V4, which vary their opening between 0 and 1, divert part of the flow into the corresponding module (see Fig. 1). In addition, V1 and V5, V2 and V6, V3 and V7, and V4 and V8, are opened or closed at the same time and at the same value in order to maintain the same flow rate at the inlets of the two channels of each module.

3.2. Greenhouse model

A simplified pseudo-physical climate model, completely described in [23], has been used for the purpose of this work. The state variables for the system are the inside air temperature ($T_{a,int}$) and the humidity ($H_{a,int}$). The three main external systems interacting with the greenhouse are the outside air, the soil surface, and the crop. Thus, the greenhouse air temperature ($T_{a,int}$) can be modelled using the following balance:

$$c_{p,a} \rho_a \frac{V_g}{A_{ss}} \frac{dT_{a,int}}{dt} = Q_{sol,a} + Q_{cnv,cv-a} + Q_{cnv,ss-a} - Q_{ven} - Q_{trp,cr}, \tag{10}$$

where $Q_{sol,a}$ represents the radiative flux heating the inside air through the cover, $Q_{cnv,cv-a}$ is the convective flux with the cover, $Q_{cnv,ss-a}$ is the convective flux with the soil surface, Q_{ven} is the heat lost by natural ventilation and infiltration, and $Q_{trp,cr}$ is the latent heat effect of crop transpiration. The remaining variables are presented in the Nomenclature section (see the appendices). Moreover, the greenhouse's inside absolute humidity ($H_{a,int}$), which is the amount of water vapour in the greenhouse air, is modelled on a vapour mass balance [23]:

$$\rho_a \frac{V_a}{A_{ss}} \frac{dH_{a,int}}{dt} = \dot{M}_{trp,cr} + \dot{M}_{hum} - \dot{M}_{dehum} - \dot{M}_{vent,int-ext}, \tag{11}$$

where $\dot{M}_{trp,cr}$ is the crop transpiration flux, which relates to the amount of water lost by the plants during the transpiration process and must be recovered by irrigation, $\dot{M}_{hum}$ is the water flux provided by the humidification system, $\dot{M}_{dehum}$ is the water flux removed by the dehumidification system, and $\dot{M}_{vent,int-ext}$ is the outflow by natural ventilation and infiltration. The remaining variables are presented in the Nomenclature section (see the appendices).

It should be noted that the cultivation area in the model was fixed at $308 \, \text{m}^2$ in order to scale the greenhouse water consumption to the production of the four MD modules.

4. Control system

The main idea is to develop a control algorithm capable of providing optimal feed flow rate distribution among the MD modules, according to the greenhouse water demand and the thermal efficiency of the MD modules at each instant. For this purpose, DMPC controllers [25,26] are an attractive approach given that, in industrial applications, the number of required MD modules significantly increases and the application of a centralized controller could prove very difficult for computational power and communications.
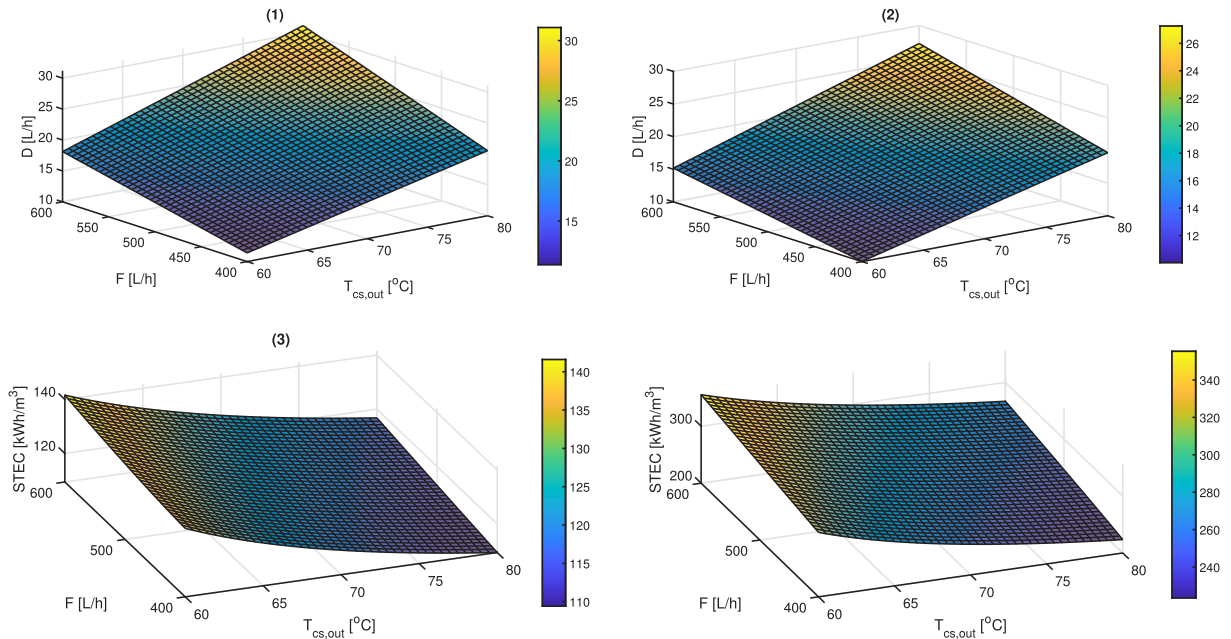

Fig. 5. 3D response surfaces. (1) Distillate production from the Aquastill module, (2) Distillate production from the Solar Spring module, (3) STEC of the Aquastill module, and (4) STEC of the Solar Spring module.

In the next section, the performance of each MD module in terms of distillate production and thermal efficiency is shown and analysed. Based on this analysis, we first formulate the centralized controller and then we present the distributed approach. Subsequently, the simulation results and some conclusions are presented.

4.1. Optimal operation of the MD modules

Before presenting the control system development, it is important to analyse and even visualize the performance of each module in order to clarify how the control system has been designed. Two of the most important metrics used in describing the performance of membrane distillation modules are the distillate production and the thermal efficiency. Thus, in this section, 3D response surface plots of each module are presented, showing the behaviour of the two metrics with respect to the evaporator inlet temperature and the feed flow rate; the two most important variables influencing them.

Conversely, the distillate production value can be directly obtained, simply by measuring the quantity of distillate produced in each sample time. The thermal efficiency of the process must be estimated using one of the performance metrics presented in the literature. In this case, the Specific Thermal Energy Consumption (STEC) has been selected [21,16,22]. This metric provides the amount of thermal energy required to produce a volume unit of distillate, and it can be calculated as follows:

$$\text{STEC}(\text{kWh/m}^3) = \frac{F \cdot \rho_{feed} \cdot c_{p,2} \cdot (T_{cs,out} - T_{cs,in})}{c_f \cdot D}. \tag{12}$$

Please note that all the variables involved in the previous equation are defined in the Nomenclature section.

Fig. 5 shows the 3D response surface plots. Regarding the distillate production, one can observe that the maximum value is obtained when operating at the maximum feed flow rate and evaporator inlet temperature for both modules (see Fig. 5-1 and Fig. 5-2). However, in the case of STEC, which must be at the minimum to obtain a higher thermal efficiency in the process, the optimal operating points are reached by working at the maximum evaporator inlet temperature and the minimum feed flow rate in both cases (see Fig. 5-3 and Fig. 5-4). In addition, when comparing the two modules, the Aquastill module has higher distillate production and thermal efficiency than the Solar Spring module. So, to summarize, the most important conclusions on which to base the control system development are that: (i) the evaporator inlet temperature should be the highest possible (this depends on solar irradiance) to obtain optimal performance, (ii) contrary operating conditions are required in the feed flow rate to maximize the distillate production and thermal efficiency in both modules, and (iii) the Aquastill module produces more distillate and is more efficient than the Solar Spring module.

4.2. Centralized control approach

MPC is a control technique that is widely used in both industry and academia. MPC can include (but is not limited to) optimal control, dead time, multivariable processes and the use of future setpoints if they are available [27]. By using a finite receding control horizon strategy, it can also deal with constraints and nonlinear processes. MPC controllers use the following structure and features (see Fig. 6):

- Explicit use of a process model to predict future process behaviour $\hat{y}(t + j|t)$.
- Minimization of a cost function to calculate the control signal $u(t|t)$. This objective function usually tries to maintain the process as closely as possible to a determined reference $w(t + j|t)$.
- The use of a finite receding control horizon, meaning that a set of control signals is calculated for the whole horizon

$(u(t|t), u(t + 1|t), ...,u(t + N_u - 1|t))$ although only the first control signal is applied whilst the rest are rejected; the procedure is then repeated for the next sampling period.

The main differences between the MPC strategies are firstly in the process model and noise model, and secondly in the cost function. These differences can cause distinct behaviour in a feedback loop.

Given the many advantages of the MPC strategy when compared to other control strategies [27], it was chosen as the most suitable for this work. Therefore, assuming prediction and control horizons with lengths of N and N_u, respectively, the cost function for a system can be formulated as follows:

$$J = \sum_{j \geq 1}^{N} \delta \cdot [\hat{y}(t + j|t) - w(t + j|t)]^2 + \sum_{j \geq 0}^{N_u - 1} \lambda \cdot [\Delta u(t + j)]^2, \tag{13}$$

where the system output prediction and the desired reference, $\hat{y}(t + j|t)$ and $w(t + j|t)$ respectively, are estimated for sample time $t + j$ using the information available at sample time t. On the other hand, $\Delta u(t + j)$ is the variation in the control action at sample time $(t + j)$ whereas δ and λ are weighting factors that penalize the future tracking errors and control efforts, respectively, along their horizons.

With regard to the constraints, there are mainly three kinds that can be found affecting system outputs and control actions:

$$\Delta u_{min} \leqslant \Delta u(t) \leqslant \Delta u_{max}, \quad \forall\, t \geqslant 0, \tag{14a}$$

$$u_{min} \leqslant u(t) \leqslant u_{max}, \quad \forall\, t \geqslant 0, \tag{14b}$$

$$y_{min} \leqslant y(t) \leqslant y_{max}, \quad \forall\, t \geqslant 0. \tag{14c}$$

In the previous equations, the first constraint, Eq. (14a), limits the control effort in order to avoid abrupt changes in the actuator that may cause disruption. The second one, Eq. (14b), relates to the physical hard constraints of the actuator. Finally, the third constraint, Eq. (14c), gives the lower and upper limits, y_{min} and y_{max} respectively, of the output variable (also applicable to predicted future values). In this work, the cost function presented in Eq. (13) has been modified to the problem at hand. Thus, for the centralized control approach, the cost function is given by:

$$J = \sum_{j \geq 1}^{N} \zeta \cdot \hat{y}_{STEC}(t + j|t) + \sum_{j \geq 1}^{N} \delta \cdot [w_{tank}(t + j) - \hat{y}_{tank}(t + j|t)]$$
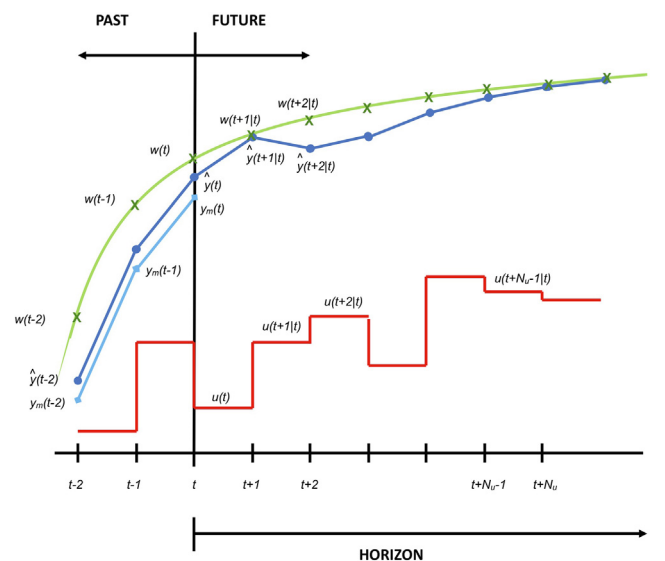$$+ \sum_{j \geq 0}^{N_u - 1} \lambda \cdot \Delta u(t + j), \tag{15}$$

Fig. 6. MPC strategy.

where $\zeta = (1 - \delta)$, $\widehat{y}_{STEC}$ is the mean STEC value for the four MD modules, $\widehat{y}_{tank}$ is the level of the tank and w_{tank} is the minimum tank level allowed. In addition, it should be pointed out that the set of inputs $\boldsymbol{u}$ is composed of the feed flow rate for each of the MD modules, according to Fig. 1, $\boldsymbol{u} = [F_{AQ-1}F_{SS-1}F_{SS-2}F_{AQ-2}]$.

4.3. Distributed control

In this work, a system composed of M subsystems or agents, i.e. the MD modules, is considered. So, for each agent, i, Eq. (15) can be rewritten as follows:

$$J_i = \sum_{j \geq 1}^{N} \zeta \cdot \widehat{y}_{STEC}(t + j|t) + \sum_{j \geq 1}^{N} \delta \cdot [w_{tank}(t + j) - \widehat{y}_{tank}(t + j|t)]$$
$$+ \sum_{j \geq 0}^{N_u-1} \lambda_i \cdot \Delta u_i(t + j).$$

(16)

Regarding the constraints, as has been indicated before, each agent, i can have its own constraints, as shown in Eqs. ((14)). However, this work is concerned with a plant that is formed by interconnecting M dynamic subsystems which share a common resource. Let $\mathscr{M} = \{1, ..., M\}$ be the set of agents or subsystems. In this case, the shared resource is the water flow supplied from the feed water tank and, to impose a limit on it, a new constraint which couples all the subsystems must be considered. Such a constraint can be defined as follows:

$$\sum_{i \geq 1}^{M} u_i(t + j) \leqslant b, \quad \forall j = 0, ..., N_u - 1,$$

(17)

where b is the allowable resource. For the problem at hand, this constraint is related to the total feed water flow supplied from the feed water tank to the whole system, which could be limited by design decisions as previously mentioned. So, the optimization problem for the whole system, including the M subsystems, can be formulated as follows:

$$P(t): \min f(\Delta u_i)$$
$$= \sum_{j \geq 1}^{N} \zeta \cdot \widehat{y}_{STEC}(t + j|t) + \sum_{j \geq 1}^{N} \delta \cdot [w_{tank}(t + j) - \widehat{y}_{tank}(t + j|t)]$$
$$+ \sum_{i \geq 1}^{M} \sum_{j \geq 0}^{N_u-1} \lambda_i \cdot \Delta u_i(t + j)$$

(18a)

$$\text{s.to: } \sum_{i \geq 1}^{M} u_i(t + j) \leqslant b, \ \forall j = 0, ..., N_u - 1$$

(18b)

$$u_{min} \leqslant u_i(t + j) \leqslant u_{max}, \ \forall j = 0, ..., N_u - 1.$$

(18c)

The optimization problem $P(t)$ defined by Eq. ((18)) would consist of a set of M decoupled subproblems if it were not for the coupling constraint in Eq. (18b). The first term, y_{STEC} in Eqs. (15) and (16), which is related to the mean STEC of the four MD modules, is added to maximize the thermal efficiency of the SMD plant operation. On the other hand, the tank level, y_{tank}, should not have a value lower than 1500 L; that is, $y_{tank} \geqslant 1500$, this value has been chosen as it ensures the greenhouse supply for two days without MD production, given that the average consumption per day is around 750 L. However, setting this constraint as a hard constraint makes the optimization problem unfeasible; thus, a soft constraint has been added to the second term of both Eqs. (15) and (16), where w_{tank} is set to 1500 L for the whole prediction horizon.

It should be mentioned that the two terms involved in the objective function require contrary operating conditions since, to maximize the thermal efficiency, the MD modules must be run at the minimum feed flow rate value, whereas to maximize the distillate production to increase the tank level, the MD modules must be fed at the maximum flow

(see Section 4.1). Nevertheless, the two objectives do not always have to be maximized at the same time; hence, the following function is used to set the weighting factors ζ and δ:

$$\zeta = \begin{cases} 0 & \text{if } x \leqslant c, \\ d \cdot x + e & \text{if } c < x < f, \\ 1 & \text{if } x \geqslant f. \end{cases}$$

(19)

In this function, x is the tank level at instant time t, c and f are specific tank levels, and d and e are the first-order polynomial factors. It should be remembered that $\delta = (1 - \zeta)$. Therefore, if the tank level is below c, only the part related to increasing the tank level is considered in the objective function. Conversely, if the tank level is above f, the objective function is aimed at maximizing the STEC, whereas if the tank level is between c and f, the two objectives are considered, calculating the weighting factors by means of a first-order polynomial, and thus obtaining a soft transition between the two objectives while avoiding chattering problems in the control signals.

Additionally, it should be pointed out that, among the set of constraints presented in Eq. (18), only the constraint related to the physical limitations of the actuators has been included in the problem. This is because it is the only limitation imposed by the system since the feed flow rate of the MD modules must be between 400 and 600 L/h, which is u_{min} equal to 400 and u_{max} equal to 600 L/h.

The procedure that each agent or subsystem i must perform at each iteration l within a sample period t is the following [20]: read the decisions made by the neighbours, coordinate its iterations and calculate its own control actions by solving problem $P(t)$. For this, the agent will need to receive the residual feed water flow from the upstream agent and the previous control signal $u_{i+1}(t - 1)$ from the downstream agent; the latest prediction for output $\widehat{y}_{i+1}(t)$ and the latest control increment $\Delta u_{i+1}(t)^l$.

Upon satisfying a convergence criterion (i.e. the difference between the results of two iterations being less than a minimum established threshold ε) or reaching the maximum number of iterations σ, the obtained control values are applied to the valves, the horizon is shifted to the next sample time, and the process is repeated. This procedure is given in pseudo-code in Algorithm 1.

Algorithm 1: Distributed optimization performed by agent i during the iteration l at sample time t

---

if agent i cannot revise its decisions in iteration l **then**
   $\lfloor \ \Delta u_i(t)^{l+1} = \Delta u_i(t)^l$
else
   - Agent i receives the available feed water flow from the upstream agent $i - 1$ and $\Delta u_{i+1}(t)^l$ from the downstream agent $i + 1$;
   - Agent i solves problem $P(t)$ to obtain $\Delta u_i(t)^{l+1}$ and the prediction of available feed water flow;

Finally, to solve this optimization problem, function *fmincon*, which can be found in the MATLAB *Optimization Toolbox* [28], has been used.

5. Results and discussion

This section shows the results of the simulation experiments carried out to evaluate the effectiveness of the proposed control strategy. The results are presented as follows: (i) the simulation set-up is presented, (ii) the controller set-up is shown and discussed, (iii) the convergence of the DMPC approach to optimal solutions is checked by comparing the results obtained from the DMPC algorithm with those of the centralized approach, (iv) the use of the DMPC approach is justified by scaling up the problem to industrial-scale plants and measuring the maximum time spent by the DMPC and the centralized formulations in solving the

control problem, and (v) the automatic operation benefits are presented by comparing the performance with a non-optimal management of the facility; namely, manual operation.

5.1. Simulation set-up

The schematic diagrams showing how the simulations were performed for the centralized and distributed approaches are presented in Figs. 7 and 8. As can be observed, the experimental campaign was performed using the temperature profiles of the SMD plant's heat generation circuit ($T_{hs,in}$ in Figs. 7 and 8), as mentioned above. These temperature profiles were connected to a simulator that emulated the behaviour of the MD modules and the greenhouse using the models presented in Section 3. To simulate the greenhouse model, meteorological data from the Experimental Station of the Cajamar Foundation were employed, on the day of July 20th, 2017. Additionally, in the simulations, both control approaches used linearized models of the system around the operating point **u** for predicting $\hat{y}_{STEC}$ and $\hat{y}_{tank}$; these are obtained at each sampling time using the technique presented in [29]. Note that the linear models are calculated only once in the distributed approach (see Fig. 8) since the strategy has been implemented in only one computer; however, in real implementations, they must be calculated for each of the agents included in the optimization problem. It should be pointed out that linearized models rather than nonlinear ones have been used in the controllers due to the high computational effort required for solving the optimization problem with the latter. Accordingly, the controllers have to cope with uncertainties caused by disturbances, modelling errors and neglected dynamics. Moreover, the use of two different kinds of MD modules, each behaving differently, increases the automatic operation complexity.

In the experiments, the maximum feed flow rate provided by pump 1 (see Fig. 1) was limited to 2000 L/h (as mentioned in Section 3.1), that is b = 2000 L/h, trying to mimic the conditions that would occur in industrial processes. One must bear in mind that, in this case study, only four modules are required to meet the water requirements of the pilot greenhouse. This pilot configuration was chosen since it accurately represents practical situations, and facilitates the visualization of the results. However, when considering industrial-scale greenhouses, the number of commercial MD modules increases considerably, and the feed flow rate may be limited either by design (as mentioned in Section 3.1) or by operational constraints, requiring adequate control algorithms to deal with these situations.

The MD modules come into operation when the evaporator inlet temperature is higher than 60 °C (the lower operational limit of the modules) and are turned off when it is lower than 60 °C. This strategy has been implemented using the procedure presented in [13], in which mean values are used for checking instead of instant ones, thus avoiding chattering problems. In this way, the MD modules are started after reaching 60 °C, specifically at 63.6 °C under the conditions used in the simulations. Moreover, as the initial point, valves V1, V2, V3 and V4 were fixed at 0.5, corresponding to a feed flow rate of 475 L/h in each MD module, and the initial distillate tank level was 1600 L.

5.2. Controller set-up

Regarding the controller set up, the sampling time was set at 10 min; this was selected considering the representative time constants of the crop transpiration inside the greenhouse and the temperature of the heat generation circuit of the SMD plant. The horizons were selected considering traditional recommendations for MPC controllers, $N_u \ll N$, and N large enough to contemplate the transient part of the response, thus ensuring stable closed-loop performance. The final values were N = 6 and N_u = 2. In the same way, λ was fixed at 0.1; this was chosen following an exhaustive simulation until the desired closed-loop response was obtained. Moreover, σ was fixed to 200. This parameter relates to the maximum number of DMPC algorithm iterations at each sample time. A large number was chosen so that the DMPC algorithm would stop when reaching the threshold criterion, instead of reaching the set one.

c was fixed at 1510 L whilst g was fixed at 1620 L. The first value was chosen since c should be slightly higher than the minimum tank level (1500 L), thus allowing the controller to consider the thermal efficiency term in the objective function as much as possible. Conversely, g was chosen to allow a soft change between the two objectives included in the objective function. Comprehensive simulations were carried out with several g values, showing that with g values closer to the ones for c, abrupt changes in the control signals might occur, which could cause chattering problems. Besides, the thermal efficiency index did not improve considerably. The polynomial factors were fixed at [d, e] = [0.0091, −13.6383], obtained by interpolating c and g. Finally, the controller was implemented in MATLAB code running on a PC with an Intel Core i5-6500T CPU 2.50 GHz with 8 GB of RAM.

5.3. Convergence of the DMPC approach to optimal solutions

This section presents the simulations performed to check the convergence of the DMPC approach to optimal solutions. It should be mentioned that the distributed controller approximates the centralized one, and the theoretical optimal solution must be the same as that of the centralized algorithm. For this reason, the same test was carried out with the centralized and the distributed algorithm in order to graphically and quantitatively compare both approaches.

The results of the simulations for the centralized and distributed controllers are shown in Figs. 9 and 10, respectively. Note that both the hot side inlet temperature of the heat exchanger (see Figs. 9-1 and 10-1) and the greenhouse consumption (see Figs. 9-4 and 10-4) directly depend on the solar irradiance. Although the global irradiance curve has not been included in the graphics for the sake of simplicity, in Almería, on a summer's day, the solar midday is at around 2.00 pm. Consequently, one can observe how the greenhouse water consumption (see Figs. 9-4 and 10-4) is maximum around this time instant. However, the temperature at the heat exchanger inlet is maximum later on due to the volume of water accumulated in the storage tank placed between the solar field and the heat exchanger (see Figs. 9-1 and 10-1). Consequently, the distillate production of the four MD modules also reaches
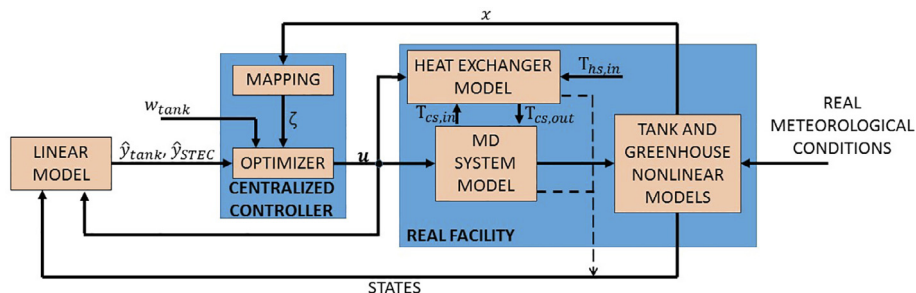
Fig. 7. Centralized approach simulation scheme.
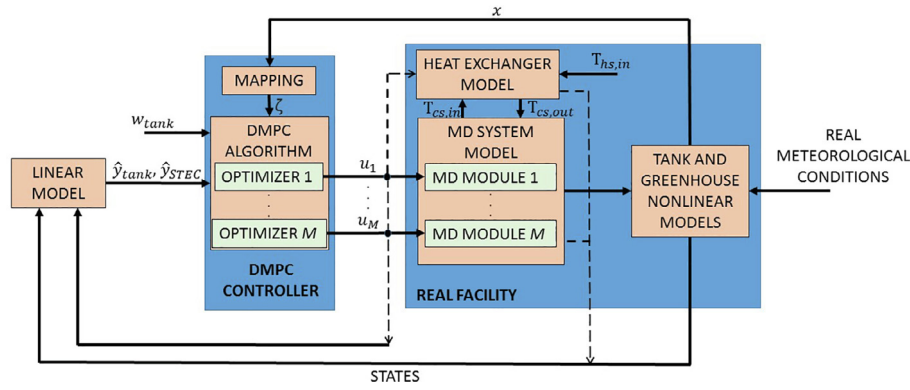
Fig. 8. Distributed approach simulation scheme.

the maximum later on since it depends on this temperature (see Figs. 9-4 and 10-4).

As pointed out before, the automatic operation starts when the inlet temperature of the evaporator channel of each MD module is higher than 60 °C (see Figs. 9-1 and 10-1). This condition is checked using the heat exchanger model, as presented in [13]. At this moment, the tank level is 1575 L (notice that the greenhouse consumes water before the modules are started); therefore, in the objective function, both the distillate production and the STEC objectives are taken into account with the weighting factors calculated using the polynomial. For this reason, in the first sampling time, the controllers increase the feed flow rate diverted for the Aquastill modules and decrease that delivered to the Solar Spring modules (see Figs. 9-2 and 10-2). This procedure is repeated for the following sampling times, until saturating the control signals. In this way, the MD modules that have a higher distillate production and a lower STEC (the Aquastill modules) are fed at the maximum feed flow rate (600 L/h) whereas the Solar Spring modules are fed at the minimum feed flow rate (400 L/h). With this optimal distribution, the mean distillate production of the four MD modules is augmented, while the mean STEC is reduced (see Figs. 9-3 and 10-3), thus achieving optimal performance and maintaining the desired level in the distillate tank. At around 16.00 h, the greenhouse water

consumption decreases and the tank level increases (see Figs. 9-4 and 10-4). Thus, in the objective function, the weighting factor part related to the STEC increases in accordance with the polynomial, while the feed flow rates of the Aquastill modules are reduced by the controller (see Figs. 9-2 and 10-2). At around 17.30 h, the distillate tank level is over 1,620 L, so only the objective function part related to the STEC is considered. Accordingly, the feed flow rates of the Aquastill modules decrease faster until they reach the minimum value (see Figs. 9-2 and 10-2); this is to increase the operation's thermal efficiency (see Figs. 9-4 and 10-4).

The performance of both controllers is very similar, and the differences between them can be observed only in the control signals during the transients. These are caused by the way in which the control signals are calculated by the DMPC algorithm (see Algorithm 1). However, these differences hardly affect the overall system performance in terms of distillate production and thermal efficiency (see Figs. 9 and 10). This fact can be quantitatively checked in Table 1, where the mean STEC of the operation and the distillate produced by the four MD modules are summarized for the centralized MPC case, and for several DMPC cases with different values of ε. All the simulations were performed under the same operating conditions as those employed in Figs. 9 and 10. Therefore, as can be seen in Table 1, for a ε equal to 10^{-5}, the same
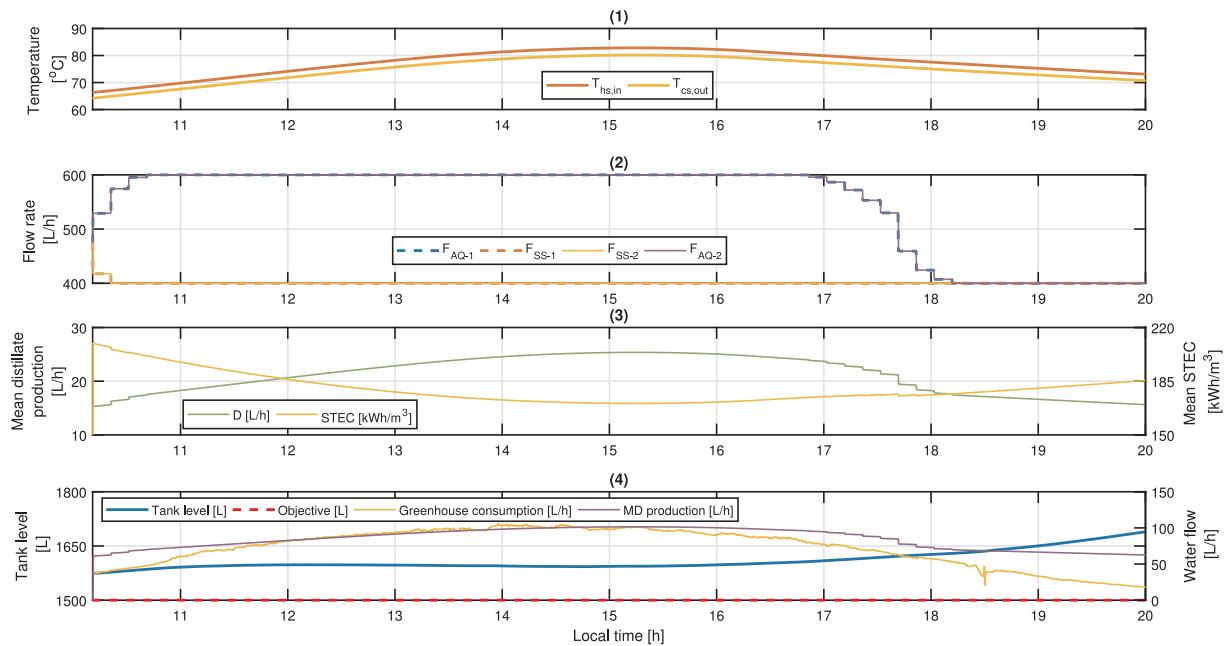
Fig. 9. Results obtained with the centralized approach. (1) Temperature at the hot side heat exchanger inlet ($T_{hs,in}$), and the temperature leaving the cold side of the heat exchanger ($T_{cs,out}$); (2) MD modules feed flow rates (F_{AQ-1}, F_{SS-1}, F_{SS-2}, and F_{AQ-2}); (3) mean distillate production from the four MD modules (D) and the mean STEC (STEC); and (4) tank level, objective (minimum allowed tank level), greenhouse water consumption, and MD production.
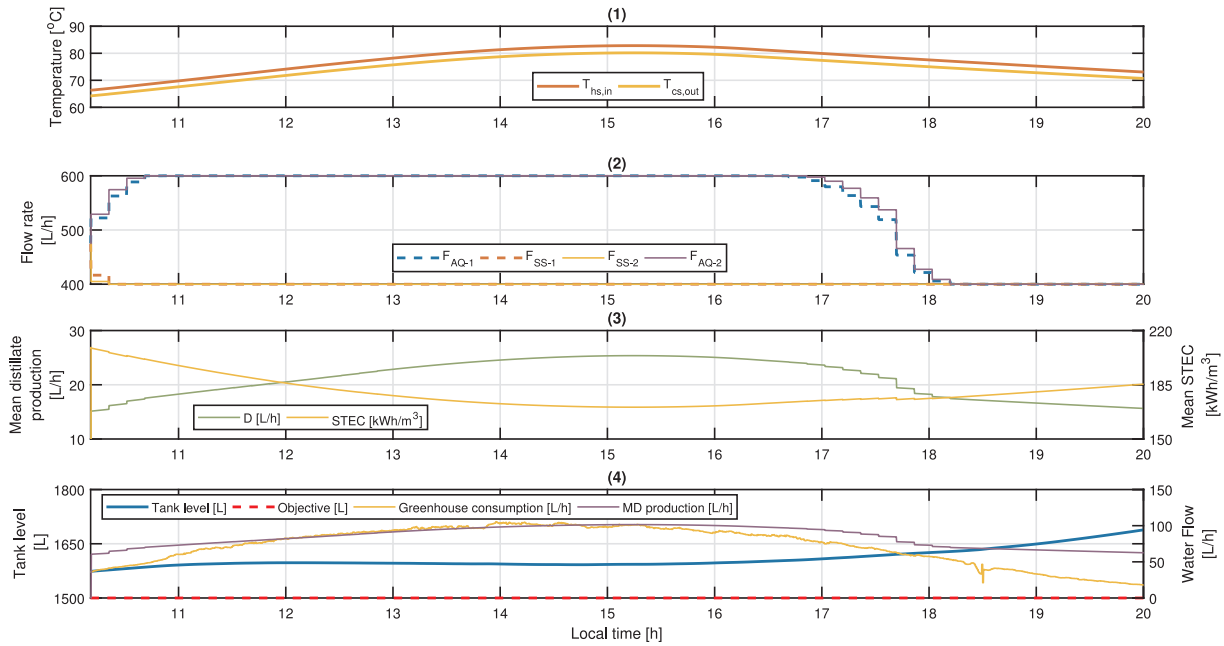
Fig. 10. Results obtained with the distributed approach ($\varepsilon = 10^{-4}$). (1) Temperature at the heat exchanger inlet, hot side ($T_{hs,in}$), and the temperature leaving the cold side of the heat exchanger ($T_{cs,out}$); (2) MD modules feed flow rates (F_{AQ-1}, F_{SS-1}, F_{SS-2}; and F_{AQ-2}) (3) mean distillate production of the four MD modules (D) and mean STEC (STEC); and (4) tank level, objective (minimum allowed tank level), greenhouse water consumption, and MD production.

Table 1

Comparison between an operation using the centralized MPC controller, an operation using several varying DMPC configurations ε, and an operation with no controller, using a static setpoint in valves V1, V2, V3 and V4 equal to 0.5.

Controller	STEC [kWh/m$_3$]	Distillate [L]
No	190.35	1719.00
MPC	180.56	1733.82
DMPC ($\varepsilon = 10^{-1}$)	180.57	1733.80
DMPC ($\varepsilon = 10^{-2}$)	180.57	1733.80
DMPC ($\varepsilon = 10^{-3}$)	180.57	1733.80
DMPC ($\varepsilon = 10^{-4}$)	180.56	1733.81
DMPC ($\varepsilon = 10^{-5}$)	180.56	1733.82

results in terms of STEC and distillate production are obtained as those for the centralized approach. In the same way, when increasing ε, the results are still almost the same until reaching the value of 10^{-1}, which is the limit. At this value, the controller still provides a stable response and an optimal distribution of the feed flow rate. However, with ε higher than 10^{-1}, the algorithm converges to solutions that are far from optimal.

5.4. Justification for using the DMPC approach

One of the main advantages of the DMPC approach is that the optimization problem that each agent has to solve is simple and small, independent of the number of agents involved in the system. This influences the time spent by the algorithm in reaching a stationary
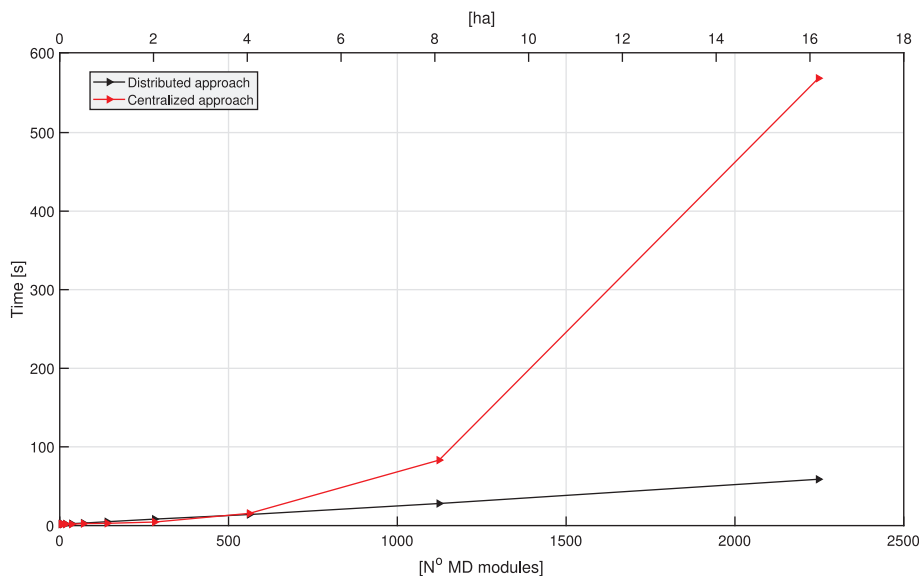
Fig. 11. Maximum time spent for each algorithm to solve the optimization problem in a sampling time depending on the number of hectares to be irrigated. The number of MD modules required for each case is also shown. These simulations have been performed fixing $\varepsilon = 10^{-4}$ in the distributed algorithm.

solution, so that it is analysed both for the centralized and the distributed approaches. The facility used in this work is a small pilot plant; thus, the centralized problem formulation is favoured. Conversely, when considering industrial-scale facilities, the number of MD modules required to meet the water requirement increases considerably, and so does the computation time. For this reason, several simulations have been carried out increasing the number of crop hectares that must be irrigated by the SMD plant; this allows us to analyse the maximum time spent for each algorithm to solve the optimization problem in a sampling time (see Fig. 11).

As can be seen in Fig. 11, and as pointed out previously, the centralized approach is slightly favoured when considering small-scale facilities (i.e. 1 or 2 hectares). Conversely, when considering extensive crops areas, the time spent by the centralized approach exponentially increases – for 16 ha, the time is almost equal to the sampling time itself and the algorithm does not provide an optimal solution within the required time period. The time required by the distributed approach also increases depending on the number of hectares but in a linear way, thus allowing optimal solutions to be obtained for large facilities in the required time period, one of the main advantages of this algorithm and one of the main reasons for choosing it for this application. It is also important to point out that expanding the algorithm for larger plants is very easy since the introduction of a new agent in the problem only requires changes in the neighbouring agents, without reprogramming the entire algorithm.

In addition to the benefits achieved regarding the time spent solving the optimization problem, the DMPC approach offers the following general advantages of these kinds of algorithms: (i) the risk of failure is reduced because the system does not depend on a centralized controller, so the greenhouse supply is not compromised, (ii) the communication between agents is easier because each agent is only connected to its neighbours, hence simplifying the communication network in an industrial facility.

5.5. Benefits of optimal operation

The results obtained with the MPC controllers were compared to an operation using static control signals of 0.5 in valves V1, V2, V3 and V4. To perform this comparison, the same operating conditions as those considered in Section 5.1 were employed. The results of this simulation are presented in Table 1. The mean STEC for the operation with static values in the valves was 190.35 kWh/m_3 while the total distillate production was 1719 L. When a controller was used to optimally distribute the feed flow rate, almost 10 kWh (around 5%) less thermal energy was required to produce $1\,m_3$ of distillate while the total distillate production increased by more than 14 L.

To analyse the energy savings achieved using the proposed MPC approach, the results obtained in this case study have been extrapolated to the industrial scale. According to the study performed in [30], a tomato crop has a water requirement of 4110 m^3/ha in a season. In addition, if the water consumed by the humidification system during a season is considered (200 L/m^2[31]), the water demand increases even more. In Fig. 12, the absolute thermal energy savings have been plotted for the case of a tomato crop (also considering the humidification system) based on the number of hectares that must be irrigated.

It should be pointed out that the improvements achieved using the control system are almost constant, independent of the operating conditions, since the worst operating conditions occur when there are passing clouds or the global irradiance level is low. However, an adequate control system for the solar field [13] and the appropriate use of a storage system reduces the irradiance disturbance effect on the MD system. It should also be pointed out that these savings could be considered in the design phase, allowing one to reduce the costs associated with oversizing the thermal energy sources. Similarly, it could be very relevant for daily operation, especially in cases where non-renewable sources are used (i.e. boilers), given that a considerable amount of fuel, biomass, multi-fuel, or any type of power can potentially be saved, thus reducing the daily operating costs.

6. Conclusions

This paper has addressed the optimal management of a distributed energy system comprising a solar membrane distillation facility and a greenhouse, connected by a buffer system. The scenario includes the generation of thermal energy using flat-plate solar collectors, and the distribution of this energy between the different MD modules included in the SMD plant to meet the greenhouse water demand.

A DMPC technique has been developed for optimal plant operation. In this control approach, each agent solves a simple MPC problem, exchanging information only with the neighbouring agents and
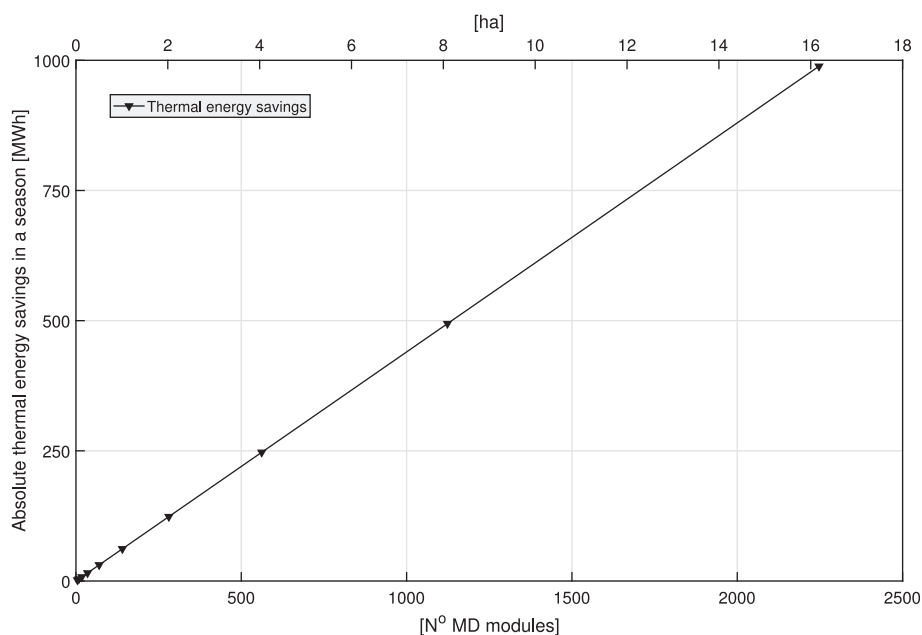

Fig. 12. Absolute energy savings in a season depending on the number of hectares to be irrigated. The number of MD modules required for each case is also shown.

optimally distributing the available resources as a whole. in addition, two weighted objectives were considered in the cost function defining the optimization problem. The first aimed to maximize the thermal efficiency of the SMD system, which is identified as one of the main weak point of this technology. The second related to the intermediate buffer level located between the SMD facility and the greenhouse, which must be higher than a specific minimum value to guarantee the greenhouse water supply. Based on these objectives, the control algorithm computes the optimal distribution of the feed flow rate for each MD module. Simulation experiments using real meteorological data from the Plataforma Solar de Almería and the Experimental Station of the Cajamar Foundation were performed, showing that:

- The DMPC controller is suitable for managing these kinds of plants, improving the thermal efficiency of the facility and maintaining the intermediate tank level above the objective.
- The same results as for a centralized approach can be achieved using the proposed DMPC controller, meaning that the DMPC controller can converge to optimal results. The DMPC approach approximates the centralized controller so the optimal results for the DMPC algorithms are those of the centralized one.
- However, when industrial-scale SMD plants are considered, where the number of MD modules included in the plant, and therefore the number of agents involved in the optimization problem, significantly increases, only the DMPC approach is able to provide optimal results.
- The application of the DMPC strategy allows us to reduce the specific thermal energy consumption of the SMD plant by 5 % compared to manual operation. These thermal energy savings mean that, for an industrial-scale cultivation area (i.e. 8 ha), around 50 MWh/season less thermal energy is required; this could be very relevant both for the design phase and for daily operation, especially when also considering non-renewable sources to feed the MD modules.

Declaration of Competing Interest

None.

Acknowledgement

References

[1] De Rafael GH, Fernández-Prados JS. Intensive agriculture, marketing and social structure: the case of South-eastern Spain. Agric Econ 2018;64(8):367–77. https://doi.org/10.17221/318/2016-AGRICECON.

[2] Cazcarro I, Duarte R, Martín-Retortillo M, Pinilla V, Serrano A. Water scarcity and agricultural growth in Spain: from curse to blessing. Nat Resour Econ Growth: Learn History Routledge, London 2015:339–61.

[3] Garcia-Caparros P, Contreras JI, Baeza R, Segura ML, Lao MT. Integral management of irrigation water in intensive horticultural systems of Almería. Sustainability 2017;9(12):2271. https://doi.org/10.3390/su9122271.

[4] Aznar-Sánchez JA, Belmonte-Ureña LJ, Velasco-Muñoz JF, Valera DL. Aquifer sustainability and the use of desalinated seawater for greenhouse irrigation in the campo de Níjar, Southeast Spain. Int J Environ Res Public Health 2019;16(5):898. https://doi.org/10.3390/ijerph16050898.

[5] Martínez-Alvarez V, González-Ortega M, Martin-Gorriz B, Soto-García M, Maestre-Valero J. The use of desalinated seawater for crop irrigation in the Segura River Basin (South-eastern Spain). Desalination 2017;422:153–64. https://doi.org/10.1016/j.desal.2017.08.022.

[6] Amy G, Ghaffour N, Li Z, Francis L, Linares RV, Missimer T, et al. Membrane-based seawater desalination: present and future prospects. Desalination 2017;401:16–21. https://doi.org/10.1016/j.desal.2016.10.002.

[7] Martínez-Álvarez V, Martin-Gorriz B, Soto-García M. Seawater desalination for crop

[8] González D, Amigo J, Suárez F. Membrane distillation: perspectives for sustainable and improved desalination. Renewable Sustainable Energy Rev 2017;80:238–59. https://doi.org/10.1016/j.rser.2017.05.078.

[9] Elzahaby AM, Kabeel A, Bassuoni M, Elbar ARA. Direct contact membrane water distillation assisted with solar energy. Energy Conversion Manage 2016;110:397–406. https://doi.org/10.1016/j.enconman.2015.12.046.

[10] Fernández-Ibáñez P, Polo-López MI, Malato S, Ruiz-Aguirre A, Zaragoza G. Solar photocatalytic disinfection of water for reuse in irrigation. Geothermal, Wind and Solar Energy Applications in Agriculture and Aquaculture CRC Press; 2017. p. 195–211.

[11] Gil JD, Roca L, Zaragoza G, Berenguel M. A feedback control system with reference governor for a solar membrane distillation pilot facility. Renewable Energy 2018;120:536–49. https://doi.org/10.1016/j.renene.2017.12.107.

[12] Porrazzo R, Cipollina A, Galluzzo M, Micale G. A neural network-based optimizing control system for a seawater-desalination solar-powered membrane distillation unit. Comput Chem Eng 2013;54:79–96.

[13] Gil JD, Roca L, Ruiz-Aguirre A, Zaragoza G, Berenguel M. Optimal operation of a solar membrane distillation pilot plant via nonlinear model predictive control. Comput Chem Eng 2018;109:151–65. https://doi.org/10.1016/j.compchemeng.2017.11.012.

[14] Rahimpour MR, Kazerooni NM, Parhoudeh M. Water treatment by renewable energy-driven membrane distillation. Current Trends and Future Developments on (Bio-) Membranes Elsevier; 2019. p. 179–211. https://doi.org/10.1016/B978-0-12-813545-7.00008-8.

[15] Miladi R, Frikha N, Kheiri A, Gabsi S. Energetic performance analysis of seawater desalination with a solar membrane distillation. Energy Conversion Manage 2019;185:143–54. https://doi.org/10.1016/j.enconman.2019.02.011.

[16] Ruiz-Aguirre A, Andrés-Mañas J, Fernández-Sevilla J, Zaragoza G. Experimental characterization and optimization of multi-channel spiral wound air gap membrane distillation modules for seawater desalination. Separation Purification Technol 2018;205:212–22. https://doi.org/10.1016/j.seppur.2018.05.044.

[17] Roca L, Sánchez-Molina JA, Rodríguez F, Bonilla J, de la Calle A, Berenguel M. Predictive control applied to a solar desalination plant connected to a greenhouse with daily variation of irrigation water demand. Energies 2016;9(3):194. https://doi.org/10.3390/en9030194.

[18] Carballo JA, Bonilla J, Roca L, De la Calle A, Palenzuela P, Alarcón-Padilla DC. Optimal operating conditions analysis for a multi-effect distillation plant according to energetic and exergetic criteria. Desalination 2018;435:70–6. https://doi.org/10.1016/j.desal.2017.12.013.

[19] Ortega-Delgado B, Giacalone F, Catrini P, Cipollina A, Piacentino A, Tamburini A, et al. Reverse electrodialysis heat engine with multi-effect distillation: Exergy analysis and perspectives. Energy Conversion Manage 2019;194:140–59. https://doi.org/10.1016/j.enconman.2019.04.056.

[20] Scherer HF, Pasamontes M, Guzmán JL, Álvarez JD, Camponogara E, Normey-Rico J. Efficient building energy management using distributed model predictive control. J Process Control 2014;24(6):740–9. https://doi.org/10.1016/j.jprocont.2013.09.024.

[21] Zaragoza G, Ruiz-Aguirre A, Guillén-Burrieza E. Efficiency in the use of solar thermal energy of small membrane desalination systems for decentralized water production. Appl Energy 2014;130:491–9. https://doi.org/10.1016/j.apenergy.2014.02.024.

[22] Ruiz-Aguirre A, Andrés-Mañas J, Fernández-Sevilla J, Zaragoza G. Modeling and optimization of a commercial permeate gap spiral wound membrane distillation module for seawater desalination. Desalination 2017;419:160–8. https://doi.org/10.1016/j.desal.2017.06.019.

[23] Rodríguez F, Berenguel M, Guzmán JL, Ramírez-Arias A. Modeling and control of greenhouse crop growth. Springer; 2015.

[24] de la Calle A, Roca L, Bonilla J, Palenzuela P. Dynamic modeling and simulation of a double-effect absorption heat pump. Int J Refrig 2016;72:171–91. https://doi.org/10.1016/j.ijrefrig.2016.07.018.

[25] Rahman M, Oo A. Distributed multi-agent based coordinated power management and control strategy for microgrids with distributed energy resources. Energy Conversion Manage 2017;139:20–32. https://doi.org/10.1016/j.enconman.2017.02.021.

[26] Rubio FR, Navas SJ, Ollero P, Lemos JM, Ortega MG. Control óptimo aplicado a campos de colectores solares distribuidos. Revista Iberoamericana de Automática e Informática industrial 2018;15:327–38. https://doi.org/10.4995/riai.2018.8944.

[27] Camacho E, Bordons C. Model predictive control. London: Springer-Verlag Ltd; 2004.

[28] Matlab optimization toolbox release 2018. 2018. The MathWorks, Natick, MA, USA.

[29] Plucenio A, Pagano D, Bruciapaglia A, Normey-Rico J. A practical approach to predictive control for nonlinear processes. IFAC Proc Vol 2007;40(12):210–5. https://doi.org/10.3182/20070822-3-ZA-2920.00035.

[30] Becerra AT, Bravo XL. La agricultura intensiva del poniente almeriense. Diagnóstico e instrumentos de gestión ambiental. M+ A Revista Electrónica de Medioambiente 2010;8:18–40.

[31] Cámara-Zapata JM, Sánchez-Molina JA, Rodríguez F, López JC. Evaluation of a dehumidifier in a mild weather greenhouse. Appl Thermal Eng 2019;146:92–103. https://doi.org/10.1016/j.applthermaleng.2018.09.107.

2.3.2 A general optimal operating strategy for commercial membrane distillation facilities

Research in this field is supported by the following journal paper:

Title	A general optimal operating strategy for commercial membrane distillation pilot facility
Authors	**J. D. Gil**, P. R. C. Mendes, E. Camponogara, L. Roca, J. D. Álvarez, J. E. Normey-Rico
Journal	Renewable Energy
Year	2020
Volume	156
Pages	220-234
DOI	`https://doi.org/10.1016/j.renene.2020.04.074`
IF (JCR 2018)	5.439
Categories	Energy & Fuels (17/103) **Q1**
	Green & Sustainable Science & Technology (7/35) Q1

Contribution of the Ph.D. candidate
The Ph.D. candidate, J. D. Gil, is the main contributor and first author of this paper.

Apart from the main work, it also gave rise to a contribution to a international conference:

- **J. D. Gil**, M. Muñoz, L. Roca, F. Rodríguez, and M. Berenguel, "An IoT based Control System for a Solar Membrane Distillation Plant used for Greenhouse Irrigation," in *Global IoT Summit (GIoTS)*. IEEE, 2019, pp. 1–6.

Also, to the following contribution to a national conference:

- **J. D. Gil**, L. Roca, M. Berenguel, and G. Zaragoza, "Aportaciones de la desalación solar térmica a la sostenibilidad del sistema agrícola en Almería," in *1er Congreso de Jóvenes Investigadores en Ciencias Agroalimentarias*. Almería, España, 2018.
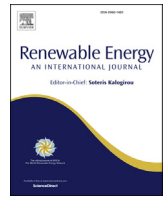
A general optimal operating strategy for commercial membrane distillation facilities

Juan D. Gil [a], Paulo R.C. Mendes [c, d], E. Camponogara [c], Lidia Roca [a, b], J.D. Álvarez [a, *], Julio E. Normey-Rico [c]

[a] Centro Mixto CIESOL, ceiA3, Universidad de Almería, Ctra, Sacramento s/n, Almería, 04120, Spain
[b] CIEMAT-Plataforma Solar de Almería, Ctra, de Senés s/n, Tabernas, 04200, Almería, Spain
[c] Federal University of Santa Catarina, Department of Automation and Systems engineering, Florianópolis, Brazil
[d] Fraunhofer Institute for Industrial Mathematics, Kaiserslautern, Germany

ARTICLE INFO

ABSTRACT

The high thermal energy consumption is one of the main drawbacks hampering the commercial implementation of Membrane Distillation (MD) technology. The development of adequate operating strategies can help to reduce these energy requirements. Accordingly, this paper focuses on the optimal management of the array of MD modules composing a commercial-scale MD plant, trying to reduce their thermal energy consumption while ensuring a given water need. For this aim, the array of MD modules is modelled as a Mixed Integer Programming (MIP) system to consider that some modules can be turned on/off depending on the operation specifications. An algorithm based on the Generalized Bender Decomposition (GBD) is then developed for the efficient solution of the problem. This algorithm is incorporated in a Model Predictive Control (MPC) strategy allowing to manage the plant in real time. The effectiveness of the proposed strategy is verified using a practical example. The obtained results are compared with a manual and a previous strategy presented in literature, showing that for a sunny day, around the 65 and 55% of the thermal energy consumed by these methodologies can be saved, which means important thermal energy savings that can be relevant for the industrial implementation of MD technology.

© 2020 Elsevier Ltd. All rights reserved.

1. Introduction

Membrane Distillation (MD) is an arising thermally driven separation method under investigation. This technology enables the use of low-grade thermal energy to desalinate water, what puts MD based processes in a competitive position to relieve water-energy stress nexus sustainably [1]. Despite this fact, its low energy efficiency, mainly caused by its high thermal energy consumption per unit of distillate produced, has hampered the industrial commercialization of the technology so far [2].

From the process point of view, MD stands out from conventional desalination technologies as: i) it is able to treat high salinity feed waters [3], ii) it has a high rejection factor [4], iii) it is driven by the partial pressure difference between both sides of the membrane, which is originated by a temperature difference instead of a mechanical power that increases exergy and costs [5], iv) it operates at low pressure around 0.1 MPa, which is much lower than the one required by Reverse Osmosis (RO) processes 2.5—8.5 MPa [5], and v) it is conducted at low temperature (lower than 90 °C), which allows MD units to be coupled with low grade solar energy [4,6]. This last advantage, together with the simplicity of the process, make MD systems especially suitable for developing stand-alone plants to be applied in offgrids locations; with good irradiance conditions and small-medium water needs [7]. Nevertheless, for making MD technology competitive at industrial-scale, its specific thermal energy consumption must be reduced by improving both the MD module design and configuration [8], and the operating strategies [6].

Regarding the design of MD modules, remarkable improvements have been reported in the literature in the last decades.

* Corresponding author.
E-mail addresses: juandiego.gil@ual.es (J.D. Gil), paulo.mendes@itwm.fraunhofer.de (P.R.C. Mendes), Eduardo.Camponogara@ufsc.br (E. Camponogara), lidia.roca@psa.es (L. Roca), jhervas@ual.es (J.D. Álvarez), julio.normey@ufsc.br (J.E. Normey-Rico).

These investigations were aimed at creating new membranes, configurations and modules, and to understand the membrane fouling [2]. These research efforts have caused a breakthrough in terms of thermal efficiency, going from a specific thermal energy consumption of 628 kWh/m^3 (MD modules without heat recovery [9]) to the current consumption of commercial-scale modules, around 100 kWh/m^3 at optimal operating conditions [10]. Note that this number is far from the consumption of conventional processes as RO, around 2—4 kWh/m^3 [11]. However, as was pointed out before, what is interesting of MD technology is that these energy requirements (around 95%) can be provided by solar energy [12]. Consequently, there are also numerous works proposing effective combinations [13] and new designs of integrated solar membrane-based desalination systems [14], showing that the overall efficiency can be improved up to 15%. Undoubtedly, the development in the design of the modules is still an open research field, but due to the growth of the technology, other research areas focused on the operation of MD modules are gaining interest in recent years. These works are mainly aimed to optimize the operating parameters of MD units [15], and to develop control and optimal management methods for improving the performance of the technology in real time [7].

With respect to the optimization of the operating parameters, several authors are working on the development of effective statistical or black-box models that allow to find optimal operating conditions of MD units [16]. The statistical model most widely used for this aim is the Response Surface Methodology (RSM). These kind of research works are based on the same procedure [17—20]: i) to design and conduct an experimental campaign in a determined operating range, ii) to adjust the selected outputs of the model by means of the RSM method, and iii) to find the optimal operating conditions within the studied operating range by applying an optimization method. Similarly, other authors used black-box models based on Artificial Neural Networks instead of RSM models with the same objectives [19,21,22]. Even though all these studies show how the thermal efficiency can be considerably improved by using the optimal static operating conditions they present, these conditions are difficult to achieve when using an energy source with an intermittent nature such as solar energy [23].

In this sense, the development of control and optimal operating strategies to be applied in real-time become essential. In Ref. [24] two control modes based on on/off controllers for the day and night were presented in simulation, trying to maintain the distillate production stable even in cloudy days. A neural network based controller that optimizes the distillate production under intermittent conditions was presented and experimentally tested in Ref. [25]. In spite of irradiance disturbances, a feedback control system with reference governor for fixing a suitable operating temperature at the inlet of the MD module was proposed and experimentally tested in Ref. [26]. Moreover, the work [7] experimentally demonstrated that the thermal energy demand of an MD module can be reduced in 1.21 kWh/m^3 by making an optimal management of the solar field powering it. In summary, the works presented above are fundamentally focused on the operation of the solar field, rejecting irradiance disturbances and maintaining desired temperature setpoints to maximize both, distillate production and thermal energy efficiency. However, not only the temperature affects the performance of MD modules but also the feed water flow rate [27]. The optimal management of this variable is especially relevant because a tradeoff solution must be adopted to maximize both thermal efficiency and distillate production in current commercial-scale MD modules [19,28], thus requiring properly formulated optimization problems.

In industrial-scale plants, the optimal operation of the feed water flow rate is even more critical. Due to the low production of current MD commercial modules (around 30 L/h in optimal operating conditions [18]), an industrial-scale plant must include multiple MD units. Accordingly, an optimal management of this variable can considerably reduce the Specific Thermal Energy Consumption (STEC) of the facility. To the best of the authors knowledge, only a previous work [29] deals with this problem. In that work, a distributed Model Predictive Control (MPC) approach was proposed aimed at reducing the STEC while assuring water needs. The tests performed in that work demonstrated how the distributed MPC controller can reduce by 5% the mean STEC of the operation. This percentage means a thermal energy saving of about 50 MWh per season in an application in which an MD industrial plant is combined with an 8 ha cultivation area. Nevertheless, it should be commented that the principal objective of that work was to demonstrate how an effective distributed MPC technique can manage the facility optimally when the water resources were limited and not all the MD modules could be fed at their optimal operating range. In this way, in the formulation of the control system, only continuous variables for the feed water flow rate (within its operating range 400—600 L/h) were considered.

Motivated by the above literature review, the main gaps observed in terms of MD operational strategies are the followings:

1. The real-time management methods proposed in the literature for Solar-powered MD (SMD) systems are focused on the heat generation circuit. The optimal operation of the feed water flow rate of the MD modules has hardly been addressed in these real-time methodologies, which can significantly improve the energy efficiency especially if the water demand is variable.
2. The developed methods are mainly applied to pilot-scale plants. In industrial plants, the presence of multiple MD modules totally alters the formulation of the problem, which has not been well discussed in the aforementioned literature.
3. The only published work that addresses the management of an industrial-scale plant uses only continuous variables in the optimization problem. With this formulation only the STEC can be minimized. If binary variables for turning on and off MD modules are introduced in the problem, the distillate production can be better adapted to the water demand.

In order to address the above issues, in the present work it is proposed a general optimal operating strategy for reducing the total thermal energy consumption of commercial-scale SMD plants connected to a consumer agent. The strategy is focused on the management of the desalination unit of the facility, as the optimal management of the solar field has been previously treated in the literature [7,25,26]. The contributions developed in this paper are the followings: firstly, conventional models used in MD systems are adapted to the Mixed Integer Programming (MIP) methodology. In this formulation, the binary variables are related to valve apertures that allows to turn on/off the MD units installed in the facility, whereas the continuous variables are related to the feed water flow rate of each MD module. Based on this model, a Mixed Integer Nonlinear Programming (MINLP) optimization problem is formulated, tasked with reducing both the STEC and the total thermal energy consumption, while assuring the water requirements. Secondly, it is proposed an efficient algorithm based on the Generalized Benders Decomposition (GBD) method [30] that enables the use of simpler optimization solvers, Mixed Integer Linear Programming (MILP) and Quadratic Programming (QP) methods rather than MINLP for solving the overall problem, which proved to reach optimal results more efficiently. This algorithm is then incorporated into an MPC controller [31] which reflects the operational strategy. Thirdly, to demonstrate the effectiveness of our proposal,

we present an exhaustive analysis by applying the developed technique in a practical case study, and comparing the obtained results to those obtained with a non-optimal management method (a manual operation) and with the ones obtained with the previous approach presented in Ref. [29]. This analysis evidences significant gains in relation to previous/manual approaches showing for example that for a sunny day, around the 65 and 55% of the thermal energy consumed by these operating methodologies can be saved, which can mean important contributions toward the commercialization of MD technology.

The rest of the paper is arranged as follows: Section 2 is dedicated to the description of the system and the optimization problem associated to the management of the facility. Section 3 is aimed at formulating the proposed operating strategy. Section 4 shows the performance of the management technique in a practical case study, and Section 5 summerizes the conclusion obtained from the results.

2. System description and problem formulation

2.1. System description

Fig. 1 shows a general schematic diagram of an SMD plant used for desalination purposes [4]. In this plant, a solar thermal field is used as thermal source. The outlet of the solar field is coupled to a storage tank that is used as buffer system for damping irradiance disturbances or storing the remaining thermal energy of the process. Then, a heat exchanger is employed to connect the MD modules and the heat generation circuit. As can be seen, the desalination unit is formed by an array of MD modules which are bonded in parallel according to Fig. 2. The feed water enters the MD unit, which uses the thermal energy transferred by the solar field to produce distillate and brine. In the process, the brine is rejected while the distillate is stored in the distillate tank. Finally, the water demand agent takes the required freshwater from this tank.

Regarding the operation of the MD modules, as illustrated in Fig. 2, the feed water is pumped by a main pipe to which all the MD modules are joined. The available valves (V_m in Fig. 2) allow to turn on/off each MD module. If a module is in operation, the feed water flows through the condenser channel. In this stage, the feed solution is preheated with the latent heat of condensation and with the sensible heat that crosses the membrane. Afterwards, the preheated solution is circulated to the heat exchanger where it is heated with the fluid coming from the solar field storage tank. Later, the hot solution flows through the evaporator channel where the volatile molecules are evaporated and pass through the membrane and the non-volatile ones are rejected in the form of brine. At the end, the volatile molecules are condensed and driven to the distillate tank. A more complete description of the process can be found elsewhere [10,18].

2.2. MD module modelling

As this work is focused on the management of the desalination unit, a model that accurately represents the behaviour of each of the MD modules contained in the unit must be used for the formulation of the problem. As was mentioned in the introduction section, most works presented in the literature use the RSM methodology as the modelling approach. This method provides linear or quadratic polynomial functions obtained from experimental data to fit the outputs of MD processes. In this work, we use the RSM models presented in Refs. [10,18,29]. By following these works, each subsystem m, i.e. each MD module included in the array, can be modelled according to Fig. 3. So, each subsystem m is characterized by:

- Input: feed water flow rate ($F_m(k) \in \Re_+$).
- Outputs: distillate production ($d_m(k) \in \Re_+$) and the temperature difference ($\Delta T_m(k) \in \Re_+$) between the outlet of the condenser channel ($T_{cout,m}$) and the inlet of the evaporator channel ($T_{ein,m}$) of the MD module. It should be remarked that this variable can be considered as the driving force of the process, which will be used to calculate the amount of thermal energy consumed by each MD module.
- Disturbances: inlet temperature of the condenser channel of the MD module ($T_{cin,m}(k) \in \Re_+$) and inlet temperature of the evaporator channel of the MD module ($T_{ein,m}(k) \in \Re_+$).

where p_i, with $i = 1, ..., 9$, are constant polynomial coefficients, and the rest of variables are defined in Appendix A.

$$d_m(k) = p_1 + p_2 \cdot T_{ein,m}(k) + p_3 \cdot T_{cin,m}(k) + p_4 \cdot F_m(k) + p_5 \cdot T_{ein,m}(k) \cdot F_m(k), \tag{1}$$

$$\Delta T_m(k) = p_6 + p_7 \cdot T_{ein,m}(k) + p_8 \cdot T_{cin,m}(k) + p_9 \cdot F_m(k), \tag{2}$$

$$d_m(k) = \alpha_{m,1}^d(k) \cdot \delta_m(k) + \alpha_{m,2}^d(k) \cdot F_m(k), \tag{3}$$

$$\Delta T_m(k) = \alpha_{m,1}^T(k) \cdot \delta_m(k) + \alpha_{m,2}^T(k) \cdot F_m(k), \tag{4}$$

where:

$$\alpha_{m,1}^d(k) = p_1 + p_2 \cdot T_{ein,m}(k) + p_3 \cdot T_{cin,m}(k), \tag{5}$$

$$\alpha_{m,2}^d(k) = p_4 + p_5 \cdot T_{ein,m}(k), \tag{6}$$
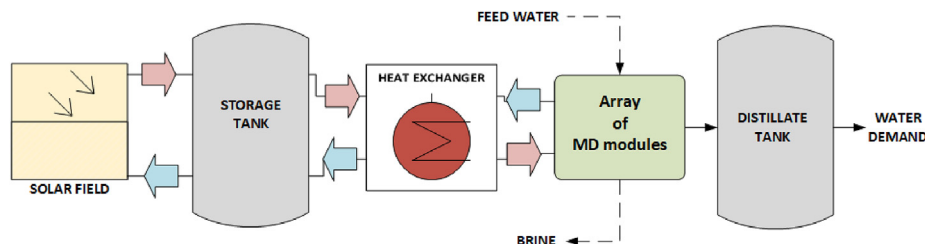
Fig. 1. Schematic diagram of an industrial-scale SMD plant.
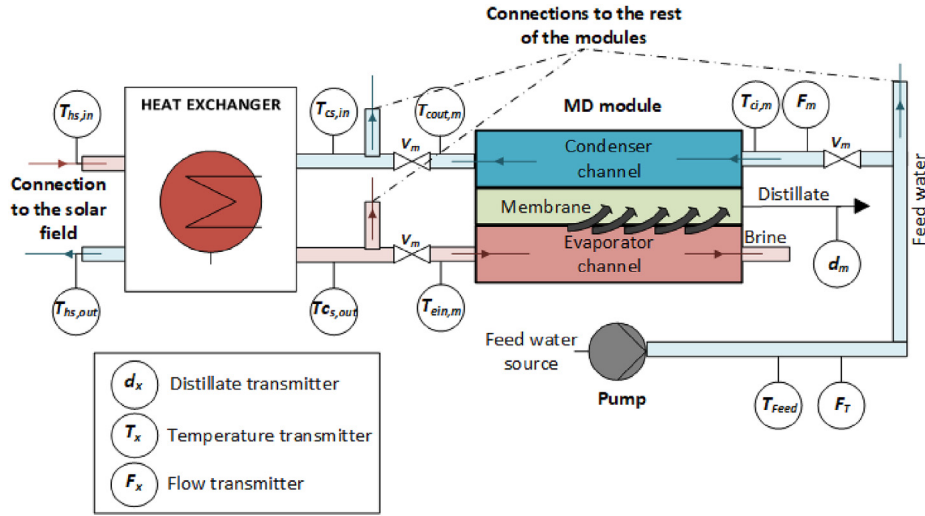
Fig. 2. Connection of a single MD module in the array of MD modules.
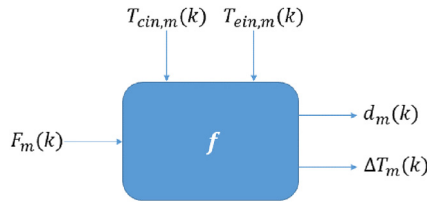
Fig. 3. Single MD module characterization. f denotes a linear function.

Note that k is related to the current time. Thus, following the ideas proposed in Refs. [10,18,29], the model of a single MD m-module can be written in a generic way as.

2.3. MIP modelling of the array of MD modules

To formulate the whole optimization problem, binary variables have been introduced in the model presented above. These variables are physically related to the valves located at the inputs and outputs of each MD module (V_m in Fig. 2). In this way, considering $\mathcal{M} = \{1, \ldots, m\}$ the set of MD modules in the array, the MIP model of the whole system can be written as, $\forall m \in \mathcal{M}$:

$$\alpha_{m,1}^{T}(k) = p_6 + p_7 \cdot T_{ein,m}(k) + p_8 \cdot T_{cin,m}(k), \tag{7}$$

$$\alpha_{m,2}^{T}(k) = p_9, \tag{8}$$

$$\delta_m(k) \in \{0, 1\}, \tag{9}$$

$$\delta_m(k) \cdot F_m^{Min} \leq F_m(k) \leq \delta_m(k) \cdot F_m^{Max}, \tag{10}$$

F_m^{Min} and F_m^{Max} are the minimum and maximum feed flow rate allowed of each MD module respectively, and δ_m denotes the binary variable related to the valve of MD m-module, which assumes value 1 if the valve is open and 0 otherwise.

In addition, it must be remarked that all the subsystems are coupled by the total distillate production, $d_T(k)$, and by the total water flow rate income $F_T(k)$, which is:

$$\sum_{m \in \mathcal{M}} d_m(k) = d_T(k), \tag{11}$$

$$\sum_{m \in \mathcal{M}} F_m(k) = F_T(k), \tag{12}$$

$$F_T^{Min} \leq F_T(k) \leq F_T^{Max}, \tag{13}$$

where F_T^{Min} and F_T^{Max} are the minimum and maximum flow rate provided by the feed water pump.

2.4. Optimization problem formulation

The main objective of the optimization problem is to minimize the total thermal energy consumption of the facility while assuring the water demand. To achieve this, the manipulated variables available in the real facility are the aperture of the V_m valve ($\delta_m(k)$) and the feed water flow rate ($F_m(k)$) of each MD module. Thus, to formulate the optimization problem, three main things must be considered.

First, the total distillate production must be equal or higher than the water demand, what can be directly included in the optimization problem as a constraint. Nevertheless, as shown in Fig. 1, there is a storage tank available between the consumer and the producer agent. So, the production constraint can be formulated according to the water level of the tank. Note that, the behaviour of this element is like an integrator which allows to filter the water demand, thus smoothing the production constraint.

Second, the total thermal energy consumption of the desalination unit can be directly reduced by turning on as few modules as possible at each moment. This can be achieve by optimally managing the binary variables according to the operating water needs.

Third, when a module is turned on, the total thermal energy it consumes can be reduced by improving its thermal efficiency. In MD processes, one of the most widely used metrics to estimate the thermal efficiency is the STEC [4,10,18]. The STEC is defined as the amount of thermal energy required to produce a volume unit of distillate (kWh/m^3). For a single m-module, it can be calculated as follows:

$$S_m(k) = \frac{c_1 \cdot F_m(k) \cdot \Delta T_m(k)}{d_m(k)}, \tag{14}$$

$$c_1 = \frac{\rho \cdot c_p}{c_f}, \tag{15}$$

where $S_m(k)$ is the STEC of MD m-module, and the rest of variables and constants are defined in Appendix A. It should be noted that to maximize the distillate production (to meet the water needs) and to minimize the STEC in current commercial MD modules, the maximun and minimum feed flow rate must be applied respectively [29]. Thus, the operation of the feed flow rate of each MD module is not trivial, and a tradeoff solution must be taken at each sample time depending on the operating conditions.

According to the above issues, the optimization problem can be formulated as:

$$\min \sum_{m \in \mathcal{M}} \frac{c_1 \cdot F_m(k) \cdot \Delta T_m(k)}{d_m(k)}, \tag{16}$$

subject to, $\forall m \in \mathcal{M}$:

$$d_m(k) = \alpha_{m,1}^d(k) \cdot \delta_m(k) + \alpha_{m,2}^d(k) \cdot F_m(k) + c_2 \cdot (1 - \delta_m(k)), \tag{17}$$

$$\Delta T_m(k) = \alpha_{m,1}^T(k) \cdot \delta_m(k) + \alpha_{m,2}^T(k) \cdot F_m(k), \tag{18}$$

$$\delta_m(k) \cdot F_m^{Min} - F_m(k) \leq 0, \tag{19}$$

$$F_m(k) - \delta_m(k) \cdot F_m^{Max} \leq 0, \tag{20}$$

$$\delta_m(k) \in \{0, 1\}, \tag{21}$$

and the constraints that couple all the MD modules and the consumer and producer agent:

$$\sum_{m \in \mathcal{M}} F_m(k) = F_T(k), \tag{22}$$

$$F_T^{Min} \leq F_T(k) \leq F_T^{Max}, \tag{23}$$

$$\sum_{m \in \mathcal{M}} d_m(k) = d_T(k), \tag{24}$$

$$(d_T(k) - D(k)) \cdot c_3 + L_T(k-1) \geq L^* \tag{25}$$

$$L_T^{Min} \leq L_T(k) \geq L_T^{Max} \tag{26}$$

where c_2 is a large number (i.e., 10_6) used to avoid division by zero in Eq. (16), $D(k)$ is the water demand of the consumer agent, c_3 is the conversion factor, $L_T(k)$ is the water level of the distillate tank, L_T^{Min} and L_T^{Max} are the maximum and minimum level of the tank, and L^* is the setpoint water level of the distillate tank. Note that all the units and description of the variables are available in Appendix A.

In the formulation of the optimization problem, the objective function, Eq. (16), is focused on minimizing the sum of the STEC of each MD module. The summation term allows to minimize the total thermal energy consumption of the whole system, while the STEC calculation allows to enhance the thermal efficiency of the modules turned on at each sampling time. The constraints in Eqs. 17–24 define the model of the system and the physical limits of the manipulated variables. Eq. (25) is related to the production needs, which have been introduced in the problem according to the water level of the distillate tank, as was explained before. Finally, it should be remarked that the disturbances and water demand are known,

and therefore, they are fixed in the optimization problem.

Note that, the formulated problem is an MINLP problem due to the nonlinearity of the objective function Eq. (16), and the presence of binary and continuous variables. Regarding the feasibility of the problem, the only constraint that can turn the problem infeasible is Eq. (25). However, as long as the desalination unit and the solar field powering it are well sized according to the water needs the problem will be feasible. In addition, the tank level setpoint can be adapted to the plant operation in the starting of the operation, if the tank starts with level zero. Nevertheless, smoothing techniques could also be applied in this constraint such as the use of slack variables if necessary.

It should be also remarked that the boundary conditions of the problem mainly change according to the operating temperature (temperature at the inlet of the evaporator channel of the MD modules), which depends on solar irradiance. Therefore, the problem must be solved in real time to achieve an optimal operation. However, the nonlinearity of the problem requires a high computational power which prevents the problem from being solved quickly by using MINLP solvers, especially when the number of agents in the array of MD modules is large. Therefore, in the following section we propose an efficient algorithm based on the GBD method for solving this problem.

3. The GBD-based MPC operating strategy

In this section the GBD and the MPC methods are introduced. Then, the MINLP problem presented in the previous section is formulated according to these two methodologies.

3.1. Benders decomposition method

Considering a generic MINLP problem:

$$[x, y]\min f(x, y). \tag{27}$$

$$\text{s.t.} \quad h(x, y) = 0, \tag{28}$$

$$g(x, y) \leq 0, \tag{29}$$

$$x \in \mathbf{X} \subseteq \mathfrak{R}^{n_x}, \tag{30}$$

$$y \in \mathbf{Y}^{n_y} = \{0, 1\}, \tag{31}$$

the basic idea of the GBD method [30] consists on solving this problem on a iterative way, computing at each iteration an upper and a lower bound in the solution space of the MINLP model. These bounds are obtained by decomposing the overall MINLP problem into two problems: the *master* problem which provides the lower bound, and the *primal* problem which provides the upper bound.

The *primal* problem corresponds to the problem defined in Eqs. 27–31 with the y-variables fixed in a particular solution 0–1, which is denoted by y^l, being l the iteration counter:

$$[x, y]\min f(x, y^l). \tag{32}$$

$$\text{s.t.} \quad h(x, y^l) = 0, \tag{33}$$

$$g(x, y^l) \leq 0, \tag{34}$$

$$x \in \boldsymbol{X} \subseteq \Re^{n_x}. \tag{35}$$

Remark 3.1. *Note that the solution of this primal problem is the global solution for problem (27)-(31).*

At this point, two different cases can be distinguished: feasible *primal*, and infeasible *primal*. If the solution of the *primal* problem is feasible at iteration l, it provides information of: i) the value of x^l, ii) the value of the upper bound, which is the value of $f(x^l,y^l)$, and iii) the value of the optimal Lagrange multipliers vectors λ^l and μ^l related to the set of equality ($\boldsymbol{h}$) and inequality ($\boldsymbol{g}$) constraints respectively. The aforementioned information allows us to formulate the following Lagrange function, which is called the optimallity cut:

$$L^l\left(x, y, \lambda^l, \mu^l\right) = f(x,y) + \lambda^{lT}\boldsymbol{h}(x,y) + \mu^{lT}\boldsymbol{g}(x,y). \tag{36}$$

On the other hand, if the solution of the *primal* problem at iteration l is infeasible, only the constraints of the *primal* problem are considered, and the following optimization problem is formulated in order to identify a feasible solution:

$$\min_{x,\gamma} \gamma \tag{37}$$

$$\text{s.t.} \quad h\left(x, y^l\right) = 0, \tag{38}$$

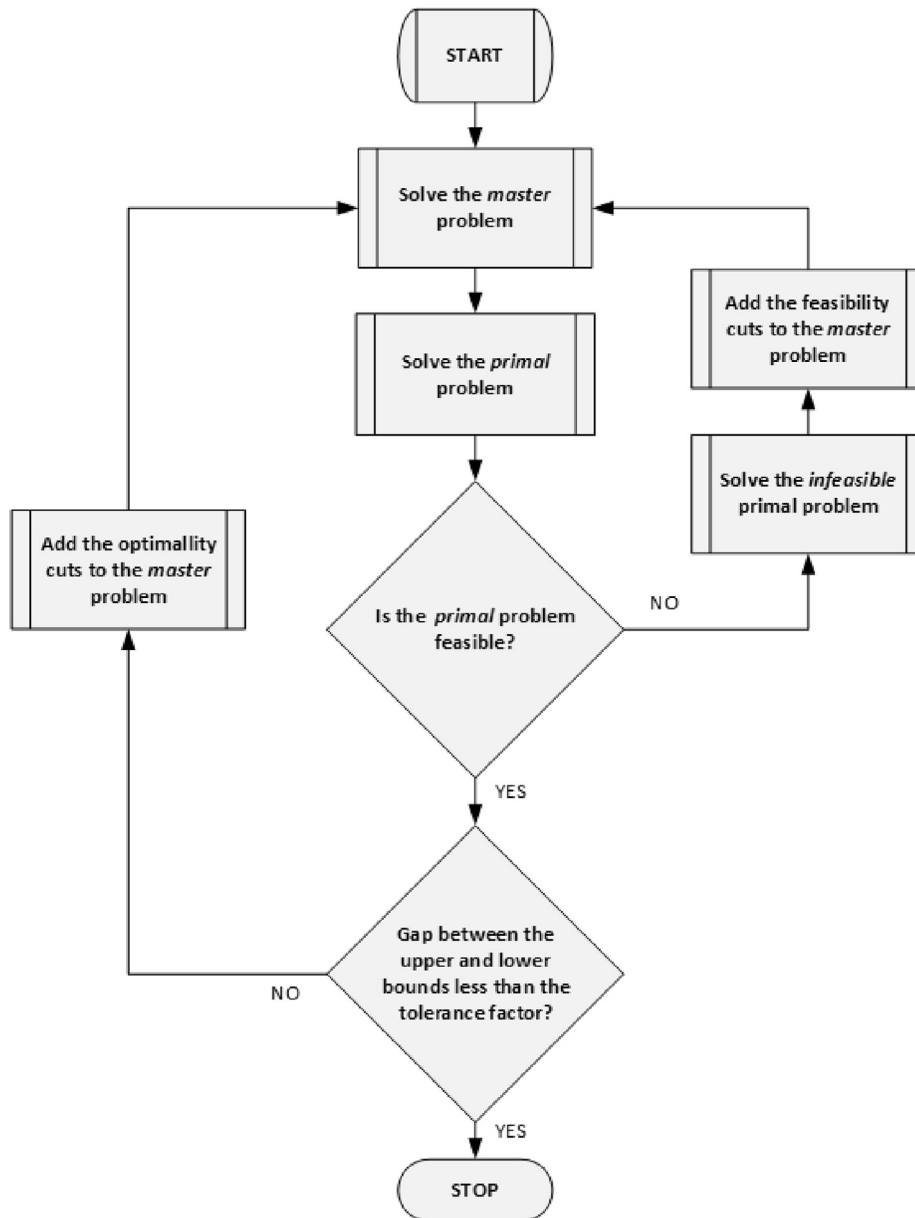$$\boldsymbol{g}\left(x, y^l\right) \leq \gamma^l, \tag{39}$$

Fig. 4. GBD algorithm.

$$\gamma \geq 0, \tag{40}$$

$$x \in \mathbf{X}. \tag{41}$$

The solution of this problem provides information about the Lagrange multipliers related to the equality and inequality constraints, which are denoted in this case as $\overline{\lambda}^l$ and $\overline{\mu}^l$ respectively. These multipliers allows us to formulate the feasibility cut as:

$$\overline{L}^l\left(x, y, \overline{\lambda}^l, \overline{\mu}^l\right) = \overline{\lambda}^{lT} \mathbf{h}(x, y) + \overline{\mu}^{lT} \mathbf{g}(x, y). \tag{42}$$

Remark 3.2. It should be noted that at each iteration only one cut is generated, depending if the *primal* problem is feasible or infeasible. In addition, the upper bound is generated only if the *primal* problem is feasible.

The *master* problem is defined according to the duality theory being based on the projection of the overall MINLP problem in the y-space (see Ref. [30] for more details):

$$[y, \mu_0]\min \mu_0 \tag{43}$$

$$\text{s.t.} \quad \mu_0 \geq L^{l^1}\left(x^{l^1}, y, \lambda^{l^1}, \mu^{l^1}\right) \ l^1 = 1, \ldots, L^1, \tag{44}$$

$$0 \geq \overline{L}^{l^2}\left(x^{l^2}, y, \overline{\lambda}^{l^2}, \overline{\mu}^{l^2}\right) \ l^2 = 1, \ldots, L^2, \tag{45}$$

where L^1 and L^2 are the last iteration counters at which the optimality and feasibility cuts were updated.

Remark 3.3. *The master problem is equivalent to the MINLP (27)-(31). Also, the value of the variable μ_0 is the value of the lower bound.*

The whole algorithm is solved on an iterative way according to the flow-chart presented in Fig. 4. The iterations terminate when the gap between the upper and the lower bound is lower than a given tolerance factor, which is, $UB \leq LB + \varepsilon$, where UB and LB are the upper and lower bounds respectively and ε is a tolerance factor.

3.2. Model Predictive Control

The MPC strategy is one of the most widespread control methodologies used in both industry and academia. The MPC is not an explicit control technique, but rather comprises a wide range of control methods based on the use of a model of the system for obtaining the control actions by minimizing an objective function [31]. Specifically, the procedure used in MPC controllers is given by (see Fig. 5):

1. The outputs of the process for a given prediction horizon N, are predicted at each time k by using a model of the system. The predicted outputs, denoted by $\hat{z}(k+j|k)$ for $j = 1, \ldots, N$, depend on past outputs, inputs and disturbances, and on the value of future control actions $u(k+j-1|k)$ for $j = 1, \ldots, N$. Note that the notation $(k+j|k)$ is related to the predicted value of a variable at the instant time $k + j$, calculated with the information available at instant k.
2. The set of future control actions is calculated by minimizing a determined objective function.
3. The control action $u(k|k)$ is sent to the system while the rest of control signals are rejected because at the next sampling time, $\hat{z}(k+1)$ will be known, allowing to repeat the first step with the
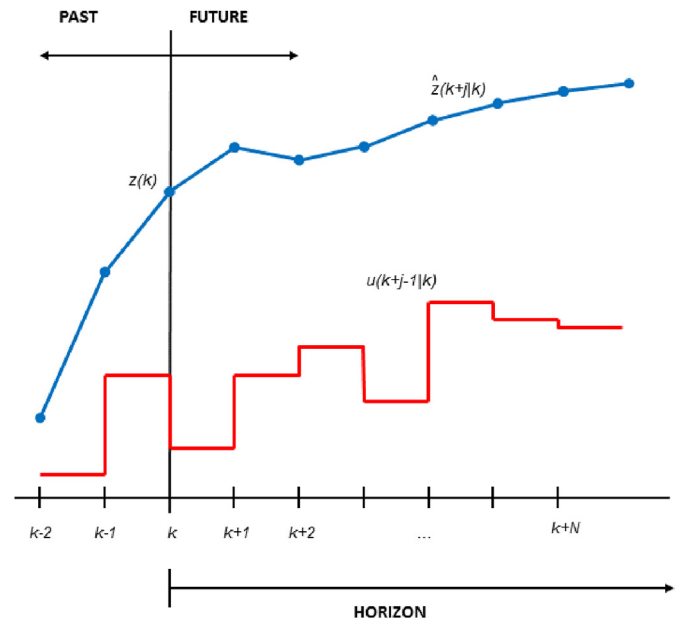
Fig. 5. MPC strategy.

updated information. This methodology is known as the receding horizon concept.

It should be remarked that, the application of the MPC technique in the problem concerning this work is specially suitable due to the presence of the distillate tank. This method allows us to predict the level of the tank taking into account future water demands, and therefore, to induce the optimal management and high performance of the desalination plant.

3.3. The GBD-based MPC algorithm

Once both techniques have been introduced, the decomposition of the overall MINLP problem (see Eqs. 16–25) is formulated according to them. It should be pointed out that the problem treated in this work has the same structure of the generic problem presented in Section 3.1, with a set of binary, δ_m, $\forall m \in \mathcal{M}$, and continuous variables, F_m, $\forall m \in \mathcal{M}$. Therefore, the *primal* problem will be the projection of the overall MINLP problem in the F_m-space, while the *master* problem will be the projection of the problem in the δ_m-space.

It should be also taken into account that the variables $\alpha_{m,1}^d$, $\alpha_{m,2}^d$, $\alpha_{m,1}^T$ and $\alpha_{m,2}^T$ can be predicted along the prediction horizon, as they depend on the measurable temperatures (see Section 2.3).

Thus, the feasible *primal* problem can cast:

$$\min \sum_{j=1}^{N} \sum_{m \in \mathcal{M}} \frac{c_1 \cdot F_m(k+j-1|k) \cdot \Delta \widehat{T}_m(k+j|k)}{\widetilde{d}_m^l(k+j-1|k)}, \tag{46}$$

subject to, $\forall m \in \mathcal{M}$ and $j = 1, \ldots, N$:

$$\widetilde{d_m}(k+j|k) = \widehat{\alpha}_{m,1}^d(k+j|k) \cdot \delta_m^l(k+j-1|k) \\ + \widehat{\alpha}_{m,2}^d(k+j|k) \cdot F_m(k+j-1|k), \tag{47}$$

$$\widetilde{d}_m^l(k+j-1|k) = \widetilde{d}_m^{l-1}(k|k) + c_2 \cdot \left(1 - \delta_m^l(k+j-1|k)\right), \tag{48}$$

$$\Delta \widehat{T}_m(k+j|k) = \widehat{\alpha}_{m,1}^T(k+j|k) \cdot \delta_m^l(k+j-1|k) + \widehat{\alpha}_{m,2}^T(k+j|k) \cdot F_m(k+j-1|k), \tag{49}$$

$$\delta_m^l\left(k+j-1|k\right) \cdot F_m^{Min} - F_m(k+j-1|k) \leq 0, \tag{50}$$

$$F_m\left(k+j-1|k\right) - \delta_m^l(k+j-1|k) \cdot F_m^{Max} \leq 0, \tag{51}$$

$$F_T^{Min} \leq F_T(k+j-1|k) \leq F_T^{Max}, \tag{52}$$

$$(\widehat{d_T}(k+j|k) - \widehat{D}(k+j|k)) \cdot c_3 + \widehat{L_T}(k+j-1|k) \geq L^*, \tag{53}$$

$$L_T^{Min} \leq L_T(k+j|k) \geq L_T^{Max} \tag{54}$$

and

$$\sum_{j=1}^{N} \sum_{m \in \mathscr{M}} F_m(k+j-1|k) = F_T(k+j-1|k), \tag{55}$$

$$\sum_{j=1}^{N} \sum_{m \in \mathscr{M}} \widehat{d_m}(k+j|k) = \widehat{d_T}(k+j|k). \tag{56}$$

As can be seen, for the calculation of the STEC in Eq. (46), an estimation of the distillate production, $\widetilde{d_m^l}$, is used instead of the actual distillate production, $\widehat{d_m}(k+j|k)$. One should highlight that the objective function of the overall MINLP problem, Eq. (16), can be rewritten as follows, by combining it with Eq. (18):

$$\min \sum_{m \in \mathscr{M}} \frac{c_1 \cdot F_m(k) \cdot \alpha_{m,1}^T(k) \cdot \delta(k)}{d_m(k)} + \sum_{m \in \mathscr{M}} \frac{c_1 \cdot \alpha_{m,2}^T(k) \cdot F_m(k)^2}{d_m(k)}, \tag{57}$$

where for $d_m(k) > 0$, the right part of the equation is convex whereas the left part is quasi-convex. The estimation of the distillate production allows us to eliminate this quasi-convex part in the objective function, rendering the objective function convex. Note that, the estimation is updated at each iteration of the algorithm as shown in Eq. (48), where $\widetilde{d_m}^{l-1}(k|k)$ is the value of $\widehat{d_m}(k|k)$ calculated in the previous iteration $l-1$. In this way, in the last iterations, $\widetilde{d_m^l}$ reaches a static value which is the optimum or very close to the optimum, ensuring the stability of the solution. In addition, by using the estimation, Eq. (46) can be formulated as:

$$\min \sum_{j=1}^{N} \sum_{m \in \mathscr{M}} \frac{c_1 \cdot F_m(k+j-1|k) \cdot \widehat{\alpha}_{m,1}^T(k+j|k) \cdot \delta_m^l(k+j-1|k)}{\widetilde{d_m}^l(k+j-1|k)} + \sum_{j=1}^{N} \sum_{m \in \mathscr{M}} \frac{c_1 \cdot \widehat{\alpha}_{m,2}^T(k+j|k) \cdot F_m(k+j-1|k)^2}{\widetilde{d_m}^l(k+j-1|k)}, \tag{58}$$

where all the parameters involved in the equation are constants, except $F_m(k+j-1|k)$, what enables the problem to be solved with a simple QP solver.

The infeasible *primal* problem can be formulated as:

$$\min \sum_{j=1}^{N} \gamma(k+j), \tag{59}$$

subject to, $\forall m \in \mathscr{M}$ and for $j = 1, ..., N$:

$$\widehat{d_m}(k+j|k) - \left[\widehat{\alpha}_{m,1}^d(k+j|k) \cdot \delta_m^l(k+j-1|k) \quad \widehat{\alpha}_{m,2}^d\left(k+j|k\right) \cdot F_m(k+j-1|k)\right)\right] - \gamma(k+j) \leq 0, \tag{60}$$

$$-\widehat{d_m}\left(k+j|k\right) + \left[\times \left(\widehat{\alpha}_{m,1}^d\left(k+j|k\right) \cdot \delta_m^l\left(k+j-1|k\right) + \widehat{\alpha}_{m,2}^d(k+j|k) \cdot F_m(k+j-1|k) \times \right] - \gamma(k+j) \leq 0, \tag{61}$$

$$\delta_m^l\left(k+j-1|k\right) \cdot F_m^{Min} - F_m(k+j-1|k) - \gamma(k+j) \leq 0, \tag{62}$$

$$F_m\left(k+j-1|k\right) - \delta_m^l(k+j-1|k) \cdot F_m^{Max} - \gamma(k+j) \leq 0, \tag{63}$$

$$F_T^{Min} - F_T(k+j-1|k) - \gamma(k+j) \leq 0, \tag{64}$$

$$F_T(k+j-1|k) - F_T^{Max} - \gamma(k+j) \leq 0, \tag{65}$$

$$L^* - [(\widehat{d_T}(k+j|k) - \widehat{D}(k+j|k)) \cdot c_3 + \widehat{L_T}(k+j-1|k)] - \gamma(k+j) \leq 0, \tag{66}$$

$$L_T^{Min} - L_T(k+j-1|k) - \gamma(k+j) \leq 0, \tag{67}$$

$$L_T(k+j-1|k) - L_T^{Max} - \gamma(k+j) \leq 0, \tag{68}$$

and

$$\sum_{j=1}^{N} \sum_{m \in \mathscr{M}} F_m(k+j-1|k) - F_T(k+j-1|k) - \gamma(k+j) \leq 0, \tag{69}$$

$$F_T\left(k+j-1|k\right) - \sum_{j=1}^{N} \sum_{m \in \mathscr{M}} F_m(k+j-1|k) - \gamma(k+j) \leq 0, \tag{70}$$

$$\sum_{j=1}^{N} \sum_{m \in \mathscr{M}} \widehat{d_m}(k+j|k) - \widehat{d_T}(k+j|k) - \gamma(k+j) \leq 0, \tag{71}$$

$$\widehat{d_T}\left(k+j|k\right) - \sum_{j=1}^{N} \sum_{m \in \mathscr{M}} \widehat{d_m}(k+j|k) - \gamma(k+j) \leq 0. \tag{72}$$

This problem is proposed only with the constraints of the feasible *primal* problem according to the GBD theory. Also, the equality constraints have been rewritten as inequality constraints for the sake of simplicity in the implementation of the method. It is worth noting that, this optimization problem can be worked out with an LP solver.

Finally, the *master* problem is written as:

$$\min \sum_{j=1}^{N} \mu_0(k+j), \tag{73}$$

subject to, $\forall j = 1...N$, $l^1 = 1,...,L^1$, and $l^2 = 1,...,L^2$

$$\mu_0(k+j) \geq \sum_{m \in M} \lambda_{1,m}^{l^1}(k+j) \cdot \left[F_m^{l^1}(k+j-1|k) - \delta_m(k+j-1|k) \cdot F_m^{Max} \right] +$$

$$\sum_{m \in M} \lambda_{2,m}^{l^1}(k+j) \cdot \left[\delta_m \left(k+j-1|k \right) \cdot F_m^{Min} - F_m^{l^1}(k+j-1|k) \right] +$$

$$J_{primal}^{l^1}(k+j|k), \tag{74}$$

$$0 \geq \sum_{m \in M} \overline{\lambda}_{1,m}^{l^2}\left(k+j\right) \cdot \left[\hat{d}_m^{l^2}\left(k+j \middle| k\right) - \left(\hat{\alpha}_{m,1}^{d}\left(k+j \middle| k\right) \right. \right.$$

$$\left. \cdot \delta_m\left(k+j-1 \middle| k\right) + \right.$$

$$\hat{\alpha}_{m,2}^{d}\left(k+j \middle| k\right) \cdot F_m^{l^2}\left(k+j-1 \middle| k\right) \right)$$

$$\times \Bigg] + \sum_{m \in M} \overline{\lambda}_{2,m}^{l^2}\left(k+j\right) \cdot \left[-\hat{d}_m^{l^2}\left(k+j \middle| k\right) + \right.$$

$$\left. \left(\hat{\alpha}_{m,1}^{d}(k+j|k) \cdot \delta_m(k+j-1|k) + \hat{\alpha}_{m,2}^{d}\left(k+j \middle| k\right) \cdot F_m^{l^2}(k+j-1|k) \right) \right] +$$

$$\sum_{m \in M} \overline{\lambda}_{3,m}^{l^2}(k+j) \cdot \left[F_m^{l^2}(k+j-1|k) - \delta_m(k+j-1|k) \cdot F_m^{Max} \right] +$$

$$\sum_{m \in M} \overline{\lambda}_{4,m}^{l^2}(k+j) \cdot \left[\delta_m \left(k+j-1|k \right) \cdot F_m^{Min} - F_m^{l^2}(k+j-1|k) \right], \tag{75}$$

where $J_{primal}^{l^1}(k+j|k)$ is the value of the objective function of the feasible *primal* problem, $\lambda_{1,m}^{l^1}(k+j)$ and $\lambda_{2,m}^{l^1}(k+j)$ are the Lagrange multipliers of the constraints Eqs. (50) and (51) at iteration l^1, obtained from the solution of the feasible *primal* problem, and $\overline{\lambda}_{1,m}^{l^2}(k+j)$, $\overline{\lambda}_{2,m}^{l^2}(k+j)$, $\overline{\lambda}_{3,m}^{l^2}(k+j)$ and $\overline{\lambda}_{4,m}^{l^2}(k+j)$ are the ones related to Eqs. (60)—(63) obtained from the solution of the infeasible *primal* problem at iteration l^2. Observe also that Eq. (74) is related with the optimallity cuts and Eq. (75) with the feasibility ones. It should be also remarked that this problem is an MILP problem that can be worked out with a suitable algorithm.

The algorithm is solved according to the resolution method presented in Fig. 4. In addition, Fig. 6 shows the variables shared between problems at each iteration. Note that, the prediction of
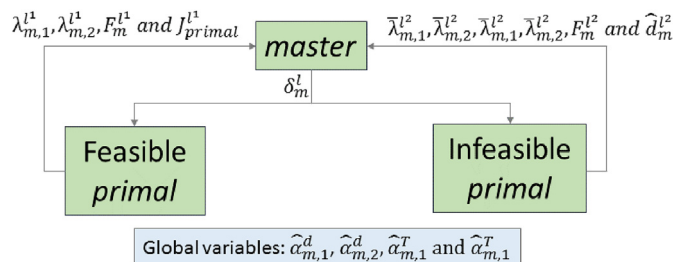

Fig. 6. Information shared between problems. The variables shared are $\forall m \in \mathcal{M}$. Observe that the MPC nomenclature has not been included in the figure for the sake of simplicity.

variables $\hat{\alpha}_{m,1}^{d}$, $\hat{\alpha}_{m,2}^{d}$, $\hat{\alpha}_{m,1}^{T}$ and $\hat{\alpha}_{m,2}^{T}$ is global information, and, therefore, it is known for all the problems.

4. Results and discussion

4.1. Case study

The case study adopted in this work is based on two real facilities located in Almería (southeast Spain). On the one hand, for the desalination unit, the SMD facility of the Plataforma Solar de Almería (PSA, www.psa.es) was used as reference [4]. Among the different commercial MD modules useable at PSA, the Aquastill unit and the Solar Spring one were chosen (see Fig. 7) to be part of the array of MD modules. These two modules were selected since they have different behaviours in terms of distillate production and thermal efficiency, what adds complexity to the problem. The Aquastill module has a lower thermal energy consumption and a higher distillate production than the Solar Spring one, as was stated in Ref. [29]. One should bear in mind that the models of these two modules were already presented and validated in literature in Ref. [10,18] for the Solar Spring and Aquastill module respectively. These models can be formulated according to the generic method described in Section 2.2 and 2.3. Table 1 presents the value of the polynomial coefficients of the RSM models of each MD module.

On the other hand, a greenhouse was selected as consumer agent. Note that the combination of greenhouses and SMD plants is a potential industrial application of MD technology [29], and of thermal powered desalination technologies in general [32]. Besides, a greenhouse presents a variable water demand according to the meteorological conditions [32], which makes the use of optimal management techniques in the desalination unit essential. In this way, a multi-span "Almeria-type" greenhouse (see Fig. 8) located at the Experimental Station of the Cajamar Foundation (also in the southeast of Spain) was employed in the simulations. The dynamical model of the greenhouse, the validation of the model, and a detailed description of the greenhouse environment were presented in [33]. Note that in this model, the water demand is decided according to the crop transpiration flux, which relates to the amount of water lost by the plants during the transpiration process and must be recovered by irrigation.

4.2. Simulation set-up

The simulations were performed following the scheme deployed in Fig. 9. As can be observed, the real facility in the simulation loop was composed by the model of the array of MD modules, the model of the heat exchanger connecting the solar field and the desalination unit, and the model of the greenhouse. Note that, for these two last elements, the same models from Ref. [29] were employed. Also, in the simulations, the array of MD modules was composed by the same number of Solar Spring and Aquastill modules, placing the Solar Spring modules in the odd numbers of the array and the Aquastill modules in the even ones. In addition, the maximum and minimum feed flow rate (F_m^{Min} and F_m^{Max}) of each MD module was stated as 400 and 600 L/h respectively, in accordance with the operating range of these commercial MD modules (see Ref. [10,18] for more details). The minimum range of the feed water pump (F_T^{Min}) was fixed at zero and the maximum (F_T^{Max}) at $N_m \cdot 600$, where N_m is the number of MD modules in the array.

It should be highlighted that, real data were used to feed the models mentioned above, what adds reliability to the simulations. In order to simplify the simulation loop, a temperature profile at the entrance of the heat exchanger was used ($T_{hs,in}$ in Fig. 9) instead of including the complete heat generation model. These profiles were obtained by simulating the complete model of the heat generation

Fig. 7. Commercial MD modules at PSA. From left to right: Solar Spring and Aquastill modules.

Table 1
Polynomial coefficients of the RSM models of the Aquastill and Solar Spring modules.

Coefficient	Module	
	Aquastill	Solar Spring
p_1 (L/h)	3.24	−10.88
p_2 (L/(h·°C))	0.072	0.24
p_3 (L/(h·°C))	−0.4896	−0.18
p_4 (−)	−0.024	−0.01
p_5 (1/°C)	0.0096	0.0006
p_6 (°C)	−0.739	−0.2018
p_7 (−)	0.078	0.1385
p_8 (−)	−0.067	−0.158
p_9 (h/(L·°C))	0.0019	0.0049

circuit (which was presented in Ref. [26]) with real meteorological data, similar to the ones used as input of the greenhouse model, and with the operational strategy presented in Ref. [7]. The model of the greenhouse was directly fed with real meteorological data (see Fig. 9), which were obtained from Experimental Station of the Cajamar Foundation. It should be remarked that, in the prediction model of the MPC strategy, the meteorological conditions as well as

inlet temperature at the hot side of the heat exchanger ($T_{hs,in}$) were maintained constant along the prediction horizon. Also, the feed temperature (T_{feed}) was fixed at 20 °C (average temperature of the Mediterranean sea).

In the simulation loop, the MPC controller received the states from the different models comprising the real simulating facility, and sent the corresponding control action $\boldsymbol{u}$ (i.e., δ_m and F_m, $\forall m \in \mathcal{M}$) to the array of MD modules at each sampling time. The sampling time of the system was established in 10 min according to the representative time constant of the greenhouse water demand and the desired closed loop behaviour [29].

All the simulations were performed using MATLAB code [34] (MATLAB version 2018a) running on a PC with an Intel Core i5-6500T CPU 2.50 GHz with 8 GB of RAM. Moreover, it should be noted that the overall MINLP problem was solved with the BARON solver (version 1.88) [35], whereas the optimization problems of the GBD method were solved with the CPLEX solver [36] (version 12.6.1).

4.3. Study of efficiency of the proposed algorithm

One of the main benefits of the developed management method is that simpler optimization problems, such as QP, LP and MILP, are

Fig. 8. Greenhouse environment. From left to right and from top to bottom: the greenhouse, the dropper and the tomato crop lines.
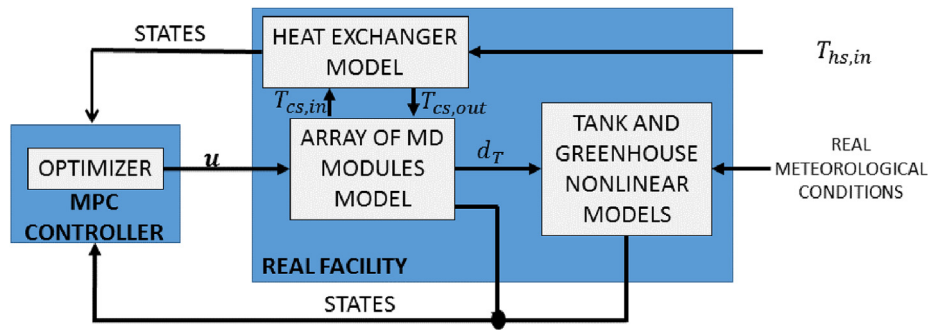
Fig. 9. Simulation scheme.

Table 2
Results reached with each resolution method when increasing the number of MD modules in the array. V-obj is the value of the objective function.

Number of MD units	GBD algorithm		MINLP algorithm	
	Time	V-obj	Time	V-obj
	[s]	[kWh/m₃]	[s]	[kWh/m₃]
4	0.29	112.25	1.50	112.25
8	0.29	112.30	1.60	112.28
16	0.30	224.50	3.77	224.50
32	1.56	382.40	102.23	382.06
64	5.67	455.20	1619.72	451.55

Fig. 10. Results reached with each resolution method when increasing the number of MD modules in the array.

solved instead of an overall MINLP one. This fact directly influences the time spent in reaching an optimal solution of the problem. So that, in this section, the GBD based method and MINLP solver are analyzed in terms of computational time. To do this, several simulations were carried out, increasing the number of agents (i.e., the number of MD modules in the array). The time spent by each resolution method to work out the overall MINLP problem in a single sampling time was measured.

Table 2 summerizes the results of the different simulations and Fig. 10 graphically represents these results. As can be observed, five cases were simulated, with 4, 8, 16, 32 and 64 MD modules. For the two first cases, in which the number of MD modules was small, both algorithms solved the problem quickly, reaching the same value in the objective function. In the third case, the time required by the MINLP solver was doubled in comparison with the two first cases, whereas the one of the GBD based approach remained almost constant. In the two last cases, the time spent by the MINLP solver increased exponentially (see Fig. 10). Note that with 64 MD modules, the time spent by the MINLP solver is much longer than the system's sampling time (600 s). This fact means that the MINLP solver cannot be used when considering a plant equal or larger than that size. It is worth noting that, this also happens when using the MPC strategy with long prediction horizons, since for the purpose of the optimization problem, it has the same effect as using a large number of MD modules in the array.

Finally, it should be remarked that the GBD algorithm reached almost the same values that the global MINLP solver in the objective function (see Table 2), which indicates convergence to optimal solutions. The slight differences are due to the value chosen for $\varepsilon = 0.5$. This value was taken considering the trade-off between resolution time and accuracy. Nevertheless, it should be remarked that the aforementioned differences are not representative in comparison to the magnitude of the objective function.
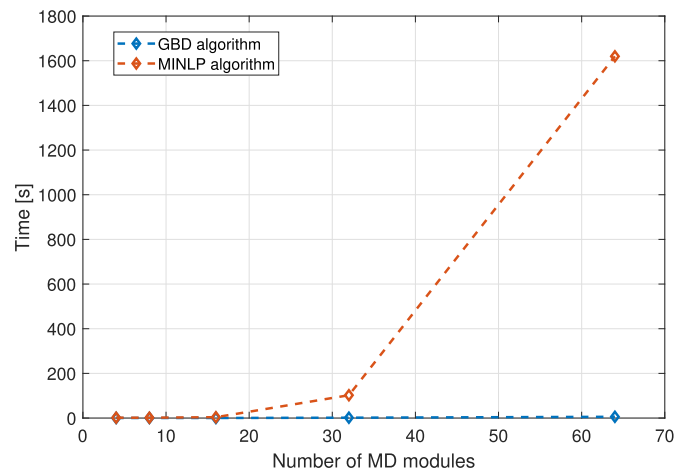
4.4. Simulation study

To assess the running of the proposed algorithm during a daily operation of the facility, different tests were executed with several values of the prediction horizon N. For these tests, the desalination unit was configured with four MD modules, and the greenhouse with a size of 308 m², as in the tests performed in Ref. [29]. It should be highlighted that, this small scale plant was chosen for being representative of the system and allowing to visualize the results on a easy way. Besides, the tests were performed with meteorological data from the Experimental Station of the Cajamar Foundation on the day of June 6th, 2017. It should be also remarked that, as the array of modules included identical modules (i.e., two of Aquastill and two of Solar Spring), a term in the objective function was added to prevent chattering problems in the switching on and off of the modules between one sampling time and the next. The term added to the *primal* and *master* problems consisted of $\sum_{m \in \mathscr{M}} (\delta_m(k+j-1|k) - \delta_m(k+j-2|k))^2$.

Figs. 11 and 12 show two representative tests with $N = 1$ and $N = 4$ respectively. Please note that the global irradiance has not been included in the figures for the sake of simplicity. However, it should be remarked that the dynamical behaviour of both, the inlet temperature at the hot side of the heat exchanger ($T_{hs,in}$) and the water demand (D) depends directly on this variable. In this way, in the simulations, the water consumption of the greenhouse was maximum around the solar midday (see Fig. 11-4,12-(4)). Nevertheless, $T_{hs,in}$ reached the maximum value later (see Fig. 11-1,12-(1)) because of the volume of water accumulated in the solar field
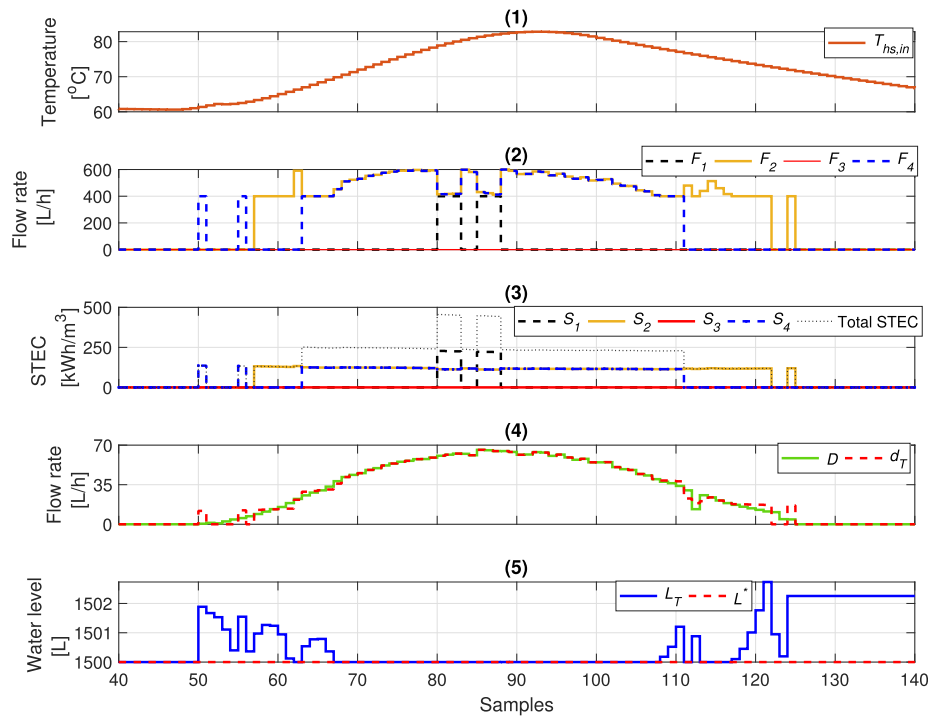
Fig. 11. Simulation results obtained during a daily operation of the plant with the proposed approach with $N = 1$. (1) Temperature at the inlet of the hot side of the heat exchanger ($T_{hs,in}$), (2) feed flow rates of each MD module included in the desalination unit (F_1, F_2, F_3 and F_4), (3) STEC of each module (S_1, S_2, S_3 and S_4) and total STEC of the whole system (total STEC), (4) water demand (D) and total distillate production (d_T), and (5) actual water level of the tank (L_T) and desire level (L^*).
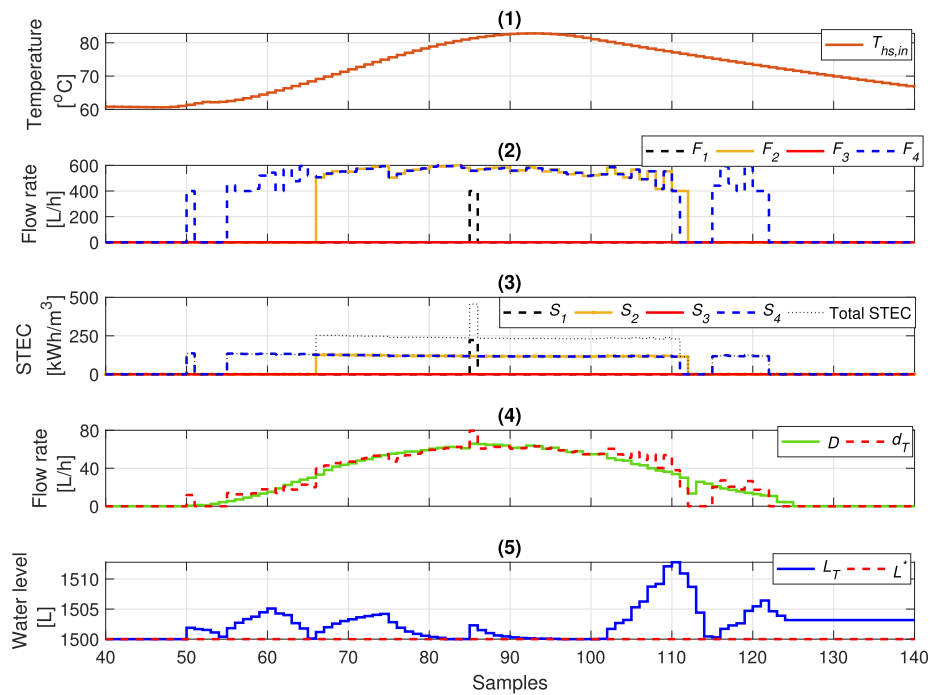
Fig. 12. Simulation results obtained during a daily operation of the plant with the proposed approach with $N = 4$. (1) Temperature at the inlet of the hot side of the heat exchanger ($T_{hs,in}$), (2) feed flow rates of each MD module included in the desalination unit (F_1, F_2, F_3 and F_4), (3) STEC of each module (S_1, S_2, S_3 and S_4) and total STEC of the whole system (total STEC), (4) water demand (D) and total distillate production (d_T), and (5) actual water level of the tank (L_T) and desire level (L^*).

storage tank (see Fig. 1).

As can be observed in Fig. 11-5,12-(5), the simulations started with a level in the distillate tank equal to the setpoint level, which was set as 1500 L. Therefore, as soon as the water demand was

higher than zero, the controller turned on one of the Aquastill modules (which are the most efficient) at its minimum feed flow rate, 400 L/h (see Fig. 11-2,12-(2)). This fact caused the level of the tank to increase as the production was higher than the demand,

and therefore, at the next sampling time, the module was turned off again. From sample 55, there were differences between the performance of the management method in both tests, which were caused by the value of the prediction horizon.

In general terms, it can be seen how the controller with $N = 1$ (see Fig. 11), which means to take into account a prediction of 10 min at each sampling time, used more modules than in the case with $N = 4$ because of the low prediction horizon. This was especially relevant around midday when the controller with $N = 1$ (see Fig. 11-(2)) turned on one of the less efficient modules twice for three and four sampling times respectively. Regarding the controller with $N = 4$ (which means to consider a prediction of 40 min at each sampling time), it can be seen that (see Fig. 12), thanks to a longer prediction horizon, the controller anticipated the increase in water demand better. In this way, it augmented the production of one of the aquastill modules progressively by increasing its feed flow rate (see Fig. 12-(2) from sample 55 to sample 66). Then, it turned on the other Aquastill module, and in the solar midday, it activated one of the Solar Spring modules only once during a single sampling time. Note that, the advantages achieved by operating the facility this way were directly reflected in the thermal energy consumption of the desalination unit. This fact can be seen in Fig. 11-3,12-(3). Observe as the total STEC (which is the sum of the STEC of the four MD modules, the value of the objective function) in the case with $N = 1$ was higher than the one of the controller with $N = 4$ from sample 62 to sample 66, due to the use of two MD modules. This happened also in the solar midday from sample 80 to 88.

Moreover, Table 3 summarizes the results obtained in the operation with different values of N. Observe as both, the total thermal energy consumption and the mean STEC of the operation decreased as the prediction horizon increased from $N = 1$ to $N = 4$. On the contrary, for higher horizons, the value of these two metrics was worse. This was caused by errors in the predictions. It is worth noting that, the water demand decreased at the end of the solar day according to the global irradiance. However, the water demand was fixed constant along the prediction horizon. This caused the production to be greater than necessary, what penalized the thermal energy consumption of the desalination unit when using a larger prediction horizon than $N = 4$.

4.5. Comparison with previous and non-optimal approaches

In this section, three representative days with different meteorological conditions were used to compare a manual operation, an operation performed with the approach presented in Ref. [29], and an operation with the management method presented in this paper. The data corresponded to July 10th, 2017, June 6th, 2017 and March 4th, 2015 (test 1, 2 and 3 respectively). The first day was a sunny day, similar to the one presented in the previous section but with a higher level of irradiance (see the cumulative global irradiance, CTI, for test 1 in Table 4). This fact caused the water

Table 3
Results obtained in the operation with different values of N. DP is the total distillate production, M-STEC is the mean STEC of the MD facility during the operation and TTEC is the total thermal energy consumption.

	DP [L]	M-STEC [kWh/m^3]	TTEC [kWh]
$N = 1$	691.86	261.03	180.59
$N = 2$	692.19	258.54	178.95
$N = 3$	692.94	257.80	178.78
$N = 4$	693.51	257.22	178.38
$N = 5$	694.26	258.11	179.19
$N = 6$	695.36	259.30	180.30

consumption of the greenhouse to be higher, and the desalination unit to operate around 80% of its capacity to cover the needs when the demand was maximum. The second day corresponded to the test presented in the previous section. Note that, in that test, the water needs required the operation of the desalination unit to be around 50% of its capacity in the moments of maximum consumption. The third test was a cloudy day, so that, the water requirements of the greenhouse were low, which could be covered with the operation of the desalination unit at less than 30% of its capacity.

It should be remarked that in both, the manual method and the one presented in Ref. [29], the four modules included in the desalination unit were turned on as long as the water demand was higher than zero. On the one hand, the manual operation were performed with the feed flow rate of each MD module fixed at 500 L/h. On the other hand, with the method presented in Ref. [29], the feed flow rate of each MD module was manipulated according to the water needs trying to reduce the STEC.

Table 4 shows the results obtained with each technique. As can be seen, in the first test, the manual procedure required 1213.57 kWh of thermal energy, whereas the approach presented in Ref. [29] 982.48 kWh (see Table 4). The amount of thermal energy saved by using the proposed technique is considerable, around 65 and 55% with respect to the manual operation and the one performed with procedure presented in Ref. [29] respectively. This was the result by two main facts. First, the total distillate production (1015.10 L) was almost totally adjusted to the water demand (1013.03 L), which was achieved by manipulating the number of MD modules turned on at each sampling time according to the water needs. This allowed the controller to use only the most efficient MD modules at the beginning and at the end of the day (when the water demand was low), thus saving a large amount of thermal energy. Second, when a module was turned on, its STEC was minimized, which also allowed to reduce the total thermal energy consumption. In the second test, the performance was similar to the previous one, but in this case, as the water needs were lower, the amount of thermal energy saved was even higher, around 85 and 80% in comparison with the manual procedure and the method proposed in Ref. [29] respectively. In the third test, the level of irradiance was lower, and therefore, the water requirements too. In this case, the benefits attained by using the proposed technique were greater as the water needs could be met using only the most efficient modules in the array during the whole operation. Thus, less than the 5% of the thermal energy required by the manual operation and the one performed with the approach in Ref. [29] was used with the application of the proposed method.

5. Conclusions

This paper proposes a general optimal operating strategy aimed at reducing the total thermal energy consumption of commercial membrane distillation facilities. The proposed approach is based on the Generalized Benders Decomposition (GBD) method, which allows us to solve the MINLP optimization problem associated to the management of the facility in a simple and efficient way. In addition, a Model Predictive Control (MPC) strategy is employed to reflect the operational strategy in real time. The developed method was applied in a practical case study, in which an SMD plant was connected to a greenhouse with a variable water demand. The obtained results allow us to draw the following conclusions:

- The developed strategy can be applied in any commercial desalination facility based on membrane distillation as long as the MD modules are modelled with the RSM method.

Table 4
Comparison of results. CTI is the cumulative global irradiance, WD is the total water demand, DP is the total cumulative distillate production, M-STEC is the mean STEC (thermal efficiency) of the MD facility during the operation and TTEC is the total thermal energy consumption.

	Test 1			Test 2			Test 3		
	CTI = 29951 [kJ/m^2]			CTI = 26488 [kJ/m^2]			CTI = 17406 [kJ/m^2]		
	WD = 1013.03 [L]			WD = 690.95 [L]			WD = 210.62 [L]		
	DP	M-STEC	TTEC	DP	M-STEC	TTEC	DP	M-STEC	TTEC
	[L]	[kWh/m^3]	[kWh]	[L]	[kWh/m^3]	[kWh]	[L]	[kWh/m^3]	[kWh]
Manual operation	1589.70	763.40	1213.57	1312.60	831.33	1091.20	1095.70	859.25	941.48
Procedure proposed in [29]	1383.34	710.23	982.48	1152.40	805.42	928.16	957.15	832.17	796.51
Proposed approach	1015.10	426.99	433.43	693.51	257.22	178.38	211.46	139.82	26.04

- The efficiency analysis performed showed as the developed technique reaches almost the same results of an MINLP solver. However, the resolution time was considerable improved. For example, for a facility with 64 MD modules, an MINLP solver required 1619.72 s for solving the problem in a single sampling time, whereas the proposed approach only 5.67 s.
- Regarding the operation, the proposed method was able to manage the facility optimally when coupled to a variable water demand, deciding at each sampling time the number of MD modules turned on and their operating feed flow rate, reducing the total thermal energy consumption of the desalination unit and ensuring the water needs.
- The comparison performed with a manual operation and with a previous proposed approach in literature showed how, in a sunny day, around the 65 and 55% of the thermal energy used by these methods can be saved with the application of the developed technique. In a cloudy day, the benefits are even higher, so that, the proposed approach used less than 5% of the energy required by the other operating methods. These improvements could be very important for both the design of SMD commercial facilities and their daily operation, especially if non-renewable sources are also taken into account to feed the desalination unit or as a backup for cloudy days.

CRediT authorship contribution statement

Juan D. Gil: Conceptualization, Software, Investigation, Writing - original draft. **Paulo R.C. Mendes:** Methodology, Investigation, Writing - review & editing. **E. Camponogara:** Methodology, Writing - review & editing. **Lidia Roca:** Conceptualization, Resources, Writing - review & editing. **J.D. Álvarez:** Conceptualization, Writing - review & editing. **Julio E. Normey-Rico:** Supervision, Writing - review & editing.

Acknowledgements

Appendix A. Nomenclature

Variable	Description	Units
c_1	Constant used in the STEC calculation	kWh/^{o}C.m$_3$
c_2	Constant for the GBD algorithm	10^6
c_3	Conversion factor for the tank level calculation	0.16 h
c_f	Conversion factor to the STEC	$3.6 \cdot 10^6$ s·W/h·kW
c_p	Specific heat capacity of sea water	J/kg·^{o}C
CTI	Cumulative global irradiance	kJ/m^3
D	Water demand	L/h
d_m	Distillate production of MD m-module	L/h
DP	Total cumulative distillate production	L
d_T	Total distillate production	L/h
F_m	Feed flow rate of MD m-module	L/h
F_m^{Max}	Maximum feed flow rate of MD m-module	L/h
F_m^{Min}	Maximum feed flow rate of MD m-module	L/h
F_T	Feed water source flow rate	L/h
F_T^{Max}	Maximum feed flow rate of feed pump	L/h
F_T^{Min}	Minimum feed flow rate of feed pump	L/h
L_T	Water level of the distillate tank	L
L_T^{Max}	Maximum water level of the distillate tank	L
L_T^{Min}	Minimum water level of the distillate tank	L
L^*	Setpoint level of the distillate tank	L
M-STEC	Mean STEC of the MD facility	kWh/m^3
p_i	with $i = 1, ..., 9$, Polynomial coefficients	−
S_m	Specific thermal energy consumption of MD m-module	kWh/m^3
$T_{cin,m}$	Inlet temperature of the condenser channel of MD m-module	^{o}C
$T_{cout,m}$	Outlet temperature of the condenser channel of MD m-module	^{o}C
$T_{cs,in}$	Inlet temperature at the cold side of the heat exchanger	^{o}C
$T_{cs,out}$	Outlet temperature at the cold side of the heat exchanger	^{o}C

(*continued*)

Variable	Description	Units
$T_{ein,m}$	Inlet temperature of the evaporator channel of MD m-module	°C
T_{Feed}	Feed water source temperature	°C
$T_{hs,in}$	Inlet temperature at the hot side of the heat exchanger	°C
$T_{hs,out}$	Outlet temperature at the hot side of the heat exchanger	°C
TTEC	Total thermal energy consumption	kWh
V_m	Valve aperture	%
WD	Total cumulative water demand	L
$\alpha_{m,j}^d$	with j = 1…,2, Auxiliary variable 1 for the MILP model	−
$\alpha_{m,j}^T$	with j = 1…2, Auxiliary variable 2 for the MILP model	−
δ_m	Valve position	0−1
ΔT_m	Temperature difference between the inlet of the evaporator channel and the outlet of the condenser channel of the MD m-module	°C
ρ	Density of sea water	kg/m³

References

[1] A. Deshmukh, C. Boo, V. Karanikola, S. Lin, A.P. Straub, T. Tong, D.M. Warsinger, M. Elimelech, Membrane distillation at the water-energy nexus: limits, opportunities, and challenges, Energy Environ. Sci. 11 (5) (2018) 1177–1196, https://doi.org/10.1039/c8ee00291f.

[2] D. González, J. Amigo, F. Suárez, Membrane distillation: perspectives for sustainable and improved desalination, Renew. Sustain. Energy Rev. 80 (2017) 238–259, https://doi.org/10.1016/j.rser.2017.05.078.

[3] Y. Kim, K. Thu, S.-H. Choi, Solar-assisted multi-stage vacuum membrane distillation system with heat recovery unit, Desalination 367 (2015) 161–171, https://doi.org/10.1016/j.desal.2015.04.003.

[4] G. Zaragoza, A. Ruiz-Aguirre, E. Guillén-Burrieza, Efficiency in the use of solar thermal energy of small membrane desalination systems for decentralized water production, Appl. Energy 130 (2014) 491–499, https://doi.org/10.1016/j.apenergy.2014.02.024.

[5] A. Luo, N. Lior, Critical review of membrane distillation performance criteria, Desalination Water Treat. 57 (43) (2016) 20093–20140, https://doi.org/10.1080/19443994.2016.1152637.

[6] R. Miladi, N. Frikha, A. Kheiri, S. Gabsi, Energetic performance analysis of seawater desalination with a solar membrane distillation, Energy Convers. Manag. 185 (2019) 143–154, https://doi.org/10.1016/j.enconman.2019.02.011.

[7] J.D. Gil, L. Roca, A. Ruiz-Aguirre, G. Zaragoza, M. Berenguel, Optimal operation of a solar membrane distillation pilot plant via nonlinear model predictive control, Comput. Chem. Eng. 109 (2018) 151–165, https://doi.org/10.1016/j.compchemeng.2017.11.012.

[8] I. Janajreh, M.N. Hussain, R. Hashaikeh, R. Ahmed, Thermal efficiency enhancement of the direct contact membrane distillation: conductive layer integration and geometrical undulation, Appl. Energy 227 (2018) 7–17, https://doi.org/10.1016/j.apenergy.2017.10.048.

[9] P. Wang, T.-S. Chung, Recent advances in membrane distillation processes: membrane development, configuration design and application exploring, J. Membr. Sci. 474 (2015) 39–56, https://doi.org/10.1016/j.memsci.2014.09.016.

[10] A. Ruiz-Aguirre, J. Andrés-Mañas, J. Fernández-Sevilla, G. Zaragoza, Experimental characterization and optimization of multi-channel spiral wound air gap membrane distillation modules for seawater desalination, Separ. Purif. Technol. 205 (2018) 212–222, https://doi.org/10.1016/j.seppur.2018.05.044.

[11] M.T. Mito, X. Ma, H. Albuflasa, P.A. Davies, Reverse osmosis (RO) membrane desalination driven by wind and solar photovoltaic (PV) energy: state of the art and challenges for large-scale implementation, Renew. Sustain. Energy Rev. 112 (2019) 669–685, https://doi.org/10.1016/j.rser.2019.06.008.

[12] R. Miladi, N. Frikha, S. Gabsi, Exergy analysis of a solar-powered vacuum membrane distillation unit using two models, Energy 120 (2017) 872–883, https://doi.org/10.1016/j.energy.2016.11.133.

[13] Q. Li, L.-J. Beier, J. Tan, C. Brown, B. Lian, W. Zhong, Y. Wang, C. Ji, P. Dai, T. Li, et al., An integrated, solar-driven membrane distillation system for water purification and energy generation, Appl. Energy 237 (2019) 534–548, https://doi.org/10.1016/j.apenergy.2018.12.069.

[14] A. Shafieian, M. Khiadani, A novel solar-driven direct contact membrane-based water desalination system, Energy Convers. Manag. 199 (2019) 112055, https://doi.org/10.1016/j.enconman.2019.112055.

[15] N. Thomas, M.O. Mavukkandy, S. Loutatidou, H.A. Arafat, Membrane distillation research & implementation: lessons from the past five decades, Separ. Purif. Technol. 189 (2017) 108–127, https://doi.org/10.1016/j.seppur.2017.07.069.

[16] R. Long, X. Lai, Z. Liu, W. Liu, Direct contact membrane distillation system for waste heat recovery: modelling and multi-objective optimization, Energy 148 (2018) 1060–1068, https://doi.org/10.1016/j.energy.2018.02.027.

[17] D. Cheng, W. Gong, N. Li, Response surface modeling and optimization of direct contact membrane distillation for water desalination, Desalination 394 (2016) 108–122, https://doi.org/10.1016/j.desal.2016.04.029.

[18] A. Ruiz-Aguirre, J. Andrés-Mañas, J. Fernández-Sevilla, G. Zaragoza, Modeling and optimization of a commercial permeate gap spiral wound membrane distillation module for seawater desalination, Desalination 419 (2017) 160–168, https://doi.org/10.1016/j.desal.2017.06.019.

[19] J.D. Gil, A. Ruiz-Aguirre, L. Roca, G. Zaragoza, M. Berenguel, Prediction models to analyse the performance of a commercial-scale membrane distillation unit for desalting brines from ro plants, Desalination 445 (2018) 15–28, https://doi.org/10.1016/j.desal.2018.07.022.

[20] H. Deng, X. Yang, R. Tian, J. Hu, B. Zhang, F. Cui, G. Guo, Modeling and optimization of solar thermal-photovoltaic vacuum membrane distillation system by response surface methodology, Sol. Energy 195 (2020) 230–238, https://doi.org/10.1016/j.solener.2019.11.006.

[21] M. Khayet, C. Cojocaru, Artificial neural network modeling and optimization of desalination by air gap membrane distillation, Separ. Purif. Technol. 86 (2012) 171–182, https://doi.org/10.1016/j.seppur.2011.11.001.

[22] W. Cao, Q. Liu, Y. Wang, I.M. Mujtaba, Modeling and simulation of vmd desalination process by ann, Comput. Chem. Eng. 84 (2016) 96–103, https://doi.org/10.1016/j.compchemeng.2015.08.019.

[23] M.-A.A. Hejazi, O.A. Bamaga, M.H. Al-Beirutty, L. Gzara, H. Abulkhair, Effect of intermittent operation on performance of a solar-powered membrane distillation system, Separ. Purif. Technol. 220 (2019) 300–308, https://doi.org/10.1016/j.seppur.2019.03.055.

[24] Y.-H. Chen, Y.-W. Li, H. Chang, Optimal design and control of solar driven air gap membrane distillation desalination systems, Appl. Energy 100 (2012) 193–204, https://doi.org/10.1016/j.apenergy.2012.03.003.

[25] R. Porrazzo, A. Cipollina, M. Galluzzo, G. Micale, A neural network-based optimizing control system for a seawater-desalination solar-powered membrane distillation unit, Comput. Chem. Eng. 54 (2013) 79–96, https://doi.org/10.1016/j.compchemeng.2013.03.015.

[26] J.D. Gil, L. Roca, G. Zaragoza, M. Berenguel, A feedback control system with reference governor for a solar membrane distillation pilot facility, Renew. Energy 120 (2018) 536–549, https://doi.org/10.1016/j.renene.2017.12.107.

[27] A. Ruiz-Aguirre, D.-C. Alarcón-Padilla, G. Zaragoza, Productivity analysis of two spiral-wound membrane distillation prototypes coupled with solar energy, Desalination Water Treat. 55 (10) (2015) 2777–2785, https://doi.org/10.1080/19443994.2014.946711.

[28] D. Cheng, N. Li, J. Zhang, Modeling and multi-objective optimization of vacuum membrane distillation for enhancement of water productivity and thermal efficiency in desalination, Chem. Eng. Res. Des. 132 (2018) 697–713, https://doi.org/10.1016/j.cherd.2018.02.017.

[29] J.D. Gil, J.D. Álvarez, L. Roca, J.A. Sánchez-Molina, M. Berenguel, F. Rodríguez, Optimal thermal energy management of a distributed energy system comprising a solar membrane distillation plant and a greenhouse, Energy Convers. Manag. 198 (2019) 111791, https://doi.org/10.1016/j.enconman.2019.111791.

[30] A.M. Geoffrion, Generalized benders decomposition, J. Optim. Theor. Appl. 10 (4) (1972) 237–260, https://doi.org/10.1007/BF00934810.

[31] E. Camacho, C. Bordons, Model Predictive Control, Springer-Verlag Ltd, London, 2004.

[32] L. Roca, J.A. Sánchez-Molina, F. Rodríguez, J. Bonilla, A. de la Calle, M. Berenguel, Predictive control applied to a solar desalination plant connected to a greenhouse with daily variation of irrigation water demand, Energies 9 (3) (2016) 194, https://doi.org/10.3390/en9030194.

[33] F. Rodríguez, M. Berenguel, J.L. Guzmán, A. Ramírez-Arias, Modeling and Control of Greenhouse Crop Growth, Springer, 2015.

[34] Matlab Release 2018a, the MathWorks, Natick, MA, USA, 2018.

[35] N.V. Sahinidis, BARON V. 2019.7.13: Global Optimization of Mixed-Integer Nonlinear Programs, User's Manual, 2018.

[36] IBM, IBM ILOG CPLEX v. 12.6.1, User's Manual, 2015.

2.4 Tutorial on modelling and control of membrane distillation technology

2.4.1 Modelado y control automático en destilación por membranas solar: fundamentos y propuestas para su desarrollo tecnológico

Research in this work is supported by the following journal paper:

Title	Modelado y control automático en destilación por membranas solar: fundamentos y propuestas para su desarrollo tecnológico
Authors	**J. D. Gil**, L. Roca, M. Berenguel
Journal	Revista Iberoamericana de Automática e Informática Industrial
Year	2020
Volume	-
Pages	-
DOI	`https://doi.org/10.4995/riai.2020.13122`
IF (JCR 2018)	1.313
Categories	Automatic & Control Systems (46/62) **Q3**
	Robotics (20/26) Q4

Contribution of the Ph.D. candidate
The Ph.D. candidate, J. D. Gil, is the main contributor and first author of this paper.

Aside to this work, the research also resulted in a contribution to a national conference:

- **J. D. Gil**, M. Berenguel, and L. Roca,"Aportaciones desde el punto de vista del control automático y la optimización a la tecnología de destilación por membranas alimentada con energía solar," in *Actas XVI Simposio CEA de Ingeniería de Control*. Almería, España, 2018.

Modelado y control automático en destilación por membranas solar: fundamentos y propuestas para su desarrollo tecnológico

Gil, J.D.[a,*], Roca, L.[b], Berenguel, M.[a]

[a]Centro Mixto CIESOL, ceiA3, Universidad de Almería, Ctra. Sacramento s/n, Almería 04120, Spain
[b]CIEMAT-Plataforma Solar de Almería, Ctra. de Senés s/n, Tabernas 04200, Almería, Spain.

Resumen

La destilación por membranas es un proceso de separación impulsado térmicamente en fase de investigación. Esta tecnología destaca principalmente por la simplicidad del proceso y su baja temperatura de operación, lo que permite que pueda ser alimentada con energía solar de media-baja temperatura. Así, la destilación por membranas se ha convertido en una solución prometedora, eficiente y sostenible para desarrollar plantas de desalación de pequeño o mediano tamaño en lugares aislados con buenas condiciones de radiación. No obstante, para que esta tecnología pueda llegar a ser implementada a escala industrial se debe seguir investigando y mejorando aspectos relacionados tanto con el diseño de las membranas y de los módulos como con la propia operación de estos. En relación con la operación, el desarrollo de modelos y técnicas de control cobran un papel fundamental. En este trabajo se presenta una revisión de las técnicas de control y modelado aplicadas en este campo, describiendo las principales metodologías empleadas y los retos futuros que quedan por abordar, incluyendo además un ejemplo ilustrativo.

Palabras clave: Modelado, Control, Destilación por membranas, Desalación, Energía solar térmica.

Modelling and automatic control in solar membrane distillation: Fundamentals and proposals for its technological development

Abstract

Membrane distillation is a termally-driven separation process under investigation. This technology stands out for the simplicity of the process and for its low operating temperature, which allows it to be combined with low grade solar energy. Thus, membrane distillation has become a promising, efficient and sustainable solution for the development of small-medium stand-alone desalination facilities to be implemented in offgrids areas with good irradiance conditions. However, in order to develop this technology on an industrial scale, research must continue to improve aspects related to both the design of membranes and modules and their operation. Regarding the operation, the development of models and control techniques play a fundamental role. This paper presents a review of the control and modeling techniques applied in this field, describing the main methodologies employed and the future challenges to be addressed, also including an illustrative example.

Keywords: Modelling, Control, Membrane distillation, Desalination, Solar thermal energy.

1. Introducción

La creciente demanda de agua asociada al crecimiento económico y de la población, así como a la disminución de las reservas de agua como consecuencia del cambio climático y la contaminación, están agravando el problema de la escasez de

agua en el mundo. Diversos estudios estiman que el 60 % de la población mundial sufrirá escasez severa de agua en 2025 (Schewe et al., 2014). Estas estadísticas demuestran que las fuentes de agua convencionales, como acuíferos, lagos, agua de lluvia o deshielo, ya no son suficientes para satisfacer las demandas humanas en áreas con escasez de agua. Este hecho entra en conflicto directo con los objetivos mundiales de desarrollo sostenible aprobados por la Organización de las Naciones Unidas (ONU) en 2015, entre los que destaca uno dirigido a "garantizar la disponibilidad de agua y su gestión sostenible y el saneamiento para todos"(Jones et al., 2018).

El agua no solo está limitada en cuanto a cantidad, sino que también en la calidad suficiente para el consumo humano. Una de las principales consecuencias del cambio climático es la degradación de los recursos hídricos, ya que los fenómenos de precipitación extremos transportan patógenos y otros contaminantes a las vías fluviales a través de escorrentías e inundaciones (DeNicola et al., 2015). Además, hay que sumar otras consecuencias del cambio climático como la sequía y la desertificación, las cuales están aumentando significativamente cubriendo áreas cada vez más amplias del planeta.

El problema de la escasez agua resulta paradójico si se tiene en cuenta que vivimos en un planeta en el que dos tercios de la superficie están cubiertos de agua. Sin embargo, alrededor del 99 % del total es demasiado salada (agua de mar) o inaccesible (capas de hielo y acuíferos). Así, el agua pura en estado líquido prácticamente no se encuentra en la naturaleza, y lo que se denomina agua en realidad es una disolución de diversas sales en agua. La Organización Mundial de la Salud (OMS) establece que el agua potable debe tener un contenido salino menor a 0.05 % (WHO, 2011). En este contexto es donde la desalación, que se define como el proceso de eliminar sales y minerales disueltos del agua salina para producir agua potable, puede ser una alternativa muy atractiva y viable para combatir el déficit hídrico.

Aunque la desalación se posiciona como una de las soluciones más prometedoras, un uso intensivo e irresponsable de esta tecnología puede ocasionar serios problemas, entre los que destacan aquellos relacionados con el alto consumo energético de las tecnologías de desalación actuales. Si las plantas de desalación se alimentan mediante fuentes de energía convencionales, se requerirá la quema de grandes cantidades de combustibles fósiles, contribuyendo a la emisión de CO_2 y, por consiguiente, a la contaminación medioambiental. Por el contrario, si dichas plantas se alimentan con energías renovables, la desalación se puede convertir en una nueva fuente de agua dulce eficiente y sostenible, que cubra las necesidades básicas y, que lo haga con un impacto mínimo en el medio ambiente. La habitual coincidencia geográfica entre la escasez de agua y la alta radiación solar, hace de la energía solar térmica la tecnología más apropiada y eficiente para alimentar las plantas de desalación. Así, la tecnología destilación por membranas (*Membrane Distillation*, MD) destaca como uno de los procesos de desalación más adecuados para ser combinado con este tipo de fuentes energéticas, debido principalmente a su baja temperatura de operación (Zaragoza et al., 2014).

MD es una tecnología de separación emergente en fase de investigación, que permite el uso de energía solar térmica de baja temperatura para la obtención de agua desalada, lo que la co-

loca en una posición competitiva para reducir la tensión a la que está sometida el binomio energía-agua en la actualidad (Deshmukh et al., 2018). Sin embargo, su baja eficiencia energética, debido principalmente a su alto consumo energético por unidad de destilado producido, ha obstaculizado su implementación a escala comercial hasta el momento. Por este motivo, para lograr que la técnica MD sea competitiva a escala industrial, los avances tecnológicos deben estar enfocados a reducir su consumo energético específico a partir de la mejora tanto en aspectos relacionados con el diseño de los módulos, como en aquellos relacionados con la propia operación.

En las últimas décadas, se han publicado numerosos trabajos que presentan mejoras notables en el diseño de los módulos MD. Estas investigaciones se han centrado en la creación de nuevas membranas, nuevos módulos y configuraciones, y en comprender el ensuciamiento de la membrana, fenómeno que se conoce como *fouling* (González et al., 2017). Estos trabajos han originado un gran progreso en términos de eficiencia energética, yendo de un consumo térmico específico de 810 kWh/m³ en módulos MD sin recuperación de calor y en condiciones de operación óptimas (Guillén-Burrieza et al., 2011), al consumo actual de los módulos comerciales, 49 kWh/m³ también referido a condiciones de operación óptimas pero en módulos con recuperación de calor (Andrés-Mañas et al., 2020b). Una de las razones que hace a la tecnología MD especialmente interesante es que estos requerimientos energéticos se pueden cubrir mediante energía solar de media-baja temperatura o mediante fuentes de energía de baja entalpía como calor residual (Wang and Chung, 2015).

Aunque el avance en el diseño de los módulos es aún una rama de investigación abierta, este ha sido uno de los temas más tratados en la literatura, y por tanto, se encuentra en una fase de madurez avanzada. Es por esto que, de acuerdo a las ideas presentadas en Thomas et al. (2017), la destilación por membranas se encuentra en una nueva fase de investigación, en la cual, el foco de los trabajos de investigación se encuentra puesto en otras áreas como son aquellas centradas en la operación de los módulos MD. Estos trabajos están dirigidos al modelado y optimización de las principales variables que intervienen en los procesos MD (Ruiz-Aguirre et al., 2018), y al desarrollo de metodologías de control y optimización para la mejora del rendimiento térmico de los módulos MD en tiempo real (Gil et al., 2018a). Se debe remarcar que este tipo de trabajos pueden ser fundamentales para el desarrollo de plantas sostenibles MD alimentadas con energía solar (*Solar Membrane Distillation*, SMD), ya que estas requieren que el sistema sea optimizado en tiempo real de acuerdo a las condiciones de irradiancia.

En este trabajo se presenta una revisión del estado del arte de las técnicas de modelado y control aplicadas a este tipo de plantas. En primer lugar, se describirá la tecnología de destilación por membranas poniendo de manifiesto sus principales ventajas y su interés para la implementación industrial. Además, se presentará un resumen de las principales instalaciones SMD que hay actualmente en el mundo. En segundo lugar, se hará un repaso de las técnicas de modelado que se han aplicado hasta el momento en esta tecnología. En tercer lugar, se revisarán los principales enfoques de control aplicados a sistemas MD, indicando los principales objetivos que se persiguen y las técnicas de control empleadas. A continuación, se expondrán

algunas de las potenciales aplicaciones industriales de la tecnología MD, mostrando cómo los algoritmos de control pueden ser un elemento fundamental para su desarrollo. Por último, se expondrán los retos futuros a abordar.

2. Tecnología de destilación por membranas

2.1. Descripción de la tecnología

La destilación por membranas es un proceso de separación impulsado térmicamente, basado en el transporte de moléculas en estado gaseoso a través de una membrana hidrófoba y microporosa (Khayet and Matsuura, 2011). Las fuerzas de tensión superficial de dicha membrana evitan el paso de las moléculas en estado líquido a través de los poros de esta, mientras que las moléculas en estado gaseoso la atraviesan gracias a la diferencia de presión parcial de vapor que se origina a ambos lados de la membrana, la cual se establece por una diferencia de temperatura.

El funcionamiento general de un módulo MD con recuperación de calor se puede explicar en base a la Figura 1. El agua de alimentación entra por el canal de alimentación donde se precalienta con el calor sensible que atraviesa el canal de condensación. Posteriormente, la solución precalentada se dirige al intercambiador de calor, donde se calienta con el fluido que proviene del circuito de generación de calor (normalmente basado en un campo solar térmico de media-baja temperatura). A continuación, la solución caliente se circula al canal de evaporación. La diferencia de temperatura que hay entre los dos lados de la membrana genera una diferencia de presión parcial de vapor, la cual fuerza a las moléculas en estado gaseoso a pasar desde el canal de evaporación al de condensación a través de la membrana. Finalmente, estas moléculas se condensan de forma que se obtiene destilado, mientras que las moléculas que no han pasado a estado gaseoso se rechazan en forma de salmuera. Se debe resaltar que se pueden encontrar diferentes configuraciones MD que se clasifican de acuerdo a la forma de generar la diferencia de presión a través de la membrana y el lugar donde tiene lugar la condensación. Por tanto, la descripción anterior varía en función de la configuración adoptada, ver Alkhudhiri et al. (2012) donde se explica este hecho en profundidad.
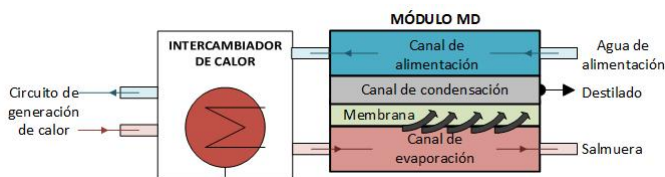

Figura 1: Diagrama esquemático de un módulo MD.

Desde el punto de vista del proceso, la tecnología MD tiene una serie de ventajas que la hacen destacar en comparación con otras tecnologías de desalación, como son:

- Su habilidad para tratar soluciones con alta concentración en sal (Kim et al., 2015; Andrés-Mañas et al., 2020b; Ruiz-Aguirre et al., 2019).

- Su alto factor de rechazo, teóricamente del 100 % (Alkhudhiri et al., 2012). Nótese que en la práctica alcanza valores mayores al 99 % (Ruiz-Aguirre et al., 2019).

- Su fuerza impulsora se origina a través de una diferencia de temperatura, en lugar de ser originada mediante fuentes mecánicas que incrementan el consumo exergético del proceso y los costes (Luo and Lior, 2016).

- Su baja presión de operación, de alrededor de 0.1 MPa, mucho menor que la requerida por tecnologías convencionales de desalación como la ósmosis inversa 2.5-8.5 MPa (Miladi et al., 2019).

- Su baja temperatura de operación (menor de 90 °C), lo que permite que pueda ser fácilmente acoplada con energía solar de baja temperatura (Zaragoza et al., 2014; Andrés-Mañas et al., 2020a) y otras fuentes como calor residual (Wang and Chung, 2015).

Esta última ventaja, junto a la simplicidad del proceso, convierten a la tecnología MD en uno de los sistemas de desalación más adecuados para el desarrollo de plantas de desalación alimentadas con energía solar en lugares aislados con buenas condiciones de radiación y requerimientos de agua no muy elevados.

2.2. Instalaciones SMD

Con el fin de evaluar el rendimiento y viabilidad de la tecnología al ser alimentada con energía solar (e implantada en lugares aislados) se han diseñado e instalado varias plantas SMD a escala piloto por todo el mundo. En concreto, en España y Jordania, se han instalado plantas piloto en el marco del proyecto "SMADES" (Koschikowski et al., 2009; Banat et al., 2007), el cual demostró la factibilidad y viabilidad del desarrollo de plantas de desalación autónomas MD alimentadas con energía solar para satisfacer demandas de agentes consumidores aislados de la red de agua pública. En la Tabla 1 se presenta un resumen de las principales instalaciones SMD en el mundo, mostrando su localización, año de construcción y capacidad de producción. Se debe destacar que solo se han incluido plantas MD no compactas, es decir, plantas en las que la unidad de desalación (módulo MD) y el sistema de generación de calor (i.e., el campo solar térmico) están separados.

Aunque las plantas SMD de la Tabla 1 se han diseñado mediante diferentes métodos y por diferentes equipos investigadores, todas ellas se pueden describir en base al diagrama esquemático mostrado en la Figura 2. De este modo, la energía térmica requerida por el proceso de destilación se consigue a través de un campo solar térmico. La salida de este campo está conectada a un tanque de almacenamiento térmicamente aislado, que se puede utilizar para almacenar energía térmica o para filtrar perturbaciones en la radiación. Además, casi todas las plantas cuentan con un circuito hidráulico que permite evitar el uso de dicho tanque y llevar a cabo la conexión directa entre el campo solar y el módulo MD cuando las condiciones de irradiancia sean favorables. Por último, el módulo MD se conecta a este sistema de generación de energía térmica mediante un intercambiador de calor. Se debe destacar que las diferentes capacidades de las plantas estudiadas se deben principalmente al número de módulos MD utilizados en la unidad de desalación o a la configuración o eficiencia de los módulos MD utilizados en cada planta.

Tabla 1: Resumen de las instalaciones SMD seleccionadas a escala piloto no compactas. PSA significa Plataforma Solar de Almería y UAL Universidad de Almería.

| Referencia	Localización	Año	Capacidad [m³/día]
Banat et al. (2007)	Áqaba (Jordania), 29º31'N	2007	0.90
Koschikowski et al. (2009)	Gran Canaria (España), 27º58'N	2009	1.60
Dow et al. (2010)	Edenhope (Australia), 37º03'S	2010	0.12
Cipollina et al. (2012)	Palermo (Italia), 28º06'N	2012	0.15
Gabsi et al. (2013)	Mahares (Túnez), 34º32'N	2013	0.21
Chafidz et al. (2014)	Riyadh, (Arabia Saudí) 24º38'N	2014	0.10
Gil et al. (2018b)	Almería, (España) situada en la PSA, 36º50'N	2014	0.60
Andrés-Mañas et al. (2020a)	Almería, (España) situada en la UAL, 36º49'N	2014	0.29
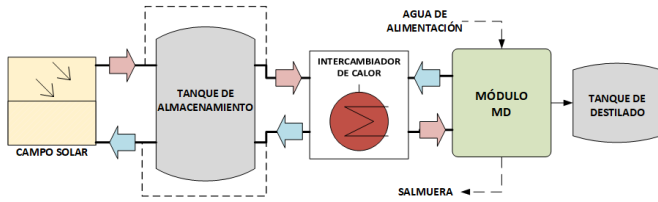
Figura 2: Diagrama esquemático general de una planta SMD.

La mayoría de los estudios llevados a cabo en las instalaciones SMD mostrados en la Tabla 1 están dedicados a evaluar diferentes tipos y diseños de módulos MD en términos de eficiencia térmica y producción de destilado. Sin embargo, en pocas instalaciones se hacen evaluaciones económicas de la tecnología. En este sentido, solo en el trabajo de Guillén-Burrieza et al. (2015) se analizó una planta piloto SMD en términos económicos, mostrando cómo el precio del agua ronda los 10-11.30 €/m³ para una instalación con capacidad de 100 m³/día. Estos resultados demostraron la viabilidad económica de la tecnología para plantas de pequeño o mediano tamaño al ser comparada con una instalación de la misma capacidad basada en la tecnología de ósmosis inversa alimentada con energía fotovoltaica, donde el precio ascendía a 11.7-15.6 €/m³. No obstante, se debe destacar que se requieren trabajos en los cuales se utilicen módulos MD más actuales y eficientes, puesto que los precios comentados anteriormente pueden ser significativamente más bajos.

2.3. *Índices de desempeño para la evaluación de la tecnología MD*

Antes de describir las estrategias de modelado y control empleadas en la tecnología MD, se deben definir los índices de desempeño que se utilizan para evaluar los módulos MD. Es importante comentar que no hay un índice estándar para la evaluación de estos procesos y por este motivo, se pueden encontrar varios métodos en la literatura (Ruiz-Aguirre et al., 2015). En primer lugar, para cuantificar la producción de los módulos MD se suele utilizar el flujo de destilado por unidad de superficie (D, medido en L/(h·m²)), el cual se puede calcular como:

$$D = \frac{\dot{m}_d}{\rho_d \cdot A_m} \cdot c_1, \tag{1}$$

donde $\dot{m}_d$ es el flujo másico de destilado (kg/s), ρ_d es la masa específica del destilado (kg/m³), A_m es la superficie de la membrana del módulo (m²) y c_1 es un factor de conversión de unidades con valor $3.6 \cdot 10^6$ (L·s/(m³·h)).

Para la evaluación de la eficiencia térmica de los módulos, en la literatura principalmente se utilizan dos índices de desempeño. Por un lado, la Razón de Salida Ganada (*Gained Output Ratio*, GOR (-)) que se define como el calor latente necesario para evaporar todo el flujo másico de destilado producido comparado con el calor externo aportado:

$$GOR = \frac{\dot{m}_d \cdot \Delta h_v}{\dot{Q}}, \tag{2}$$

donde Δh_v es la entalpía de vaporización (kJ/kg) y $\dot{Q}$ es el flujo de calor que se le aporta al sistema (kJ/s). Por otro lado, también se suele usar un índice denominado Consumo Específico de Energía Térmica (*Specific Thermal Energy Consumption*, STEC (kWh/m³)), el cual da información acerca de la cantidad de energía necesaria para producir una unidad de volumen de destilado. El STEC se puede calcular como:

$$STEC = \frac{\dot{Q} \cdot \rho_d}{\dot{m}_d \cdot c_2}\cdot, \tag{3}$$

donde c_2 es un factor de conversión de unidades con valor 3600 (kJ/kWh).

3. Modelado de plantas MD

En esta sección se hace una revisión de las principales técnicas de modelado propuestas en este campo. En primer lugar, se describen las técnicas de modelado usadas para caracterizar los módulos MD y, posteriormente, las utilizadas para modelar el resto de componentes de una planta piloto SMD como la descrita en la subsección anterior.

3.1. *Modelado de módulos MD*

El desarrollo de modelos de módulos MD, ya sean basados en primeros principios o en datos empíricos, se ha convertido en una herramienta fundamental para predecir el funcionamiento de estos procesos bajo diferentes condiciones de operación. Estos modelos no solo ayudan a analizar el comportamiento de los módulos MD bajo las condiciones de operación requeridas, sino que también son esenciales para el desarrollo de técnicas de control (Porrazzo et al., 2013; Gil et al., 2019a) y para el desarrollo de algoritmos dirigidos a obtener un diseño óptimo de la planta (Chen et al., 2012). De este modo, a continuación se hace una revisión de los enfoques de modelado utilizados hasta el momento en la literatura abordando, tanto los modelos basados en datos experimentales como los basados en primeros principios.

3.1.1. Modelos basados en datos experimentales de módulos MD

En el caso particular de la tecnología MD, la existencia de diferentes diseños internos (diferentes longitudes del canal, anchuras del canal, número de canales, etc.) así como de tipos de módulos y membranas dificulta la construcción de modelos basados en primeros principios. Se debe tener en cuenta que la variación de estos parámetros no resulta en un cambio proporcional en el rendimiento del proceso, haciendo que no se pueda establecer fácilmente un modelo general (Ruiz-Aguirre et al., 2018). Además, en la mayoría de los módulos MD a escala comercial no se dispone de la información suficiente para realizar dichos modelos teóricos, por lo que se necesita una colaboración más estrecha entre el mundo académico y los desarrolladores industriales de módulos MD. Por estas razones, la mayoría de los procesos MD (especialmente los módulos comerciales) se modelan mediante modelos basados en datos experimentales. Dos de las técnicas de modelado más utilizadas en este campo son la Metodología de Superficie de Respuesta (*Response Surface Methodology*, RSM) y las Redes Neuronales Artificiales (*Artificial Neural Network*, ANN). Estos modelos son válidos para ajustar procesos lineales y no lineales multivariables. Su principal ventaja radica en la rapidez a la hora de obtenerlos una vez se dispone del conjunto de datos experimentales. Sin embargo, se debe tener en cuenta que no se pueden usar para extrapolar los resultados a otros sistemas, y que son solo válidos para el rango de operación en el cual se han obtenido. Además, este tipo de modelos representan directamente la salida final del modelo, y no permiten estudiar el fenómeno físico que ocurre en el sistema. Por el contrario, sí que son válidos para visualizar y analizar el rango de operación del módulo y entender el comportamiento del sistema.

La metodología RSM (Hill and Hunter, 1966) es una técnica estadística que utiliza funciones cuadráticas para caracterizar procesos lineales o con no linealidades suaves. En esta metodología se diseñan campañas experimentales centradas en aplicar cambios en forma de escalón, llamados niveles, a uno de los grados de libertad (entradas) mientras que los otros se mantienen constantes. Posteriormente, se ajusta un modelo polinomial en base a la respuesta experimental observada en cada nivel para cada variable independiente. El modelo RSM tiene la siguiente estructura:

$$q = \gamma_0 + \sum_{i=1}^{v} \gamma_i \cdot w_i + \sum_{i=1}^{v} \gamma_{ii} \cdot w_i^2 + \sum_{1 \leq i \leq j}^{v} \gamma_{ij} \cdot w_i \cdot w_j, \quad (4)$$

donde v es el número de variables, γ_0 es el coeficiente de compensación (*offset*), γ_i son los coeficientes de los términos lineales, w_i y w_j son entradas del modelo, γ_{ii} representa los coeficientes de los términos cuadráticos, γ_{ij} los coeficientes de interacción entre entradas del modelo y q la salida del modelo.

Por su parte, la metodología ANN (más conocida en el ámbito de la Automática) consiste también en un modelo matemático compuesto por elementos simples interconectados y organizados en una estructura de capas, los cuales procesan información en respuesta a entradas externas tratando de imitar el comportamiento de las neuronas biológicas (Demuth et al., 2014). Esta técnica se ha convertido en una herramienta emergente durante los últimos años en el campo de la MD ya que,

en comparación con la técnica RSM, es capaz de ajustar con éxito casi todos los procesos no lineales, tanto estáticos como dinámicos. Así, cobra especial importancia cuando se utilizan variables independientes que inducen comportamientos no lineales en el sistema, como es el caso de la salinidad de la solución de alimentación del módulo MD.

De este modo, se pueden encontrar diferentes trabajos de modelado basados en RSM en la literatura. En la mayoría de ellos se utiliza la metodología RSM para predecir el flujo de destilado, como es el caso de Fadhil et al. (2019); El-zahaby et al. (2016); Khalifa and Lawal (2016); Bouguecha et al. (2016); Mohammadi et al. (2015); Boubakri et al. (2014); Khayet and Matsuura (2011); Khayet and Cojocaru (2012a); Khayet et al. (2007). Por el contrario, solo unos pocos predicen aparte del flujo del destilado algún índice de desempeño relacionado con el consumo térmico del módulo como el STEC o el GOR (Gil et al., 2018c; Ruiz-Aguirre et al., 2018; Cheng et al., 2018; Ruiz-Aguirre et al., 2017; He et al., 2014). Además, en casi todos los trabajos se utilizan como variables de entrada la temperatura y caudal del agua de alimentación y la temperatura a la entrada del canal de evaporación del módulo, y solo en Gil et al. (2018c); Mohammadi et al. (2015); Khayet et al. (2007) se incluye la salinidad del agua de alimentación como entrada del modelo. De forma similar, se pueden encontrar trabajos basados en la metodología ANN para predecir el flujo de destilado como es el caso de Yang et al. (2020); Cao et al. (2016); Porrazzo et al. (2013); Khayet and Cojocaru (2013, 2012b); Tavakolmoghadam and Safavi (2012). Por otra parte, solo en Gil et al. (2018c); Shirazian and Alibabaei (2017) se tienen en cuenta como salida también índices de desempeño como el STEC o el GOR. Sin embargo, únicamente en Gil et al. (2018c); Cao et al. (2016) se utiliza como entrada la salinidad del agua de alimentación.

En base a los trabajos revisados se puede observar cómo las entradas más utilizadas en este tipo de modelos son la temperatura y caudal del agua de alimentación y la temperatura de entrada del canal de evaporación del módulo MD, y la variable de salida más utilizada es el flujo de destilado. Se debe destacar que solo unos pocos trabajos tienen en cuenta la salinidad como variable de entrada en la metodología RSM y además, utilizan rangos de entrada pequeños para dicha variable. De acuerdo a las ideas presentadas en Gil et al. (2018c), la metodología ANN es más adecuada para realizar modelos cuando se considera esta variable debido a su comportamiento no lineal. Nótese que el estudio de la influencia de esta variable es importante, ya que una de las principales aplicaciones industriales de la tecnología MD consiste en tratar salmueras procedentes de otras tecnologías de desalación, como se verá más adelante en la sección 5. También cabe destacar que hay pocos trabajos que utilicen como variable de salida algún índice de desempeño relacionado con el rendimiento térmico del módulo, lo cual es especialmente relevante, ya que es uno de los principales puntos débiles de la tecnología. El estudio del comportamiento de esta variable bajo diferentes condiciones de operación puede ser determinante para el desarrollo comercial de la tecnología MD. Por último, se debe destacar que muchos de los modelos desarrollados están basados en datos obtenidos en módulos a escala de laboratorio y solo en unos pocos trabajos (Gil et al., 2018c; Ruiz-Aguirre et al., 2018, 2017; Porrazzo et al., 2013) se utilizan módulos

de MD a escala comercial, por lo que aún se necesita el desarrollo de trabajos de investigación para estudiar y optimizar el comportamiento de los módulos comerciales MD.

3.1.2. Modelos basados en primeros principios de módulos MD

En la literatura también se han presentado diferentes trabajos tratando el modelado basado en primeros principios de este tipo de sistemas. El objetivo principal de dichos trabajos consiste en estudiar el comportamiento temporal de los módulos en base a diversos parámetros de diseño, como son el tamaño de la membrana o su porosidad, y diferentes condiciones de operación, con variaciones en temperatura de entrada a ambos canales del módulo, en la concentración, y en el caudal del agua de alimentación. A continuación, se presenta una revisión somera de estos tipos de trabajos.

En Chang et al. (2010) se presentó un modelo dinámico basado en balances de masa y energía para estudiar la resistencia de transferencia de materia y calor del módulo. En Tang et al. (2011) se presentó el modelo de un módulo MD mediante la metodología de Dinámica de Fluidos Computacional (*Computational Fluid Dynamics*, CFD), el cual tiene como objetivo estudiar la transmisión de masa y de calor en los poros de la membranas. En Yu et al. (2011) se propuso también un modelo basado en CFD para analizar la transferencia de masa y materia en un módulo MD. En Alsaadi et al. (2013) se presentó un modelo basado en balances de energía y masa con el objetivo de predecir el flujo de vapor de destilado. En Zhang et al. (2015) se utilizó un modelo CFD para estudiar la distribución de vapor y líquido en la membrana del módulo. En Hayer et al. (2015) se incorporaron los efectos de la difusión de Knudsen, difusión molecular y flujo viscoso a la metodología CFD para estudiar el coeficiente de polarización de temperatura del módulo. En Karanikola et al. (2015) se presentó un modelo basado en balances de masa y energía para estudiar los perfiles de temperatura y producción de destilado del módulo. En Gustafson et al. (2016) se presentó un enfoque similar al anterior, pero que permite también predecir la concentración del destilado. En Eleiwi et al. (2016) se modeló un módulo MD mediante ecuaciones de advección-difusión, las cuales describen los mecanismos de transferencia de calor y de masa que se dan lugar dentro del módulo. En Karam and Laleg-Kirati (2016) se presentó un modelo dinámico basado en la analogía entre los sistemas térmicos y eléctricos. Este modelo captura las respuestas espaciales y temporales de la distribución de temperatura a lo largo de la dirección del flujo, y predice la salida del flujo de agua destilada. En Karam et al. (2017) se realizó un modelo con los mismos objetivos mencionados anteriormente, pero en este caso, el sistema se caracterizó mediante un modelo de parámetros concentrados. En Perfilov et al. (2018) se propuso un modelo de predicción general basado en la metodología CFD, con el objetivo de obtener perfiles detallados de temperatura, presión, concentración y flujo de salida de destilado. Otro enfoque interesante se propuso en el trabajo de Amigo et al. (2018) en el cual se presentó un modelo basado en CFD para comprender la relación entre la hidrodinámica y el *fouling*. En Esfandiari et al. (2019) se introduce un modelo basado en CFD para predecir el flujo de destilado del módulo, el cual contiene ecuaciones de masa, energía y fenómenos de transferencia de impulso.

En base a la revisión realizada, se puede observar que la metodología de modelado más usada es la CFD. Esta metodología de modelado se basa en el uso de una aproximación numérica para simular el flujo de caudal. Además, esta técnica permite predecir temperaturas y concentraciones a lo largo del módulo (Hitsov et al., 2015). Del mismo modo, se puede ver cómo la mayoría de estos modelos se han desarrollado para estudiar y analizar los fenómenos de transferencia de materia y calor dentro del módulo con el fin de optimizar su diseño y funcionamiento. Por otra parte, se debe comentar que aunque todos los modelos mencionados en el párrafo anterior fueron validados experimentalmente, en la mayoría de casos los datos fueron obtenidos con módulos a escala de laboratorio. Las validaciones de este tipo de modelos en módulos a escala comercial son escasas y solo se pueden encontrar algunos ejemplos en la literatura como es el caso de los trabajos de Winter (2015) y Hitsov et al. (2017). Una de las principales dificultades que impiden dichas validaciones se debe a que, para el desarrollo de este tipo de modelos, algunos de los fenómenos físicos que ocurren dentro del módulo MD se simplifican, lo que hace que los modelos pierdan fiabilidad y sea más complicado validarlos en módulos comerciales.

3.2. Modelado de plantas SMD

Tal y como se mostró en la Figura 2, los dispositivos que se incluyen en este tipo de instalaciones, además del módulo de MD, son los típicos de un campo solar térmico: captadores solares, tanques de almacenamiento aislados térmicamente e intercambiadores de calor. Para este tipo de dispositivos existen modelos basados en primeros principios bien conocidos y validados en sistemas reales en la literatura (Duffie and Beckman, 2013). Es por esto que en la mayoría de trabajos de modelado de este tipo de plantas se utilizan estos modelos (Ding et al., 2005; Chang et al., 2010; Abdallah et al., 2013; Gil et al., 2018a,b). Además, en Gil et al. (2019b) se adaptaron dichos modelos a la metodología de modelado dinámico lógico mixto (*Mixed-Logical Dynamical*, MLD) con el fin de representar el carácter híbrido de la planta SMD. También se debe comentar que los trabajos de modelado en este ámbito no se han limitado a los mencionados modelos basados en primeros principios, sino que también se han presentado modelos basados en ANN para modelar la planta completa (Porrazzo et al., 2013).

4. Sistemas de control para plantas SMD

Aunque la tecnología MD este todavía en fase experimental, se encuentra en un estado de madurez avanzado, y los trabajos de investigación centrados en la mejora de las estrategias de operación para este tipo de sistemas están cobrando cada vez más importancia. En este ámbito, los sistemas de control tienen un papel fundamental ya que, al utilizar una fuente de energía intermitente como la energía solar, se debe realizar una gestión óptima de la planta de acuerdo al comportamiento de la irradiancia solar, la cual se puede conseguir mediante técnicas de control avanzadas. En esta sección se hace una revisión de los principales enfoques de control aplicados hasta el momento en plantas SMD, los cuales se resumen en la Tabla 2, remarcando los principales objetivos que se persiguen y las metodologías de control empleadas.

4.1. Objetivos

Antes de describir las metodologías de control empleadas, se deben establecer los objetivos de control de este tipo de instalaciones, los cuales se pueden dividir en dos niveles. En primer lugar, se pueden diferenciar los objetivos de bajo nivel, que consisten en mantener las principales variables que intervienen en el proceso, como caudal y temperatura, en torno a valores deseados. Esto es fundamental para asegurar un régimen estacionario y poder llevar a cabo la evaluación de los módulos en distintas condiciones de operación. En segundo lugar, se encuentran los objetivos de alto nivel, los cuales están relacionados con el funcionamiento del módulo de desalación y consisten en maximizar su producción y rendimiento energético.

Las estructuras de control de bajo nivel tienen como objetivo tareas clásicas de regulación en sistemas alimentados con energía solar térmica (Camacho et al., 2012). Así, los objetivos que se buscan se pueden resumir en: i) controlar los distintos caudales de la instalación haciendo uso de los variadores de frecuencia de las bombas de la instalación, ii) controlar la temperatura y rechazar las perturbaciones de radiación actuando sobre el caudal del campo solar, y iii) mantener una temperatura estable a la entrada del intercambiador de calor encargado de proporcionar la energía térmica al módulo de destilación por membranas.

Por otra parte, los objetivos de los bucles de control de alto nivel están relacionados con la mejora de los índices de desempeño del módulo MD. Para establecer dichos objetivos conviene analizar las variables que afectan al funcionamiento del módulo las cuales son: caudal del agua de alimentación, temperatura de alimentación, concentración de la solución de alimentación, y temperatura a la entrada del canal de evaporación. De estas variables, la temperatura y concentración del agua de alimentación son perturbaciones y vienen impuestas por la solución de alimentación con la que se este trabajando. Por el contrario, la temperatura a la entrada del canal de evaporación se puede manipular actuando sobre los bucles de bajo nivel del campo solar, al igual que el caudal de alimentación el cual se puede variar actuando sobre la bomba de alimentación. Una vez descritas las variables, los objetivos de alto nivel que se han tratado hasta el momento en la literatura consiste en maximizar la producción de destilado y la eficiencia energética del módulo. Como se mostró en Ruiz-Aguirre et al. (2017, 2018), para maximizar la producción de destilado tanto el caudal de alimentación como la temperatura a la entrada del canal de evaporación del módulo deben ser máximos, lo que se traduce en que los bucles de alto nivel deben tratar de maximizar estas variables. Para maximizar la eficiencia energética del módulo MD, se suele minimizar el índice de desempeño STEC o maximizar el GOR, de forma que se reduzca la cantidad de energía térmica necesaria para producir una unidad de volumen de destilado. Para minimizar el STEC o maximizar el GOR la temperatura a la entrada del canal de condensación también debe ser máxima (Ruiz-Aguirre et al., 2017, 2018) sin embargo, en la mayoría de módulos MD el caudal de alimentación debe ser mínimo (al contrario que para maximizar la producción de destilado). Este hecho da a lugar a problemas de optimización multiobjetivo en el caso de que se tenga en cuenta tanto la producción de destilado como el STEC, tal y como se presentó en Gil et al. (2018c).

4.2. Lazos de control básicos/clásicos

En esta subsección se revisan las arquitecturas de control de bajo nivel propuestas para plantas SMD. Se debe mencionar que la mayoría de las estructuras de control incluidas en este apartado utilizan lazos de control simples basados en controladores todo/nada y controladores Proporcionales, Integrales y Derivativos (PID) (Mercader et al., 2019). Del mismo modo, los sistemas de control desarrollados para los objetivos de bajo nivel en plantas SMD suelen incorporar controladores anticipativos los cuales se utilizan como complemento a los controladores por realimentación con el fin de mejorar el seguimiento a referencias y el rechazo a perturbaciones. Una descripción más detallada de estos tipos de sistemas de control se puede encontrar en Åström and Hägglund (2006).

En Chang et al. (2010) se presentó una arquitectura de control de bajo nivel compuesta por controladores todo/nada y controladores PI para mantener la temperatura de entrada al intercambiador de calor de un planta SMD a un nivel deseado a pesar de las perturbaciones de radiación. En Chen et al. (2012) se propusieron dos modos de control basados en controladores PI, uno para el día, el cual estaba encargado de controlar la temperatura a la entrada del intercambiador de calor manipulando el caudal de entrada por la parte del campo solar del tanque de almacenamiento, y otro para la noche, encargado de controlar dicha temperatura manipulando el caudal de entrada del tanque de almacenamiento térmico por la parte del intercambiador de calor. En Porrazzo et al. (2013) se presentó un enfoque de control más completo el cual utiliza un control anticipativo basado en un modelo de red neuronal que proporciona la referencia de caudal de alimentación del módulo MD en base a las condiciones de operación de las principales perturbaciones del sistema: irradiancia y temperatura del agua de alimentación. En la Figura 3 se presenta el diagrama esquemático de la arquitectura de control propuesta. Además, se debe destacar que esta arquitectura de control se probó experimentalmente en la planta SMD descrita en Cipollina et al. (2012), a diferencia de los dos trabajos mencionados previamente los cuales fueron desarrollados en simulación.

En Gil et al. (2018b) se presentó y probó experimentalmente en la planta SMD de la PSA una arquitectura de control completa para el sistema de generación de energía térmica de la instalación. La arquitectura de control tiene como objetivo principal mantener la temperatura a la entrada del intercambiador de calor a un nivel deseado. Para ello, se desarrollaron diferentes bucles de control clásicos encargados de controlar la temperatura a la salida del campo solar (bucle de control 1 en la Figura 4), la temperatura a la entrada del intercambiador de calor (bucle de control 3 en la Figura 4), y el caudal a la entrada del intercambiador de calor (bucle de control 4 en la Figura 4). Los bucles de control de las tres últimas variables mencionadas están basados en controladores PID clásicos. Por el contrario, para controlar la temperatura a la salida del campo solar se utilizó un esquema de control en cascada (ver Figura 5). En este esquema, el controlador esclavo tiene como objetivo controlar el caudal del campo solar actuando sobre el variador de frecuencia de la bomba del mismo. Por su parte, el controlador maestro se encarga de controlar la temperatura de salida del campo solar actuando sobre el caudal. Además, este esquema de control en cascada incluye un controlador anticipativo
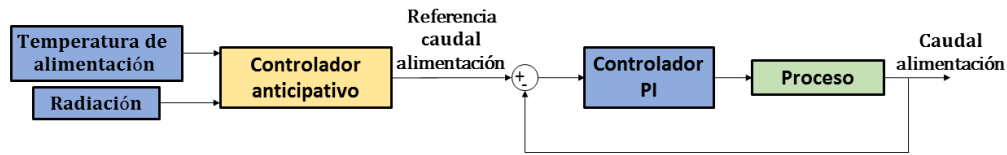
Figura 3: Adaptación del diagrama esquemático de la estructura de control propuesta en Porrazzo et al. (2013).
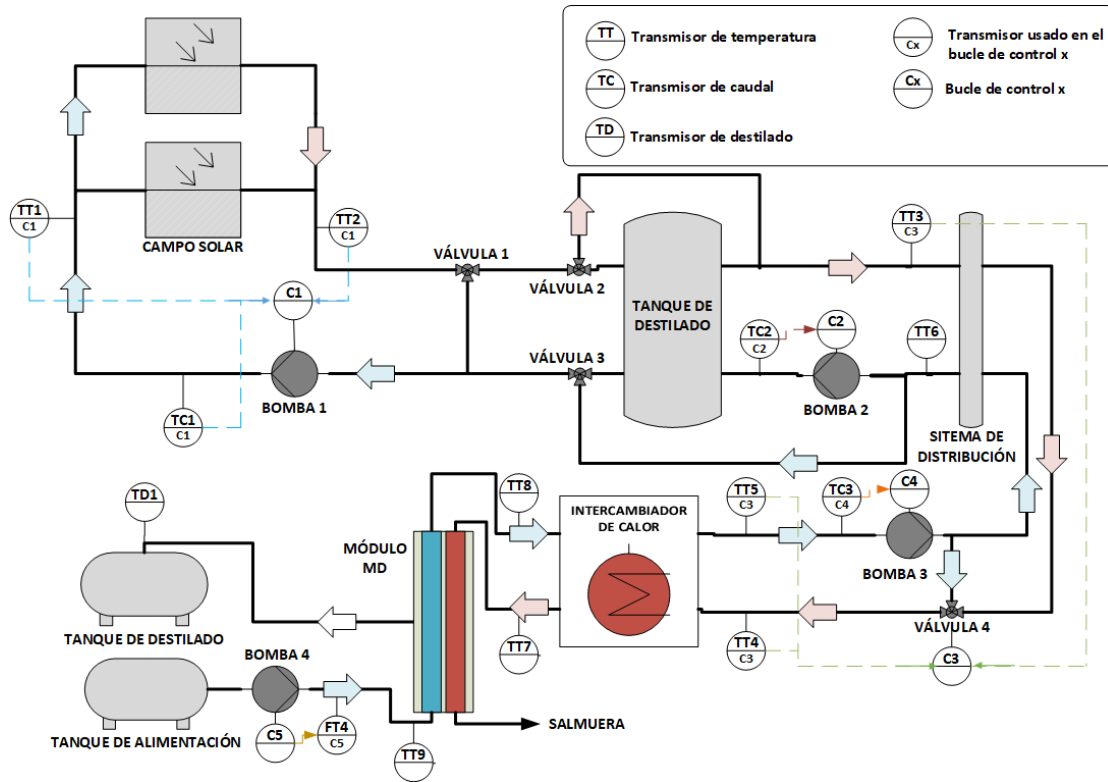

Figura 4: Adaptación del diagrama esquemático de la planta SMD de la PSA con los bucles de control de bajo nivel, adaptados de Gil et al. (2018a,b)

que tiene implementado un modelo basado en primeros principios del campo solar, de forma que se calcula el caudal de operación en base a las principales perturbaciones del proceso (irradiancia, temperatura ambiente y temperatura de entrada al campo) y la referencia de temperatura. También se debe mencionar que aunque el bucle de control de la temperatura a la entrada del intercambiador (bucle de control 3 en la Figura 4) está basado en un controlador PID el cual manipula la apertura de la válvula de tres vías en base a la referencia establecida, este se complementó con un controlador anticipativo para rechazar las perturbaciones de temperatura provenientes del sistema de distribución. Este controlador anticipativo también tiene implementado un modelo basado en primeros principios pero en este caso, el correspondiente a la mezcla que se produce en la válvula de tres vías y proporciona la apertura de la válvula en base a la referencia de temperatura y a las principales perturbaciones (TT3 y TT5 en la Figura 4). Por último, se debe mencionar que en este trabajo también se propuso un generador de referencias que calcula las referencias de cada uno de los bucles de control mencionados anteriormente en base a la temperatura deseada a la entrada del intercambiador de calor.

Hay que destacar que en la Figura 4 también se han incluido dos bucles de control de bajo nivel presentados en Gil et al.

(2018a) con el fin de que el lector pueda visualizar la estructura de control completa implementada en la planta piloto de la PSA. Estos bucles tienen como objetivo controlar el caudal a la salida del tanque de almacenamiento por la parte del sistema de distribución y el caudal de alimentación del módulo MD, bucles de control 2 y 5 respectivamente en la Figura 4. Estas variables se controlan actuando sobre el variador de frecuencia de las bombas 2 y 4 respectivamente (ver Figura 4).

4.3. Sistemas de control avanzados

La mayoría de sistemas de control avanzados presentados en el ámbito de MD utilizan la metodología de Control Predictivo Basado en Modelo (*Model Predictive Control*, MPC), y tratan de maximizar los objetivos de alto nivel mencionados anteriormente. La metodología MPC es especialmente adecuada para este tipos de objetivos ya que puede ser utilizada para controlar sistemas con dinámicas complejas, como la que presenta la planta SMD a causa de las perturbaciones de irradiancia. Además, incorpora intrínsecamente compensaciones para retardos y trata de forma natural el rechazo a perturbaciones, dos de los principales problemas presentes en plantas SMD. Una descripción más detallada de la estrategia MPC se puede encontrar en Camacho and Bordons (2004) y en Rubio et al. (2018). A
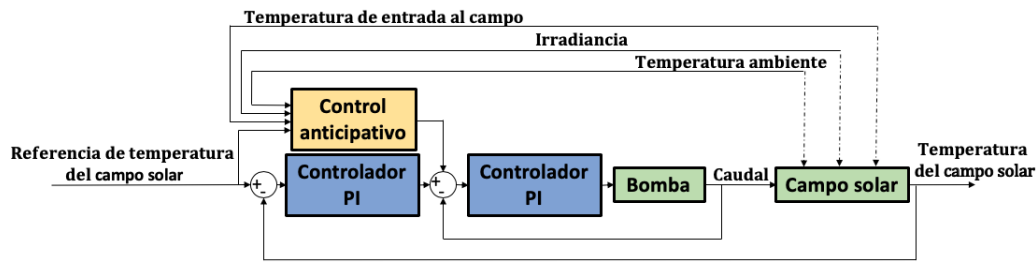
Figura 5: Adaptación del diagrama esquemático del controlador en cascada para la temperatura del campo solar presentado en Gil et al. (2018b).

continuación se muestran los principales enfoques de control aplicado a plantas SMD en este sentido.

En Karam and Laleg-Kirati (2015) se presentó un sistema de control en tiempo real basado en la metodología MPC y en la técnica de búsqueda del extremo de Newton. El objetivo de la estructura de control consiste en maximizar la producción de destilado actuando sobre el caudal de alimentación y teniendo en cuenta las perturbaciones de temperatura de alimentación y temperatura a la entrada al canal de evaporación del módulo. Los resultados en simulación mostraron cómo el controlador buscó en cada momento el máximo de la función objetivo (la máxima producción de destilado posible) dependiendo de la temperatura de la alimentación. En Gil et al. (2018a) se propuso un enfoque más complejo basado en una arquitectura de control jerárquica de dos capas que fue probada experimentalmente en la planta SMD de la PSA. El diagrama esquemático de la arquitectura de control se muestra en la Figura 6. En esta estructura, la capa superior está formada por un controlador MPC no lineal el cual calcula las referencias óptimas para la capa de control directa, formada por los bucles de control de bajo nivel propuestos en Gil et al. (2018b). Se debe mencionar que la capa superior incluye métodos de predicción de perturbaciones y que la capa inferior cuenta con controladores anticipativos para rechazar perturbaciones. Además, se propusieron dos modos de control para la operación eficiente de la instalación SMD en base a las condiciones de operación, al igual que un procedimiento de arranque automático para el campo solar y el módulo MD. La arquitectura de control fue probada tanto en simulación como en la planta real, utilizando tres funciones objetivo diferentes en la capa superior del controlador jerárquico, las cuales tratan de maximizar la producción de destilado, minimizar el STEC y la relación entre la producción de destilado y los costes de operación. Los resultados obtenidos mostraron cómo, en comparación con una operación manual, la producción de destilado se puede mejorar en 14-20 L/día (5-7 %), el consumo térmico se puede reducir entre 0.41-1.21 kWh/m^3 (0.5-1 %) y los costes se pueden disminuir entre 0.11-0.14 €/m^3 (9-10 %) dependiendo de la función objetivo utilizada en la capa superior.

En Gil et al. (2019b) se presentó una mejora al trabajo mencionado anteriormente desarrollando un controlador MPC híbrido, el cual incluye un modelo MLD de la instalación SMD. Este hecho permite considerar la naturaleza híbrida de la planta en la formulación del problema de control, teniendo en cuenta cambios entre modos de operación a lo largo del horizonte de predicción. El objetivo principal de la arquitectura de control consistió en maximizar el número de horas de operación de la

instalación así como la producción de destilado. El controlador se probó en simulación, utilizando el modelo de la planta SMD de la PSA. Los resultados mostraron cómo la operación se puede alargar en un 11 %, mientras que la producción de destilado se aumenta en un 1.40 % en comparación con operaciones manuales. En Bendevis et al. (2020) se propuso un controlador simplificado libre de modelo, obtenido a partir de una estrategia MPC. El controlador resultante incluye dos modos de operación, uno para el día y otro para la noche, en los que se utiliza un controlador bang-bang y un controlador con consignas fijas respectivamente. El objetivo de la técnica propuesta consistió en maximizar la producción de destilado de un módulo MD actuando sobre el caudal de alimentación del mismo. Los resultados en simulación mostraron cómo se puede aumentar la producción mensual en torno al 30 % en comparación con una operación manual. Por último, en Guo et al. (2020) se presentó una estrategia de control MPC basado en un observador de estados no lineal para maximizar la producción de destilado del módulo MD. Además, en el problema de optimización de la estrategia MPC se tuvieron en cuentan los costes económicos asociados a la operación de la bomba de alimentación del módulo MD.
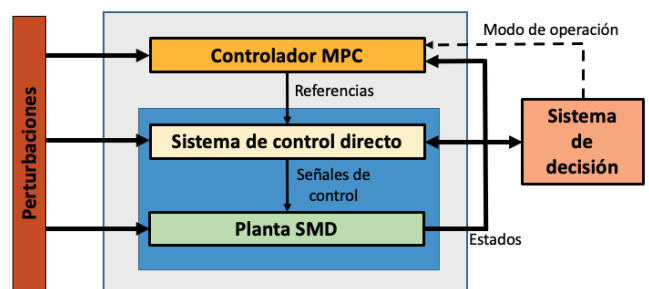
Figura 6: Adaptación del diagrama esquemático de la estructura de control jerárquica propuesta en Gil et al. (2018a).

5. Sistemas de control para aplicaciones MD industriales: Combinación entre plantas SMD e invernaderos

Como se ha mencionado anteriormente, la tecnología MD es interesante en campos donde otras tecnologías de separación no pueden ser aplicadas. Así, es especialmente relevante su habilidad para trabajar con soluciones de alimentación con alta concentración, lo que convierte a MD en una solución sostenible para tratar las salmueras producidas por otras tecnologías de desalación como la ósmosis inversa, lo cual fue ensayado

Tabla 2: Enfoques de control existentes hasta la fecha para plantas SMD.

Referencia	Tipo de estudio	Metodologías de control	Objetivos
Chang et al. (2010)	Simulación	Controladores ON/OFF Controladores PID	De bajo nivel: mantener una temperatura estable a la entrada del intercambiador de calor por la parte del campo solar.
Chen et al. (2012)	Simulación	Controladores PID	De bajo nivel: mantener una temperatura estable a la entrada del intercambiador de calor por la parte del campo solar.
Porrazzo et al. (2013)	Experimental	Controladores PID Controladores anticipativos	De bajo nivel: controlar el caudal de alimentación del módulo MD en base a las perturbaciones de radiación y temperatura de alimentación.
Gil et al. (2018b)	Experimental	Controladores PID Controladores anticipativos Controladores en cascada	De bajo nivel: mantener una temperatura estable a la entrada del intercambiador de calor por la parte del campo solar.
Karam and Laleg-Kirati (2015)	Simulación	Controlador MPC	De alto nivel: maximizar la producción de destilado
Gil et al. (2018a)	Experimental	Controlador jerárquico Controlador MPC no lineal Controladores PID	De alto nivel: maximizar producción de destilado, minimizar STEC y reducir la relación entre costes de operación y producción de destilado. *Los tres objetivos mencionados se probaron por separado.
Gil et al. (2019b)	Simulación	Controlador MPC híbrido	De alto nivel: maximizar la producción de destilado del módulo MD y sus horas de operación.
Bendevis et al. (2020)	Simulación	Controlador libre de modelo	De alto nivel: maximizar la producción de destilado del módulo MD.
Guo et al. (2020)	Simulación	Controlador MPC	De alto nivel: maximizar la producción de destilado del módulo MD.

a escala piloto en Gil et al. (2018c). Además, aparte de las características mencionadas en la sección 2.1, MD destaca ya que es menos complicada y barata de instalar que otras tecnologías, tiene pocos requerimientos de mantenimiento, y el ensuciamiento de la membrana es mínimo. Todas estas características permiten que las plantas SMD puedan ser totalmente automatizadas, desarrollando plantas de desalación de pequeño-medio tamaño autónomas, que puedan ser implantadas en lugares donde otras tecnologías de desalación no sean viables desde el punto de vista técnico o económico.

Una de las posibles aplicaciones de la tecnología MD consiste en alimentar cultivos en zonas aisladas y cercanas a la costa. Tal y como se propuso en Gil et al. (2019a), Almería (sureste de España) es una de las zonas potenciales de aplicación de dicha tecnología debido a la creciente escasez de agua que está sufriendo y las grandes superficies de cultivo bajo invernadero que tiene, las cuales se han convertido en el principal motor económico de la provincia. Sin embargo, para que la combinación entre plantas SMD e invernaderos sea exitosa, se deben desarrollar estrategias de control que gestionen en tiempo real la instalación SMD de acuerdo a las condiciones de irradiancia y a la demanda de agua variable de los cultivos. La Figura 7 presenta el diagrama esquemático del caso de estudio adoptado en Gil et al. (2019a) para analizar la viabilidad de este tipo de instalaciones operadas mediante técnicas de control avanzadas. Como se puede apreciar, en este tipo de instalaciones industriales hay una diferencia principal respecto a las plantas piloto

SMD estudiadas hasta el momento en la literatura (ver Figura 2); la unidad de desalación que ya no está compuesta por un solo módulo MD sino que se requieren múltiples módulos para satisfacer las necesidades de agua. Esto es debido a que la producción de destilado de los módulos MD comerciales actuales es relativamente baja, en torno a 60 L/h en condiciones de operación óptimas (Andrés-Mañas et al., 2020b). Así, las estrategias de control propuestas hasta ahora en la literatura centradas en objetivos de bajo nivel, como mantener la temperatura de entrada al intercambiador de calor por la parte del campo solar en niveles deseados, siguen siendo válidas. Por el contrario, la inclusión de múltiples módulos MD en la unidad de desalación cambia totalmente el paradigma de control de las estrategias propuestas para maximizar la producción de destilado o la eficiencia térmica en plantas piloto, lo que requiere la formulación de nuevos enfoques de control. En Gil et al. (2019a) se propuso un controlador distribuido MPC encargado de calcular los caudales óptimos de alimentación para cada módulo MD, tratando de minimizar el consumo térmico específico de la unidad de desalación al mismo tiempo que se satisface los requerimientos de agua del invernadero. En la formulación del controlador, cada módulo MD se consideró como un agente independiente de modo que, cada agente resuelve un problema MPC con los objetivos mencionados anteriormente, intercambiando información solamente con los agentes vecinos. Los resultados mostraron cómo el problema de control se resuelve de una forma más eficiente en términos temporales que con una estrategia centra-
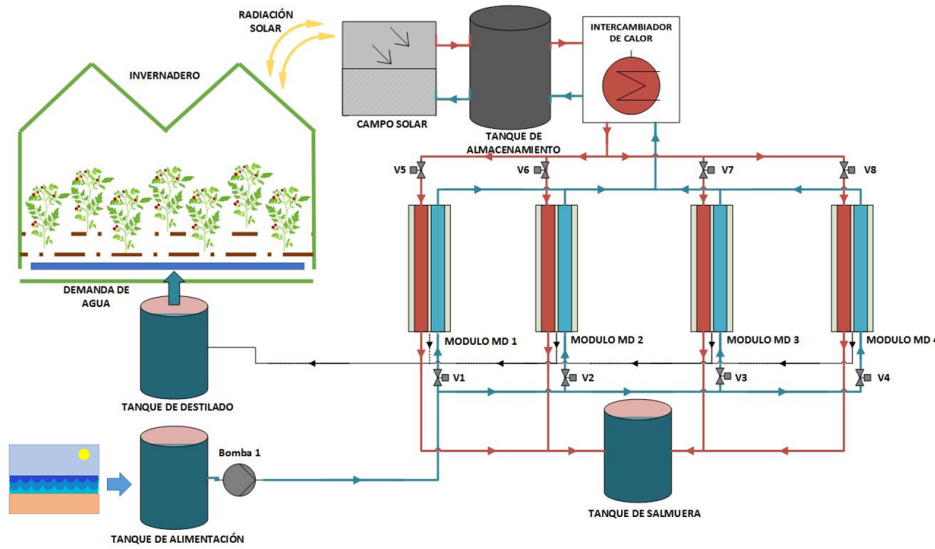
Figura 7: Adaptación del diagrama esquemático del caso de estudio utilizado en Gil et al. (2019a).

lizada y que, el consumo térmico de la planta se puede llegar a reducir en un 5 % de media respecto a operaciones manuales. Estos ahorros significan que para una superficie de 8 ha, se puede llegar a ahorrar 50 MWh de energía térmica por campaña, lo cual puede ser muy relevante para tener en cuenta en la fase de diseño de la planta y en la operación diaria de la misma.

No obstante, los resultados presentados en Gil et al. (2019a) se pueden seguir mejorando si se introducen variables binarias en el problema de control que permitan encender y apagar los módulos MD dependiendo de los requerimientos de agua del invernadero. El problema de control MPC a resolver en ese caso se puede formular de forma general como:

$$\text{mín } J = \sum_{i=1}^{4} \sum_{j=1}^{N} \text{STEC}_i(t + j|t). \tag{5}$$

Sujeto a:

$$\sum_{i=1}^{4} \sum_{j=1}^{N} P_i(t + j|t) \leq \sum_{j=1}^{N} D(t + j|t), \tag{6}$$

$\forall i = 1, 2, 3, 4 \, y \, \forall j = 0, \ldots, N - 1$:

$$\delta_i(t + j) \cdot Q_{min} \leq Q_i(t + j) \leq \delta_i(t + j) \cdot Q_{max} \tag{7}$$

$$\delta_i(t + j) \in \{0, 1\}, \tag{8}$$

donde $\text{STEC}_i(t + j|t)$ es el STEC para cada uno de los módulo i, con $i = 1, 2, 3, 4$, de los mostrados en la Figura 7, calculado para el instante de tiempo $t + j$ con la información disponible en el instante t. $P_i(t + j|t)$ es la producción de destilado de cada módulo en L/h y $D(t + j|t)$ la demanda de agua del invernadero en L/h. Q_{min} y Q_{max} son los rangos de caudal máximo y mínimo de cada módulos MD los cuales, para los módulos utilizados (los mismos que en Gil et al. (2019a)), son 400 y 600 L/h respectivamente y Q_i es el caudal de agua de alimentación del módulo i. Las variables δ_i están referidas a la posición 0-1 de las válvulas V1, V2, V3 y V4 de la Figura 7, donde 0 significa válvula cerrada, es decir módulo apagado y 1, módulo encendido. Por último N es el horizonte de predicción. Como se puede apreciar, el problema de control consiste en minimizar el valor

del STEC total de la planta, asegurando que la producción de la planta MD sea mayor que los requerimientos de agua del invernadero. Se debe resaltar que el STEC para cada módulo se calcula de acuerdo a la ecuación (3) mientras que la producción de destilado con los modelos RSM presentados en Gil et al. (2019a). Del mismo modo, se debe remarcar que las variables de decisión del problema son Q_i y δ_i, $\forall i = 1, 2, 3, 4$. Además, es importante destacar que si δ_i es igual a 0 entonces, tanto el STEC como la producción de destilado del módulo i también lo son. Nótese que el problema de optimización resultante es un problema de Optimización Entera Mixta No Lineal (*Mixed Integer Non Linear Optimization*, MINLP).

Con el objetivo de visualizar los resultados que se pueden llegar a conseguir se ha realizado una simulación representativa con datos reales de temperatura y demanda de agua obtenidos de la PSA y la Estación Experimental de la Fundación Cajamar (ubicada también en la provincia de Almería) respectivamente. Además, se han comparado los resultados obtenidos con una operación manual con consignas estáticas de 500 L/h para el agua de alimentación de cada módulo y con todos los módulos encendidos en todo momento. Los resultados se presentan en la Figura 8.

En la Figura 8-2 se puede apreciar, que los ahorros de energía térmica son considerables al aplicar la técnica de control cuando se consideran demandas de agua variables como la del invernadero. El STEC medio de la operación automática es de 412.80 kWh/m^3, mientras que el de la operación manual de 1142.2 kWh/m^3. Se puede observar cómo el mayor ahorro se produce al inicio y final del día ya que el controlador solo arranca los módulos necesarios para cubrir la demanda de agua. Este hecho puede ser muy relevante en aplicaciones industriales, ya que permite no tener que sobredimensionar el campo solar o la fuente de energía térmica, lo que supone un ahorro económico en la fase de diseño. Del mismo modo, en la Figura 8-3 se puede ver cómo la demanda de agua del invernadero se satisface en todo momento.

Se debe remarcar que el caso simulado con cuatro módulos MD y un invernadero de tamaño 392 m^2 corresponde a un ca-
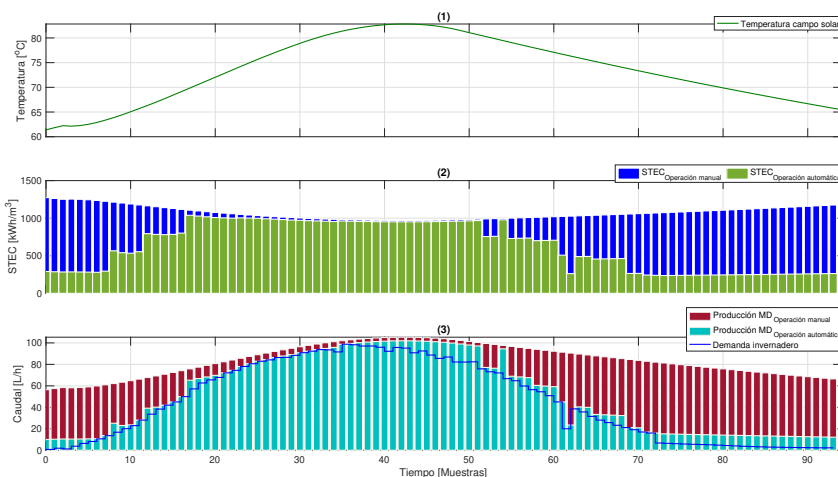
Figura 8: Comparación de resultados entre una operación automática y una manual.

so de estudio a escala piloto. Información más detallada acerca del caso de estudio se puede encontrar en el trabajo Gil et al. (2019a). Además, se ha utilizado un horizonte de predicción pequeño de $N = 5$ con un tiempo de muestreo de 10 min y los modelos con los que se trabajan son estáticos de acuerdo a la metodología RSM. En casos reales con superficies de cultivos más grandes, el número de módulos requeridos aumenta considerablemente, por lo que aumenta también el número de variables binarias en el problema y, por tanto, los problemas combinatorios y de no convexidades asociados a los problemas de optimización MINLP.

6. Retos futuros

Aunque en la bibliografía especializada se pueden encontrar una gran cantidad de contribuciones científicas relacionados con el modelado y, en menor medida, con el control en MD, existen numerosos retos futuros y brechas por cubrir en la literatura en ambas áreas, las cuales se resumen a continuación.

En lo que concierne a los modelos basados en datos experimentales, los trabajos futuros deben estar centrados en modelar módulos comerciales considerando la eficiencia térmica de estos como un parámetro de salida del modelo. La eficiencia térmica es un parámetro crucial en estos tipos de procesos alimentados con energía térmica y además, destaca como uno de los puntos más débiles de la tecnología. Por esta razón, es determinante incluir este parámetro como salida de los modelos, pudiendo así analizar su comportamiento bajo diferentes condiciones de operación y permitiendo que se tenga en cuenta a la hora de diseñar plantas MD, lo cual puede ayudar a la correcta implementación industrial de la tecnología. Del mismo modo, se debe incluir la concentración del agua de alimentación como parámetro de entrada de los modelos, lo cual ha sido brevemente discutido en la literatura hasta el momento. Este hecho permite estudiar la aplicación de módulos MD para tratar salmueras procedentes de otras plantas de desalación, una de las ramas de aplicación con más futuro de la tecnología MD. Respecto a los modelos basados en primeros principios, la principal brecha observada radica en que estos tipos de modelos han sido

principalmente validados a escala de laboratorio. Las simplificaciones asumidas a la hora de realizar estos modelos hacen que su validación con módulos comerciales sea difícil de llevar a cabo. Así, se requieren nuevos trabajos de investigación dedicados a desarrollar modelos más detallados y precisos que puedan ser ajustados y calibrados para módulos MD comerciales. Además, de manera general es importante destacar la necesidad de definir una norma enfocada a homogeneizar la calidad de los resultados evaluados durante las campañas experimentales, tanto para procesos de obtención de modelos como para la propia evaluación de los módulos MD empleados. Esta norma debería especificar bajo qué criterios se pueden dar como válidos los valores experimentales obtenidos y su aplicación daría como resultado la garantía de los resultados proporcionados.

Por otra parte, las líneas de investigación abiertas relacionadas con el control automático de procesos MD son aún mayores ya que, tal y como se ha podido ver a lo largo del presente artículo, se han presentado muy pocos trabajos en este ámbito hasta el momento. En este sentido, los tipos de trabajos de control se pueden dividir en dos partes de acuerdo a los objetivos de control que se persiguen. Desde el punto de vista de objetivos de bajo nivel los trabajos futuros son más limitados, ya que esta rama se centra principalmente en controlar el sistema de generación de energía térmica de la instalación SMD, el cual está basado en un campo solar térmico. Para este tipo de sistemas se han presentado numerosas publicaciones detallando arquitecturas de control precisas y testadas experimentalmente (Camacho et al., 2012; Rubio et al., 2018). Por el contrario, se han presentado muy pocos trabajos centrados en objetivos de alto nivel como maximizar la producción de destilado o la eficiencia térmica del módulo. Además, en los enfoques propuestos, estos índices de desempeño se tratan por separado los cuales en la mayoría de casos requieren condiciones de operación contrapuestas (Gil et al., 2018c). Por lo que uno de los trabajos que quedan por abordar consiste en desarrollar algoritmos de control multiobjetivo que gestionen en tiempo real (Rodríguez-Blanco et al., 2018) la instalación SMD tratando de maximizar ambos objetivos. Del mismo modo, se requiere la inclusión de términos económicos en la estrategias de control de forma que

se minimicen los costes de producción del agua desalada, lo cual solo ha sido tratado en Gil et al. (2018a) donde solo se tuvieron en cuenta los costes de operación del sistema de generación de energía térmica. También se requieren trabajos de control centrados en gestionar instalaciones industriales MD ya que, como se ha visto para el caso de aplicación de MD para el riego de cultivos, en estos sistemas se dispone de múltiples módulos MD. En este sentido, el único trabajo de control presentado hasta la fecha es el propuesto en Gil et al. (2019a) en el cual se gestionó el caudal de alimentación en base a la demanda de agua del invernadero y tratando de minimizar el STEC. Sin embargo, también se pueden introducir variables binarias en este tipo de enfoques de control de modo que en cada momento únicamente los módulos estrictamente necesarios para satisfacer la demanda de agua estén encendidos, ahorrando así tanto energía térmica como costes de operación como se ha mostrado en la simulación incluida en el apartado anterior. En estas aplicaciones se abre otra línea de trabajo de control ya que, si se trabajan con demandas de aguas grandes el número de módulos MD requeridos también lo será. Por tanto, el numero de variables de control aumenta a medida que aumenta el número de módulos MD de la unidad de desalación, requiriendo algoritmos de control distribuidos (Gil et al., 2019a) o algoritmos para descomponer enfoques centralizados de forma que los problemas de control se puedan resolver de forma sencilla y rápida. Por último, cabe destacar que también se necesitan enfoques de control centrados en las demás aplicaciones industriales de la tecnología MD como es el caso del tratamiento de salmueras. En este tipo de procesos, aparte de las perturbaciones clásicas del módulo MD como temperatura de entrada al canal de evaporación y temperatura de la solución de alimentación, se añade una nueva, la concentración de la solución de alimentación que va aumentando a lo largo de la operación hasta que se consiguen separar completamente las partículas volátiles y no volátiles de esta (Ghaffour et al., 2019).

7. Conclusiones

Este trabajo ha presentado una revisión del estado del arte de las metodologías de modelado y control propuestas para sistemas MD. Se muestra cómo esta tecnología presenta una serie de características interesantes que permiten cubrir nichos de aplicación a los que no pueden acceder otros procesos de separación, como son el desarrollo de plantas de desalación de pequeño o mediado tamaño para lugares aislados o el tratamiento de soluciones de alimentación con alta concentración. Sin embargo, para que estas aplicaciones se lleguen a implementar a nivel industrial, se requiere el desarrollo de modelos precisos y de algoritmos de control adecuados para su correcta operación. En base a la revisión de la literatura llevada a cabo en este sentido se concluye que:

1. Es necesario el desarrollo de modelos basados en datos experimentales que consideren el rendimiento térmico del módulo MD como variable de salida y la concentración de la solución de alimentación como variable de entrada, de forma que se puedan tener en cuenta estas variables en el proceso de diseño de la planta y en las estrategias de control formuladas para su operación.

2. Se requiere el desarrollo de modelos basados en primeros principios para módulos MD comerciales. La mayoría de los enfoques presentados hasta el momento se validan en módulos a escala de laboratorio cuyos resultados no pueden extrapolarse exitosamente a módulos comerciales.

3. En los enfoques de control aún queda un largo camino por recorrer ya que hasta el momento este tema ha sido tratado escasamente en la literatura. Se precisan enfoques de control multiobjetivo para maximizar la producción de destilado y la eficiencia energética de los módulos MD en operaciones en tiempo real, formulaciones de control que tengan en cuentan criterios económicos y sobre todo, estrategias de control dirigidas a mejorar el rendimiento de la tecnología en las aplicaciones industriales mencionadas con antelación.

Agradecimientos

Referencias

Abdallah, S. B., Frikha, N., Gabsi, S., 2013. Simulation of solar vacuum membrane distillation unit. Desalination 324, 87–92.
    DOI: 10.1016/j.desal.2013.06.001
Alkhudhiri, A., Darwish, N., Hilal, N., 2012. Membrane distillation: A comprehensive review. Desalination 287, 2–18.
    DOI: 10.1016/j.desal.2013.06.001
Alsaadi, A. S., Ghaffour, N., Li, J.-D., Gray, S., Francis, L., Maab, H., Amy, G. L., 2013. Modeling of air-gap membrane distillation process: A theoretical and experimental study. Journal of Membrane Science 445, 53–65.
    DOI: 10.1016/j.memsci.2013.05.049
Amigo, J., Urtubia, R., Suárez, F., 2018. Exploring the interactions between hydrodynamics and fouling in membrane distillation systems–A multiscale approach using CFD. Desalination 444, 63–74.
    DOI: 10.1016/j.desal.2018.07.009
Andrés-Mañas, J., Roca, L., Ruiz-Aguirre, A., Acién, F., Gil, J. D., Zaragoza, G., 2020a. Application of solar energy to seawater desalination in a pilot system based on vacuum multi-effect membrane distillation. Applied Energy 258, 114068.
    DOI: 10.1016/j.apenergy.2019.114068
Andrés-Mañas, J., Ruiz-Aguirre, A., Acién, F., Zaragoza, G., 2020b. Performance increase of membrane distillation pilot scale modules operating in vacuum-enhanced air-gap configuration. Desalination 475, 114202.
    DOI: 10.1016/j.desal.2019.114202
Åström, K. J., Hägglund, T., 2006. Advanced PID control. ISA-The Instrumentation, Systems, and Automation Society Research Triangle.
Banat, F., Jwaied, N., Rommel, M., Koschikowski, J., Wieghaus, M., 2007. Performance evaluation of the "large SMADES" autonomous desalination solar-driven membrane distillation plant in Aqaba, Jordan. Desalination 217 (1-3), 17–28.
    DOI: 10.1016/j.desal.2006.11.027
Bendevis, P., Karam, A., Laleg-Kirati, T.-M., 2020. Optimal model-free control of solar thermal membrane distillation system. Computers & Chemical Engineering 133, 106622.
    DOI: 10.1016/j.compchemeng.2019.106622
Boubakri, A., Hafiane, A., Bouguecha, S. A. T., 2014. Application of response surface methodology for modeling and optimization of membrane distillation desalination process. Journal of Industrial and Engineering Chemistry 20 (5), 3163–3169.
    DOI: 0.1016/j.jiec.2013.11.060

Bouguecha, S. T., Boubakri, A., Aly, S. E., Al-Beirutty, M. H., Hamdi, M. M., 2016. Optimization of permeate flux produced by solar energy driven membrane distillation process using central composite design approach. Water Science and Technology 74 (1), 87–98.
DOI: 10.2166/wst.2016.126

Camacho, E. F., Berenguel, M., Rubio, F. R., Martínez, D., 2012. Control of Solar Energy Systems. Springer.

Camacho, E. F., Bordons, C., 2004. Model Predictive Control. Springer-Verlag Ltd, London.

Cao, W., Liu, Q., Wang, Y., Mujtaba, I. M., 2016. Modeling and simulation of VMD desalination process by ANN. Computers & Chemical Engineering 84, 96–103.
DOI: 10.1016/j.compchemeng.2015.08.019

Chafidz, A., Al-Zahrani, S., Al-Otaibi, M. N., Hoong, C. F., Lai, T. F., Prabu, M., 2014. Portable and integrated solar-driven desalination system using membrane distillation for arid remote areas in Saudi Arabia. Desalination 345, 36–49.
DOI: 10.1016/j.desal.2014.04.017

Chang, H., Wang, G.-B., Chen, Y.-H., Li, C.-C., Chang, C.-L., 2010. Modeling and optimization of a solar driven membrane distillation desalination system. Renewable Energy 35 (12), 2714–2722.
DOI: 10.1016/j.renene.2010.04.020

Chen, Y.-H., Li, Y.-W., Chang, H., 2012. Optimal design and control of solar driven air gap membrane distillation desalination systems. Applied Energy 100, 193–204.
DOI: 10.1016/j.apenergy.2012.03.003

Cheng, D., Li, N., Zhang, J., 2018. Modeling and multi-objective optimization of vacuum membrane distillation for enhancement of water productivity and thermal efficiency in desalination. Chemical Engineering Research and Design 132, 697–713.
DOI: 10.1016/j.cherd.2018.02.017

Cipollina, A., Di Sparti, M., Tamburini, A., Micale, G., 2012. Development of a membrane distillation module for solar energy seawater desalination. Chemical Engineering Research and Design 90 (12), 2101–2121.
DOI: 10.1016/j.cherd.2012.05.021

Demuth, H. B., Beale, M. H., De Jess, O., Hagan, M. T., 2014. Neural network design. PWS Publishing Co.

DeNicola, E., Aburizaiza, O. S., Siddique, A., Khwaja, H., Carpenter, D. O., 2015. Climate change and water scarcity: The case of Saudi Arabia. Annals of Global Health 81 (3), 342–353.
DOI: 10.1016/j.aogh.2015.08.005

Deshmukh, A., Boo, C., Karanikola, V., Lin, S., Straub, A. P., Tong, T., Warsinger, D. M., Elimelech, M., 2018. Membrane distillation at the water-energy nexus: Limits, opportunities, and challenges. Energy & Environmental Science 11 (5), 1177–1196.
DOI: 10.1039/c8ee00291f

Ding, Z., Liu, L., El-Bourawi, M. S., Ma, R., 2005. Analysis of a solar-powered membrane distillation system. Desalination 172 (1), 27–40.
DOI: 10.1016/j.desal.2004.06.195

Dow, N., Duke, M., Zhang, J., O'Rielly, T., Li, J., Gray, S., Ostarcevic, E., Atherton, P., 2010. Demonstration of solar driven membrane distillation in remote Victoria. In: Australian Water Association (AWA) Ozwater Conference and Exhibition, Brisbane, Australia. Vol. 810.

Duffie, J. A., Beckman, W. A., 2013. Solar engineering of thermal processes. John Wiley & Sons.

Eleiwi, F., Ghaffour, N., Alsaadi, A. S., Francis, L., Laleg-Kirati, T. M., 2016. Dynamic modeling and experimental validation for direct contact membrane distillation (DCMD) process. Desalination 384, 1–11.
DOI: 10.1016/j.desal.2016.01.004

Elzahaby, A. M., Kabeel, A., Bassuoni, M., Elbar, A. R. A., 2016. Direct contact membrane water distillation assisted with solar energy. Energy Conversion and Management 110, 397–406.
DOI: 10.1016/j.enconman.2015.12.046

Esfandiari, A., Monjezi, A. H., Rezakazemi, M., Younas, M., 2019. Computational fluid dynamic modeling of water desalination using low-energy continuous direct contact membrane distillation process. Applied Thermal Engineering 163, 114391.
DOI: 10.1016/j.applthermaleng.2019.114391

Fadhil, S., Alsalhy, Q. F., Makki, H. F., Ruby-Figueroa, R., Marino, T., Criscuoli, A., Macedonio, F., Giorno, L., Drioli, E., Figoli, A., 2019. Seawater desalination using PVDF-HFP membrane in DCMD process: Assessment of operating condition by response surface method. Chemical Engineering Communications 206 (2), 237–246.
DOI: 10.1080/00986445.2018.1483349

Gabsi, S., Frikha, N., Chaouachi, B., 2013. Performance of a solar vacuum membrane distillation pilot plant, for seawater desalination in Mahares, Tunisia. International Journal of Water Resources and Arid Environments 2 (4), 213–217.

Ghaffour, N., Soukane, S., Lee, J.-G., Kim, Y., Alpatova, A., 2019. Membrane distillation hybrids for water production and energy efficiency enhancement: A critical review. Applied Energy 254, 113698.
DOI: 10.1016/j.apenergy.2019.113698

Gil, J. D., Álvarez, J., Roca, L., Sánchez-Molina, J., Berenguel, M., Rodríguez, F., 2019a. Optimal thermal energy management of a distributed energy system comprising a solar membrane distillation plant and a greenhouse. Energy Conversion and Management 198, 111791.
DOI: 10.1016/j.enconman.2019.111791

Gil, J. D., Mendes, P. R., Andrade, G., Roca, L., Normey-Rico, J. E., Berenguel, M., 2019b. Hybrid NMPC applied to a solar-powered membrane distillation system. IFAC-PapersOnLine 52 (1), 124 – 129, 12th IFAC Symposium on Dynamics and Control of Process Systems, including Biosystems DYCOPS 2019.
DOI: 10.1016/j.ifacol.2019.06.048

Gil, J. D., Roca, L., Ruiz-Aguirre, A., Zaragoza, G., Berenguel, M., 2018a. Optimal operation of a solar membrane distillation pilot plant via nonlinear model predictive control. Computers & Chemical Engineering 109, 151–165.
DOI: 10.1016/j.compchemeng.2017.11.012

Gil, J. D., Roca, L., Zaragoza, G., Berenguel, M., 2018b. A feedback control system with reference governor for a solar membrane distillation pilot facility. Renewable Energy 120, 536–549.
DOI: 10.1016/j.renene.2017.12.107

Gil, J. D., Ruiz-Aguirre, A., Roca, L., Zaragoza, G., Berenguel, M., 2018c. Prediction models to analyse the performance of a commercial-scale membrane distillation unit for desalting brines from RO plants. Desalination 445, 15–28.
DOI: 10.1016/j.desal.2018.07.022

González, D., Amigo, J., Suárez, F., 2017. Membrane distillation: Perspectives for sustainable and improved desalination. Renewable and Sustainable Energy Reviews 80, 238–259.
DOI: 10.1016/j.rser.2017.05.078

Guillén-Burrieza, E., Alarcón-Padilla, D.-C., Palenzuela, P., Zaragoza, G., 2015. Techno-economic assessment of a pilot-scale plant for solar desalination based on existing plate and frame MD technology. Desalination 374, 70–80.
DOI: 10.1016/j.desal.2015.07.014

Guillén-Burrieza, E., Blanco, J., Zaragoza, G., Alarcón, D.-C., Palenzuela, P., Ibarra, M., Gernjak, W., 2011. Experimental analysis of an air gap membrane distillation solar desalination pilot system. Journal of Membrane Science 379 (1-2), 386–396.
DOI: 10.1016/j.memsci.2011.06.009

Guo, X., Albalawi, F., Laleg-Kirati, T.-M., 2020. Observer-based economic model predictive control for direct contact membrane distillation. Chemical Engineering Research and Design 156, 86–99.
DOI: 10.1016/j.cherd.2020.01.027

Gustafson, R. D., Murphy, J. R., Achilli, A., 2016. A stepwise model of direct contact membrane distillation for application to large-scale systems: Experimental results and model predictions. Desalination 378, 14–27.
DOI: 0.1016/j.desal.2015.09.022

Hayer, H., Bakhtiari, O., Mohammadi, T., 2015. Simulation of momentum, heat and mass transfer in direct contact membrane distillation: A computational fluid dynamics approach. Journal of Industrial and Engineering Chemistry 21, 1379–1382.
DOI: 10.1016/j.jiec.2014.06.009

He, Q., Li, P., Geng, H., Zhang, C., Wang, J., Chang, H., 2014. Modeling and optimization of air gap membrane distillation system for desalination. Desalination 354, 68–75.
DOI: 10.1016/j.desal.2014.09.022

Hill, W. J., Hunter, W. G., 1966. A review of response surface methodology: A literature survey. Technometrics 8 (4), 571–590.

Hitsov, I., Eykens, L., De Schepper, W., De Sitter, K., Dotremont, C., Nopens, I., 2017. Full-scale direct contact membrane distillation (DCMD) model including membrane compaction effects. Journal of Membrane Science 524, 245–256.
DOI: 10.1016/j.memsci.2016.11.044

Hitsov, I., Maere, T., De Sitter, K., Dotremont, C., Nopens, I., 2015. Modelling approaches in membrane distillation: A critical review. Separation and Purification Technology 142, 48–64.

DOI: 10.1016/j.seppur.2014.12.026

Jones, E., Qadir, M., van Vliet, M. T., Smakhtin, V., Kang, S.-m., 2018. The state of desalination and brine production: A global outlook. Science of the Total Environment 657, 1343–1356.
DOI: 10.1016/j.scitotenv.2018.12.076

Karam, A. M., Alsaadi, A. S., Ghaffour, N., Laleg-Kirati, T. M., 2017. Analysis of direct contact membrane distillation based on a lumped-parameter dynamic predictive model. Desalination 402, 50–61.
DOI: 0.1016/j.desal.2016.09.002

Karam, A. M., Laleg-Kirati, T. M., 2015. Real time optimization of solar powered direct contact membrane distillation based on multivariable extremum seeking. In: 2015 IEEE Conference on Control Applications (CCA). IEEE, pp. 1618–1623.
DOI: 10.1109/CCA.2015.7320841

Karam, A. M., Laleg-Kirati, T. M., 2016. Electrical equivalent thermal network for direct contact membrane distillation modeling and analysis. Journal of Process Control 47, 87–97.
DOI: 10.1016/j.jprocont.2016.08.001

Karanikola, V., Corral, A. F., Jiang, H., Sáez, A. E., Ela, W. P., Arnold, R. G., 2015. Sweeping gas membrane distillation: numerical simulation of mass and heat transfer in a hollow fiber membrane module. Journal of Membrane Science 483, 15–24.
DOI: 10.1016/j.memsci.2015.02.010

Khalifa, A. E., Lawal, D. U., 2016. Application of response surface and Taguchi optimization techniques to air gap membrane distillation for water desalination: A comparative study. Desalination and Water Treatment 57 (59), 28513–28530.
DOI: 0.1080/19443994.2016.1189850

Khayet, M., Cojocaru, C., 2012a. Air gap membrane distillation: Desalination, modeling and optimization. Desalination 287, 138–145.
DOI: 10.1016/j.desal.2011.09.017

Khayet, M., Cojocaru, C., 2012b. Artificial neural network modeling and optimization of desalination by air gap membrane distillation. Separation and Purification Technology 86, 171–182.
DOI: 10.1016/j.seppur.2011.11.001

Khayet, M., Cojocaru, C., 2013. Artificial neural network model for desalination by sweeping gas membrane distillation. Desalination 308, 102–110.
DOI: 10.1016/j.desal.2012.06.023

Khayet, M., Cojocaru, C., García-Payo, C., 2007. Application of response surface methodology and experimental design in direct contact membrane distillation. Industrial & Engineering Chemistry Research 46 (17), 5673–5685.
DOI: 10.1021/ie070446p

Khayet, M., Matsuura, T., 2011. Membrane distillation: Principles and applications. Elsevier.

Kim, Y., Thu, K., Choi, S.-H., 2015. Solar-assisted multi-stage vacuum membrane distillation system with heat recovery unit. Desalination 367, 161–171.
DOI: 10.1016/j.desal.2015.04.003

Koschikowski, J., Wieghaus, M., Rommel, M., Ortin, V. S., Suarez, B. P., Rodríguez, J. R. B., 2009. Experimental investigations on solar driven stand-alone membrane distillation systems for remote areas. Desalination 248 (1-3), 125–131.
DOI: 10.1016/j.desal.2008.05.047

Luo, A., Lior, N., 2016. Critical review of membrane distillation performance criteria. Desalination and Water Treatment 57 (43), 20093–20140.
DOI: 10.1080/19443994.2016.1152637

Mercader, P., Cánovas, C., Baños, A., 2019. Control PID multivariable de una caldera de vapor. Revista Iberoamericana de Automática e Informática industrial 16 (1), 15–25.
DOI: 10.4995/riai.2018.9034

Miladi, R., Frikha, N., Kheiri, A., Gabsi, S., 2019. Energetic performance analysis of seawater desalination with a solar membrane distillation. Energy Conversion and Management 185, 143–154.
DOI: 10.1016/j.enconman.2019.02.011

Mohammadi, T., Kazemi, P., Peydayesh, M., 2015. Optimization of vacuum membrane distillation parameters for water desalination using Box–Behnken design. Desalination and Water Treatment 56 (9), 2306–2315.
DOI: 10.1080/19443994.2014.961173

Perfilov, V., Fila, V., Marcano, J. S., 2018. A general predictive model for sweeping gas membrane distillation. Desalination 443, 285–306.
DOI: 10.1016/j.desal.2018.06.007

Porrazzo, R., Cipollina, A., Galluzzo, M., Micale, G., 2013. A neural network-based optimizing control system for a seawater-desalination solar-powered membrane distillation unit. Computers & Chemical Engineering 54, 79–96.

DOI: 10.1016/j.compchemeng.2013.03.015

Rodríguez-Blanco, T., Sarabia, D., de Prada, C., 2018. Optimización en tiempo real utilizando la metodología de adaptación de modificadores. Revista Iberoamericana de Automática e Informática industrial 15 (2), 133–144.
DOI: 10.4995/riai.2017.8846

Rubio, F. R., Navas, S. J., Ollero, P., Lemos, J. M., Ortega, M. G., 2018. Control óptimo aplicado a campos de colectores solares distribuidos. Revista Iberoamericana de Automática e Informática industrial 15 (3), 327–338.
DOI: 10.4995/riai.2018.8944

Ruiz-Aguirre, A., Alarcón-Padilla, D.-C., Zaragoza, G., 2015. Productivity analysis of two spiral-wound membrane distillation prototypes coupled with solar energy. Desalination and Water Treatment 55 (10), 2777–2785.
DOI: 10.1080/19443994.2014.946711

Ruiz-Aguirre, A., Andrés-Mañas, J., Fernández-Sevilla, J., Zaragoza, G., 2017. Modeling and optimization of a commercial permeate gap spiral wound membrane distillation module for seawater desalination. Desalination 419, 160–168.
DOI: 10.1016/j.desal.2017.06.019

Ruiz-Aguirre, A., Andrés-Mañas, J., Fernández-Sevilla, J., Zaragoza, G., 2018. Experimental characterization and optimization of multi-channel spiral wound air gap membrane distillation modules for seawater desalination. Separation and Purification Technology 205, 212–222.
DOI: doi:10.1016/j.seppur.2018.05.044

Ruiz-Aguirre, A., Andrés-Mañas, J. A., Zaragoza, G., 2019. Evaluation of permeate quality in pilot scale membrane distillation systems. Membranes 9 (6), 69.
DOI: 10.3390/membranes9060069

Schewe, J., Heinke, J., Gerten, D., Haddeland, I., Arnell, N. W., Clark, D. B., Dankers, R., Eisner, S., Fekete, B. M., Colón-González, F. J., et al., 2014. Multimodel assessment of water scarcity under climate change. Proceedings of the National Academy of Sciences 111 (9), 3245–3250.
DOI: 10.1073/pnas.1222460110

Shirazian, S., Alibabaei, M., 2017. Using neural networks coupled with particle swarm optimization technique for mathematical modeling of air gap membrane distillation (AGMD) systems for desalination process. Neural Computing and Applications 28 (8), 2099–2104.
DOI: 10.1007/s00521-016-2184-0

Tang, N., Zhang, H., Wang, W., 2011. Computational fluid dynamics numerical simulation of vacuum membrane distillation for aqueous NaCl solution. Desalination 274 (1-3), 120–129.
DOI: 10.1016/j.desal.2011.01.078

Tavakolmoghadam, M., Safavi, M., 2012. An optimized neural network model of desalination by vacuum membrane distillation using genetic algorithm. Procedia Engineering 42, 106–112.
DOI: 10.1016/j.proeng.2012.07.400

Thomas, N., Mavukkandy, M. O., Loutatidou, S., Arafat, H. A., 2017. Membrane distillation research & implementation: Lessons from the past five decades. Separation and Purification Technology 189, 108–127.
DOI: 10.1016/j.seppur.2017.07.069

Wang, P., Chung, T.-S., 2015. Recent advances in membrane distillation processes: Membrane development, configuration design and application exploring. Journal of Membrane Science 474, 39–56.
DOI: 10.1016/j.memsci.2014.09.016

WHO, 2011. Guidelines for drinking-water quality. World Health Organization, Chronicle 38 (4), 104–8.

Winter, D., 2015. Membrane distillation: A thermodynamic, technological and economic analysis. Shaker Verlag.

Yang, C., Peng, X., Zhao, Y., Wang, X., Fu, J., Liu, K., Li, Y., Li, P., 2020. Prediction model to analyze the performance of VMD desalination process. Computers & Chemical Engineering 132, 106619.
DOI: 10.1016/j.compchemeng.2019.106619

Yu, H., Yang, X., Wang, R., Fane, A. G., 2011. Numerical simulation of heat and mass transfer in direct membrane distillation in a hollow fiber module with laminar flow. Journal of Membrane Science 384 (1-2), 107–116.
DOI: 10.1016/j.memsci.2011.09.011

Zaragoza, G., Ruiz-Aguirre, A., Guillén-Burrieza, E., 2014. Efficiency in the use of solar thermal energy of small membrane desalination systems for decentralized water production. Applied Energy 130, 491–499.
DOI: 10.1016/j.apenergy.2014.02.024

Zhang, L., Xiang, J., Cheng, P. G., Tang, N., Han, H., Yuan, L., Zhang, H., Wang, S., Wang, X., 2015. Three-dimensional numerical simulation of aqueous NaCl solution in vacuum membrane distillation process. Chemical Engineering and Processing: Process Intensification 87, 9–15.
DOI: 10.1016/j.cep.2014.11.002

3. Conclusions and future works

In this Ph.D. thesis, several operating methodologies, developed from an automatic control point of view, have been proposed for the optimal operation of MD based facilities. The different works presented along the Ph.D. thesis have been carried out according to the development phases of a control engineering project as mentioned. In this way, the first research work focused on the development of a complete model and a regulation control layer for SMD plants. The second research line was devoted to the design of hierarchical control strategies for the optimal operation of SMD plants, mainly focused on the management of the heat generation circuit powering the MD unit. The third research work dealt with the development of control structures for MD industrial plants. In this case, the control algorithms were tasked with the optimal management of the desalination unit, which was composed by multiple MD modules. Finally, the thesis project culminated with a tutorial on modelling and control methodologies for MD plants, which was developed based on the experience acquired up through the thesis development and a literature review of the state-of-art in this field.

The main conclusion of the whole work is that adequate control algorithms, developed using accurate models, could be essential tools for the industrial implementation of MD technology. Their use can help to improve fundamental performance parameters in MD processes as to reduce the thermal energy consumption of the MD modules and to augment their distillate production according to operating conditions. Additionally, they can be used to reduce operational costs. This overall conclusion is supported by the specific conclusions of each of the research lines addressed in this thesis, which are summarized in the following sections. Based on these findings, some ideas for future research works are provided as well.

3.1 Conclusions on modelling and low-level control of solar membrane distillation plants

The conclusions in this research line can be divided into two parts according to the two scientific contributions presented. The first work was included in Section 2.1.1, and the main conclusions

that can be drawn from the results obtained are:

- It is possible to accurately characterize the heat generation circuit of an SMD plant by using the set of models proposed. The validation of the whole model in the SMD plant of the PSA confirmed it. For example, the mean square error in most parts of the plant (i.e., storage tank, distribution system, heat exchanger, etc.) was around 0.5 $^{\circ}$C, whereas the one at the outlet of the solar field was around 1 $^{\circ}$C. Besides, the whole dynamic model resulted in a powerful tool to develop and test control strategies to be applied in SMD plants.
- The settling time to establish the desired operating temperature at the entrance of the MD module in SMD plants can be considerably reduced by using an adequate direct control structure formed by PID controllers. This was experimentally demonstrated as the settling time achieved with the proposed control algorithm was around 20 min, whereas the time spent in manual operations performed by qualify operators amounted to 40-50 min, meaning a reduction in time of around 50 %.
- The disturbance rejection when using the direct connection mode, i.e., when the solar field is directly connected to the MD modules without using thermal storage, can also be improved by using a direct control layer. In manual mode, this task was highly difficult to perform due to the intermittent nature of solar energy.

Regarding the second contribution, which was included in Section 2.1.2 and was aimed at presenting the modelling of a commercial MD module and determining its optimal operating conditions, the following conclusions can be drawn:

- The ANN methodology is more appropriate than the RSM one when using inputs that induce nonlinear behavior, such as salinity of feed solution. This is supported by the comparison of predictive abilities performed between the two modelling techniques, which revealed that the coefficient of determination (R^2) achieved by the RSM technique was 0.770 while the one of the ANN was 0.982 to adjust the specific thermal energy consumption of the module; the output which presented nonlinear behavior concerning feed solution salt concentration.
- Real-time management methods are required to optimally perform batch operations aimed at desalting brines from other desalination techniques. This was revealed by the multi-objective optimization study carried out using the ANN model, which evidenced how different operating conditions are required depending on the level of the feed water salinity.

3.2 Conclusions on hierarchical controllers for the optimal operation of solar membrane distillation plants

In this research line hierarchical controllers were developed from the models and direct control system proposed during the first phase. In this case, the conclusion can be also divided according to the journal papers published. Firstly, a hierarchical control structure for the optimal operation of SMD plants was proposed (see Section 2.2.1). This controller was tasked with improved high-level control objectives in SMD plants, as to maximize the distillate production or thermal efficiency or to minimize operating costs. The controller was tested both in simulation, to carry out comparisons, and experimentally in the pilot plant of the PSA to validate the control performance. The obtained results derived in the following conclusions:

- Hierarchical control techniques are useful methodologies to develop optimal operating

management strategies for SMD plants. This was supported by the experimental results obtained with the application of the proposed controller in the pilot plant of the PSA and the improvement achieved in comparison to conventional manual operations.

- The distillate production and thermal efficiency of an SMD plant can be increased by using these real-time control techniques. This was demonstrated in the simulations performed using a week of data with different meteorological conditions obtained from PSA. The relative improvements achieved were 5-7 % and 0.5-1 % in comparison to manual operations for the distillate production and thermal efficiency respectively. Note that the figure depends on the objective function chosen in the upper layer of the hierarchical controller.

- Operating costs can be reduced as well. In this case the relative improvements with respect to a manual operation ranged between 9-10 %, also depending on the objective function selected in the upper layer.

The second hierarchical controller proposed was aimed at improving the start phase of SMD plants (see Section 2.2.2). This controller was also tested in both simulation and experimentally, and the obtained results allows us to draw the following conclusions:

- As in the previous case, the experimental tests showed as hierarchical controllers are powerful tools to improve the start-up phase of SMD plants, dealing with irradiance disturbances and stratification problems in the storage tank in real-time.

- Specifically, the time in reaching the required operating temperature in the storage tank of an SMD plant can be considerably reduced by means of the proposed hierarchical controller. For example, the time is reduced by 9 and 11 % compared to a manual and a previous control procedure previously published in literature respectively. This is mainly due to the fact that the controller considered irradiance disturbances and operating conditions at each sampling time, the upper layer was based on a receding control strategy, and the control system used the mixing valve apart from the flow rate as control variable.

3.3 Conclusions on control and optimization strategies for membrane distillation industrial applications

The research carried out in this line was focused on the management of the desalination unit of industrial SMD plants, in which multiple MD units must be used to meet the water requirements. The first work (see Section 2.3.1) was tasked with the development of a DMPC strategy in charge of calculating the feed flow rate for each of the MD modules trying to reduce the specific thermal energy consumption while meeting water needs. The main findings of this work are summarized below:

- The proposed DMPC algorithm showed satisfactory results for the management of SMD industrial plants reaching the same solutions as those obtained with a centralized MPC approach, which demonstrated its convergence to optimal results.

- The benefit achieved in terms of resolution time makes the DMPC algorithm more suitable than the centralized one for these facilities. For example, when dealing with a large number of MD modules, the problem concerning the optimal management of the plant could only be solved by the DMPC algorithm.

- The thermal energy consumption in these MD industrial applications can be significantly reduced by using an adequate control technique. The results obtained with the application

of the DMPC strategy showed a reduction in the specific thermal energy consumption of 5 % in comparison to a manual operation.

In the second work of this research line, which was included in Section 2.3.2, the objectives were the same but apart from the feed flow rate, binary variables to turn ON/OFF the different MD modules at each sampling time were also considered in the control problem, leading to an MINLP problem. Therefore, a general and efficient method for solving the problem and reflecting the operating strategy was proposed. The outcomes of that paper allow us to draw the following conclusions:

- The developed strategy can be applied in any MD plant independently of the power source, as long as the MD modules are modelled by the RSM method.
- The developed technique considerably improves the time spent in solving the problem by an MINLP solver. This was supported by the comparison performed among the proposed technique and an MINLP solver, which revealed that for a case with 64 MD modules the MINLP solver required 1619.72 s while the proposed algorithm only 5.67 s.
- The improvements achieved in terms of energy savings are meaningful with the application of the proposed management method. For example, on a sunny day, around 65 and 55 % of the thermal energy required by manual operation and by the one performed with the DMPC algorithm mentioned above, respectively, was saved. In cloudy days, the proposed technique used less than 5 % required by the aforementioned operating methods.

3.4 Conclusion on the tutorial on modelling and control of membrane distillation technology

The last work developed in the framework of the thesis was a tutorial on modelling and control approaches for the MD technology. In this work, the different proposals made in this thesis project as well as others published papers in the literature related to this emerging research field were summarized and reviewed, describing the main techniques used and presenting the technological development achieved trough their application in MD plants. The main conclusions that arise from the review performed are:

- Concerning the modelling of MD modules, it is necessary to develop models based on experimental data that take into account the thermal efficiency of the MD module as output, and the salinity of the feed solution as input. These models could be the basis for the development of operating strategies or to design an MD plant for potential applications as desalting brines from other desalination plants.
- Similarly, the development of first principles models for commercial MD modules is required. Most current approaches are validated with lab-scale MD modules whose results cannot be extrapolated to commercial MD modules successfully.
- Regarding control approaches, there is still a long way to go since this topic has been sparingly addressed in literature so far. So that, multiobjective control approaches to maximize the distillate production and energy efficiency of MD modules in real-time as well as control formulations that take into account economic criteria are required, and above all, control strategies aimed at improving the performance of MD technology in its potential industrial applications.

3.5 Recommendations for future research

This thesis provides a wide range of tools based on modelling and automatic control for efficient management of the operation of MD based plants. Although it may serve as a reference in this new research field in the MD technology, there is still room for investigating and developing new models and operating strategies. In what follows, the future challenges and gaps to be filled in both areas are summarized.

As described, there are well-known models in the literature that can be successfully adapted to characterize the heat generation circuit of an SMD plant. Conversely, the models for the MD module are more limited. Most approaches proposed so far only predict the distillate production and they use limited input variables that do not allow to explore the entire field of application of MD technology. Consequently, it is required the development of models that consider also the thermal efficiency of MD modules as an output. This parameter is crucial in these kinds of thermal powered processes, in addition, it stands out as one of the main drawbacks of the technology. The development of these models could be relevant for the design of new operating strategies that optimize both the distillate production and thermal efficiency in real-time. In the same line, it is necessary to include variables as the salinity of the feed solution as input in the models. As a result, the performance of the MD modules in potential applications as desalting brines from other desalination technologies could be better assessed.

Moreover, and as said before, most of the published models are based on experimental data. The models based on first principles for MD modules are scarce and they are mainly validated in lab-scale MD modules. The simplifications assumed when formulating these models make their validation with commercial modules difficult to carry out. Thus, research efforts must be devoted to developing more detailed and accurate models than can be adjusted and calibrated for commercial MD modules. At this point, perhaps, closer collaboration between MD developers and academia is required. This could help to better understand the dynamics that occur inside the MD module opening new research opportunities in the control field, as the development of low-level controllers aimed at improving the MD module performance.

With regard to automatic control approaches, the related open research lines are even greater, since, as it has been pointed out throughout this thesis, very few works have been presented in this field so far. The kinds of works required can be divided into two branches according to the control objectives being pursued or the type of control methodology employed. On the one hand, the future work concerning low-level control structures is more limited since this branch is mainly focused on controlling the heat generation circuit of the SMD plant, which is based on a thermal solar field. For these systems numerous works have been published detailing accurate and experimentally tested control architectures [78]. However, a new line coul be opened for improving aspects related to the performance of the MD modules. But, for this purpose, it is fundamental to develop accurate dynamic models for commercial MD modules as said above.

On the other hand, very few papers focused on high-level control objectives, i.e., maximizing distillate production or thermal efficiency, have been presented. For example, in the one developed in this thesis [4], these parameters were optimized using as decision variable only the operating temperature, leading to control structures with only one objective. Nevertheless, in most commercial MD modules these objectives require contrary operating conditions in the feed flow rate to be optimized [64]. Accordingly, future research works could be focused on the development of multiobjective control algorithms to manage the SMD facility in real-time trying

to optimize both goals. Again, models capable of predicting both variables are needed to the proper design of these control structures as previously mentioned. Likewise, the inclusion of economic terms in the control strategies is needed in order to decrease the costs of desalinated water. A first attempt was presented in [4], but only the operational costs of the heat generation circuit were taken into account. Therefore, the control formulation must be extended to the whole SMD plant.

Another interesting research line is the development of control structures for industrial applications. In this sense, the works developed in this thesis [7, 138] have evidenced that the control formulations change with respect to the ones developed for MD pilot plants, as multiple MD modules are required instead of a single one. The main problems that arise here are related to the computing time, since the number of control variables in the problem increases according to the number of MD modules in the desalination unit. Therefore, distributed approaches or algorithms to decompose centralized approaches, so that the problems can be easily and quickly solved, should be developed. Note that the works in [7, 138] are based on these control techniques, but other algorithms or control structures can be tested to improve the obtained results. Finally, control approaches focused on the other industrial applications of the MD technology such as brine treatment should be also formulated. In these types of applications, apart from the classic disturbances of the MD modules as inlet temperature of the evaporator channel and temperature of the feed solution, a new one must be considered: the salinity concentration of the feed solution. This variable increases throughout the operation until the volatile and non-volatile particles of the feed solution are completely separated. Thus, real-time control approaches to improve module performance must be formulated as was stated in [5].

4. Other contributions

As specified in the previous contents, the main research work of this thesis is supported by: i) 7 papers in JCR journals (4 in Q1, 2 in Q2 and 1 in Q3), ii) 6 contributions to international conferences, iii) 6 contributions to national conferences, iv) 1 article in a general outreach magazine, and v) 2 research stays. Aside from this work, several collaborations have been performed resulting in publications derived directly from the thesis. In addition, the Ph.D. candidate has participated in two research projects and contributed as a reviewer on several occasions. Apart from the aforementioned research activities, the Ph.D. candidate has also been involved in teaching activities and has collaborated in one group of innovation and good teaching practices, resulting in a publication in a national conference. All this information is summarized in this chapter.

4.1 Derived publications and research work

4.1.1 Scientific journals

During the development of the thesis, several collaborations with partners from the University of Almería, Plataforma Solar de Almería, Salesian University of Ecuador, and the Federal University of Santa Catarina were performed. This research work resulted in 4 publications in JCR journals ranked in Q1. The topic of each of the publications was: i) the inclusion of MD technology in an agroindustrial environment and its management through Internet of Things tools, ii) the evaluation of a novel vacuum multi-effect MD module powered with solar energy, iii) the analysis of the apparent delays of flat-plate solar fields, and iv) the modelling of a flat-plate solar field used to power thermal desalination facilities. The works are referenced below according to the previous order:

- M. Muñoz, **J. D. Gil**, L. Roca, F. Rodríguez, and M. Berenguel, "An IoT Architecture for Water Resource Management in Agroindustrial Environments: A Case Study in Almería (Spain)," *Sensors*, vol. 20, pp. 596, 2020.
- J. A. Andrés-Mañas, L. Roca, A. Ruiz-Aguirre, F. G. Acién, **J. D. Gil**, and G. Zaragoza,

"Application of solar energy to seawater desalination in a pilot system based on vacuum multi-effect membrane distillation," *Applied Energy*, vol. 258, pp. 114068, 2020.

- G. Ampuño, L. Roca, **J. D. Gil**, M. Berenguel, and J. E. Normey-Rico, "Apparent delay analysis for a flat-plate solar field model designed for control purposes". *Solar Energy*, vol. 177, pp. 241-254, 2019.
- G. Ampuño, L. Roca, M. Berenguel, **J. D. Gil**, M. Pérez, and J. E. Normey-Rico, "Modeling and simulation of a solar field based on flat-plate collectors". *Solar Energy*, vol. 170, pp. 369-378, 2018.

4.1.2 International conferences

Similarly, the different collaborations mentioned above and other performed with partners from the University of Sevilla and the Università degli Studi di Brescia (Italy) resulted in four contributions to international conferences also covering topics related to the thesis as modelling and control of solar thermal fields or other thermal processes as refrigerated chambers:

- J. L. Guzmán, M. Berenguel, A. Merchan, **J. D. Gil**, and J. D. Álvarez, "A virtual lab for modeling and control of a solar collector field," *IFAC–PapersOnLine* (In press).
- A. Tosi, L. Roca, **J. D. Gil**, A. Visioli, and M. Berenguel,"Multivariable controller for stationary flat plate solar collectors," in *7th International Conference on Systems and Control*, pp. 7-12, IEEE, 2018.
- G. Bejarano, D. Rodríguez, J. A. Alfaya, **J. D. Gil**, and M. G. Ortega,"Optimization and cascade robust temperature control of a refrigerated chamber," *IFAC–PapersOnLine*, vol. 51(25), pp. 110-115, 2018.
- G. Ampuño, L. Roca, M. Berenguel, **J. D. Gil**, M. Pérez, "Modeling and simulation of a heat generation system for a Multi-Effect Desalination plant based on solar flat-plate collectors," in *11th ISES European Solar Energy Congress*, 2016.

4.1.3 National conferences

Additionally, the Ph.D. candidate has actively participated in the different conferences organized by the Department of Informatics of the University of Almería. This participation gave rise to the following publications:

- **J. D. Gil**, "Estrategias de control jerárquico y optimización aplicadas a plantas de destilación por membranas alimentadas con energía solar," in *I Jornadas de Doctorado en Informática de la Universidad de Almería, JSIDI*, 2019.
- **J. D. Gil**, "Aportaciones desde el punto de vista del modelado y del control automático a la tecnología de destilación por membranas alimentadas con energía solar" in *II Jornadas de Doctorado en Informática de la Universidad de Almería, JSIDI*, 2019.
- **J. D. Gil**, "Sistemas de control para las fases de arranque y operación en plantas de destilación solar por membranas a escala industrial," in *III Jornadas de Doctorado en Informática de la Universidad de Almería, JSIDI*, 2019.

4.1.4 Collaboration in research projects

The research activity developed in this thesis has contributed to the development of two national research projects in which the Ph.D candidate got involved in the work team:

- Control and energy management strategies in production environments with support of renewable energy (**ENERPRO**).

Ref.: DPI2014-56364-C2-1-R.
Funded: Spanish Ministry of Economy, Industry and Competitiveness and ERDF funds.

- Control and optimal management of heterogeneous resources in agroindustrial production districts integrating renewable energies (**CHROMAE**).
Ref.: DPI2017-85007-R.
Funded: Spanish Ministry of Science, Innovation and Universities and ERDF funds.

4.1.5 Contribution as reviewer

The Ph.D. candidate has also contributed to research by accepting invitations to participate as reviewer. Specifically, the Ph.D. candidate has been invited to review contributions to: i) international conferences such as "The 2018 IFAC Conference on Advances in Proportional-Integral-Derivative Control" and the "21st IFAC World Congress", ii) national conferences as the "Jornadas de Automática", and iii) JCR journals such as *Energy Conversion and Management*, *Computer & Chemical Engineering*, and *Revista Iberoamericana de Automática e Informática industrial*. All the topics covered were related to those treated in the thesis as control algorithms and MD technology.

4.2 Teaching activities

As a complement to the research work, the Ph.D. candidate has participated in teaching activities, namely 225 hours, related to the research topics treated in the thesis. The subjects taught include Electrical Machines and Drives Controls, Control of Production Processes and Systems, Big Data Applications, and Real Time Systems. Moreover, the Ph.D. candidate has also participated in an Innovation and Good Teaching Practices group, devoted to the improvement of teaching activity and the quality of learning of students of the University of Almería. In particular, the one in which the Ph.D. student took part was:

- Desarrollo de una plataforma de simulación de plantas industriales para su utilización en prácticas de automatización de procesos (Development of an industrial plant simulation platform for use in process automation practices).

One of the results of this project was presented as a contribution to the following national conference:

- J. A. Sánchez-Molina, J. D. Álvarez, M. Berenguel, **J. D. Gil**, J. García-Donaire, J. L. Guzmán, A. Hoyo, J. C. Moreno and F. Rodríguez, "Innovation and Good Teaching Practices groups: Desarrollo de una plataforma de simulación de plantas industriales para su utilización en prácticas de automatización de procesos (Development of an industrial plant simulation platform for use in process automation practices)," in *Jornadas de Innovación Docente y Experiencias Profesionales en la Universidad de Almería*. 2019.

Bibliography

[1] WWAP, *The United Nations World Water Development Report 2019: Leaving no One Behind*. Paris, UNESCO, 2019.

[2] K. Mohammadi, M. Saghafifar, K. Ellingwood, and K. Powell, "Hybrid concentrated solar power (CSP)-desalination systems: A review," *Desalination*, vol. 468, p. 114083, 2019.

[3] G. Zaragoza, A. Ruiz-Aguirre, and E. Guillén-Burrieza, "Efficiency in the use of solar thermal energy of small membrane desalination systems for decentralized water production," *Applied Energy*, vol. 130, pp. 491–499, 2014.

[4] J. D. Gil, L. Roca, A. Ruiz-Aguirre, G. Zaragoza, and M. Berenguel, "Optimal operation of a solar membrane distillation pilot plant via nonlinear model predictive control," *Computers & Chemical Engineering*, vol. 109, pp. 151–165, 2018.

[5] J. D. Gil, A. Ruiz-Aguirre, L. Roca, G. Zaragoza, and M. Berenguel, "Prediction models to analyse the performance of a commercial-scale membrane distillation unit for desalting brines from RO plants," *Desalination*, vol. 445, pp. 15–28, 2018.

[6] K. J. Åström and T. Hägglund, *Advanced PID control*. ISA-The Instrumentation, Systems, and Automation Society Research Triangle, 2006, vol. 461.

[7] J. D. Gil, J. D. Álvarez, L. Roca, J. A. Sánchez-Molina, M. Berenguel, and F. Rodríguez, "Optimal thermal energy management of a distributed energy system comprising a solar membrane distillation plant and a greenhouse," *Energy Conversion and Management*, vol. 198, p. 111791, 2019.

[8] E. F. Camacho and C. Bordons, *Model Predictive Control*. London: Springer-Verlag Ltd, 2004.

[9] J. D. Gil, L. Roca, G. Zaragoza, J. E. Normey-Rico, and M. Berenguel, "Hierarchical control for the start-up procedure of solar thermal fields with direct storage," *Control Engineering Practice*, vol. 95, p. 104254, 2020.

[10] E. Jones, M. Qadir, M. T. H. van Vliet, V. Smakhtin, and S. Kang, "The state of desalination and brine production: A global outlook," *Science of the Total Environment*, vol. 657, pp. 1343–1356, 2018.

[11] M. Qadir, "Policy Note:" Addressing trade-offs to promote safely managed wastewater in developing countries"," *Water Economics and Policy*, vol. 4, no. 02, p. 1871002, 2018.

[12] WWAP, *The United Nations World Water Development Report 2018: Nature-based Solutions for Water.* Paris, UNESCO, 2018.

[13] E. Dalampira and S. A. Nastis, "Mapping sustainable development goals: A network analysis framework," *Sustainable Development*, vol. 28, no. 1, pp. 46–55, 2020.

[14] G. Fiorenza, V. K. Sharma, and G. Braccio, "Techno-economic evaluation of a solar powered water desalination plant," *Energy Conversion and Management*, vol. 44, no. 14, pp. 2217–2240, 2003.

[15] E. DeNicola, O. S. Aburizaiza, A. Siddique, H. Khwaja, and D. O. Carpenter, "Climate change and water scarcity: The case of Saudi Arabia," *Annals of Global Health*, vol. 81, no. 3, pp. 342–353, 2015.

[16] M. A. Eltawil, Z. Zhengming, and L. Yuan, "A review of renewable energy technologies integrated with desalination systems," *Renewable and Sustainable Energy Reviews*, vol. 13, no. 9, pp. 2245–2262, 2009.

[17] M. T. van Vliet, M. Flörke, and Y. Wada, "Quality matters for water scarcity," *Nature Geoscience*, vol. 10, no. 11, pp. 800–802, 2017.

[18] F. G. Brière, *Drinking-water distribution, sewage, and rainfall collection.* Presses inter Polytechnique, 2014.

[19] WHO, "Guidelines for drinking-water quality," *Chronicle of the World Health Organization*, vol. 38, no. 4, pp. 104–8, 2011.

[20] M. Elimelech and W. A. Phillip, "The future of seawater desalination: Energy, technology, and the environment," *Science*, vol. 333, no. 6043, pp. 712–717, 2011.

[21] N. Ghaffour, T. M. Missimer, and G. L. Amy, "Technical review and evaluation of the economics of water desalination: Current and future challenges for better water supply sustainability," *Desalination*, vol. 309, pp. 197–207, 2013.

[22] N. Ghaffour, S. Lattemann, T. Missimer, K. C. Ng, S. Sinha, and G. Amy, "Renewable energy-driven innovative energy-efficient desalination technologies," *Applied Energy*, vol. 136, pp. 1155–1165, 2014.

[23] V. G. Gude, "Desalination and water reuse to address global water scarcity," *Reviews in Environmental Science and Bio/Technology*, vol. 16, no. 4, pp. 591–609, 2017.

[24] J. H. Lienhard, G. P. Thiel, D. M. Warsinger, and L. D. Banchik, "Low carbon desalination: Status and research, development, and demonstration needs," *Report of a Workshop conducted at the Massachusetts Institute of Technology in association with the Global Clean Water Desalination Alliance*, 2016.

[25] A. Kylili, P. A. Fokaides, A. Ioannides, and S. Kalogirou, "Environmental assessment of solar thermal systems for the industrial sector," *Journal of Cleaner Production*, vol. 176, pp. 99–109, 2018.

[26] A. B. Pouyfaucon and L. García-Rodríguez, "Solar thermal-powered desalination: A viable solution for a potential market," *Desalination*, vol. 435, pp. 60–69, 2018.

[27] A. Al-Karaghouli and L. L. Kazmerski, "Energy consumption and water production cost of conventional and renewable-energy-powered desalination processes," *Renewable and Sustainable Energy Reviews*, vol. 24, pp. 343–356, 2013.

[28] F. E. Ahmed, R. Hashaikeh, and N. Hilal, "Solar powered desalination–Technology, energy and future outlook," *Desalination*, vol. 453, pp. 54–76, 2019.

[29] N. Ghaffour, J. Bundschuh, H. Mahmoudi, and M. F. A. Goosen, "Renewable energy-driven desalination technologies: A comprehensive review on challenges and potential applications of integrated systems," *Desalination*, vol. 356, pp. 94–114, 2015.

[30] T. M. Missimer, Y. Kim, R. Rachman, and K. C. Ng, "Sustainable renewable energy seawater desalination using combined-cycle solar and geothermal heat sources," *Desalination and Water Treatment*, vol. 51, no. 4-6, pp. 1161–1170, 2013.

[31] P. Wang and T. Chung, "Recent advances in membrane distillation processes: Membrane development, configuration design and application exploring," *Journal of Membrane Science*, vol. 474, pp. 39–56, 2015.

[32] D. González, J. Amigo, and F. Suárez, "Membrane distillation: Perspectives for sustainable and improved desalination," *Renewable and Sustainable Energy Reviews*, vol. 80, pp. 238–259, 2017.

[33] M. Khayet and T. Matsuura, *Membrane distillation: principles and applications*. Elsevier, 2011.

[34] T. Chen and C.-D. Ho, "Immediate assisted solar direct contact membrane distillation in saline water desalination," *Journal of Membrane Science*, vol. 358, no. 1-2, pp. 122–130, 2010.

[35] A. M. Alklaibi and N. Lior, "Transport analysis of air-gap membrane distillation," *Journal of Membrane Science*, vol. 255, no. 1-2, pp. 239–253, 2005.

[36] J. Koschikowski, M. Wieghaus, and M. Rommel, "Solar thermal-driven desalination plants based on membrane distillation," *Desalination*, vol. 156, no. 1-3, pp. 295–304, 2003.

[37] D. Winter, J. Koschikowski, and M. Wieghaus, "Desalination using membrane distillation: Experimental studies on full scale spiral wound modules," *Journal of Membrane Science*, vol. 375, no. 1-2, pp. 104–112, 2011.

[38] K. Charfi, M. Khayet, and M. J. Safi, "Numerical simulation and experimental studies on heat and mass transfer using sweeping gas membrane distillation," *Desalination*, vol. 259, no. 1-3, pp. 84–96, 2010.

[39] J. Mengual, M. Khayet, and M. Godino, "Heat and mass transfer in vacuum membrane distillation," *International Journal of Heat and Mass Transfer*, vol. 47, no. 4, pp. 865–875, 2004.

[40] D. Winter, *Membrane distillation: A thermodynamic, technological and economic analysis*. Shaker Verlag, 2015.

[41] Y. Kim, K. Thu, and S.-H. Choi, "Solar-assisted multi-stage vacuum membrane distillation system with heat recovery unit," *Desalination*, vol. 367, pp. 161–171, 2015.

[42] J. A. Andrés-Mañas, A. Ruiz-Aguirre, F. G. Acién, and G. Zaragoza, "Performance increase of membrane distillation pilot scale modules operating in vacuum-enhanced air-gap configuration," *Desalination*, vol. 475, p. 114202, 2020.

[43] A. Ruiz-Aguirre, J. A. Andrés-Mañas, and G. Zaragoza, "Evaluation of permeate quality in pilot scale membrane distillation systems," *Membranes*, vol. 9, no. 6, p. 69, 2019.

[44] A. Alkhudhiri, N. Darwish, and N. Hilal, "Membrane distillation: A comprehensive review," *Desalination*, vol. 287, pp. 2–18, 2012.

[45] A. Luo and N. Lior, "Critical review of membrane distillation performance criteria," *Desalination and Water Treatment*, vol. 57, no. 43, pp. 20 093–20 140, 2016.

[46] R. Miladi, N. Frikha, A. Kheiri, and S. Gabsi, "Energetic performance analysis of seawater desalination with a solar membrane distillation," *Energy Conversion and Management*, vol. 185, pp. 143–154, 2019.

[47] E. Tzen, G. Zaragoza, and D. C. Alarcón-Padilla, "Solar desalination," pp. 529–565, 2012.

[48] E. Guillén-Burrieza, D. C. Alarcón-Padilla, P. Palenzuela, and G. Zaragoza, "Techno-economic assessment of a pilot-scale plant for solar desalination based on existing plate and frame MD technology," *Desalination*, vol. 374, pp. 70–80, 2015.

[49] A. Giwa, V. Dufour, F. Al Marzooqi, M. Al Kaabi, and S. W. Hasan, "Brine management methods: Recent innovations and current status," *Desalination*, vol. 407, pp. 1–23, 2017.

[50] R. Bouchrit, A. Boubakri, A. Hafiane, and S. A. Bouguecha, "Direct contact membrane distillation: Capability to treat hyper-saline solution," *Desalination*, vol. 376, pp. 117–129, 2015.

[51] D. A. Roberts, E. L. Johnston, and N. A. Knott, "Impacts of desalination plant discharges on the marine environment: A critical review of published studies," *Water research*, vol. 44, no. 18, pp. 5117–5128, 2010.

[52] H. C. Duong, A. R. Chivas, B. Nelemans, M. Duke, S. Gray, T. Y. Cath, and L. D. Nghiem, "Treatment of RO brine from CSG produced water by spiral-wound air gap membrane distillation–A pilot study," *Desalination*, vol. 366, pp. 121–129, 2015.

[53] J. Koschikowski, M. Wieghaus, M. Rommel, V. S. Ortin, B. P. Suarez, and J. R. B. Rodríguez, "Experimental investigations on solar driven stand-alone membrane distillation systems for remote areas," *Desalination*, vol. 248, no. 1-3, pp. 125–131, 2009.

[54] R. B. Saffarini, E. K. Summers, H. A. Arafat, and J. H. Lienhard, "Technical evaluation of stand-alone solar powered membrane distillation systems," *Desalination*, vol. 286, pp. 332–341, 2012.

[55] N. Thomas, M. O. Mavukkandy, S. Loutatidou, and H. A. Arafat, "Membrane distillation research & implementation: Lessons from the past five decades," *Separation and Purification Technology*, vol. 189, pp. 108–127, 2017.

[56] J. Amigo, R. Urtubia, and F. Suárez, "Exploring the interactions between hydrodynamics and fouling in membrane distillation systems–A multiscale approach using CFD," *Desalination*, vol. 444, pp. 63–74, 2018.

[57] L. D. Tijing, Y. C. Woo, J.-S. Choi, S. Lee, S.-H. Kim, and H. K. Shon, "Fouling and its control in membrane distillation–A review," *Journal of Membrane Science*, vol. 475, pp. 215–244, 2015.

[58] E. Guillén-Burrieza, J. Blanco, G. Zaragoza, D. C. Alarcón-Padilla, P. Palenzuela, M. Ibarra, and W. Gernjak, "Experimental analysis of an air gap membrane distillation solar desalination pilot system," *Journal of Membrane Science*, vol. 379, no. 1-2, pp. 386–396, 2011.

[59] Q. Li, L. Beier, J. Tan, C. Brown, B. Lian, W. Zhong, Y. Wang, C. Ji, P. Dai, T. Li *et al.*, "An integrated, solar-driven membrane distillation system for water purification and energy generation," *Applied Energy*, vol. 237, pp. 534–548, 2019.

[60] A. Shafieian and M. Khiadani, "A novel solar-driven direct contact membrane-based water desalination system," *Energy Conversion and Management*, vol. 199, p. 112055, 2019.

[61] R. Schwantes, A. Cipollina, F. Gross, J. Koschikowski, D. Pfeifle, M. Rolletschek, and V. Subiela, "Membrane distillation: Solar and waste heat driven demonstration plants for desalination," *Desalination*, vol. 323, pp. 93–106, 2013.

[62] A. Ruiz-Aguirre, J. A. Andrés-Mañas, J. M. Fernández-Sevilla, and G. Zaragoza, "Experimental characterization and optimization of multi-channel spiral wound air gap membrane distillation modules for seawater desalination," *Separation and Purification Technology*, vol. 205, pp. 212–222, 2018.

[63] R. Porrazzo, A. Cipollina, M. Galluzzo, and G. Micale, "A neural network-based optimizing control system for a seawater-desalination solar-powered membrane distillation unit," *Computers & Chemical Engineering*, vol. 54, pp. 79–96, 2013.

[64] A. Ruiz-Aguirre, J. A. Andrés-Mañas, J. M. Fernández-Sevilla, and G. Zaragoza, "Modeling and optimization of a commercial permeate gap spiral wound membrane distillation module for seawater desalination," *Desalination*, vol. 419, pp. 160–168, 2017.

[65] D. Cheng, W. Gong, and N. Li, "Response surface modeling and optimization of direct contact membrane distillation for water desalination," *Desalination*, vol. 394, pp. 108–122, 2016.

[66] F. Banat, N. Jwaied, M. Rommel, J. Koschikowski, and M. Wieghaus, "Performance evaluation of the "large SMADES" autonomous desalination solar-driven membrane distillation plant in Aqaba, Jordan," *Desalination*, vol. 217, no. 1-3, pp. 17–28, 2007.

[67] N. Dow, M. Duke, J. Zhang, T. O'Rielly, J. Li, S. Gray, E. Ostarcevic, and P. Atherton, "Demonstration of solar driven membrane distillation in remote Victoria," in *Australian Water Association (AWA) Ozwater Conference and Exhibition, Brisbane, Australia*, vol. 810, 2010.

[68] A. Cipollina, M. G. Di Sparti, A. Tamburini, and G. Micale, "Development of a membrane distillation module for solar energy seawater desalination," *Chemical Engineering Research and Design*, vol. 90, no. 12, pp. 2101–2121, 2012.

[69] H. Chang, G.-B. Wang, Y. Chen, C.-C. Li, and C.-L. Chang, "Modeling and optimization of a solar driven membrane distillation desalination system," *Renewable Energy*, vol. 35, no. 12, pp. 2714–2722, 2010.

[70] Y. Chen, Y. Li, and H. Chang, "Optimal design and control of solar driven air gap membrane distillation desalination systems," *Applied Energy*, vol. 100, pp. 193–204, 2012.

[71] A. M. Karam and T. M. Laleg-Kirati, "Real time optimization of solar powered direct contact membrane distillation based on multivariable extremum seeking," in *2015 IEEE Conference on Control Applications (CCA)*.   IEEE, 2015, pp. 1618–1623.

[72] P. Bendevis, A. M. Karam, and T. M. Laleg-Kirati, "Optimal model-free control of solar thermal membrane distillation system," *Computers & Chemical Engineering*, vol. 133, p. 106622, 2020.

[73] X. Guo, F. Albalawi, and T. M. Laleg-Kirati, "Observer-based economic model predictive control for direct contact membrane distillation," *Chemical Engineering Research and Design*, vol. 156, pp. 86–99, 2020.

[74] J. D. Gil, L. Roca, G. Zaragoza, and M. Berenguel, "A feedback control system with reference governor for a solar membrane distillation pilot facility," *Renewable Energy*, vol. 120, pp. 536–549, 2018.

[75] K. Ogata, *Modern control engineering*.   Fifth edition, Prentice Hall, 2010.

[76] M. Khayet and C. Cojocaru, "Artificial neural network modeling and optimization of desalination by air gap membrane distillation," *Separation and Purification Technology*, vol. 86, pp. 171–182, 2012.

[77] J. A. Duffie and W. A. Beckman, *Solar Engineering of Thermal Processes*.   John Wiley & Sons, 2013.

[78] E. F. Camacho, M. Berenguel, F. R. Rubio, and D. Martínez, *Control of Solar Energy Systems*.   Springer, 2012.

[79] Z. Ding, L. Liu, M. S. El-Bourawi, and R. Ma, "Analysis of a solar-powered membrane distillation system," *Desalination*, vol. 172, no. 1, pp. 27–40, 2005.

[80] S. B. Abdallah, N. Frikha, and S. Gabsi, "Simulation of solar vacuum membrane distillation unit," *Desalination*, vol. 324, pp. 87–92, 2013.

[81] N. Tang, H. Zhang, and W. Wang, "Computational fluid dynamics numerical simulation of vacuum membrane distillation for aqueous NaCl solution," *Desalination*, vol. 274, no. 1-3, pp. 120–129, 2011.

[82] H. Yu, X. Yang, R. Wang, and A. G. Fane, "Numerical simulation of heat and mass transfer in direct membrane distillation in a hollow fiber module with laminar flow," *Journal of Membrane Science*, vol. 384, no. 1-2, pp. 107–116, 2011.
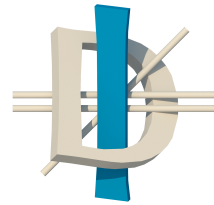
[83] A. S. Alsaadi, N. Ghaffour, J.-D. Li, S. Gray, L. Francis, H. Maab, and G. L. Amy, "Modeling of air-gap membrane distillation process: A theoretical and experimental study," *Journal of Membrane Science*, vol. 445, pp. 53–65, 2013.

[84] L. Zhang, J. Xiang, P. G. Cheng, N. Tang, H. Han, L. Yuan, H. Zhang, S. Wang, and X. Wang, "Three-dimensional numerical simulation of aqueous NaCl solution in vacuum membrane distillation process," *Chemical Engineering and Processing: Process Intensification*, vol. 87, pp. 9–15, 2015.

[85] H. Hayer, O. Bakhtiari, and T. Mohammadi, "Simulation of momentum, heat and mass transfer in direct contact membrane distillation: A computational fluid dynamics approach," *Journal of Industrial and Engineering Chemistry*, vol. 21, pp. 1379–1382, 2015.

[86] V. Karanikola, A. F. Corral, H. Jiang, A. E. Sáez, W. P. Ela, and R. G. Arnold, "Sweeping gas membrane distillation: Numerical simulation of mass and heat transfer in a hollow fiber membrane module," *Journal of Membrane Science*, vol. 483, pp. 15–24, 2015.

[87] R. D. Gustafson, J. R. Murphy, and A. Achilli, "A stepwise model of direct contact membrane distillation for application to large-scale systems: Experimental results and model predictions," *Desalination*, vol. 378, pp. 14–27, 2016.

[88] F. Eleiwi, N. Ghaffour, A. S. Alsaadi, L. Francis, and T. M. Laleg-Kirati, "Dynamic modeling and experimental validation for direct contact membrane distillation (DCMD) process," *Desalination*, vol. 384, pp. 1–11, 2016.

[89] V. Perfilov, V. Fila, and J. S. Marcano, "A general predictive model for sweeping gas membrane distillation," *Desalination*, vol. 443, pp. 285–306, 2018.

[90] I. Hitsov, L. Eykens, W. De Schepper, K. De Sitter, C. Dotremont, and I. Nopens, "Full-scale direct contact membrane distillation (DCMD) model including membrane compaction effects," *Journal of Membrane Science*, vol. 524, pp. 245–256, 2017.

[91] I. Hitsov, T. Maere, K. De Sitter, C. Dotremont, and I. Nopens, "Modelling approaches in membrane distillation: A critical review," *Separation and Purification Technology*, vol. 142, pp. 48–64, 2015.

[92] W. J. Hill and W. G. Hunter, "A review of response surface methodology: A literature survey," *Technometrics*, vol. 8, no. 4, pp. 571–590, 1966.

[93] S. Fadhil, Q. F. Alsalhy, H. F. Makki, R. Ruby-Figueroa, T. Marino, A. Criscuoli, F. Macedonio, L. Giorno, E. Drioli, and A. Figoli, "Seawater desalination using PVDF-HFP membrane in DCMD process: Assessment of operating condition by response surface method," *Chemical Engineering Communications*, vol. 206, no. 2, pp. 237–246, 2019.

[94] A. E. Khalifa and D. U. Lawal, "Application of response surface and Taguchi optimization techniques to air gap membrane distillation for water desalination: A comparative study," *Desalination and Water Treatment*, vol. 57, no. 59, pp. 28 513–28 530, 2016.

[95] S. T. Bouguecha, A. Boubakri, S. E. Aly, M. H. Al-Beirutty, and M. M. Hamdi, "Optimization of permeate flux produced by solar energy driven membrane distillation process using central composite design approach," *Water Science and Technology*, vol. 74, no. 1, pp. 87–98, 2016.

[96] T. Mohammadi, P. Kazemi, and M. Peydayesh, "Optimization of vacuum membrane distillation parameters for water desalination using Box–Behnken design," *Desalination and Water Treatment*, vol. 56, no. 9, pp. 2306–2315, 2015.

[97] A. Boubakri, A. Hafiane, and S. A. T. Bouguecha, "Application of response surface methodology for modeling and optimization of membrane distillation desalination process," *Journal of Industrial and Engineering Chemistry*, vol. 20, no. 5, pp. 3163–3169, 2014.

[98] M. Khayet and C. Cojocaru, "Air gap membrane distillation: Desalination, modeling and optimization," *Desalination*, vol. 287, pp. 138–145, 2012.

[99] M. Khayet, C. Cojocaru, and C. García-Payo, "Application of response surface methodology and experimental design in direct contact membrane distillation," *Industrial & Engineering Chemistry Research*, vol. 46, no. 17, pp. 5673–5685, 2007.

[100] H. B. Demuth, M. H. Beale, O. De Jess, and M. T. Hagan, *Neural Network Design*. PWS Publishing Co., 2014.

[101] M. Khayet, C. Cojocaru, and M. Essalhi, "Artificial neural network modeling and response surface methodology of desalination by reverse osmosis," *Journal of Membrane Science*, vol. 368, no. 1-2, pp. 202–214, 2011.

[102] W. Cao, Q. Liu, Y. Wang, and I. M. Mujtaba, "Modeling and simulation of VMD desalination process by ANN," *Computers & Chemical Engineering*, vol. 84, pp. 96–103, 2016.

[103] C. Yang, X. Peng, Y. Zhao, X. Wang, J. Fu, K. Liu, Y. Li, and P. Li, "Prediction model to analyze the performance of VMD desalination process," *Computers & Chemical Engineering*, vol. 132, p. 106619, 2020.

[104] M. Khayet and C. Cojocaru, "Artificial neural network model for desalination by sweeping gas membrane distillation," *Desalination*, vol. 308, pp. 102–110, 2013.

[105] M. Tavakolmoghadam and M. Safavi, "An optimized neural network model of desalination by vacuum membrane distillation using genetic algorithm," *Procedia Engineering*, vol. 42, pp. 106–112, 2012.

[106] W. S. Levine, *The Control Handbook (three volume set)*. CRC press, 2018.

[107] C. V. Miranda, *Sistemas de Control Continuos y Discretos*. Editorial Paraninfo, 2012.

[108] G. A. Andrade, D. J. Pagano, J. D. Álvarez, and M. Berenguel, "A practical NMPC with robustness of stability applied to distributed solar power plants," *Solar Energy*, vol. 92, pp. 106–122, 2013.

[109] J. D. Álvarez, J. L. Redondo, E. Camponogara, J. E. Normey-Rico, M. Berenguel, and P. Ortigosa, "Optimizing building comfort temperature regulation via model predictive control," *Energy and Buildings*, vol. 57, pp. 361–372, 2013.

[110] M. Brdys and P. Tatjewski, *Iterative Algorithms for Multilayer Optimizing Control*. World Scientific, 2005.

[111] M. D. Mesarovic, D. Macko, and Y. Takahara, *Theory of Hierarchical, Multilevel, Systems*. Elsevier, 2000.

[112] W. Findeisen, F. N. Bailey, M. Brdys, K. Malinowski, P. Tatjewski, and A. Wozniak, *Control and Coordination in Hierarchical Systems.* John Wiley & Sons, 1980.

[113] S. Boyd, S. P. Boyd, and L. Vandenberghe, *Convex Optimization.* Cambridge University Press, 2004.

[114] G. B. Dantzig, A. Orden, and P. Wolfe, "The generalized simplex method for minimizing a linear form under linear inequality restraints," *Pacific Journal of Mathematics*, vol. 5, no. 2, pp. 183–195, 1955.

[115] S. Mehrotra, "On the implementation of a primal-dual interior point method," *SIAM Journal on Optimization*, vol. 2, no. 4, pp. 575–601, 1992.

[116] T. F. Coleman and Y. Li, "A reflective Newton method for minimizing a quadratic function subject to bounds on some of the variables," *SIAM Journal on Optimization*, vol. 6, no. 4, pp. 1040–1058, 1996.

[117] P. E. Gill, W. Murray, and M. H. Wright, *Practical Optimization.* SIAM, 2019.

[118] C. A. Floudas, *Nonlinear and Mixed-Integer Optimization: Fundamentals and Applications.* Oxford University Press, 1995.

[119] S. Salhi, *Heuristic search: The Emerging Science of Problem Solving.* Springer, 2017.

[120] A. M. Geoffrion, "Generalized benders decomposition," *Journal of optimization theory and applications*, vol. 10, no. 4, pp. 237–260, 1972.

[121] H. Chang, S. G. Lyu, C. M. Tsai, Y. H. Chen, T. W. Cheng, and Y. H. Chou, "Experimental and simulation study of a solar thermal driven membrane distillation desalination process," *Desalination*, vol. 286, pp. 400–411, 2012.

[122] J. D. Gil, A. Ruiz-Aguirre, L. Roca, G. Zaragoza, and M. Berenguel, "Solar membrane distillation: A control perspective," in *23th Mediterranean Conference on Control and Automation (MED 2015).* Torremolinos, Spain, 2015, pp. 796–802.

[123] J. D. Gil, A. Ruiz-Aguirre, L. Roca, G. Zaragoza, M. Berenguel, and J. L. Guzmán, "Control de plantas de destilación por membranas con apoyo de energía solar–parte 1: Esquemas," in *XXXVI Jornadas de Automática.* Bilbao, España, 2015.

[124] ——, "Control de plantas de destilación por membranas con apoyo de energía solar–parte 2: Resultados," in *XXXVI Jornadas de Automática.* Bilbao, España, 2015.

[125] Q. He, P. Li, H. Geng, C. Zhang, J. Wang, and H. Chang, "Modeling and optimization of air gap membrane distillation system for desalination," *Desalination*, vol. 354, pp. 68–75, 2014.

[126] M. López-Alvarez, A. Flores-Tlacuahuac, L. Ricardez-Sandoval, and C. Rivera-Solorio, "Optimal start-up policies for a solar thermal power plant," *Industrial & Engineering Chemistry Research*, vol. 57, no. 3, pp. 1026–1038, 2018.

[127] J. D. Gil, L. Roca, A. Ruiz-Aguirre, G. Zaragoza, J. L. Guzmán, and M. Berenguel, "Using a nonlinear model predictive control strategy for the efficient operation of a solar-powered membrane distillation system," in *25th Mediterranean Conference on Control and Automation (MED).* Valleta, Malta, 2017, pp. 1189–1194.

[128] J. D. Gil, P. R. C. Mendes, G. A. Andrade, L. Roca, J. E. Normey-Rico, and M. Berenguel, "Hybrid NMPC applied to a solar-powered membrane distillation system," *IFAC-PapersOnLine*, vol. 52, no. 1, pp. 124–129, 2019.

[129] J. D. Gil, L. Roca, M. Berenguel, and J. L. Guzmán, "Optimización del arranque de una planta de destilación por membranas solar," in *Actas IV Simposio CEA de Modelado, Simulación y Optimización.* Valladolid (Spain), 2018.

[130] J. D. Gil, L. Roca, M. Berenguel, and J. L. Guzmán, "A multivariable controller for the start-up procedure of a solar membrane distillation facility," *IFAC-PapersOnLine*, vol. 51, no. 4, pp. 376–381, 2018.

[131] J. D. Gil, L. Roca, and M. Berenguel, "Starting-up strategies for solar thermal fields attending to time and economic criteria: Application of hierarchical control," *IFAC-PapersOnLine (In press)*.

[132] A. Ruiz-Aguirre, D. C. Alarcón-Padilla, and G. Zaragoza, "Productivity analysis of two spiral-wound membrane distillation prototypes coupled with solar energy," *Desalination and Water Treatment*, vol. 55, no. 10, pp. 2777–2785, 2015.

[133] L. Roca, J. A. Sánchez-Molina, F. Rodríguez, J. Bonilla, A. de la Calle, and M. Berenguel, "Predictive control applied to a solar desalination plant connected to a greenhouse with daily variation of irrigation water demand," *Energies*, vol. 9, no. 3, p. 194, 2016.

[134] N. Shekarchi and F. Shahnia, "A comprehensive review of solar-driven desalination technologies for off-grid greenhouses," *International Journal of Energy Research*, vol. 43, no. 4, pp. 1357–1386, 2019.

[135] H. F. Scherer, M. Pasamontes, J. L. Guzmán, J. D. Álvarez, E. Camponogara, and J. E. Normey-Rico, "Efficient building energy management using distributed model predictive control," *Journal of Process Control*, vol. 24, no. 6, pp. 740–749, 2014.

[136] J. D. Gil, L. Roca, M. Berenguel, A. Ruiz-Aguirre, and A. Giménez, "Control predictivo para la operación eficiente de una planta formada por un sistema de desalación solar y un invernadero," in *XXXVIII Jornadas de Automática.* Gijón, España, 2017.

[137] J. D. Gil, L. Roca, M. Berenguel, and G. Zaragoza, "Destilación por membranas. Aportaciones de la desalación solar térmica y el control automático en el suministro de agua en invernaderos," *Era Solar: Energías Renovables*, no. 201, pp. 16–25, 2017.

[138] J. D. Gil, P. R. C. Mendes, E. Camponogara, L. Roca, J. D. Álvarez, and J. E. Normey-Rico, "A general optimal operating strategy for commercial membrane distillation facilities," *Renewable Energy*, vol. 156, pp. 220–234, 2020.

[139] J. D. Gil, L. Roca, M. Berenguel, and G. Zaragoza, "Aportaciones de la desalación solar térmica a la sostenibilidad del sistema agrícola en Almería," in *1er Congreso de Jóvenes Investigadores en Ciencias Agroalimentarias.* Almería, España, 2018.

[140] J. D. Gil, M. Muñoz, L. Roca, F. Rodríguez, and M. Berenguel, "An IoT based Control System for a Solar Membrane Distillation Plant used for Greenhouse Irrigation," in *Global IoT Summit (GIoTS).* IEEE, 2019, pp. 1–6.

[141] J. D. Gil, L. Roca, and M. Berenguel, "Modelling and automatic control in solar membrane distillation: Fundamentals and proposals for its technological development," *Revista Iberoamericana de Automática e Informática Industrial (In press)*, 2020.

[142] J. D. Gil, M. Berenguel, and L. Roca, "Aportaciones desde el punto de vista del control automático y la optimización a la tecnologıa de destilación por membranas alimentada con energıa solar," in *Actas XVI Simposio CEA de Ingeniería de Control*. Almería, España, 2018.

UNIVERSITY OF ALMERÍA

DEPARTAMENTO
DE INFORMÁTICA
UNIVERSIDAD DE ALMERÍA

ARM
Automática, Robótica y Mecatrónica

TEP197